THE UNIVERSITY
of EDINBURGH

Bimetallic Uranium and Cerium Tetraphenolate Complexes for the Activation and Functionalisation of Small Molecules

Megan L. Seymour

The University of Edinburgh

Submitted for the degree of Doctor of Philosophy

October 2018

Declaration

The work described in this thesis is my own, except where I have given reference to a published source or acknowledged help from a named person. This thesis has not been submitted, in whole or in part, for any degree at this or any other university. The work herein was carried out under the supervision of Professor Polly L. Arnold from September 2015 to October 2018.

Signature:

Date:

Abstract

This thesis describes the synthesis of bimetallic *f*-element complexes of *meta*-functionalised tetraphenol arene ligands, **(*m*TP)**, and their reactivity, primarily towards small molecular substrates such as dinitrogen.

Chapter one introduces the principles of uranium chemistry and the suitability of aryloxides as ligands for low oxidation state uranium. The synthesis and reactivity of selected examples of U(III) and U(IV) complexes are described and an overview of dinitrogen activation by selected transition metal complexes is provided.

Chapter two reports the synthesis and characterisation of two *meta*-functionalised tetraphenol arene ligand precursors **H_4(*m*TP^m)** and **H_4(*m*TP^t)** and describes reactions designed to target closely related analogues. In 1:1 salt metathesis or protonolysis reactions, two tetradentate ligands and two U(IV) centres are combined to yield **[U_2(*m*TP)$_2$]** complexes with a novel 'letterbox' architecture. The reduction of some of these complexes under an atmosphere of dinitrogen yields bound $[N_2H_2]^{2-}$ following an intramolecular reaction of an activated N_2 fragment with benzylic C−H bonds provided by the ligand. The $[N_2H_2]^{2-}$ moiety is susceptible to further functionalisation through reactions with external electrophiles. Stoichiometric and catalytic functionalisation reactions are discussed and a mechanistic pathway for these transformations is proposed.

Chapter three presents the synthesis of another set of bimetallic complexes, **[U_2(*m*TP)X_4]** (X = one electron donor ligand), derived from 2:1 reactions of uranium(IV) with **H_4(*m*TP)**. The redox chemistry of these complexes is explored through cyclic voltammetry and the structure and reactivity of these 'half-letterbox' complexes is compared to the complexes reported in Chapter two.

The work described in Chapter four returns to complexes with a 'letterbox' geometry but employs Ce(III) and potassium cations to prepare a set of heterobimetallic analogues, **[K][Ce_2(*m*TP)$_2$K]**. The oxidation chemistry of these complexes is investigated and an EPR study is used to examine the magnetic behaviour of the two $4f^1$ Ce(III) centres.

Chapter five details the experimental procedures and characterisation data for the work described in the preceding chapters.

Lay Summary

Industrially, the amount of ammonia, NH_3, produced is greater than that of any other compound, with production exceeding 150 million tonnes annually, and consuming 2 % of the global energy supply. For over 100 years the Haber-Bosch process has provided NH_3 by combining N_2 with H_2 at high pressures and temperatures over an iron catalyst bed. This thesis describes the synthesis and reactivity of a series of new uranium complexes. A number of the uranium compounds synthesised can mediate the activation of dinitrogen to yield NH_3 and other nitrogen functionalisation products at low temperatures and ambient pressures.

The synthesis of cerium analogues of these uranium complexes is also described. The structure and reactivity of these complexes is compared with the uranium compounds, and the magnetic behaviour of electrons located on the cerium centres is briefly examined.

Acknowledgements

Firstly, I wish to thank my supervisor, Professor Polly Arnold, for her guidance throughout my PhD and the University of Edinburgh Principal's Career Development Scholarship for funding. Additionally, I would like to thank Professor Karsten Meyer for hosting me in Erlangen, and COST for funding my placement with a Short Term Scientific Mission grant.

I am grateful to Dr Lorna Murray and Mr Juraj Bella for assistance with NMR and to Dr Jordann Wells, Dr Marketa Suvova, Max Curcio, Connor Halliday and Francis Lam for their help with X-ray crystallography. Additionally, thank you to Matze Miehlich for helping me with EPR spectroscopy.

A special thank you goes to Dr Nicola Bell, who I respect and admire so much, for going above and beyond to make sure I got to this point. I would also like to thank the other members of the Larnold groups, past and present, for their many contributions. Jordann and Danny for introducing me to whisky, and Marketa and Cath for introducing me to breakfast wine. Both have been essential. Dr James Pankhurst, I am grateful for your assistance with electrochemistry, even if you were not the most supportive ceilidh partner. Thanks to Max McMullon, whose ballet skills have been an inspiration, and to Steven Gray, Scotland's own Billy Joel. Thank you Dr Brad Cowie for all of your advice and assistance, for proofreading this thesis and finally, for not murdering me and hiding my body in a suitcase. Rory, Laura, Tatsumi, Liam, Lotte, Jamie, Amy, Kai, Johann and Paul, it has been an absolute pleasure, thank you for all of the great memories. My thanks also go to the able assistant manager of my FPL team, and honorary flat mate, Dr Tom West, for putting up with my terrible company for longer than you should have had to, I wish you all the best aboard the Dog House express.

I thank my family and friends, especially my Mum and Dad, and sister Polly, who have always been so kind and supportive, especially when things have been difficult. Thank you for always believing in me, I love you and I hope I have made you proud.

Ryan Kerr, thank you for not letting me drown in Loch Tay, teaching me to speak fluent Scottish, and for providing supplies of emergency chocolate and hugs. You have helped me so so much, and I can't wait for our next adventures.

List of abbreviations

General

[O]	Oxidant
[PyH]Cl	Pyridinium chloride
18-c-6	18-crown-6
3D	3 dimensional
Ad	Adamantyl
APPI	Atmospheric pressure photoionisation
Ar	Aryl
Ar^{P}O	2-*tert*-butyl-4-methyl-6-(diphenylphosphino)phenolate
Atm	Atmosphere
Avg	Average
BMP	2,2'-Methylenebis(6-*tert*-butyl-4-methylphenolate
Bn	Benzyl
btpyan	1,8-bis(2,2':6',2''-terpyridyl)anthracene
Cat	Catalyst
COT	Cyclooctatetraenyl
COT_{TIPS}	(tri-*iso*-propylsilyl)cyclooctatetraenyl
COT_{TIPS2}	bis(tri-*iso*-propylsilyl)cyclooctatetraenyl
Cp	Cyclopentadienyl
Cp*	1,2,3,4,5-Pentamethylcyclopentadienyl
Crypt	Cryptand
CSD	Cambridge Structural Database
CV	Cyclic voltammetry
Cy	Cyclohexyl
Depf	Ferrocenyldiphosphine
DFT	Density functional theory
DHA	9,10-Dihydroanthracene
Dme	Dimethoxyethane
Dmso	Dimethyl sulfoxide
DOSY	Diffusion Ordered Spectroscopy
E	Element

EPR	Electron paramagnetic resonance
Equivs	Equivalents
ESI	Electrospray ionisation
Fc	Ferrocene
Fc^+	Ferrocenium
FTIR	Fourier-transform infrared
GC	Gas chromatography
GCMS	Gas chromatography- mass spectrometry
h	Hours
HAT	Hydrogen atom transfer
HBBN	9-Bora-9-bicyclononane
HIPT	3,5-(2,4,6-*i*-$Pr_3C_6H_2)_2C_6H_3$
HMBC	Heteronuclear Multiple Bond Correlation
HOMO	Highest occupied molecular orbital
HRMS	High resolution mass spectrometry
HSQC	Heteronuclear single quantum correlation
INEPT	Insensitive nuclei enhanced by polarisation transfer
IR	Infrared
Ln	Lanthanide
LUMO	Lowest unoccupied molecular orbital
Lut	2,6-Dimethylpyridine
LutH	2,6-Dimethylpyridinium
M	Metal
MALDI	Matrix Assisted Laser Desorption Ionisation
Me	Methyl
Me-Bim-PCP	5,6-Dimethyl-1,3-bis((di-tert-butylphosphino)methyl)benzimidazol-2-ylidene
Mes	Mesityl
Mins	Minutes
***m*TP**	*Meta*-tetraphenol
N''	$N(SiMe_3)_2$
N_3N	$N\{CH_2CH_2N(SiMe_2{}^tBu)\}_3$
^{n}Bu	Normal-butyl

NCS	N-Chlorosuccinimide
NHC	N-heterocyclic carbene
NMR	Nuclear Magnetic resonance
OAr	Aryloxide
ODtbp	O-2,6-$^{t}Bu_2C_6H_3$
OTf	SO_3CF_3
OTtbp	O-2,4,6-$^{t}Bu_3C_6H_3$
P_2N_2	$PhP(CH_2SiMe_2NSiMe_2CH_2)_2PPh$
PCET	Proton coupled electron transfer
Ph	Phenyl
***p*-Me_2bp**	*p*-$C(CH_3)_2C_6H_2Me_2O^-$
PNP	*N,N'*-bis(diphenylphosphine)-2,6-diaminopyridine
ppm	Parts per million
***p*TP**	*Para*-tetraphenol
***p*-TSA**	*Para*-toluenesulfonic acid
Py	Pyridine
Quant	Quantitative
qui	benzoquinone
R	Alkyl
RE	Rare earth
RT	Room temperature
SCE	Saturated calomel electrode
SHE	Standard hydrogen electrode
Solv	Solvent
SQUID	Superconducting quantum interference device
^{t}Bu	*Tertiary*-butyl
TEMPO	2,2,6,6-Tetramethyl-1-piperidinyloxy
Thf	Tetrahydrofuran
TLC	Thin layer chromotography
TOF	Turnover frequency
TON	Turnover number
Tp*	Hydrotris(3,5-dimethylpyrazolyl)borate
TS	Transition state

UV-Vis	Ultraviolet–visible
XRD	X-ray diffraction
Xs	Excess
ΔEp	Separation between the anodic and cathodic peak potentials

NMR

br	Broad
d	Doublet
{^{1}H}	Proton Decoupled
m	Multiplet
ppm	Parts Per Million
q	Quartet
s	Singlet
t	Triplet

Publications based on the work described in this thesis

Wells, J. A. L., Seymour, M. L., Suvova, M., & Arnold, P. L. (2016). Dinuclear uranium complexation and manipulation using robust tetraaryloxides. *Dalton Transactions*, *45*(40), 16026–16032. https://doi.org/10.1039/C6DT02630C

Contents

Chapter 1: Introduction

1.1 Fundamentals of uranium chemistry

The stockpiling of depleted uranium in nuclear wastes is not only a matter of acute scientific interest, but also a globally contentious issue with huge societal and economic impact. A waste product of uranium enrichment, depleted uranium contains just 0.2 - 0.4 % of the fissile ^{235}U isotope.[1] The more stable ^{238}U isotope has a half-life of 4.46 billion years and is only a weak α emitter. Over 1.6 million tonnes of depleted uranium are stored globally with stockpiles increasing by every 50,000 tonnes each year, and in view of this, ^{238}U is an attractive alternative to many less abundant, more toxic transition metals typically used in catalytic applications.[2]

Whilst uranium catalysts remain rare, the last 15 years have seen the development of organometallic uranium complexes for the activation and functionalisation of small molecules[3]- neutral, low molecular weight molecules that are thermodynamically stable or kinetically inert. Many represent important industrial feedstock chemicals, for example CO, CO_2, and N_2.[4] These seminal studies have revealed many unique and diverse modes of novel reactivity by organometallic uranium.

Central to its use in small molecule activation processes is the range of oxidation states available to uranium. The 5*f* orbitals of the actinide metals possess an additional radial node relative to the 4*f* lanthanides; resulting in increased shielding of the valence electrons from the effective nuclear charge.[5] Additionally, relativistic effects that result from the large mass of uranium cause a contraction of the core orbitals and an expansion of the 5*f* orbitals of the actinides, approximately halving the binding energy of a uranium 5*f* electron compared to the theoretical case of an unrelativistic 5*f* electron. This accounts for the accessibility of formal oxidation states U(II) to U(VI). The large, diffuse 5*f* orbitals are more able to overlap with neighbouring orbitals, leading to increased covalency relative to the lighter lanthanides.[3] Figure 1-1 highlights these differences by comparing the relativistic radial distribution functions of Sm(III) and Pu(III).[6]

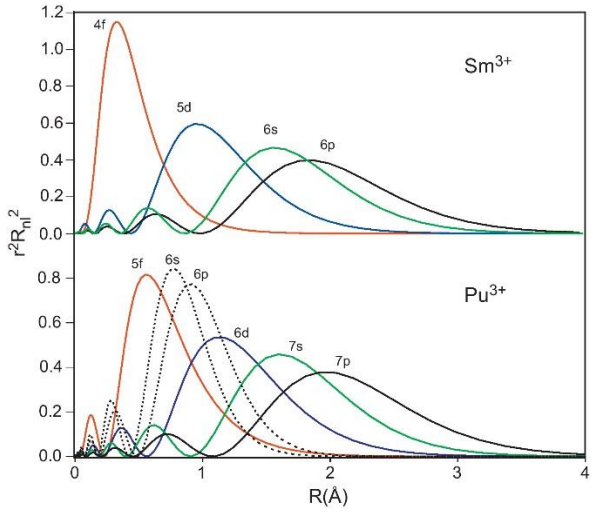

Figure 1-1 Relativistic radial distribution functions for Pu^{3+} and Sm^{3+}, showing the additional radial node in 5*f* orbitals and the contraction in core orbitals for the actinides relative to the lanthanides.[6]

Uranium(IV) and uranium(VI) are the most abundant oxidation states, and the latter is most commonly found in the form of the rigorously inert uranyl dication, $[UO_2]^{2+}$.[7] Uranium(II) is very rarely observed and requires strongly stabilising ligands, the orbitals of which are thought to partially or fully accommodate the additional electron (see **AM**, Section 1.4.1).[8,9] Although uranium(V) is often kinetically unstable with respect to disproportionation to uranium(IV) and uranium(VI), it can act as a strong oxidant, along with (VI), whereas uranium(III) is strongly reducing.[3]

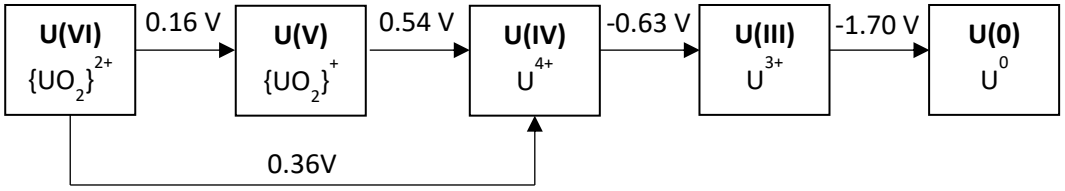

Figure 1-2 Formal uranium reduction potentials (in V vs. standard hydrogen electrode in 1M $HClO_4$ at 298 K).[1]

The U(III)/U(IV) redox couple has produced a wealth of stoichiometric reductive activation chemistry but with the exception of one electrocatalytic system,[10] examples of homogenous catalytic transformations are yet to widely emerge.

This thesis will investigate dinitrogen functionalisation by bimetallic uranium tetraphenolate complexes. The following review will introduce the synthesis and reactivity of seminal U(III)

and U(IV) complexes followed by a discussion of the suitability of aryloxides as ligands for low oxidation state uranium. Additionally, an overview of nitrogen activation by transition metal complexes is provided and selected examples of N−H, N−C and N−Si bond formation mediated by transition metal complexes are described. This discussion will highlight the importance of multimetallic cooperative reactivity in such systems. Finally, the small number of reported uranium dinitrogen complexes are described and compared.

1.2 U(III) mediated small molecule activation

The strong reducing potential of the uranium(III) ion provides unique small molecule reactivity. Typically the one electron oxidation of U(III) to U(IV) enables transfer of an electron to an unsaturated substrate, often providing bimetallic structures bridged by a single, doubly reduced substrate. This reactivity is increasingly being exploited in reductive carbon monoxide coupling,[11,12] carbon dioxide activation,[13] arene activation,[14] and even dinitrogen reduction.[15,16]

Cloke and coworkers have used simple arene ligands to prepare a series of U(III) mixed sandwich complexes which provide cyclic, aromatic ring systems *via* the reductive coupling and oligomerisation of CO (Scheme 1-1). [U(C_5Me_5)(COT_{TIPS})], **A** (COT_{TIPS} = bis(tri-iso-propylsilyl)cyclooctatetraenyl) was prepared from the sequential addition of KCp* and $K_2[COT_{TIPS}]$ to [UI_3]. The reaction of **A** with one bar of CO at –78 °C, yields the cyclic deltate dianion ($C_3O_3^{2-}$) bridged bimetallic species **D**.[11] More recent studies revealed that the nature of the oxocarbon anion generated can be controlled by the steric demand of the Cp^R ligand. Removing steric bulk by replacing Cp* with Cp^{Me4H}, (**B**) leads to the formation of a squarate ($C_4O_4^{2-}$) dianion, (**E**)[17] whereas the introduction of a single Et substituent (Cp^{Me4Et}) (**C**) increases steric demand sufficiently to impart almost complete selectivity for the ynediolate ($C_2O_2^{2-}$) product, (**F**) (with the deltate species formed as a minor product depending on the reaction conditions) (Scheme 1-1).[18] Quenching reactions with Me_3SiCl have demonstrated that the bridging oxocarbon moiety can be removed, yielding $C_4O_2(OSiMe_3)_2$ from **E**, proving the concept that reductive homologation of CO provides a new route for the synthesis of complex organic molecules.

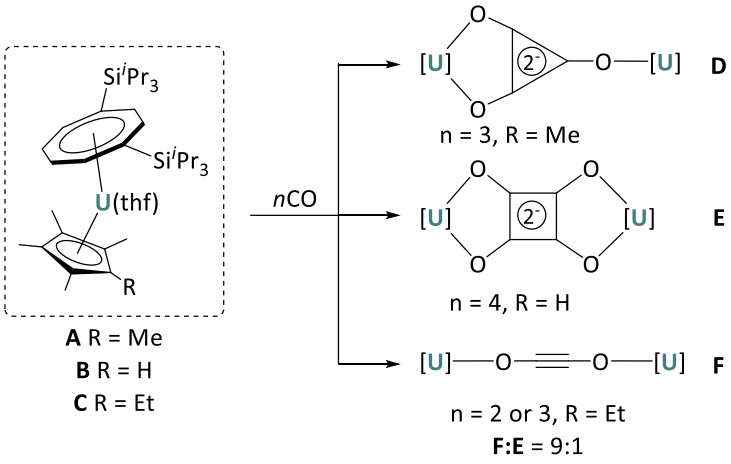

Scheme 1-1 Synthesis of different size oxocarbons by manipulating the steric environment around U(III) mixed sandwich complexes.[11,17,18]

Another potential route to organic molecules is the fixation of CO_2. CO_2 activation mediated by transition metal alkyl compounds is well established.[19] U(III) alkyl complexes on the other hand remain rare, and are typically unstable towards disproportionation. Bart and coworkers have employed the sterically demanding pyrazolyl ligand, Tp*, (hydrotris(3,5-dimethylpyrazolyl)borate) to stabilise an unusual U(III) alkyl complex and report unprecedented insertion reactivity towards CO_2. [Tp*$_2$U(CH_2Ph)], **H**, was exposed to 1 atmosphere of CO_2 to yield the uranium carboxylate complex [Tp*$_2$U(κ^2-O_2CCH_2Ph)], **I**, *via* insertion of one equivalent of CO_2 into the uranium alkyl bond. Notably, quenching with $SiMe_3I$ yields the silyl ester $Me_3SiOC(O)CH_2Ph$ and regenerates the **H** precursor, Tp*$_2$UX, **G**, (Scheme 1-2).[20]

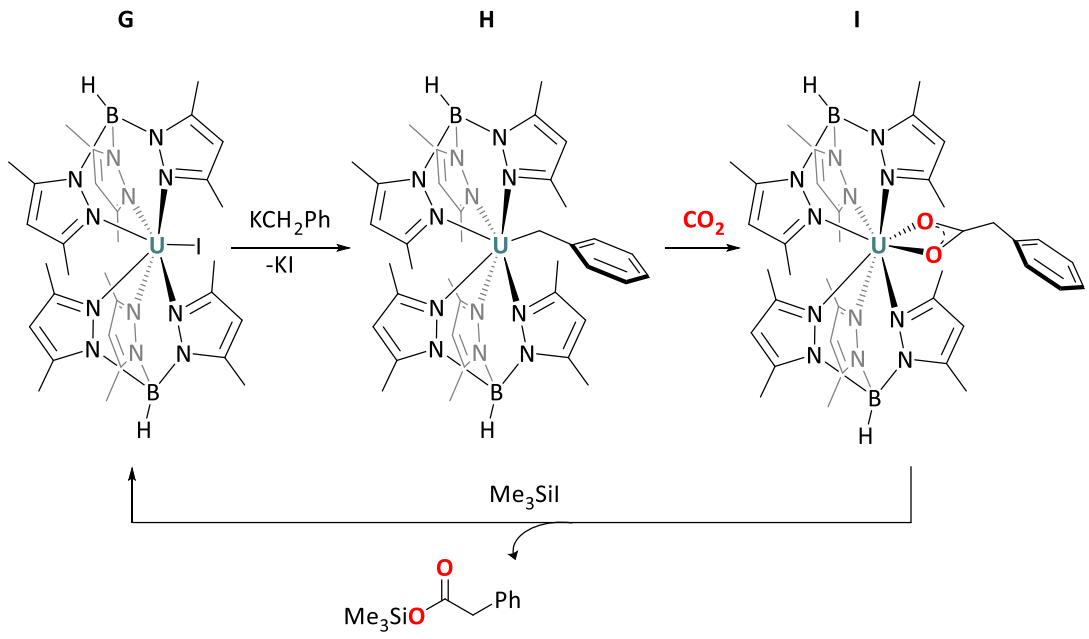

Scheme 1-2 CO_2 functionalisation mediated by **G**.[20]

Bart's pyrazole complex represents small molecule binding mediated by a single uranium centre. Cloke's arene complex is more typical of many U(III) systems in that small molecule activation is mediated by two discrete monometallic complexes acting cooperatively to reduce a substrate and yield a bimetallic, substrate bridged product. Mazzanti has exploited the power of combining two reducing uranium centres in a single molecule, and the double oxo-bridged bimetallic complex $[\{U(OR)_2(\mu\text{-}OR)\}_2]$ (**J**) (R = $Si(O^tBu)_3$), can independently afford two electron reduction of CS_2 and CO_2 (Scheme 1-3).[21] Complex **J** was also shown to reduce toluene to a dianionic η^6:η^6 bridging fragment, yielding an inverse-sandwich complex (**M**). These metal–activated-arene–metal species are attractive targets with potentially useful chemical[22] and magnetic[23] properties, but remain extremely rare owing to the highly inert nature of aromatic fragments in accordance with Hückel theory.[24]

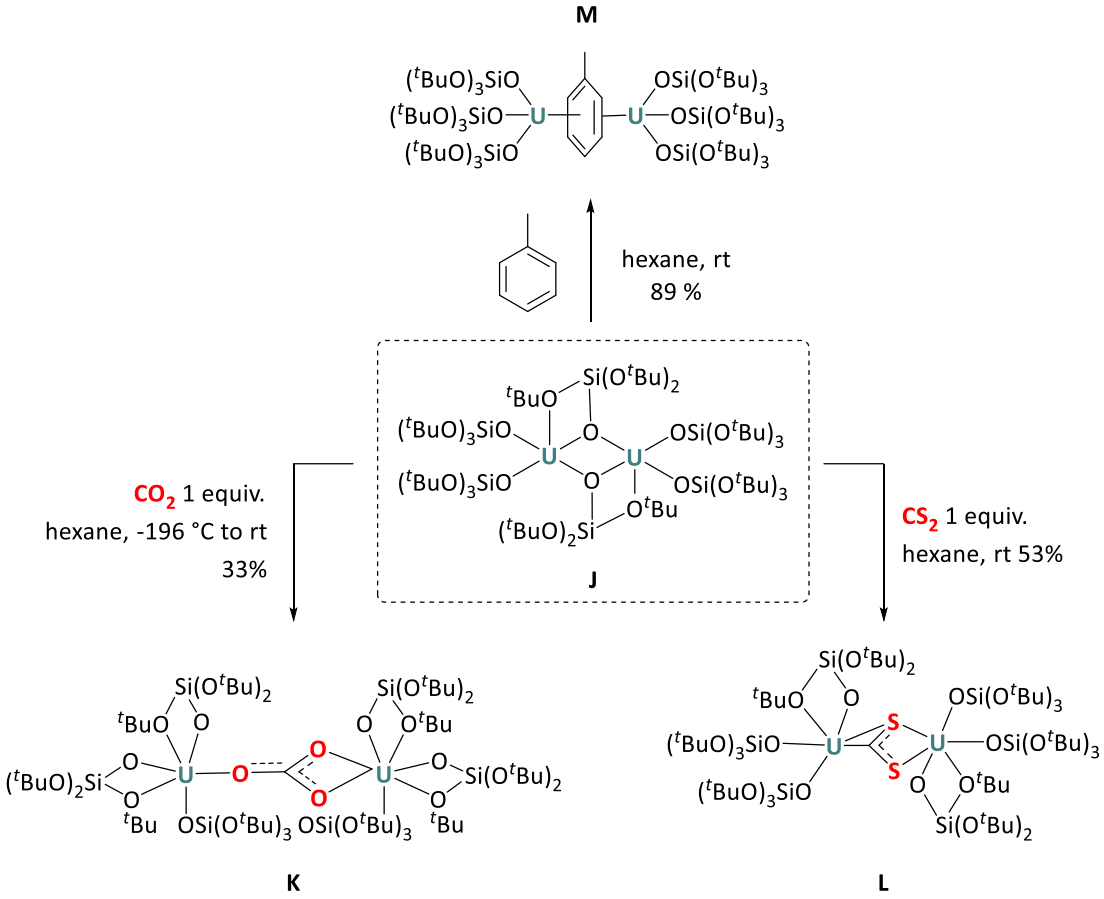

Scheme 1-3 Reductive activation of CO_2, CS_2 and toluene by $[\{U(OSi(O^tBu)_3)_2(\mu\text{-}OSi(O^tBu)_3)\}_2]$.[21]

Later studies by Mazzanti and coworkers revealed that **J** also reductively activates azides, providing dinuclear U(IV)-imido and -nitrido complexes, depending on the azide species used (Scheme 1-4).[25] The reaction of **J** with four equivalents of AdN_3 (Ad = adamantly) in toluene led to the formation of two products: the U(IV) siloxide, $[U(OR)_4]$, and the dinuclear bis-imido complex, $[U_2(NAd)_4\{OR\}_4]$ (R = $Si(O^tBu)_3$) (**N**). The use of CsN_3, however, resulted in the formation of a bridged-nitride species, **P**, with an almost linear U=N=U motif and caesium incorporation. The linear U(IV)=N=U(IV) fragment has only been reported in one previous study[26] and has been identified as a potentially useful nitrogen transfer agent in further reactions with other small molecules.[25]

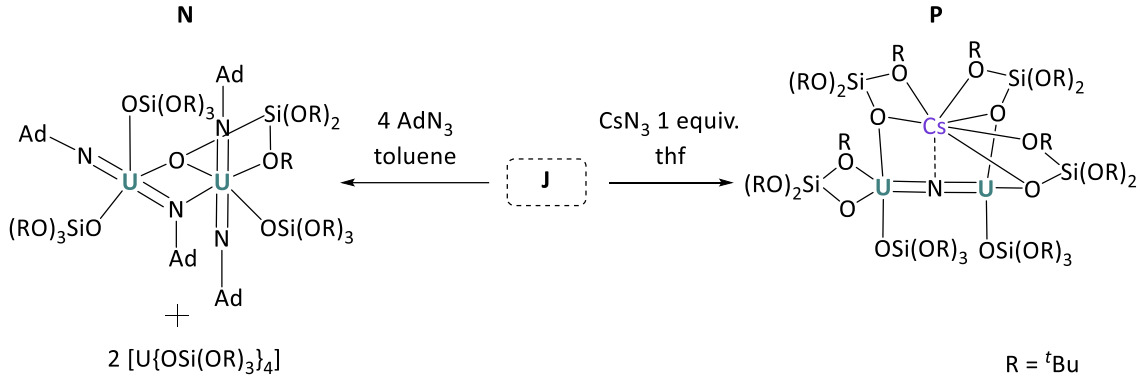

Scheme 1-4 Reductive azide activation facilitated by [{U{OSi(O^{t}Bu)$_3$}$_2${μ-OSi(O^{t}Bu)$_3$}}$_2$].[25]

1.3 U(IV) complexes and small molecule activation

Whilst the small molecule activation chemistry of uranium is dominated by the reducing U(III) oxidation state, higher oxidation states, including U(IV), show a different range of reactivity. Typically, the relative stability of uranium(IV) complexes has rendered them an attractive alternative to those investigating synthetic routes to novel uranium-ligand multiple bonding interactions, or uranium-transition metal bonding interactions.[27,3]

A computational study on a series of bimetallic U(IV)/M (M = Ni, Pd, Pt) complexes for example, confirmed that uranium employs both 5*f* and 6*d* orbitals in covalent bonding to the group 10 metal.[27] The complexes were synthesised *via* [IU(OAr^P-κ^{2}O,P)$_3$ ([Ar^{P}O]$^-$ = 2-tert-butyl-4-methyl-6-(diphenylphosphino)phenolate) as shown in Scheme 1-5.

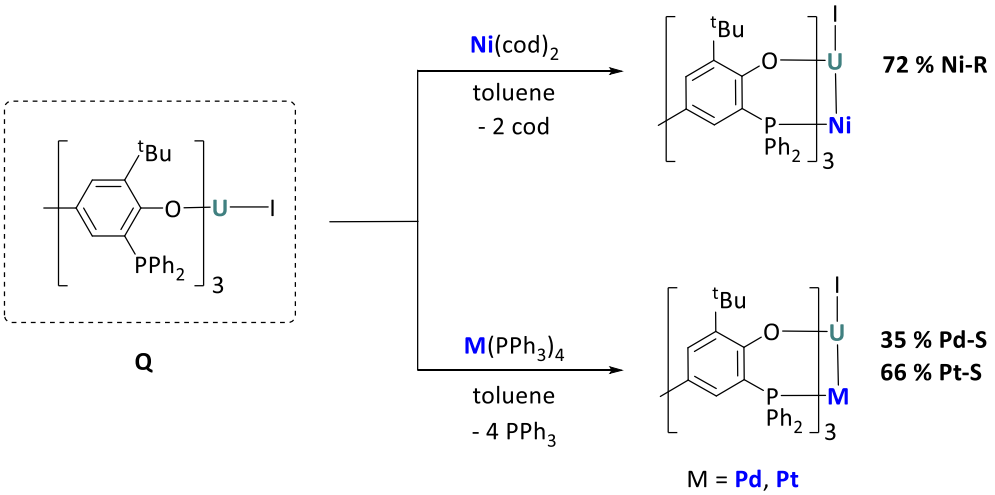

Scheme 1-5 Synthesis of bimetallic U/group 10 metal complexes.[27]

Although small molecule activation by U(IV) complexes is more unusual, reductive activation is still possible. A variety of U(IV) complexes such as $[(Cp)_2UMe_2]$ have been reported as convenient catalytic precursors for the oligomerization of terminal alkynes for example.[28]

Judicious design can yield U(IV) complexes with highly reactive metal–ligand bonds able to mediate insertion, rather than reduction of CO and CO_2. Evans and coworkers reported the synthesis of the silylalkyl double "tuck-in" complex, $[(\eta^5{:}\kappa^1\text{-}C_5Me_4SiMe_2CH_2)_2U]$, **T**, *via* thermally induced intramolecular C–H activation of the substituted metallocene $[(C_5Me_4SiMe_3)_2UMe_2]$.[29] The reactive alkyl ligands are tethered to cyclopentadienyl ligands as shown in Scheme 1-6. Insertion reactivity of the unsubstituted metallocene $[(C_5Me_5)_2UMe_2]$ is not well defined and insertion products have not been observed cystallographically.[30] **T** on the other hand reacts with substrates including CO, CO_2, isocyanides and acetylenes in to give well defined, fully characterised insertion products (**V**-**Z**).[31]

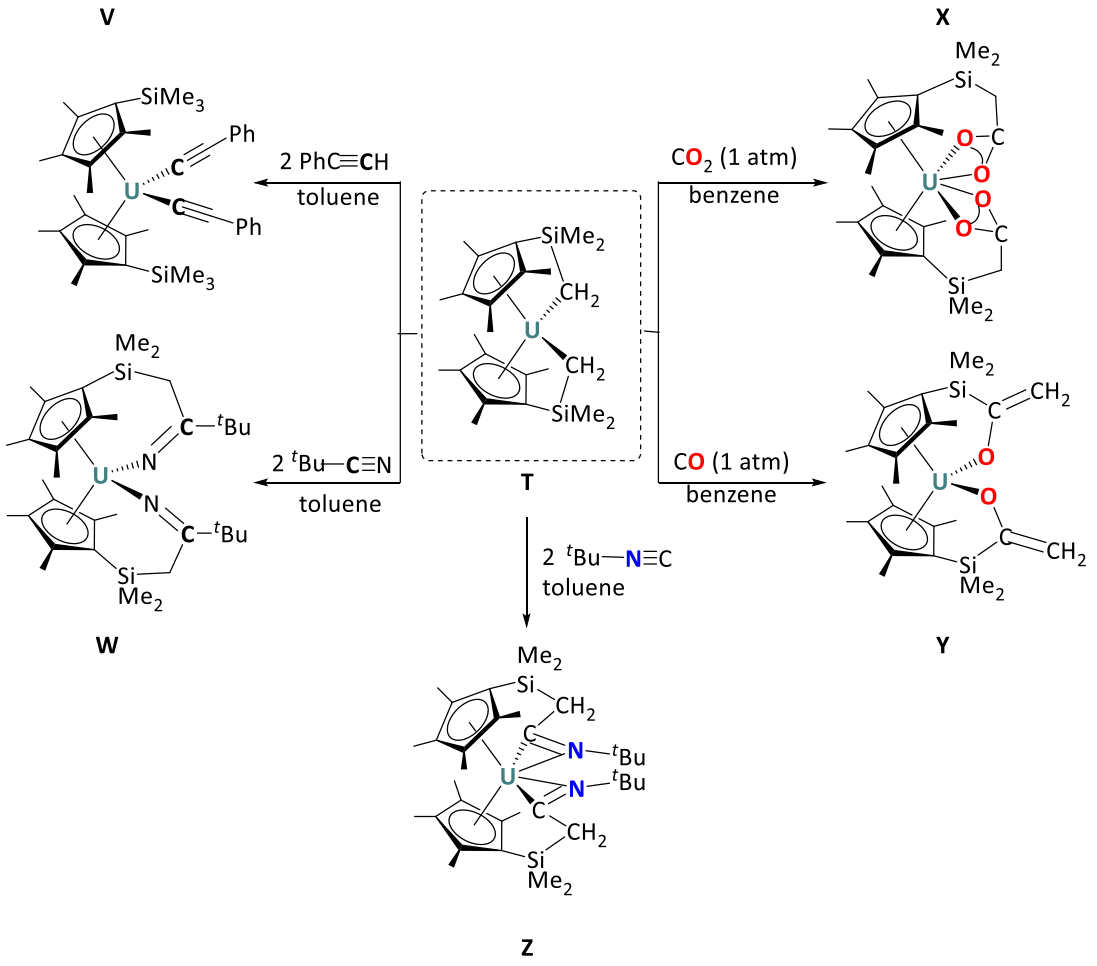

Scheme 1-6 Reactivity of $[(\eta^5{:}\kappa^1\text{-}C_5Me_4SiMe_2CH_2)_2U]$ towards small molecule substrates.[29]

A similar "tuck-in" complex, [U(COT^{TIPS2})(η^5:η^1-C$_5$Me$_4$CH$_2$)], **AA**, was observed by Cloke, as an unanticipated decomposition product of U(IV) alkyl complexes, **AB**. Exposure of **AA** to one equivalent of CO_2 yielded the dimeric insertion product [{U(COT^{TIPS2})-(η^5:η^1-C$_5$Me$_4$H$_2$-μ^1:μ^1-O$_2$C)}$_2$], **AC**, (Scheme 1-7) in contrast to the simple 'untethered' alkyl complexes which provided monometallic single insertion products.[32]

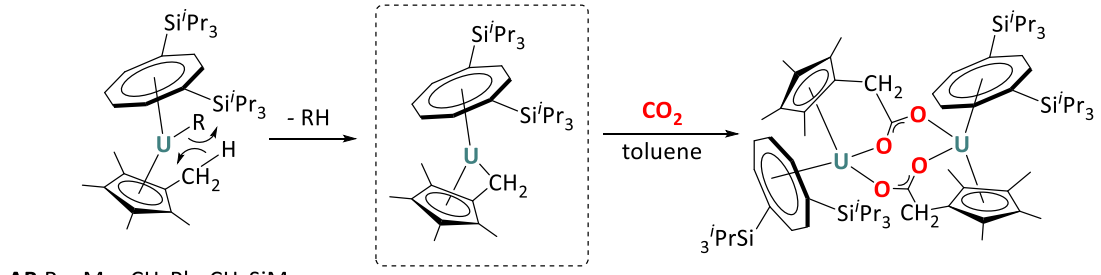

AB R = Me, CH_2Ph, CH_2SiMe_3, $CH(SiMe_3)_2$

AA

AC

Scheme 1-7 Synthesis and reactivity of [U(COT^{TIPS2})(η^5:η^1-C$_5$Me$_4$CH$_2$)].[32]

1.4 Aryloxides as ligands for uranium

Several of the above examples use arene ligands to stabilise low oxidation state uranium. In contrast, many authors choose to explore hard, anionic donors such as amides,[33,34] siloxides,[21,25,35,36] and alkoxides.[33,37,38]

Aryloxide ligands represent a major class of anionic donor ligands. Perfectly suited to forming robust linkages, they can be subtly manipulated by substitution of the aromatic ring. Substitution can not only provide steric control, protecting a uranium centre against unwanted reactivity, but can be used to tune the electronics *via* addition of electron donating or withdrawing groups. These strategies are being increasingly exploited in ligand design, especially for the oxophilic +3 to +6 oxidation states of uranium.[39,40,15,41]

Simple U(III) tris(aryloxide) complexes such as [U(ODtbp)$_3$], **AD**, have been extensively investigated by authors including Arnold,[14,15] Sattelberger,[42] Smith[43] and many others. It was recently reported by reported by Arnold however, that over a period of several days, such aryloxides are unstable in arene solvents, to spontaneous disproportionation (to two

equivalents of [U(ODtbp)$_4$] and one equivalent of [U(ODtbp)$_2$]) which allows the resulting [U(ODtbp)$_2$] fragments to bind and reduce arenes, yielding inverse sandwich complexes (**AD^{Ar}**) able to mediate the first C–H borylation of a trapped arene fragment (**AD^{B}**) (Scheme 1-8).[22]

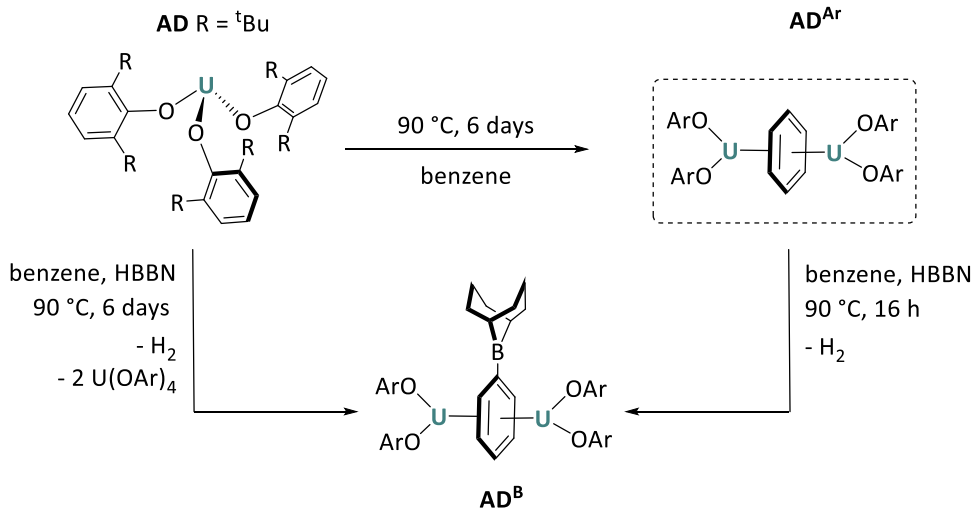

Scheme 1-8 reduction and C–H borylation of arenes mediated by [U(ODtbp)$_3$] disproportionation.[14]

[U(ODtbp)$_3$], **AD**, and the closely related analogue [U(OTtbp)$_3$], **AE**, have also been found to couple CO under ambient conditions to yield the ynediolate complexes [U(OAr)$_3$]$_2$(μ-η^1:η^1-C$_2$O$_2$) **AF**, **AG**.[15] Both complexes also react with N_2 to yield side-on, dinitrogen bridged [U(OAr)$_3$]$_2$(μ-η^2:η^2-N$_2$) complexes, **AH**, **AI**. Structural parameters, Raman spectroscopy and computational analysis indicate two electron reduction to afford [U(IV)]$_2$(N_2^{2-}) with considerable lengthening of the N−N bond to 1.189 Å. Despite this, dinitrogen binding is reversible, and nitrogen is removed from both complexes upon heating to 80 °C. Interestingly, (OTtbP) provides a much more stable N_2 complex than the *di*-^{t}Bu analogue (ODtbp) (N_2 can be removed from [U(ODtbp)$_3$]$_2$(μ-η^2:η^2-N$_2$) in solution at room temperature by freeze-pump-thaw degassing). The increased electron donation from the third alkyl substituent on the aryloxide is proposed to enhance the reducing power of the U(III) centre, demonstrating the remarkable control exerted by simple modifications to aryloxide ligands. The reactivity of [U(OAr)$_3$] towards CO_2 is less well controlled. On exposure to 1 bar of CO_2, [U(ODtbp)$_3$], **AD**, undergoes metal oxidation and ligand redistribution to yield [U(ODtbp)$_4$], **AJ**, with no observed CO_2 insertion. At elevated temperatures, [U(OTtbp)$_3$], **AE**, does mediate CO_2 reduction and incorporation of an abstracted oxo, but ligand dissociation is also observed

allowing CO_2 insertion between U−OAr bonds yielding the U(IV) carbonate **AK**, $U_2(OTtbp)_4(\mu\text{-}O)(\mu\text{-}\eta^1\text{:}\eta^1\text{-}O_2COC_6H_2\text{-}^t\text{Bu-3-2,4,6})_2$ (Scheme 1-9).

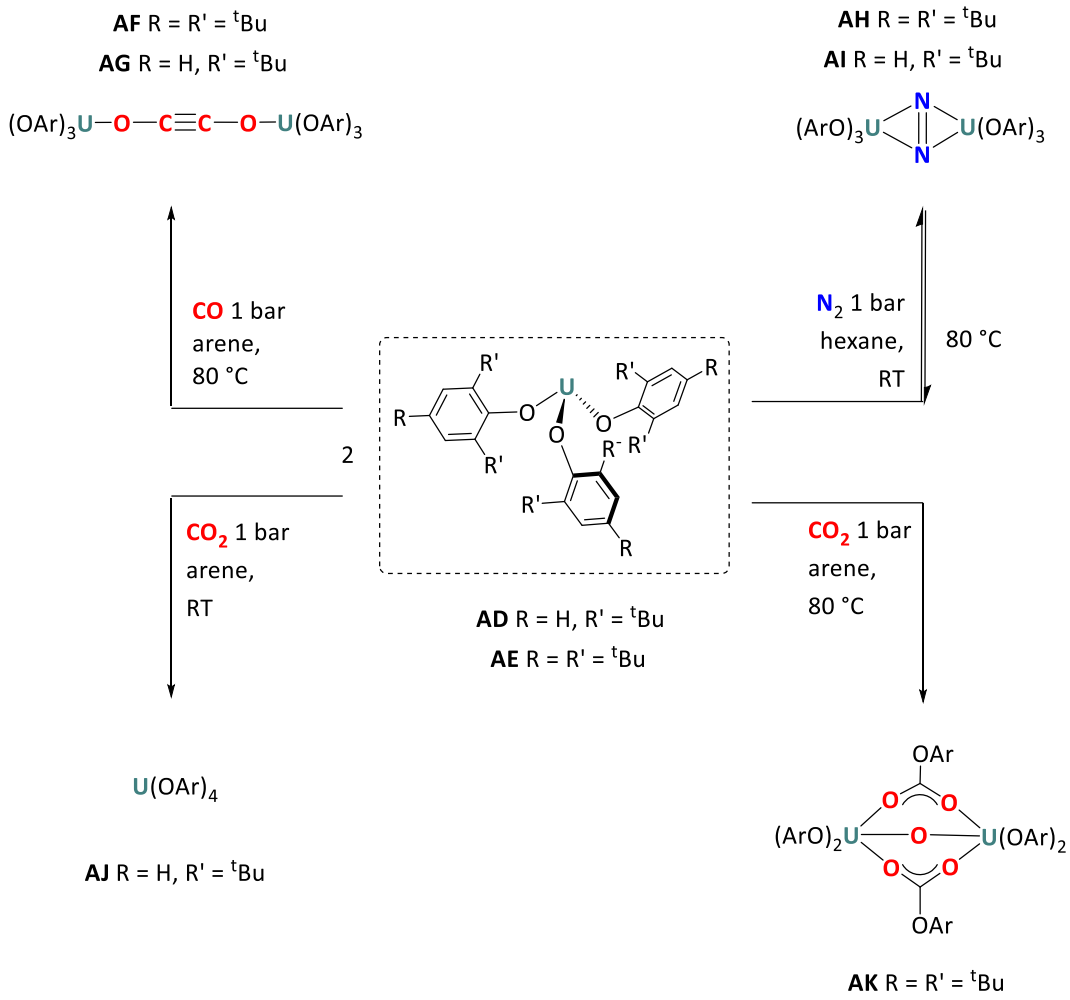

Scheme 1-9 Small molecule activation mediated by $[U(OAr)_3]$.[15]

1.4.1 Poly(aryloxides) as ligands for uranium

In order to prevent ligand dissociation, some authors have exploited the chelate effect to access more robust complexes through the use of poly(aryloxide) ligands. In many cases this has led to well-defined, well-controlled reactivity with small molecule substrates.

Often, multiple bulky aryloxide donors are tethered by an additional aromatic ring that can provide electronic stabilisation through U–arene δ bonding interactions in complex multidentate ligand systems (Scheme 1-10). Meyer *at al.* have pioneered the use of such ligands in the successful synthesis of the first molecular formal U(II) complex, [K(2.2.2-

crypt)]-[((^{Ad,Me}ArO)$_3$mes)U] (mes = mesity), **AN**,[44] and more recently the electrocatalytic generation of dihydrogen from water by the parent, [{(^{Ad,Me}ArO)$_3$mes}U] complex, **AM**.[10,45]

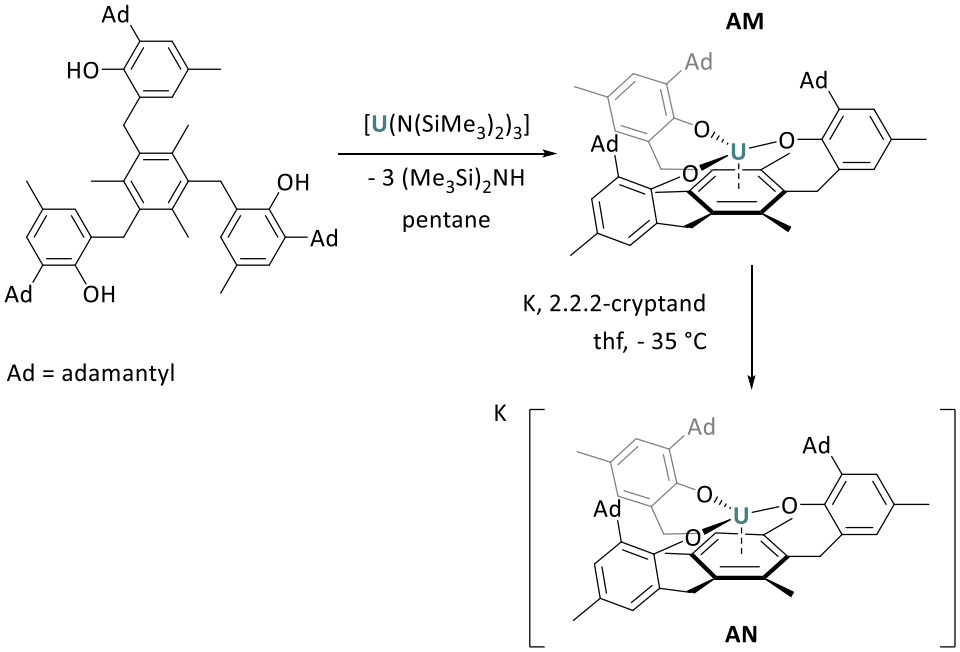

Scheme 1-10 The tripodal aryloxide ligand {(^{Ad,Me}ArO)$_3$mes} used by Meyer and coworkers.[10,44–46]

The dianionic ligand C_6H_4{ *p*-Me_2bp}$_2$ (*p*-Me_2bp = *p*-$C(CH_3)_2C_6H_2Me_2O^-$) is another recent example, featuring two aryloxide donors and a central arene ring. The U(III) compound [U(Cp*)(*p*-Me_2bp)], **AO**, (Cp* = 1,2,3,4,5-pentamethylcyclopentadiene), whose coordination sphere is saturated by a stabilising η^5 interaction with the Cp* ligand, was prepared and exposed to CO_2. Carbonate and oxalate bridged U(IV) complexes [U(Cp*)(*p*-Me_2bp)}$_2$(μ-η^1:η^2-CO_3)], **AQ**, and {U(Cp*)(*p*-Me_2bp)}$_2$(μ-η^2:η^2-C_2O_2)], **AP**, could be formed selectively under kinetic or thermodynamic control respectively (Scheme 1-11).[41]

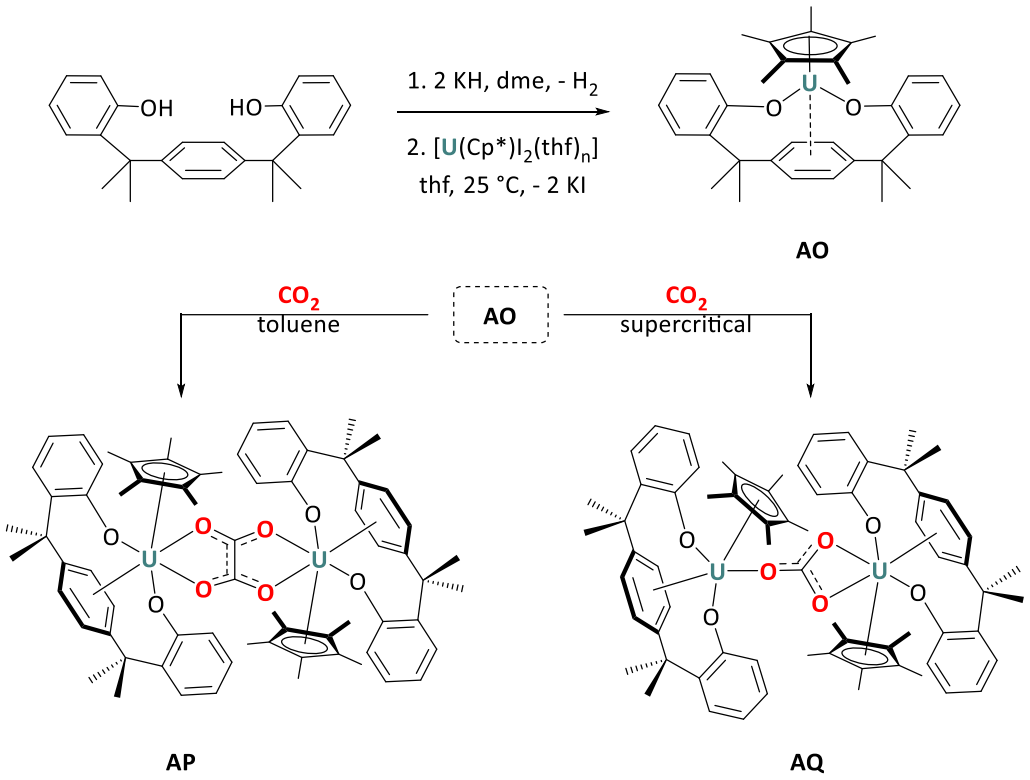

Scheme 1-11 Temperature controlled CO_2 reaction of **AO**.[41]

1.5 Nitrogen activation and functionalisation by transition metal complexes

Despite considerable advances in uranium small molecule activation chemistry over the past 15 years, the field of dinitrogen activation is still dominated by transition metal systems. Molecular dinitrogen is a kinetically inert and thermodynamically stable gas making up 78 % by volume of the earth's atmosphere.[47] Functionalisation of dinitrogen is extremely challenging due to its high bond dissociation energy (946 KJ mol^{-1}),[48] large HOMO-LUMO energy gap, and absence of bond polarity.

In biology, nitrogen fixation is achieved under ambient conditions by nitrogenase enzymes. Although this process is not yet fully understood, the transition metals iron, molybdenum and vanadium are known to play distinct, but essential roles at the enzyme active sites.[49]

For over 100 years the Haber-Bosch process has provided an industrial route for the fixation of nitrogen from the atmosphere, combining N_2 with H_2 at high pressures and temperatures over a heterogeneous iron catalyst bed. The catalyst particles contain a magnetite (Fe_3O_4)

core, encapsulated by an inner wustite (FeO) shell and an outer iron metal shell. K_2O and Al_2O_3 are typically used as promoters.[50]

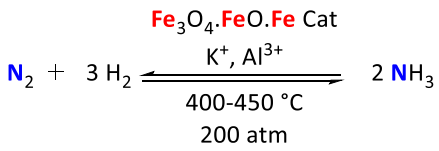

Scheme 1-12 The Haber-Bosch process uses a catalyst bed consisting of particles of Fe_3O_4 coated in FeO, and in turn coated in Fe metal.

The Haber-Bosch process is the only industrial scale process that uses dinitrogen as a feedstock. Despite significant research attention, no commercial process exists to use N_2 as a direct precursor to high value organonitrogen products.[47]

Accordingly, since the discovery of the first transition metal dinitrogen complex, $[Ru(NH_3)_5(N_2)]^{2+}$, in 1965,[51] chemists have been searching for complexes able to afford catalytic dinitrogen reduction and functionalisation under mild conditions, and most work has focused on iron and molybdenum complexes. Over 850 transition metal complexes able to bind N_2 have been identified, and a number are capable of its reduction and functionalisation. Catalytic transformations however remain challenging, and examples are limited to a small fraction of these.

Although these reactions require conditions such as low temperatures and strong reductants and acids that render them industrially non-viable, they provide valuable insights into dinitrogen reactivity, identify new transformations and bring facile organonitrogen synthesis closer to reality.[47,48,52,53]

1.5.1 N–H bond formation by transition metal complexes

The most fundamental target of dinitrogen functionalisation chemistry is the formation of N–H bonds to give N_xH_y products, most commonly ammonia. It is well known that 2 % of global energy supply is consumed in the steam reforming of methane to generate high purity H_2, and achieving the high temperatures and pressures required by the Haber-Bosch process. NH_3 is essential to satisfy global demand for fertilizers, commercial cleaning products and as a reagent in many chemical and pharmaceutical processes.[54] In 2014, 176 million tonnes of ammonia were produced.[55] It is therefore not surprising that chemists seek a more energy and cost-effective route to NH_3 synthesis.

Most commonly, ammonia formation from dinitrogen complexes is thought to proceed *via* a series of proton and electron transfer steps. Recent studies by Peters[56] and Mock[57] have suggested N−H bond forming reactions that proceed *via* the alternative mechanism of proton coupled electron transfer (PCET), invoking NH_3 formation from a metal dinitrogen complex by the concerted delivery of an electron and a proton as a hydrogen atom (hydrogen atom transfer or HAT).

Herein, turnover numbers (TON) of catalysts will be reported as the molar equivalents of nitrogen products relative to moles of metal, such that for bimetallic catalysts, TONs will be based on half an equivalent of catalyst.

A small number of homogeneous systems have accomplished catalytic conversion of dinitrogen to NH_3, with three exploiting molybdenum as the metal centre. The first, in 2003, $[Mo(HIPTN_3N)(N_2)]$ ($HIPTN_3N$ = $[\{3,5\text{-}(2,4,6\text{-}i\text{-}Pr_3C_6H_2)_2C_6H_3NCH_2CH_2\}_3N]^{3-}$) (**AR**) achieved just 4 turnovers, (Scheme 1-13)[58] but more recently TONs in excess of 100 have been reported using a modified dimolybdenum complex (**AS**).[59]

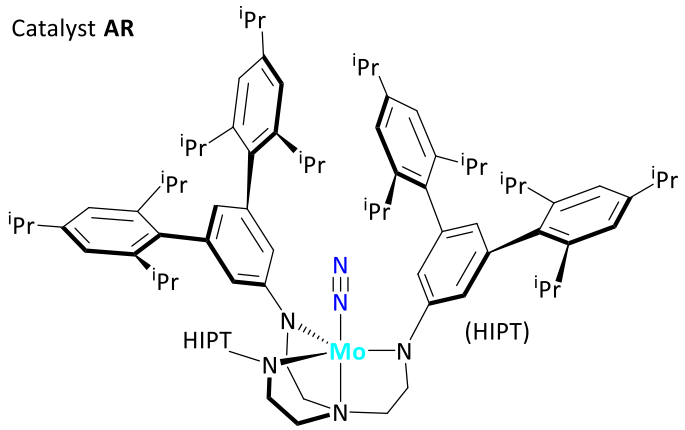

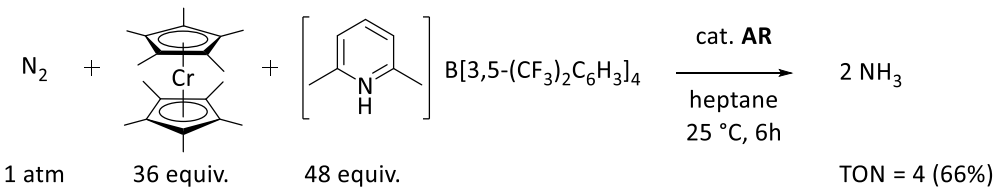

Scheme 1-13 Catalytic N_2 reduction to NH_3 by **AR**.[58]

[{Mo(N_2)$_2$(Me-Bim-PCP)}$_2$(μ-N_2)] (**AS**) where Me-Bim-PCP is the phosphine-NHC-phosphine pincer ligand, (5,6-dimethyl-1,3-bis((di-tert-butylphosphino)methyl)benzimidazol-2-ylidene) is shown in Scheme 1-14.[59] PCP ligands are more electron donating than the more common PNP-type pincer ligands (in which a pyridine moiety forms the central ligand unit), resulting in stronger binding to the metal centre.[60,61] In the presence of decamethylchromocene ([CrCp*$_2$]) (1440 equivalents) which acts as a single electron reductant, reducing the axially bound N≡N ligands, and 2,6-lutidinium triflate ([LutH]OTf) (1920 equivalents) which acts as a proton source providing the requisite H^+ to generate NH_3, **AS** is the most effective catalyst known under ambient conditions, yielding 115 equivalents of ammonia, with high turnover frequency (TOF) (53 h^{-1}) and catalyst stability. The remarkable catalytic activity is attributed to the unique electronic properties of the Me-Bim-PCP ligand. Density functional theory (DFT) calculations reveal that Me-Bim-PCP acts not only a strong σ-donor but also a π-acceptor, which is responsible for: (1) increasing the π-backdonating ability of molybdenum to the bridging dinitrogen ligand, (2) inhibiting dissociation of the ligand during the catalytic cycle, and (3) helping to preserve the Mo–N≡N–Mo core. Together these effects render **AS** more catalytically active in ammonia formation than closely related complexes tested in the study, namely those with ethylene bridged phosphine arms instead of methylene, or those with an imidazole instead of a benzimidazole central NHC.

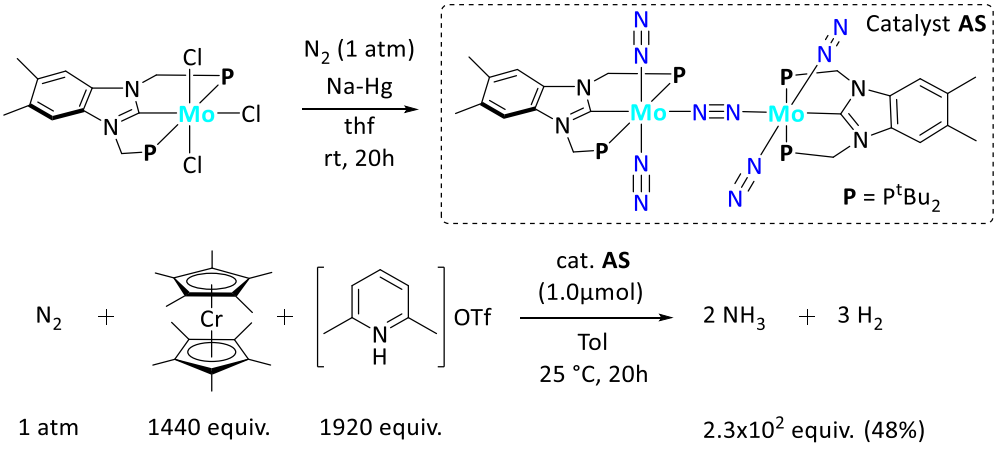

Scheme 1-14 Catalytic N_2 reduction to NH_3 by **AS**.[59]

Interestingly, DFT calculations show that one molybdenum moiety of the dinuclear molybdenum–dinitrogen complex **AS** works as a stabilising metallo-ligand to the other

molybdenum moiety which is the active site, in an equivalent manner to the multimetallic systems for nitrogen functionalisation in nearly all of the examples discussed below (*vide infra*).

Catalyst **AR** exhibits end-on terminal N_2 binding, which is the most commonly observed binding mode, closely followed by end-on bridging N_2.[62] Catalyst **AS** shows both modes of N_2 binding, but it is the terminally bound dinitrogen that reacts to provide NH_3. Terminal end-on binding of dinitrogen polarises the N–N bond such that the distal nitrogen (the non-coordinated atom) becomes nucleophilic. It is this polarisation that allows reactivity between electrophiles, such as H^+, and the non-bonding lone pair of electrons in an *sp*-hybridised orbital on the distal nitrogen atom.[63,64] Following this initial electrophilic addition, further additions may occur at either the distal or metal-coordinated nitrogen *via* 'alternating', 'distal', or 'hybrid' pathways.[65]

Catalysts **AR** and **AS** both demonstrate the use of sterically bulky, electron-donating ligands and a coordinatively saturated molybdenum centre. The steric bulk of the ligands is vital in shielding the metal ion and directing electrophiles instead to the dinitrogen ligand. Electron donation from the ligand is important in enhancing π-backdonation from the metal into the π* N_2 orbitals, reducing the tendency for premature N_2 dissociation by strengthening M–N bond.[66–68] The orbital interactions in end-on bound dinitrogen complexes (terminal and bridging) are summarised in Figure 1.3.

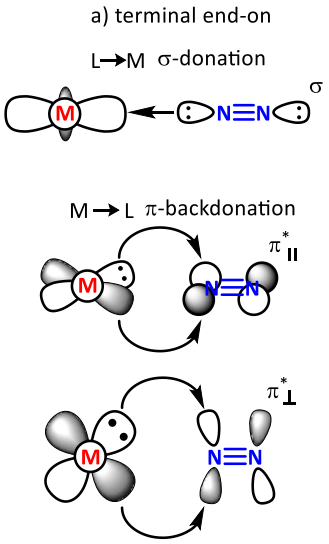

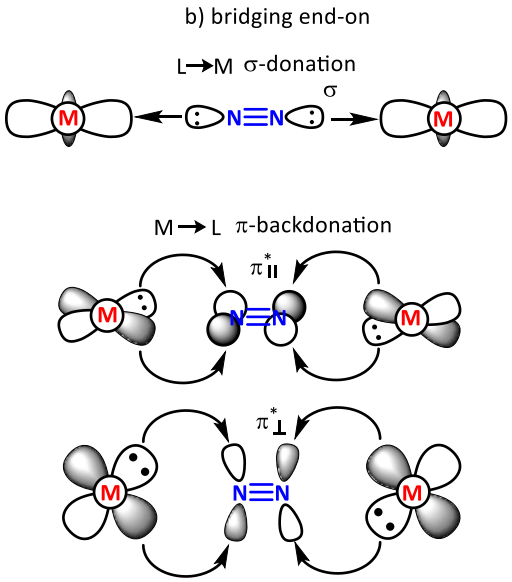

Figure 1-3 Orbital interactions in end-on bound dinitrogen metal complexes, a) terminal and b) bridging.

This bonding description can be extended to explain why, in catalyst **AS**, no functionalisation of the central end-on bridging dinitrogen ligand is observed. In this bridging mode, bonding to the two metal centres involves both of the N-centred σ orbitals, depleting the nitrogen atoms of electron density. The electron density is instead delocalised throughout the M–N–N–M motif, and as a result, neither nitrogen atom is appreciably nucleophilic.[69] For this reason, no examples of end-on bridging N_2 ligands reacting with external electrophiles are known, with electrophilic addition occurring instead at the metal with concomitant N_2 dissociation.[66–68]

The special case in which end-on bridging dinitrogen is reductively cleaved to give terminal nitride ligands which in contrast, are nucleophilic, will be discussed with reference to N–C bond forming transformations in Section 1.2.3.

1.5.2 N–Si bond formation by transition metal complexes

Silylamines are finding increasing use as important industrial chemicals, from silicon-nitride semiconductors[70] to thermally resistant polymers,[71] as well as being recognised as important tools in organic synthesis for masking primary and secondary amines. Their formation from direct functionalisation of dinitrogen therefore represents an important synthetic target. The

earliest catalytic silylation predates even the first homogeneous system for ammonia synthesis.[72] A study by Yoshizawa,[73] which exploited ferrocenyldiphosphine (depf) ligands for molybdenum (catalyst **AT**), (Scheme 1-15) has become somewhat of a benchmark in catalytic dinitrogen silylation. A TON of 226 was achieved for the production of $N(SiMe_3)_3$ (200 hours, 25 °C) from Me_3SiCl and sodium metal with 0.025 % catalyst loading of **AT**. DFT calculations were used to propose a mechanism for the catalytic cycle, which indicates that the Fe metalloligands play a crucial role in mediating the impressive activity. This TON was approximately an order of magnitude higher than previous transition metal catalysts[53,63] and set a challenging precedent for future systems.

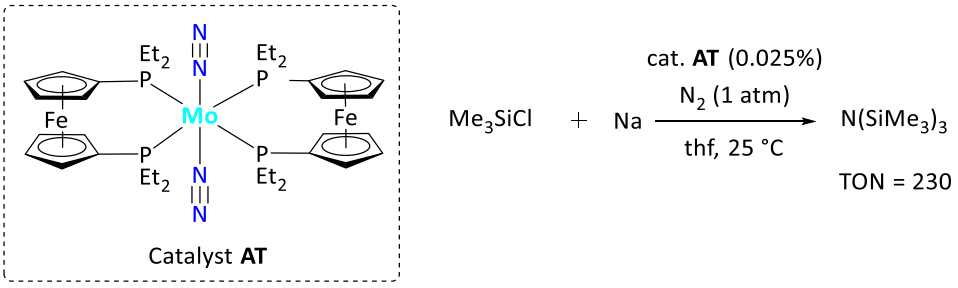

Scheme 1-15 Catalytic conversion of N_2 to $N(SiMe_3)_3$ by **AT**.[73]

Recently a dicobalt complex, Co_2L (L = $N(PhNCH_2P^iPr_2)_3$), **AU**, was investigated for catalytic silylation and found to be highly competitive with **AT**.[74] This time, using KC_8 as the reductant, Me_3SiCl was converted into $N(SiMe_3)_3$ with TON of 195 (12 hours, 299 K) with 0.05 % catalyst loading of **AU** (Scheme 1-16). Detailed mechanistic studies confirmed that although only one Co was involved in directly binding and reducing N_2, the second was critical in electronically stabilising redox events at the active centre. Substitution of the second cobalt for aluminium, **AV**, for example, reduced the TON to 30. In the parent Co_2L **AU**, the Co–Co bond length is consistent with that of a single bond. Following the binding and reduction of nitrogen, the Co–Co distance is significantly increased, suggesting only a weak metal-metal interaction. Finally, when $[N_2(SiMe_3)_3]^-$ (which combines with one equivalent of $ClSiMe_3$ and two $\cdot SiMe_3$ radicals to spontaneously form two equivalents of $N(SiMe_3)_3$) is released from the catalyst, the Co–Co single bond is reinstated.

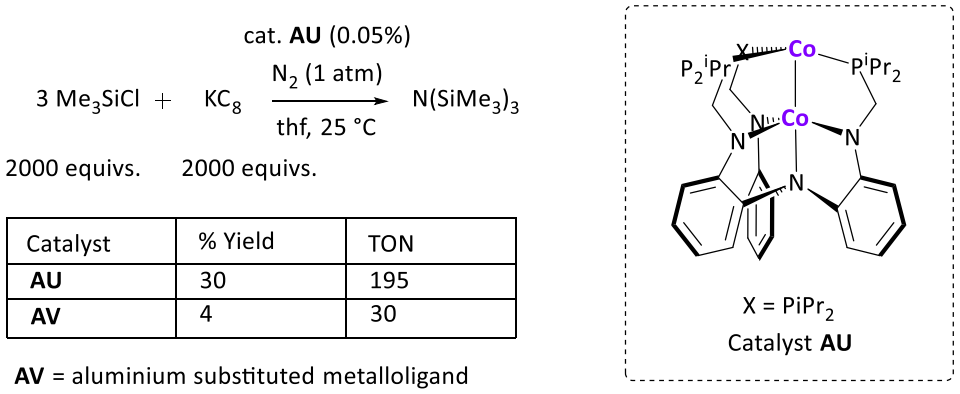

Scheme 1-16 Catalytic conversion of N_2 to $N(SiMe_3)_3$ by **AU**.[74]

It is evident that in both of the above examples, the involvement of more than one metal is paramount to achieving catalytic silylation. In contrast, work by Jonas Peters and coworkers found that direct silylation of a mononuclear iron dinitrogen complex gave *highly stable*, LFe–N_2SiR_3, **AX**, (L = $Si(PhP^iPr_2)_3$) diazenido products.[75] Whilst protonation of the parent $LFeN_2$, **AW**, leads to liberation of N_2H_4, no cleavage of the Fe–N_2SiR_3 bond (in **AX**) to liberate the silylated ligand could be achieved preventing turnover (Scheme 1-17).

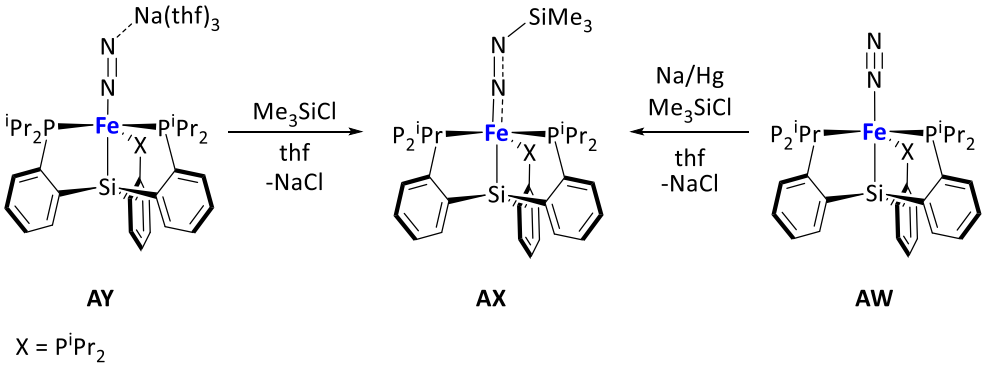

Scheme 1-17 Synthesis of LFe–N_2SiR_3.[75]

The silylation systems described above all proceed *via* electrophilic addition to terminal end-on bound dinitrogen, in an analogous manner to the N–H bond forming catalysts discussed in Section 1.2.1. In all cases, the first electrophilic addition occurs at the nucleophilic distal nitrogen. For both catalytic cases (**AT** and **AU**) the further silylation relies on continuous generation of $Me_3Si\cdot$ radicals as shown in Scheme 1-18.[76]

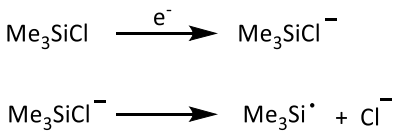

Scheme 1-18 Generation of ·$SiMe_3$ radicals *via* reduction of Me_3SiCl.

1.5.3 N–C bond formation by transition metal complexes

The preparation of alkylated organonitrogen products from molecular dinitrogen requires functionalisation of coordinated N_2 to from new N–C bonds, yielding value-added primary, secondary and tertiary amines. In a study by Holland and coworkers, a bis(nitrido)tetrairon complex, **AZ** (R = R' = R' = Me, Scheme 1-19), derived from reduction of a bimetallic iron β-diketiminate complex, $\mathbf{BA^{MeMe}}$, in the presence of dinitrogen, was reacted with MeOTs, (OTs = $CH_3C_6H_4SO_3$), forming a new N–CH_3 bond (**BB**).[77] A thf solution of the parent $Fe_2L_2Cl_2$ **BA**, (L = 2,4-bis(2,6-dimethylphenylimido)-3-methylpentyl) was treated with two equivalents of KC_8 to yield **AZ**. It was found that in the presence of 18-crown-6, no **AZ** formation was observed. This finding was consistent with computational results that suggest the importance of K^+ ions in the reductive cleavage of nitrogen, with their positive charge critical to the stabilisation of the nitride complex to which they remain coordinated. The *N*-alkylation step requires abstraction of these stabilising K^+ ions and proceeds in the presence of 2 equivalents of 18-crown-6 and 1 equivalent of MeOTs. The reaction with electrophilic CH_3^+ yielded a new methylimido complex, **BB**, which contains one bridging nitrido ligand and a mixed oxidation state triiron core, $[(LFe^{III})_2(LFe^{II})(\mu\text{-}N)(NCH_3)]$. This strategy of using alkali metal ions to reduce and cleave dinitrogen and subsequently removing them to 'turn-on' further reactivity was termed 'alkali-control', and has also been exploited by Holland to control intramolecular C–H bond cleavage in other studies.[77]

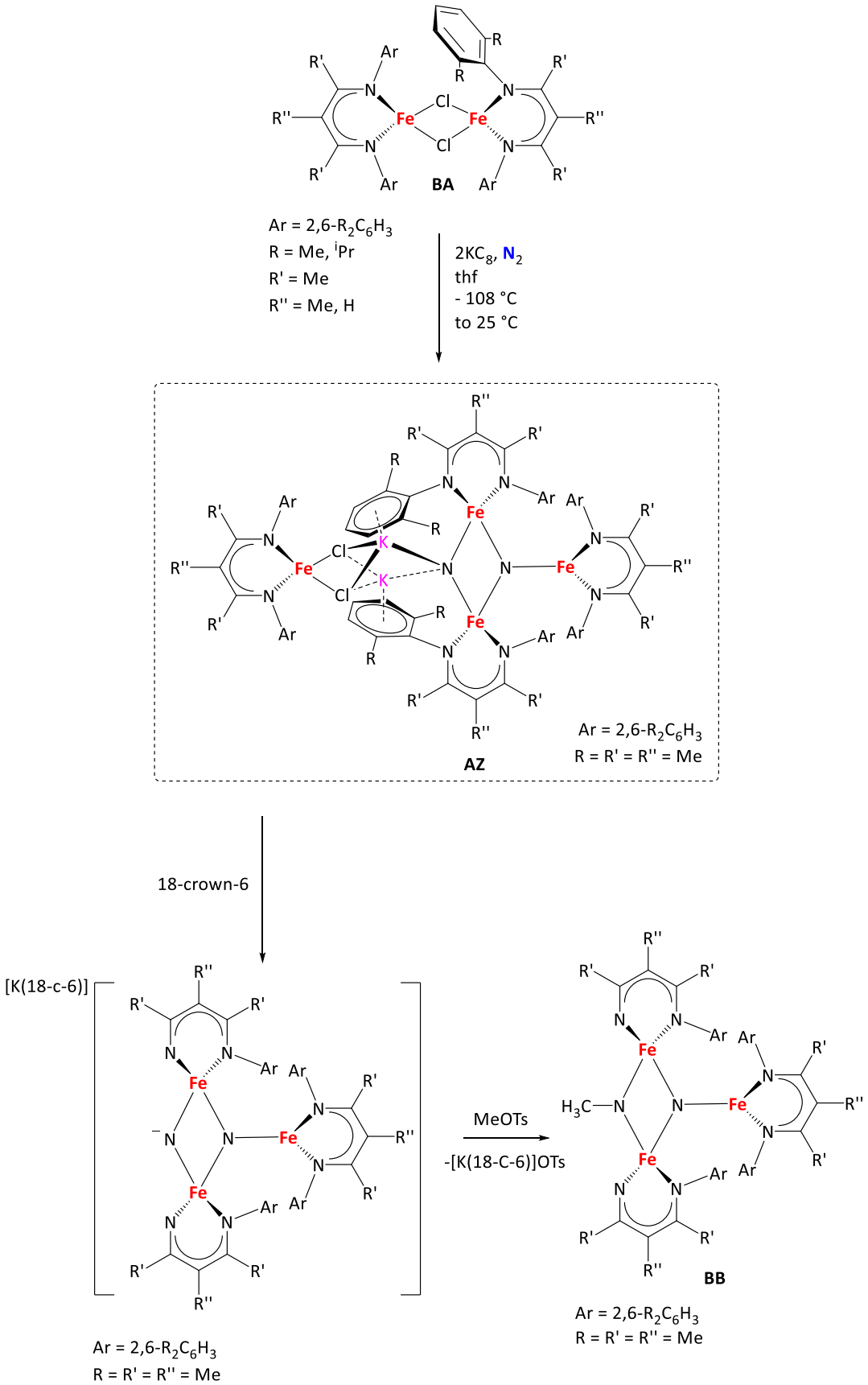

Scheme 1-19 N–C bond formation, yielding the methylmide complex **BB**.[77]

In an earlier study, Holland and coworkers reported the reduction of **BA**^{iPrH} (R = ^{i}Pr, R' = Me, R'' = H) to give the isolable end-on bridging dinitrogen complex, [Fe(L)]$_2$(μ-N$_2$).[78] Further functionalisation of the end-on bridging N$_2$, as discussed in Section 1.2.1, was not possible. By subtly manipulating the ligand, namely by reducing the steric demand of R and increasing that of R'', **AZ** was provided under identical reducing conditions. In **AZ**, the bridging dinitrogen has been reductively cleaved *in-situ* to provide the tetrairon dinitride. The nitride, as discussed above, is able to undergo electrophilic addition to provide **BB**. This cleavage is only possible due to the bonding interactions between the potassium cations and the dinitrogen ligand.

Whilst Holland's alkali control system is very promising, the new N–C fragment remains bonded to the iron complex. Liberation of the newly formed organonitrogen product is frequently the most challenging step in potential catalytic functionalisations. Despite this, catalytic reactions have been achieved by Mori and coworkers in as early as 1994 using a mixture of TiCl$_4$, Li (xs) and TMSCl (xs),[79] but mechanistic details remain unknown. Conversely, in a recent study, Schrock and coworkers presented the synthesis of several proposed intermediates in the *hypothetical* catalytic reduction of dinitrogen to triethylamine using the bulky monometallic molybdenum(III) complex, [(HIPTN$_3$N)Mo], **AR**, but attempts to actually provide NEt$_3$ catalytically were not successful (Scheme 1-20, see also Scheme 1-13).[80]

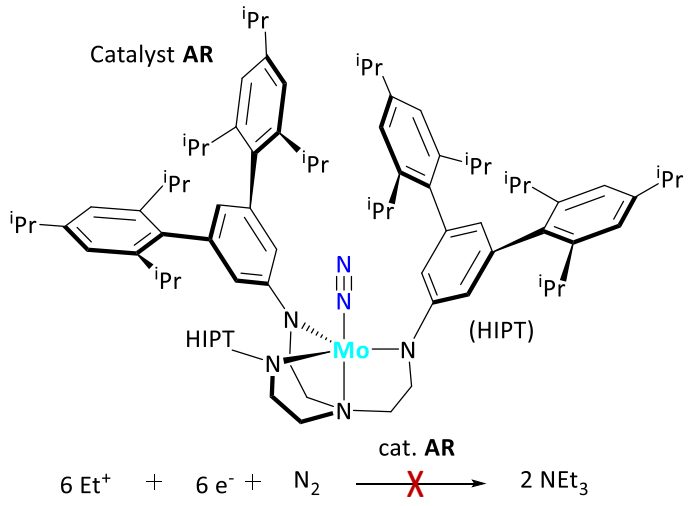

Scheme 1-20 Study of monometallic molybdenum(III) complex, **AR**, for dinitrogen alkylation by Schrock and coworkers.[80]

1.6 Uranium mediated dinitrogen activation

It is unsurprising, given the predominance of bi-, or multimetallic systems in the above examples, that cooperativity between multiple metal centres is thought to be crucial in the N_2 reduction step of both of our model systems: the Haber-Bosch process and the biological fixation of N_2 by nitrogenase.[52,81] Catalysts based on iron and molybdenum have aimed to provide a better understanding of the biological nitrogenase enzymes responsible for nitrogen fixation, but it was noted by Haber that uranium and uranium nitrides are also highly active heterogeneous catalysts for ammonia formation.[82] To this day, this result motivates many chemists to investigate the potential of uranium complexes in catalysis.

In total, only nine uranium dinitrogen complexes have been reported. These are summarised in Figure 1-4.

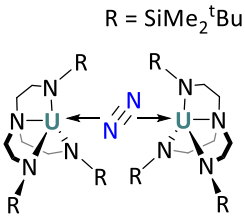

BC
1997, Scott
1.109(7) Å

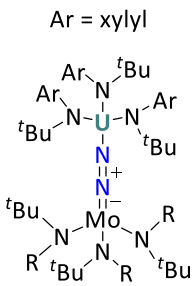

BD^{Ph} R = Ph **BD^{Ad}** R = Ad
1998, Cummins
1.232(11) Å
1568 cm^{-1}

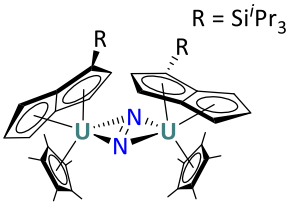

BE
Cloke, 2002
1.232(10) Å

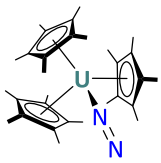

BF
Evans, 2003
1.120(14) Å
2207 cm^{-1}

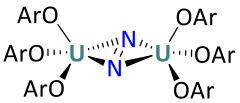

Arnold, 2011
BG^{D}: OAr = ODtbp: 1.189(19) Å
BG^{T}: OAr = OTtb: 1.236(5) Å, 1451 cm^{-1}

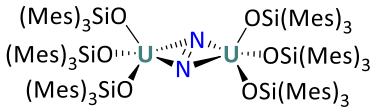

BH
Arnold, 2013
1.124(12) Å
1437 cm^{-1}

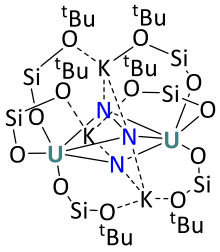

BI
Mazzanti, 2017
1.521(18) Å
817 cm^{-1}

Scheme 1-4 Uranium dinitrogen complexes, where available, N–N bond lengths and stretching frequencies are provided.[15,16,36,83–86]

All except Evans' [Cp*$_3$U(N$_2$)] (**BF**)[86] are bimetallic, and **BD**, **BE**, **BG**, and **BH** are the result of two separate monometallic complexes combining around one N_2 molecule, each donating electrons..[15,83,85,87,4,41,88]

The first uranium nitrogen complex, **BC**, was reported 21 years ago in 1997 by Scott.[83] The synthesis of the U(III) precursors $[UI_3(solv)_4]$ (solv = dme, thf) and $[U\{N(SiMe_3)_2\}_3]$[89] facilitated the advent of U(III) coordination chemistry and subsequently, the first uranium mediated small molecule activation studies.[90] $[U(N_3N)]$ (N_3N = $N\{CH_2CH_2N(SiMe_2{}^tBu)\}_3$) (**BJ**), was found to reversibly bind to dinitrogen when exposed to an N_2 atmosphere at –20 °C to yield $[\{U(N_3N)\}_2(\mu^2{:}\eta^2,\eta^2\text{-}N_2)]$ (**BC**) (Scheme 1-21)[83]. In the solid-state, nitrogen is bound in a side-on fashion, bridging the two uranium centres. The authors reported that rather than affording any formal reduction of the dinitrogen ligand, the electron deficient uranium centres are simply involved in Lewis acidic-type interactions with N_2, which is readily removed under vacuum. However, more recent calculations suggest that there is significant 5f→π*NN back bonding and suggests that N_2 has been partially reduced, despite the measured bond length.[15]

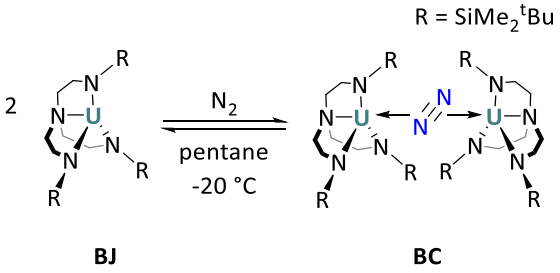

Scheme 1-21 Reversible binding of dinitrogen to $[U(N_3N)]$, **XI**, to yield **XII**.[83]

Side-on binding of N_2 is the third binding mode available to dinitrogen following terminal end-on and bridging end-on. The orbital interactions concerned are summarised in Figure 1-5. This type of binding is considerably less common than the other two, but dominates for uranium systems. The degree of activation, and therefore the reactivity of side-on bound dinitrogen is highly variable and depends wholly on the available electron-density at the metal centres for M–L backdonation. **BC** is a useful example of the limiting case in which the N_2 ligand is not reduced: the bonding orbitals of dinitrogen in this example remain largely unchanged and are not accessible to external electrophiles.

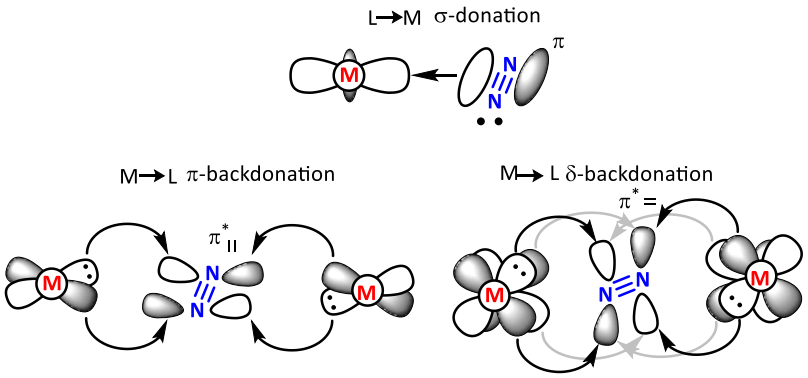

Figure 1-5 Orbital interactions for side-on dinitrogen metal complexes.

Cloke's complex was formed *via* the reaction of two equivalents of monometallic [U(η-Cp*)(η-C_8H_4{Si^{i}Pr$_3$-1,4}$_2$)] with N_2. [U(η-Cp*)(η-C_8H_4{Si^{i}Pr$_3$-1,4}$_2$)]$_2$(μ-N_2), **BE**, contains two formally U(IV) centres and an $[N_2]^{2-}$ reduced dinitrogen ligand. The extent of reduction was here characterised only by the N−N bond length in the solid-state structure (1.232(10) Å), and not by measuring the N−N stretching frequency, which is now regarded as a more reliable measure of reduction. The N_2 binding is reversed under vacuum.[91]

The two complexes reported by Arnold with aryloxide, **BG** (briefly described in Section 1.4), and siloxide, **BH**, supporting ligands are very similar to **BE.** Isolated by the exposure of two equivalents of [U(OAr)$_3$] or [U{N(SiMe$_3$)$_2$}$_3$] (in the presence of three equivalents of HOSi(Mes)$_3$) to dinitrogen respectively.[15,16] Raman spectroscopy was used to confirm the formal description of the electronic structure as $(U^{IV})_2(N_2)^{2-}$ in both cases.

In contrast to **BC**, **BE**, **BG** and **BH**, the heterobimetallic complexes reported by Cummins contain end-on bridging N_2, as was seen in the homobimetallic molybdenum catalyst **AS**.[59] The complexes were obtained by the reaction of [U(N(^{t}Bu)Ar)$_3$] with [Mo(N[^{t}Bu]Ph)$_3$] or [Mo(N[Ad]Ar)$_3$] and N_2 in toluene at room temperature. Cummins reports an N−N stretching frequency of 1568 cm^{-1} for **BD^{Ad}**, and an 1.232(11) Å N−N bond length for the solid-state structure of **BD^{Ph}**, which is also indicative of the formal electronic structure $(M^{IV})_2(N_2)^{2-}$.[87]

These studies demonstrate the ability of two separate monometallic complexes to cooperatively reduce dinitrogen. Further to the discussion in Section 1.2, it follows that molecules in which two reducing U centres are pre-arranged in a single molecule should be even more powerful tools for N_2 activation. The recent reduction of N_2 to NH_3 by Mazzanti and coworkers is powerful evidence of this.

No examples of molecular uranium complexes able to convert N_2 into ammonia or organonitrogen compounds had been reported until 2017. Mazzanti and coworkers reported the synthesis of $[K_3\{[U(OR)_3]_2(\mu\text{-}N)(\mu\text{-}\eta^2\text{:}\eta^2\text{-}N_2)\}]$ (R = $Si(OtBu)_3$), **BI**, formed by exposing the diuranium(III) nitride precursor, $[K_3\{[U(OR)_3]_2(\mu\text{-}N)\}]$, **BK**, to dinitrogen. In contrast to the above examples, dinitrogen has been reduced by a total of four electrons and **BI** is formally assigned as $(U^V)_2(N_2)^{4-}$ by virtue of the N–N bond length (1.521(18) Å), stretching frequency (817 cm^{-1}) and superconducting quantum interference device (SQUID) and electron paramagnetic resonance (EPR) measurements to confirm the metal oxidation state.

BI reacts with one equivalent of 2,4,6-tri-tert-butylphenol to give the singly-protonated compound, $[K_2\{[U(OR)_3]_2(\mu\text{-}NH)(\mu\text{-}\eta^2\text{:}\eta^2\text{-}N_2)\}]$, **BL**, or with stronger proton sources, namely two equivalents of [PyH]Cl to yield the doubly protonated species $[K_2\{[U(OR)_3]_2(\mu\text{-}NH)_2(\mu\text{-}Cl)\}]$, **BM** (isolated as a minor product as single crystals). An excess (20 equivalents) of [PyH]Cl, led to the complete cleavage of dinitrogen and the formation of NH_4Cl in modest (25%–42%) yield. It was found that the yield of ammonia could be increased to an impressive 77% when H_2 was added to **BI** followed by a proton source (HCl). Whilst all of the reactions of **BI** are stoichiometric in nature, they are the first to mediate further N_2 functionalisation and demonstrate that uranium should be considered as an alternative candidate in the design of catalytic nitrogen functionalisation systems.

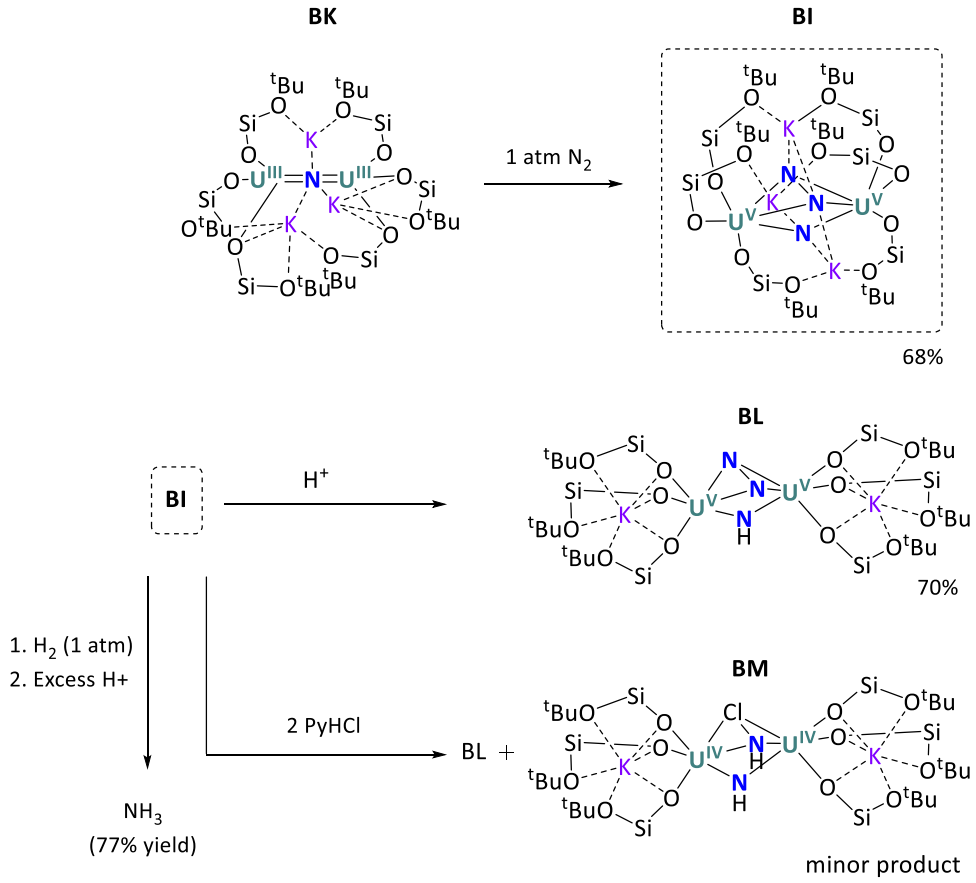

Scheme 1-22 Synthesis of **BI** and stoichiometric protonation reactions.[36]

In the examples discussed in Section 1.5, sterically demanding, electron rich ancillary ligands were frequently found to favour the most notable levels of dinitrogen activation and facilitate further functionalisation, at the same time inhibiting preferential electrophilic addition to the metal and dissociation of bound N_2. The importance of judicious ligand design is again highlighted by contrasting **BI** with **BC**, in which side on bound N_2 was bound by the Lewis acidic metals, but not reduced. **BI** exemplifies the other limiting case of side-on bound dinitrogen. The electron rich uranium centres supported by hard, anionic donor ligands are able to donate considerable electron density into the π* antibonding orbitals of the dinitrogen ligand. The highly nucleophilic nature of the bound $[N_2]^{4-}$ is responsible for the diverse nitrogen functionalisation reactions available to **BI**.[36]

The remaining uranium dinitrogen complex **BF**[86] is unique. To date it is the only monometallic example of uranium mediated nitrogen activation. $[(C_5Me_5)_3U(\eta^1\text{-}N_2)]$, **BF**, is obtained when $[(C_5Me_5)_3U]$ is exposed to overpressures (80 psi) of N_2. The N_2 is released when pressures are

lowered. The IR stretching frequency (2207 cm^{-1}) and bond length (1.120(14) Å) of the N−N bond are almost identical to those in free N_2, and accordingly complex **BF** is formulated as U(III) with a neutral N_2 donor ligand. This unique complex helps to illustrate that the performance of bimetallic systems is superior to that of monometallic complexes with respect to dinitrogen reduction.

1.7 Summary and outlook

The field of dinitrogen activation and functionalisation presents both a fundamental and applied challenge for synthetic chemists and remains an area of intense interest. The most notable breakthroughs have afforded homogenous catalysts for the protonation and silylation of dinitrogen but the challenge remains to discover industrially viable, atom efficient processes.

From the discussion presented in Sections 1.2 - 1.6 it is evident that the cooperative reactivity of multiple metal centres is critical to achieving the highest levels of dinitrogen activation and functionalisation and providing the highest performing catalysts.

Although nitrogen reduction by uranium remains rare, the ability of uranium to perform other small molecule transformations in addition to the dinitrogen activation functionalisation by the seminal report by Mazzanti and coworkers,[36] attest to the suitability of bimetallic uranium complexes, specifically in the U(III)/U(IV) oxidation states, for further studies into dinitrogen activation.

The nucleophilicity of bound dinitrogen, (i.e. the level of reduction) at one or both N atoms, and accordingly its availability for further reactions is determined by the manner in which it is coordinated. Of the common binding modes available to bimetallic systems, namely end-on and side-on bridging, and terminal end-on, only terminal end-on bound N_2 complexes have afforded catalytic transformations thus far. Side-on bound N_2 complexes however have demonstrated the highest level of reduction (to $[N_2]^{4-}$) and allow for the widest array of reactivity pathways. The extent of dinitrogen reduction afforded by side-on binding is variable and highly dependent on ligand design.

Aryloxide ligands appear to be ideal candidates to provide highly reduced, side-on bridging dinitrogen complexes. They are well suited to binding uranium in the oxophilic (III) and (IV) oxidation states, they are hard anionic donors and they are amenable to facile steric and

electronic modification to provide electron-rich metals that are at the same time, shielded from electrophilic attack.

1.8 Thesis aims

This thesis aims to build on preliminary work in the Arnold group to design and synthesise a poly(aryloxide) ligand platform able to support two low oxidation state uranium centres in a single molecule.[15,92] The steric and electronic effects of varying substituents around aryloxide ligands on the synthesis and reactivity of bimetallic uranium complexes will be investigated.

With bimetallic uranium poly(aryloxide) complexes in hand, small molecule activation and functionalisation, including dinitrogen reduction, using the cooperative reactivity of two low oxidation state uranium centres will be targeted.

Finally, the poly(aryloxide) ligand framework will be used to target bimetallic complexes of the lanthanide metal cerium. Their structure and reactivity will be contrasted with uranium analogues and the controlled oxidation of Ce(III) complexes to yield Ce(IV) will be targeted.

1.9 References for chapter 1

(1) Greenwood, N. N. (Norman N.; Earnshaw, A. (Alan). *Chemistry of the Elements*; Butterworth-Heinemann, 1997.

(2) OECD Nuclear Energy Agency.; International Atomic Energy Agency. *Management of depleted uranium : a joint report*; Nuclear Energy Agency, Organisation for Economic Co-operation and Development, 2001.

(3) Liddle, S. T. *Angew. Chem. Int. Ed.* **2015**, *54* (30), 8604–8641.

(4) Arnold, P. L. *Chem. Commun.* **2011**, *47* (32), 9005.

(5) Salmon, L.; Thuéry, P.; Rivière, E.; Girerd, J.-J.; Ephritikhine, M. *Chem. Commun.* **2003**, *0* (6), 762–763.

(6) Neidig, M. L.; Clark, D. L.; Martin, R. L. *Coord. Chem. Rev.* **2013**, *257* (2), 394–406.

(7) Arnold, P. L.; Hollis, E.; White, F. J.; Magnani, N.; Caciuffo, R.; Love, J. B. *Angew. Chem. Int. Ed.* **2011**, *123* (4), 917–920.

(8) MacDonald, M. R.; Fieser, M. E.; Bates, J. E.; Ziller, J. W.; Furche, F.; Evans, W. J. *J. Am. Chem. Soc.* **2013**, *135* (36), 13310–13313.

(9) La Pierre, H. S.; Scheurer, A.; Heinemann, F. W.; Hieringer, W.; Meyer, K. *Angew. Chem. Int. Ed.* **2014**, *53* (28), 7158–7162.

(10) Halter, D. P.; Heinemann, F. W.; Bachmann, J.; Meyer, K. *Nature* **2016**, *530* (7590), 317–321.

(11) Summerscales, O. T.; Cloke, F. G. N.; Hitchcock, P. B.; Green, J. C.; Hazari, N. *Science* **2006**, *311* (5762), 829–831.

(12) Arnold, P. L.; Turner, Z. R.; Bellabarba, R. M.; Tooze, R. P. *Chem. Sci.* **2011**, *2* (1), 77–79.

(13) Lam, O. P.; Meyer, K. *Polyhedron* **2012**, *32* (1), 1–9.

(14) Arnold, P. L.; Mansell, S. M.; Maron, L.; McKay, D. *Nat. Chem.* **2012**, *4* (8), 668–674.

(15) Mansell, S. M.; Kaltsoyannis, N.; Arnold, P. L. *J. Am. Chem. Soc.* **2011**, *133* (23), 9036–9051.

(16) Mansell, S. M.; Farnaby, J. H.; Germeroth, A. I.; Arnold, P. L. *Organometallics* **2013**, *32* (15), 4214–4222.

(17) Summerscales, O. T.; Cloke, F. G. N.; Hitchcock, P. B.; Green, J. C.; Hazari, N. *J. Am. Chem. Soc.*, **2006**, *128* (30), 9602–9603

(18) Tsoureas, N.; Summerscales, O. T.; Cloke, F. G. N.; Roe, S. M. *Organometallics*, **2013**,

32 (5), pp 1353–1362

(19) Braunstein, P.; Matt, D.; Nobel, D. *Chem. Rev.*, **1988**, *88* (5)

(20) Matson, E. M.; Forrest, W. P.; Fanwick, P. E.; Bart, S. C. *J. Am. Chem. Soc.* **2011**, *133*, 4948–4954.

(21) Mougel, V.; Camp, C.; Pécaut, J.; Copéret, C.; Maron, L.; Kefalidis, C. E.; Mazzanti, M. *Angew. Chem. Int. Ed.* **2012**, *124* (49), 12446–12450.

(22) Arnold, P. L.; Mansell, S. M.; Maron, L.; McKay, D. *Nat. Chem.* **2012**, *4* (8), 668–674.

(23) Arnold, P. L.; Mansell, S. M.; Maron, L.; McKay, D. *Nat. Chem.* **2012**, *4* (8), 668–674.

(24) Hückel, E. *Z. Phys. Chem*. **1931**, 70, 204-286

(25) Camp, C.; Pécaut, J.; Mazzanti, M. *J. Am. Chem. Soc.* **2013**, *135* (32), 12101–12111.

(26) Fox, A. R.; Arnold, P. L.; Cummins, C. C. *J. Am. Chem. Soc.* **2010**, *132* (10), 3250–3251.

(27) Hlina, J. A.; Pankhurst, J. R.; Kaltsoyannis, N.; Arnold, P. L. *J. Am. Chem. Soc.* **2016**, *138*, 3.

(28) Barnea, E.; Andrea, T.; Kapon, M.; Berthet, J.-C.; Ephritikhine, M.; Eisen, M. S. *J. Am. Chem. Soc.* **2004**, *126* (35), 10860–10861.

(29) Evans, W. J.; Siladke, N. A.; Ziller, J. W. *Chem. A Eur. J.* **2010**, *16* (3), 796–800.

(30) Manriquez, J. M.; Fagan, P. J.; Marks, T. J.; Day, C. S.; Day, V. W. *J. Am. Chem. Soc.* **1978**, *100* (22), 7112–7114.

(31) Evans, W. J.; Siladke, N. A.; Ziller, J. W. *Comptes Rendus Chim.* **2010**, *13* (6–7), 775–780.

(32) Higgins, J. A.; Cloke, F. G. N.; Roe, S. M. *Organometallics* **2013**, *32* (19), 5244–5252.

(33) Jones, R. G.; Karmas, G.; Martin, G. A.; Gilman, H. *J. Am. Chem. Soc.* **1956**, *78* (17), 4285–4286

(34) Reynolds, J. G.; Zalkin, A.; Templeton, D. H.; Edelstein, N. M.; Templeton, L. K. *Inorg. Chem.* **1976**, *15* (10), 2498–2502.

(35) Mansell, S. M.; Farnaby, J. H.; Germeroth, A. I.; Arnold, P. L. *Organometallics* **2013**, *32* (15), 4214–4222.

(36) Falcone, M.; Chatelain, L.; Scopelliti, R.; Živković, I.; Mazzanti, M. *Nature* **2017**, *547* (7663), 332–335.

(37) Bradley, D. C.; Chatterjee, A. K.; Chatterjee, A. K. *J. Inorg. Nucl. Chem.* **1959**, *12* (1–2), 71–78.

(38) Cotton, F. A.; Marler, D. O.; Schwotzer, W. *Inorg. Chem.* **1984**, *23* (25), 4211–4215.

(39) Van der Sluys, W. G.; Sattelberger, A. P. *Inorg. Chem.* **1989**, *28* (12), 2496–2498.

(40) Wilkerson, M. P.; Burns, C. J.; Morris, D. E.; Paine, R. T.; Scott, B. L. *Inorg. Chem.* **2002**, *41* (12), 3110–3120.

(41) Inman, C. J.; Frey, A. S. P.; Kilpatrick, A. F. R.; Cloke, F. G. N.; Roe, S. M. *Organometallics* **2017**, *36* (23), 4539–4545.

(42) Van der Sluys, W. G., Burns, C. J., Huffman, J. C., Sattelberger, A. P. *J. Am. Chem. Soc.*, **1988**, *110* (17), 5924–5925

(43) Avens, L. R.; Barnhart, D. M.; Burns, C. J.; McKee, S. D.; Smith, W. H. *Inorg. Chem.* **1994**, *33* (19), 4245–4254.

(44) La Pierre, H. S.; Scheurer, A.; Heinemann, F. W.; Hieringer, W.; Meyer, K. *Angew. Chem. Int. Ed.* **2014**, *126* (28), 7286–7290.

(45) La Pierre, H. S.; Kameo, H.; Halter, D. P.; Heinemann, F. W.; Meyer, K. *Angew. Chem. Int. Ed.* **2014**, *53* (28), 7154–7157.

(46) Bart, S. C.; Heinemann, F. W.; Anthon, C.; Hauser, C.; Meyer, K. *Inorg. Chem.* **2009**, *48* (19), 9419–9426.

(47) Burford, R. J.; Fryzuk, M. D. *Nat. Rev. Chem.* **2017**, *1* (4), 0026.

(48) Fryzuk, M. D.; Johnson, S. A. *Coord. Chem. Rev.* **2000,** *200*, 379–409

(49) Eady, R., R. *Coordination Chem. Rev.* **2003**, 237 (1) 23-30

(50) Scepaniak, J. J.; Vogel, C. S.; Khusniyarov, M. M.; Heinemann, F. W.; Meyer, K.; Smith, J. M. *Science* **2011**, *331* (6020), 1049–1052.

(51) Allen, A. D.; Senoff, C. V. *Chem. Commun.* **1965**, No. 24, 621.

(52) MacKay, B. A.; Fryzuk, M. D. *Chem. Rev.* **2004**, *104* (2), 385–402.

(53) Mori, M. *J. Organomet. Chem.* **2004**, *689* (24), 4210–4227.

(54) Smil, V. *Enriching the earth : Fritz Haber, Carl Bosch, and the transformation of world food production*; MIT Press, 2001.

(55) *Mineral Commodity Summaries*; 2017. DOI 10.3133/70180197.

(56) Chalkley, M. J.; Del Castillo, T. J.; Matson, B. D.; Roddy, J. P.; Peters, J. C. *ACS Cent. Sci.* **2017**, *3* (3), 217–223.

(57) Kendall, A. J.; Johnson, S. I.; Bullock, R. M.; Mock, M. T. *J. Am. Chem. Soc.* **2018**, *140* (7), 2528–2536

(58) Yandulov, D. V; Schrock, R. R. *Science.* **2003**, 301 (5629), 76-78

(59) Eizawa, A.; Arashiba, K.; Tanaka, H.; Kuriyama, S.; Matsuo, Y.; Nakajima, K.; Yoshizawa, K.; Nishibayashi, Y. *Nat. Commun.* **2017**, *8*, 14874.

(60) Ohki, Y.; Seino, H. *Dalton Trans.***, 2016**, *45,* 874-880

(61) Trnka, T. M.; Grubbs, R. H. *Acc. Chem. Res.* **2001**, *34* (1), 18–29.

(62) Leigh, G. J. *Acc. Chem. Res.* **1992**, *25* (4), 177–181.

(63) Komori, K.; Oshita, H.; Mizobe, Y.; Hidai, M. *J. Am. Chem. Soc.* **1989**, *111* (5), 1939–1940.

(64) Takahashi, T.; Mizobe, Y.; Sato, M.; Uchida, Y.; Hidai, M. *J. Am. Chem. Soc.* **1980**, *102* (25), 7461–7467.

(65) Rittle, J.; Peters, J. C. *J. Am. Chem. Soc.* **2016**, *138* (12), 4243–4248.

(66) Margulieux, G. W.; Turner, Z. R.; Chirik, P. J. *Angew. Chem. Int. Ed.* **2014**, *53* (51), 14211–14215.

(67) Zhang, Y.; Williard, P. G.; Bernskoetter, W. H. *Organometallics* **2016**, *35* (6), 860–865.

(68) Jiménez-Tenorio, M.; Puerta, M. C.; Valerga, P. *Organometallics* **2016**, *35* (3), 388–399.

(69) Bezdek, M. J.; Guo, S.; Chirik, P. J. *Inorg. Chem.* **2016**, *55* (6), 3117–3127.

(70) Nishi, Y.; Doering, R. *Handbook of semiconductor manufacturing technology*; 2000.

(71) Riley, F. L. *J. Am. Ceram. Soc.* **2004**, *83* (2), 245–265.

(72) Shiina, K. *J. Am. Chem. Soc.* **1972**, *94* (26), 9266–9267.

(73) Tanaka, H.; Sasada, A.; Kouno, T.; Yuki, M.; Miyake, Y.; Nakanishi, H.; Nishibayashi, Y.; Yoshizawa, K. *J. Am. Chem. Soc.* **2011**, *133* (10), 3498–3506.

(74) Siedschlag, R. B.; Bernales, V.; Vogiatzis, K. D.; Planas, N.; Clouston, L. J.; Bill, E.; Gagliardi, L.; Lu, C. C. *J. Am. Chem. Soc.* **2015**, *137* (14), 4638–4641.

(75) Lee, Y.; Mankad, N. P.; Peters, J. C. *Nat. Chem.* **2010**, *2* (7), 558–565.

(76) Liao, Q.; Saffon-Merceron, N.; Mézailles, N. *ACS Catal.* **2015**, *5* (11), 6902–6906.

(77) MacLeod, K. C.; Menges, F. S.; McWilliams, S. F.; Craig, S. M.; Mercado, B. Q.; Johnson, M. A.; Holland, P. L. *J. Am. Chem. Soc.* **2016**, *138* (35), 11185–11191.

(78) Smith, J. M.; Sadique, A. R.; Cundari, T. R.; Rodgers, K. R.; Lukat-Rodgers, G.; Lachicotte, R. J.; Flaschenriem, C. J.; Vela, J.; Holland, P. L. *J. Am. Chem. Soc.* **2006**, *128* (3), 756–769.

(79) Hori, M.; Mori, M. *J. Org. Chem.* **1995**, *60* (6), 1480–1481.

(80) Kupfer, T.; Schrock, R. R. *J. Am. Chem. Soc.* **2009**, *131* (35), 12829–12837.

(81) MacLeod, K. C.; Holland, P. L. *Nat. Chem.* **2013**, *5* (7), 559–565.

(82) Haber, F. Verfahren zur Herstellung von Ammoniak durch katalytische Vereinigung von Stickstoff und Wasserstoff, zweckmäßig unter hohem Druch., 1909.

(83) Roussel, P.; Scott, P. *J. Am. Chem. Soc.*, **1998**, *120* (5), 1070–1071

(84) Odom, A. L.; Arnold, P. L.; Cummins, C. C. *J. Am. Chem. Soc.* **1998**, *120* (23), 5836–5837.

(85) Cloke, F. G. N.; Hitchcock, P. B. *J. Am. Chem. Soc.* **2002**, *124* (32), 9352–9353.

(86) Evans, W. J.; Lee, D. S.; Ziller, J. W. *J. Am. Chem. Soc.*, **2004**, *126* (2), 454–455

(87) Odom, A. L.; Arnold, P. L.; Cummins, C. C. *J. Am. Chem. Soc.* **1998**, *120* (23), 5836–5837.

(88) La Pierre, H. S.; Meyer, K. John Wiley & Sons, Inc., **2014**; 303–416.

(89) Berg, J. M.; Clark, D. L.; Huffman, J. C.; Morris, D. E.; Sattelberger, A. P.; Streib, W. E.; Van der Sluys, W. G.; Watkin, J. G. *J. Am. Chem. Soc.* **1992**, *114* (27), 10811–10821.

(90) Andersen, R. A. *Inorg. Chem.* **1979**, *18* (6), 1507–1509.

(91) Cloke, F. G. N.; Hitchcock, P. B. *J. Am. Chem. Soc.* **2002**, *124* (32), 9352–9353.

(92) Wells, J. A. L. *PhD Thesis*, Bimetallic actinide complexes for small molecule activation, **2018**, University of Edinburgh

Chapter 2: Uranium Letterbox Complexes for Nitrogen Activation and Functionalisation

2.1 Introduction and aims

As discussed in Chapter 1, the highest levels of nitrogen activation require at least two metal centres that can act cooperatively to trap and reduce substrates. Bimetallic uranium complexes in which the metals are prearranged for cooperative reactivity are proposed to be well suited to this purpose. Judicious choice of ligand to optimise electron density at the uranium centre whilst providing steric protection to shield the metal from electrophile attack is important for both the initial nitrogen reduction, and subsequent electrophilic functionalisation of bound N_2.

Meta- and *para*-substituted arene teraphenolate ligands **(*m*TP, *p*TP)** first emerged in a study of bulky alkylaluminium catalysts for the polymerization of ethylene oxide and propylene oxide by Wasserman and coworkers.[1] In a more recent study, Christiansen and coworkers reported a series of organophosphites based on **(*m*TP)** ligands and proposed that they may represent useful catalyst precursors.[2] A short time later, Wu described the syntheses of alkali metal salts of closely related *para*- and *meta*-substituted tetraphenolates, establishing by X-ray diffraction (XRD) that, in the solid state, the **(*m*TP)** complexes demonstrate a ligand flexibility that enables two or more alkali metal cations to occupy positions on the same or opposite sides of the central arene bridge, whereas the *para*-ligands **(*p*TP)** were found to always provide complexes with metals on opposite sides of the central arene.[3] These findings were consistent with those of Redshaw in the synthesis of niobium and tantalum complexes for the ring opening polymerization of ε-caprolactone from the same class of ligand.[4] We therefore propose that the **(*m*TP)** ligand backbone is a good candidate for combining two uranium centres in a single molecule and may favour the binding of the two metals on the same side of the central arene bridge, in a geometry amenable to cooperative substrate reduction by the two metals.

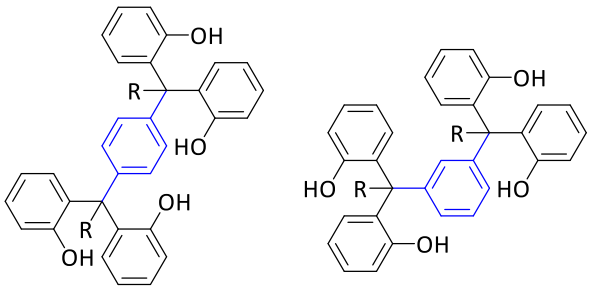

Figure 2-1 Arene-bridged tetraphenol ligand backbone used by Wasserman,[1] Christiansen,[2] Wu[3] and Redshaw.[4] The central arene ring is highlighted in blue. The left-hand figure shows *para* substitution (*p*TP) and the right shows *meta* substitution (*m*TP) around the central arene.

This chapter aims to investigate chelating aryloxide ligands, specifically *meta*-substituted arene-bridged tetraphenolates **(*m*TP)** in the synthesis of bimetallic uranium complexes in the U(III) and U(IV) oxidation states. Thorium analogues of selected uranium complexes described in this chapter have been synthesised by Dr Tatsumi Ochiai in the Arnold group. The reactivity of the uranium complexes towards small molecules will be explored, and the reactivity of the thorium analogues will be briefly referenced.

2.2 Synthesis of arene-bridged tetraphenolate ligand precursor H_4(*m*TP^m)

Around the **(*m*TP)** backbone, highly substituted phenols should provide steric congestion and simultaneously deliver a positive inductive effect, increasing electron density at the metal. Initial ligand synthesis reactions were therefore attempted using 2-*tert*-butyl-4-methylphenol.

Christiansen and coworkers used eight equivalents of phenol in HCl-catalysed condensation reactions to provide arene-bridged tetraphenols, which were then purified by a laborious process of steam distillation to remove the excess phenol.[2] A solvent-free, *p*-TSA (*para*-toluenesulfonic acid) catalysed condensation with an improved atom economy (2.2 equivalents of phenol) was pioneered by Mobinikhaledi in 2013 for the synthesis of a series of arene-tethered bis(phenols) and xanthenes.[5] Meyer's tripodal ligand (Chapter 1, compounds **AM** and **AN**) was synthesised *via* salt metathesis of 2,4,6-tris(halomethyl)-mesitylene (halo = Cl^-, Br^-) with three equivalents of 2,4-di-*tert*-butyl phenol in $CHCl_3$ with

$ZnCl_2$ as a Lewis acid catalyst.[6] A solvent free condensation reaction based on the Mobinikhaledi procedure was employed to yield Cloke's bisphenol ligand (Chapter 1, compounds **AP** and **AQ**):[7] α,α,α′,α′-tetramethyl-1,4-benzenedimethanol and 2,4-dimethylphenol (excess, as solvent) were heated with 3 mol % *para*-toluenesulfonic acid and the product was recrystalised from Et_2O to yield the analytically pure ligand in moderate yield.

Here, the Mobinikhaledi procedure was adapted and carried out using benzene-1,3-dicarboxaldehyde and 4.4 equivalents of 2-*tert*-butyl-4-methylphenol. This procedure afforded the target ligand, **H_4(*m*TP^m)**, in excellent yields (82 %) after 2-3 hours in solvent-free conditions (Scheme 2-1).

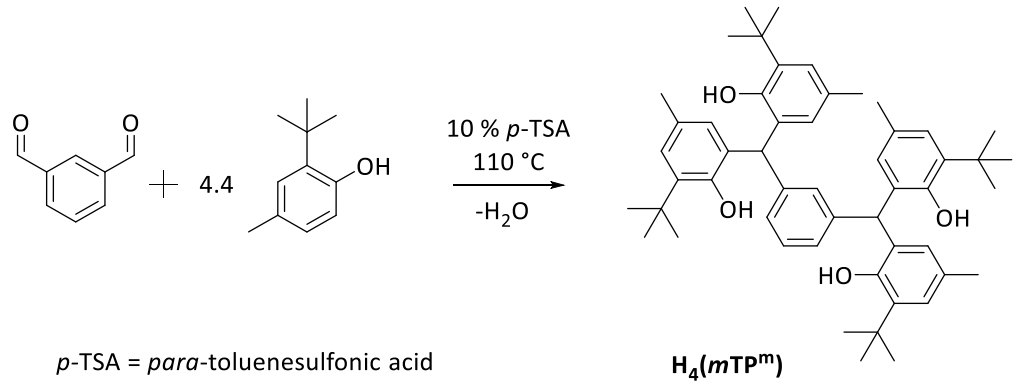

Scheme 2-1 Synthesis of **H_4(*m*TP^m)**.

The melt of benzene-1,3-dicarboxaldehyde and 2-*tert*-butyl-4-methylphenol with 10 mol % *para*-toluenesulfonic acid (*p*-TSA) was heated to 110 °C for two hours to afford a tacky red solid. **H_4(*m*TP^m)** was obtained as an analytically pure colourless solid (86% yield) after the red solid was sonicated in acetonitrile, then washed twice with more accetonitrile to remove unreacted phenol and other impurities. The product was fully characterised by multinuclear NMR spectroscopy, with HSQC and HMBC experiments used to fully assign the $\{^1H\}^{13}C$ NMR spectrum, elemental microanalysis and electrospray mass spectrometry. The ^1H NMR spectrum is shown in Figure 2-2.

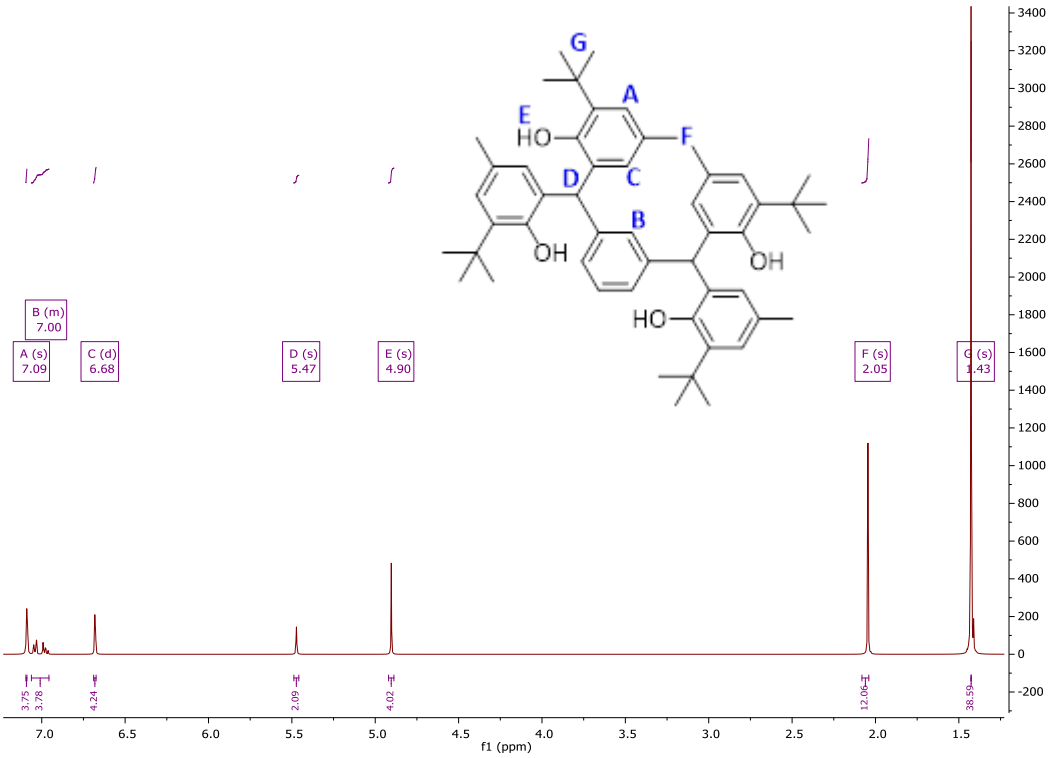

Figure 2-2 ^{1}H NMR spectrum of **H$_4$(*m*TP^m)** in C_6D_6, 500 MHz.

H$_4$(*m*TP^m) has nine distinct hydrogen environments, although the four aromatic protons on the central arene ring overlap, appearing as one multiplet, B (7.06-6.96 ppm). Resonances A (7.09 ppm) and C (6.68 ppm) are assigned as the protons on the aryloxide rings, resonance D (5.47 ppm) is assigned as the benzylic protons, and the signals labelled E (4.90 ppm), F (2.05 ppm) and G (1.43 ppm) are attributed to the phenolic, methyl and *tert*-butyl hydrogens, respectively.

In order to further simplify the preparation of **H$_4$(*m*TP^m)**, the use of a microwave reactor was investigated. Typically, solids were added to a glass microwave vial and heated to 110 °C for 1 hour. At various microwave powers these reactions led to complex product mixtures that proved challenging to separate; therefore, the method was not further investigated.

2.3 Reactions to target H$_4$(*m*TP) derivatives

The pK_a of the tertiary proton in triphenylmethane is 33.[8] The protons in the benzylic positions of **H$_4$(*m*TP^m)** are therefore expected to be relatively acidic. Anticipating that the presence of acidic hydrogen atoms might lead to competing side reactions in the

coordination chemistry of **H_4(*m*TP^m)**, analogues with alkyl- or aryl-substituted benzylic positions were targeted.

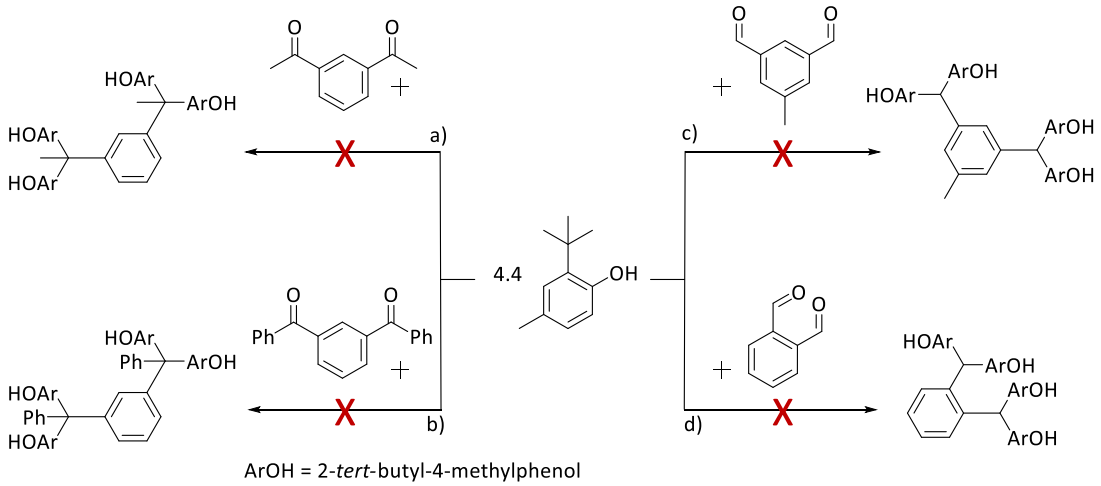

Scheme 2-2 Reactions to target **H_4(*m*TP^m)** derivatives.

Scheme 2-2 shows the reactions of (a) 1,3-diacetyl-benzene, and (b) 1,3-phenyl-benzene, with 2-*tert*-butyl-4-methylphenol. These reactions were carried out using the optimised solvent-free condensation conditions shown in Scheme 2-1, but thin layer chromatography (TLC) and ^{1}H NMR spectroscopy of the resulting reaction mixtures showed only unreacted starting materials and their decomposition products. Systematic variation of reaction time, temperature, and the amount and nature of the acid catalyst used also failed to yield the desired products. In a procedure adapted from the work of Jaikumar, the reagents were dissolved in a 1:2 mixture of acetic acid and concentrated HCl, and then heated to 60 °C.[9] Following basic work-up, unreacted starting materials were again recovered. Direct synthesis of benzylic-substituted ligands was not further investigated at this stage, but the reactivity of the benzylic hydrogens in bimetallic uranium complexes of (*m*TP^m) is discussed in Sections 2.7 and 2.8.

Additionally, reactions to target a tetraphenol with a methylisopthalaldehyde derived central arene (c), and a benzene-1,2-dicarboxaldehyde derived analogue (d), were attempted. It was anticipated that the targeted ligand precursors could favour the binding of two metals very close to each other, providing a geometry more likely to facilitate cooperative substrate reduction by the two bound metals. However, the reactions conditions described above were

unsuccessful in yielding the desired products. Further attempts to use a microwave reactor at varying pressure and temperature to yield the target products only resulted in unreacted starting materials along with product mixtures that could not be successfully separated, as indicated by ^{1}H NMR spectroscopy.

2.4 Synthesis of arene-bridged tetraphenolate ligand precursor H_4(*m*TP^t)

The condensation reaction appeared to be more tolerant towards different phenols than the different aldehydes described above. 2,4-di-*tert*butylphenol was reacted with benzene-1,3-dicarboxaldehyde to yield **H_4(*m*TP^t)** (79% yield) without need for modification of the optimised solvent-free condensation conditions shown in Scheme 2-1. **H_4(*m*TP^t)** is already known in the literature, but previous syntheses have required a 20-fold excess of phenol, and 13 hours of heating using a HCl catalyst.[3,4,10]

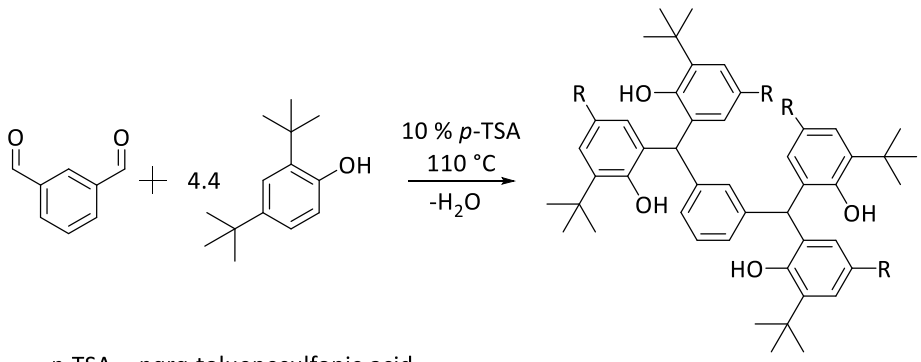

Scheme 2-3 Synthesis of **H_4(*m*TP^t)**.

H_4(*m*TP^t) was fully characterised by NMR spectroscopy, elemental microanalysis and electrospray mass spectrometry. All data are consistent with literature reports.[3,4,10] As discussed in Chapter 1, it was anticipated that the additional steric bulk and more positive inductive effect provided by **H_4(*m*TP^t)** relative to **H_4(*m*TP^m)** could impact not only the coordination chemistry of the ligands, but also the reactivity of the derived uranium complexes with small molecules.

2.5 Synthesis of Group 1 and 2 salts of H_4(*m*TP)

NMR-scale reactions of **H_4(*m*TP)** with two equivalents of either $[CaN(SiMe_3)_2]_2$ or $[MgN(SiMe_3)_2]_2$, or four equivalents of either $[KN(SiMe_3)_2]$ or $[NaN(SiMe_3)_2]$, respectively, were carried out in either C_6D_6 or d_8-thf, as shown in Scheme 2-4. These reactions resulted in the formation of a bright purple, insoluble salt for magnesium, but yielded soluble, colourless products for calcium, sodium and potassium, assigned as **[Ca_2(*m*TP)]**, **[Na_4(*m*TP)]** and **[K_4(*m*TP)]** respectively by ^{1}H NMR spectroscopy. Room and high temperature spectra indicated the loss of phenolic protons and a loss in symmetry of the aromatic and aryloxide hydrogens compared to **H_4(*m*TP)**, consistent with the interaction of bound alkali metal cations with the ligand arenes.

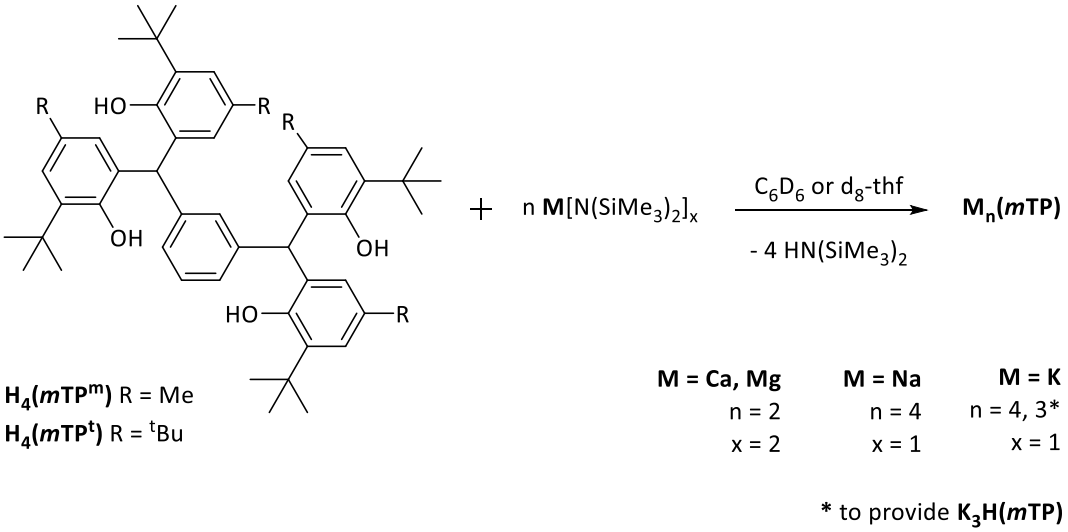

Scheme 2-4 Synthesis of group 1 and 2 salts of **H_4(*m*TP)**, **M_n(*m*TP)**.

$[KN(SiMe_3)_2]$ and $[NaN(SiMe_3)_2]$ are more convenient to prepare than $[CaN(SiMe_3)_2]_2$, which is typically synthesised *via* transmetalation of $[KN(SiMe_3)_2]$.[11,12] Metathesis reactions with **Na_4(*m*TP)** eliminated NaX (X = Cl, I) salts as by-products which are partially soluble in polar organic solvents, making isolation of analytically pure products challenging. On the other hand, metathesis reactions with **K_4(*m*TP)** eliminated KX salts which were more easily removed from the target products due to their less soluble nature. **K_4(*m*TP)** was accordingly identified as the most promising metathesis precursor to uranium complexes of **(*m*TP)**.

Addition of four equivalents of $[KN(SiMe_3)_2]$ to a thf, 1,4-dioxane or pyridine solution of **H_4(*m*TP^m)** or **H_4(*m*TP^t)** at room temperature yielded yellow solutions, which could be treated *in situ* with uranium and cerium iodides or chlorides after 10 – 30 minutes to provide

bimetallic metathesis products in good yields (Section 2.6), with all four aryloxide groups binding to the metals.

In the absence of any metal halide, however, the full deprotonation reaction remains incomplete after 24 hours. Attempts to isolate **K_4(*m*TP)** *via* the addition of hexanes to a reaction mixture of [$KN(SiMe_3)_2$] and **H_4(*m*TP^m)** provide products of incomplete deprotonation, such as **[K_3(*m*TP^m)H$(thf)_6$]**, **1(*m*TP^m)**, which is described below. Wu and coworkers have previously reported the closely related structure of [K_3(*m*TP^t)H$(thf)_6$] from the reaction of three equivalents of [$KN(SiMe_3)_2$] with **H_4(*m*TP^t)**.[3]

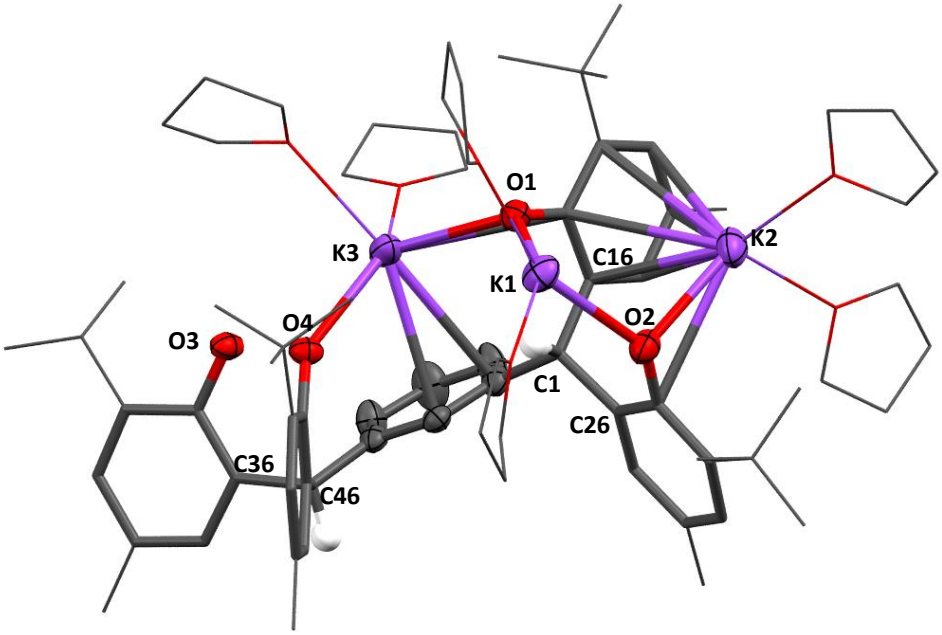

Figure 2-3 Solid-state structure of **[K_3(*m*TP^m)H$(thf)_6$]·hexane**. For clarity, backbone hydrogen atoms and lattice solvent molecules are omitted. Potassium, selected oxygen and carbon atoms and the benzylic hydrogens are shown as displacement ellipsoids at 50% probability. The remaining atoms and bonds are shown as capped stick or wireframe. Selected bond lengths (Å) and angles (°) for **[K_3(*m*TP^m)H$(thf)_6$]** are given in Table 2-1.

Parameter	[K_3(*m*TP^m)H$(thf)_6$]·hexane	[K_3(*m*TP^t)H$(thf)_6$][3]
K(1)–O(1)	2.626(4)	2.629(6)
K(1)–O(2)	2.583(4)	2.567(5)
K(2)–O(2)	2.686(4)	2.681(6)
K(3)–O(1)	2.685(4)	2.685(6)
K(3)–O(3)	3.416(4)	3.175(6)
K(3)–O(4)	2.644(3)	2.633(5)
K(2)–centroid	2.870	2.577
K(1)–O(2)–K(2)	106.9(1)	

O(1)–K(1)–O(2)	85.3(1)
O(4)–K(3)–O(1)	115.0(1)
O(3)–K(3)–O(1)	159.3(1)
O(3)–K(3)–O(4)	45.14(9)

Table 2-1 Selected bond lengths and angles for **1(mTP^{m})·hexane** and **[K$_3$(mTP^{t})H(thf)$_6$]**[3]

The solid-state structure of **[K$_3$(*m*TP^{m})H(thf)$_6$]·hexane, 1(*m*TP^{m})**, is shown in Figure 2-3. The connectivity is identical to that of the structure of [K$_3$(*m*TP^{t})H(thf)$_6$] reported by Wu and coworkers, but some parameters are significantly different, as summarised in Table 2-1.[3] The three K^+ ions are distinct, occupying different positions. K(1) is coordinated by two thf molecules and by O(1) and O(2) of the aryloxide ligand fragments, with bond distances of 2.626(4) Å (K(1)–O(1)) and 2.583(4) Å (K(1)–O(2)). K(2) is coordinated to two thf molecules, the arene ring of the O(1) aryloxide ligand fragment in an η^6 fashion, and the arene ring of the O(2) aryloxide ligand fragment in an η^2 fashion. The distance from K(2) to the centroid of the η^6 coordinated ring is 2.870 Å, and the K(2)–O(2) bond distance is 2.686(4) Å. K(3) is coordinated to two thf molecules, three aryloxide ligand fragments, and to the central arene ring in an η^2 fashion. The K(3)–O(1), K(3)–O(3) and K(3)–O(4) bond lengths are 2.629(6) Å, 3.416(4) Å and 2.644(3) Å respectively. The K(3)–O(3) bond is significantly lengthened relative to the K(3)–O(3) bond in **[K$_3$(*m*TP^{t})H(thf)$_6$]**[3] (3.175(6) Å). The ligand backbone is twisted, with a dihedral angle of 73 ° intersecting the planes C(1),C(16),C(26) and C(8),C(36),C(46).

2.6 Synthesis of [{U(*m*TP)(solv)$_2$}$_2$], 2(*m*TP), *via* salt metathesis reactions

Meyer[13,14] and Cloke[15] have reported several examples of 1:1 reactions of bis- and tris-phenolate ligands with uranium to afford monometallic, chelated [U(L)]-type complexes (compounds **AM**, **AN, AP** and **AQ**; described in Chapter 1). Unpublished work within the Arnold group has also provided monometallic [U(*p*TP)] structures from *para*-substituted arene-bridged tetraphenol ligands derived from **H$_4$(*p*TP)** (see Figure 2-1).

Complexes of the strongly reducing uranium(III) ion are most likely to afford reductive small molecule activation or catalysis, and were therefore the initial target of this work. Direct synthesis of U(III) complexes of **(*m*TP)** from the uranium(III) iodide, [UI$_3$(1,4-dioxane)$_{1.5}$], and the ligand potassium salt, **[K$_4$(*m*TP)]**, however, were not successful, and yielded U(IV)

complexes as the major products. Disproportionation of U(III) to yield U(IV) complexes is common in literature examples, especially in the presence of arenes.[16,17]

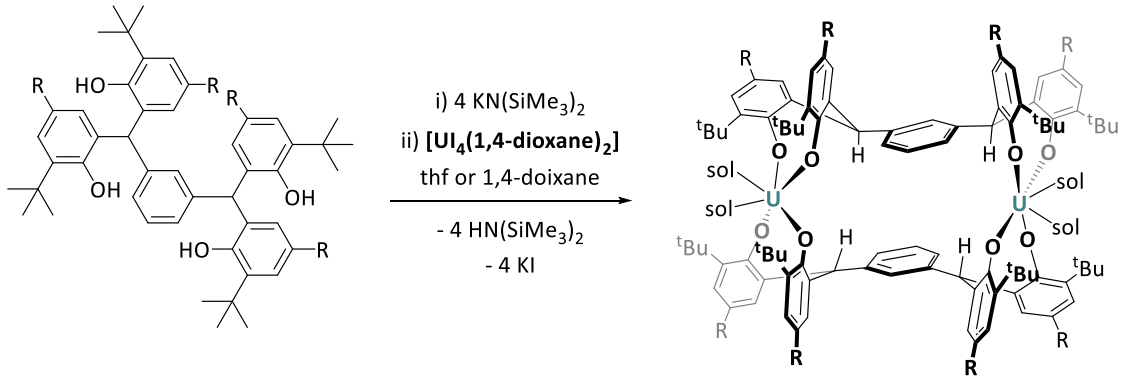

H_4(*m*TP^m) R = Me
H_4(*m*TP^t) R = ^{t}Bu

2(*m*TP^m) R = Me
2(*m*TP^t) R = ^{t}Bu

Scheme 2-5 Synthesis of **2(*m*TP)**.

Complexes of U(IV) are typically more stable and were subsequently targeted. A solution of **K_4(*m*TP)** was synthesised *in situ* by mixing **H_4(*m*TP)** with four equivalents of [$KN(SiMe_3)_2$] in 1,4-dioxane or thf. To this yellow solution, one equivalent of **[UI_4(1,4-dioxane)$_2$]** was added. The resulting dark green solution was stirred at room temperature overnight, yielding a brown suspension from which colourless KI was removed by filtration. From the resulting green solution, the product could be isolated in moderate yield (41 %) as a green powder by removal of solvent under reduced pressure then washing the solid with hexane, or as single crystals by slow diffusion of hexanes into a concentrated thf or 1,4-dioxane solution.

The procedure was repeated using **H_4(*m*TP^t)** to yield **2(*m*TP^t)**. X-ray quality single crystals of **[{U(*m*TP^t)(thf)$_2$}$_2$].toluene**, **2(*m*TP^t),** were obtained by storing a concentrated thf solution of **2(*m*TP^t)** at –30 ° C.

Analysis by single crystal XRD reveals a bimetallic structure of two U(IV) centres bridged by two ligands. The crystal structures of **[{U(*m*TP^m)(1,4-dioxane)$_2$}$_2$]·4(1,4-dioxane)**, **2(*m*TP^m)** and **[{U(*m*TP^t)(thf)$_2$}$_2$]·toluene**, **2(*m*TP^t)**, are shown in Figures 2-4 and 2-5, below.

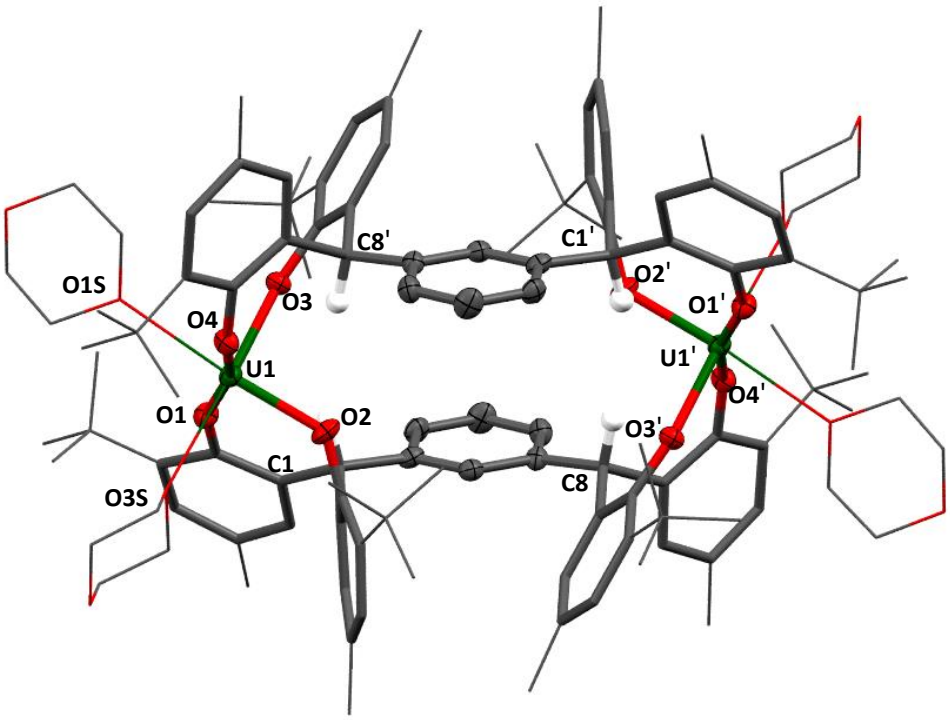

Figure 2-4 Solid-state structure of **[{U(*m*TP^{m})(1,4-dioxane)$_2$}$_2$]·4(1,4-dioxane), 2(*m*TP^{m})**. For clarity, backbone hydrogen atoms and lattice solvent molecules are omitted. Uranium, selected oxygen and carbon, and benzylic hydrogen atoms are shown as displacement ellipsoids drawn at 50 % probability. The remaining atoms and bonds are shown as capped stick or wireframe. Selected bond lengths (Å) and angles (°) for **[{U(*m*TP^{m})(1,4-dioxane)$_2$}$_2$]·4(1,4-dioxane)** are given in Table 2-2.

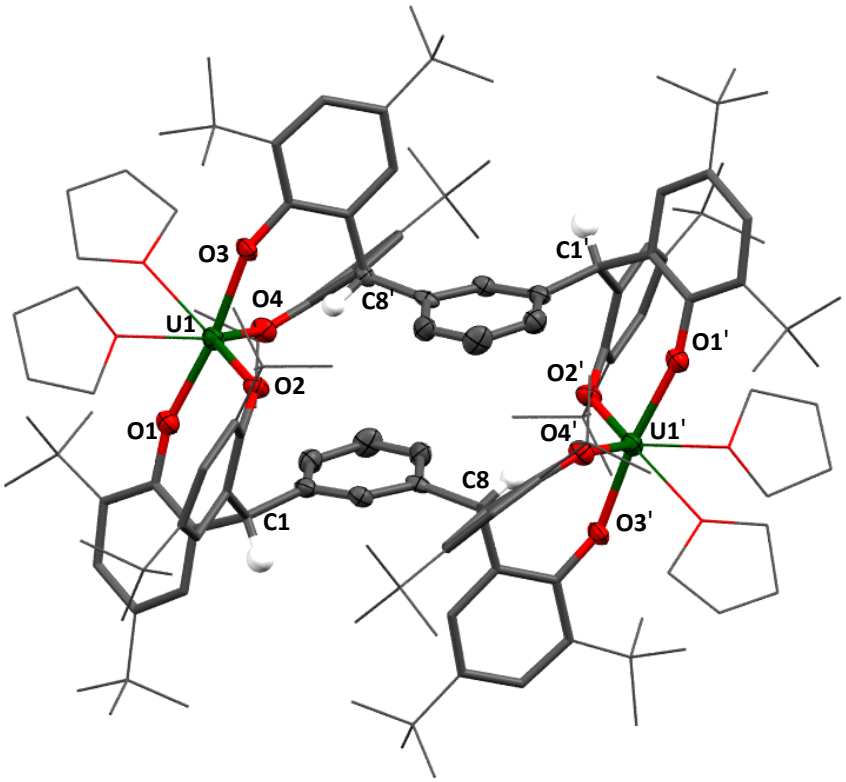

Figure 2-5 Solid-state structure of **[{U(*m*TP^t)(thf)$_2$}$_2$]·toluene, 2(*m*TP^t).** For clarity, backbone hydrogen atoms and lattice solvent molecules are omitted. Uranium, selected oxygen and carbon, and benzylic hydrogen atoms are shown as displacement ellipsoids drawn at 50 % probability. The remaining atoms and bonds are shown as capped stick or wireframe. Selected bond lengths (Å) and angles (°) for **[{U(*m*TP^t)(thf)$_2$}$_2$]·toluene** are given in Table 2-2.

Parameter	[{U(*m*TP^m)(1,4-dioxane)$_2$}$_2$]·4(1,4-dioxane)	[{U(*m*TP^t)(thf)$_2$}$_2$]·toluene
U(1)–O(1)	2.168(4)	2.144(7)
U(1)–O(2)	2.166(4)	2.191(7)
U(1)–O(3)	2.121(4)	2.167(7)
U(1)–O(4)	2.185(4)	2.179(7)
U(1)···U(1')	9.4974(7)	9.3073(7)
U(1)···C(8')	3.684(5)	3.567(6)
O(1)–U(1)–O(2)	99.6(2)	90.6(3)
O(2)–U(1)–O(3)	95.8(2)	92.1(2)
O(2)–U(1)–O(4)	91.1(2)	119.5(2)
O(3)–U(1)–O(4)	93.1(2)	92.1(3)
O(1)–U(1)–O(3)	96.6(2)	93.13(6)

Table 2-2 Selected bond lengths and angles for **2(*m*TP^m) and 2(*m*TP^t)**.

Figure 2-4 shows the solid-state structure of **[{U(*m*TP^{m})(1,4-dioxane)$_2$}$_2$]**, **2(*m*TP^{m})**. The two crystallographically identical uranium (IV) centres adopt a distorted octahedral coordination geometry with four aryloxide ligand moieties and two coordinated 1,4-dioxane molecules. The average O–U–O angle is 95.24(2)°, and the average U–O bond distance is 2.160(4) Å, which is similar to other U(IV) aryloxide bonds. The heteroleptic complex [U(ODtbp)[N(SiMe$_3$)$_2$]$_3$ (ODtbp = 2,6-di-*tert*butylphenol) has a U−O bond length of 2.145(8) Å for example.[18] 9.497(7) Å separates the two metals and 7.605 Å separates the centroids of the two bridging arene rings. The volume of the internal cavity is therefore approximately calculated as 463.5 Å^3 (where the width, 6.417 Å, is taken as the smallest C–C distance across the cavity). The central arenes are not eclipsed but fully offset; the angle between the plane of each ring and the vector linking their two centroids is 43 ° away from vertical.

Figure 2-5 shows the solid-state structure of **[{U(*m*TP^{t})(thf)$_2$}$_2$]·toluene**, **2(*m*TP^{t})**. The two uranium(IV) cations occupy identical coordination sites in a pseudo-octahedral geometry. Four coordination sites are occupied by ligand aryloxide moieties and the remaining two by coordinated thf molecules. The mean U–O bond length is 2.170(7) Å, which is longer than that of **2(*m*TP^{m})** taking calculated error into account, and closer to the corresponding length in [U(ODtbp)[N(SiMe$_3$)$_2$]$_3$ 2.145(8) Å than the homoleptic analogue [U(ODtbp)$_4$] (2.135(4) Å).[18] The mean O–U(1)–O bond angle, however, is significantly more acute (91.35(3)°) than the corresponding angle in **2(*m*TP^{m})** (95.24(15)°). This contraction presumably occurs to alleviate the additional steric congestion afforded by the larger ^{t}Bu substituents in **2(*m*TP^{t})**. The U–U distance is also significantly reduced, at 9.3076(7) Å compared to 9.497(7) Å in **2(*m*TP^{m})**, possibly also caused by the puckering of the bulkier ligand framework. An even greater reduction is seen in the distance between the centroids of the bridging arene rings, reduced from 7.605 Å to just 4.437 Å, resulting in a calculated cavity volume of 379 Å^3, 84.4 Å^3 smaller than that of **2(*m*TP^{m})**. The arene rings are still not eclipsed but offset from each other to a slightly lesser extent, the angle between the plane of each ring and the vector linking their two centroids is 37 ° away from vertical.

Ligand coordination to uranium can be readily identified by ^{1}H NMR spectroscopy owing to the paramagnetic nature of uranium (U(IV) = 4*f*^{2}). Paramagnetic NMR spectra feature peak broadening, obscured couplings and very broad chemical shift ranges caused by the magnetic

field of the unpaired metal electrons and spin polarisation transfer through shared molecular orbitals.

The C_2 symmetry of **2(*m*TP)** in the solid-state is retained in solution, resulting in only eight ligand resonances in the ^{1}H NMR spectra. These resonances occur between 34.60 ppm and –13.43 ppm at room temperature for **2(*m*TP^m)**, compared to just 7.09 ppm to 1.43 ppm in the diamagnetic **H$_4$(*m*TP^m)**. In addition to NMR spectroscopy and XRD, **2(*m*TP)** were characterised by elemental microanalyses which are consistent with the proposed molecular formulations.

The approximately 'letterbox' shaped rectangular cavity in the centre of these complexes is a new feature in organometallic uranium chemistry and may afford interesting new reactivity.

2.7 Synthesis of [{U(*m*TP)}$_2$], 3(*m*TP^m), *via* protonolysis reactions

The U–U separation distance in the N_2 cluster compound $[K_3\{[U(OR)_3]_2(\mu\text{-}N)(\mu\text{-}\eta^2\text{:}\eta^2\text{-}N_2)\}]$, **BI**, reported by Mazzanti is just 3.505 Å, indicating that very close proximity of the metal centres may be important in targeting N_2 activation.[19] Although the bridged bimetallic structures of **2(*m*TP)** are promising, the metal-metal separation distance is over 9 Å. Furthermore, in **2(*m*TP)**, both metal centres are coordinatively saturated. With no vacant coordination site available, it is unlikely that N_2 could displace another donor. Complexes **2(*m*TP)** were exposed to dynamic vacuum (20 – 60 °C) to target removal of coordinated solvent, yielding a coordinatively unsaturated analogue. However, the complexes were highly stable to vacuum, and no solvent loss was observed.

In targeting a base-free analogue of complexes **2(*m*TP)**, a protonolysis route using uranium silyamide metallacycle **[U(N")$_2$(N{SiMe$_3$}SiMe$_2$CH$_2$)]**[20] (N" = N(SiMe$_3$)$_2$) was investigated.

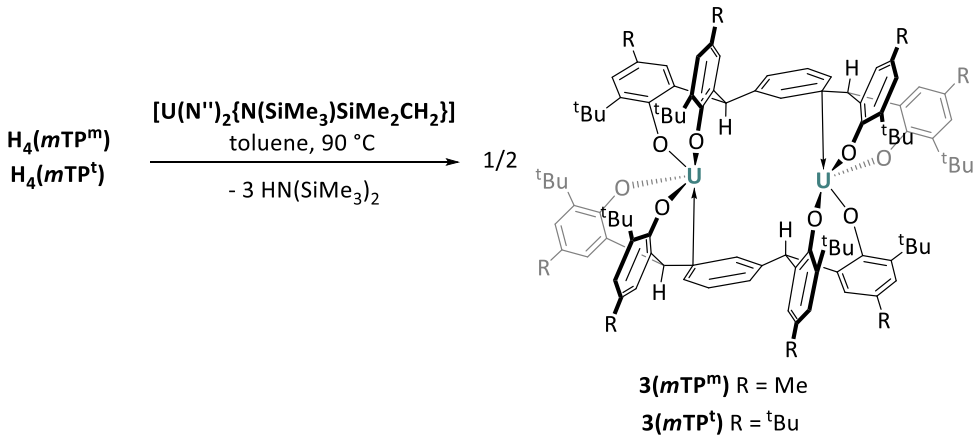

Scheme 2-6 Synthesis of **3(*m*TP)**.

The reaction of one equivalent of **H_4(*m*TP)** with **[U(N'')$_2$(N{SiMe$_3$}SiMe$_2$CH$_2$)]** in toluene yielded the desired product, with precipitation of the bright green solid from the dark brown reaction mixture after stirring at 90 °C overnight. The product was washed several times with hexanes, and then thoroughly dried under reduced pressure to ensure complete removal of the volatile byproduct, $HN(SiMe_3)_2$. Under these conditions, the yield of the product is poor (15 %). Synthesis in heptane increases yield to around 60 % but product purity is significantly reduced and byproducts are not easily removed. It is suggested that the low yield of product in toluene may be due to the formation of $[U(mTP)]_n$ oligomers which are not visible by NMR spectroscopy. Efforts to increase yield by varying concentration, the reaction temperature and the reaction time have not been successful.

Recrystallisation of **3(*m*TP^m)** from benzene, toluene or hexane gave yellow block-shaped crystals, allowing for analysis by single crystal XRD.

The molecular structure of **3(*m*TP^m)** (Figure 2-6) is considerably altered with respect to the solvated analogues, **2(*m*TP)**. The metal–metal separation is significantly reduced and the coordinatively unsaturated uranium centres now participate in π-bonding with one end of the arene. Uranium–arene interactions are often seen in U(III) compounds[13–15] but remain very rare for U(IV) complexes.

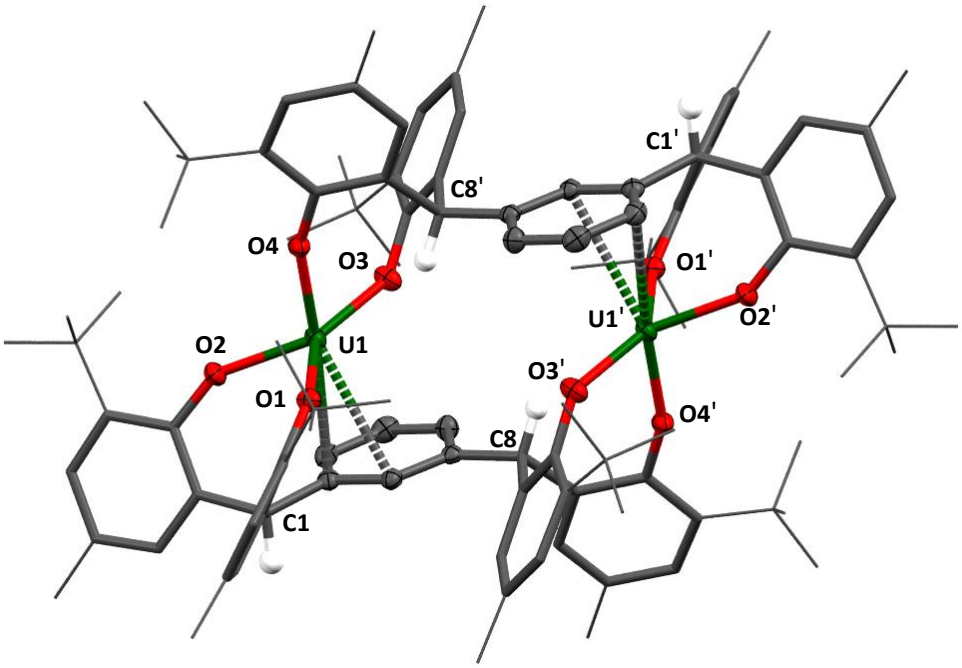

Figure 2-6 Solid-state structure of **3(m*TP*^{m})·3benzene**. For clarity, all backbone hydrogen atoms and lattice solvent molecules are omitted. Uranium, oxygen, selected carbon, and benzylic hydrogen atoms are shown as displacement ellipsoids drawn at 50 % probability. The remaining atoms and bonds are shown as capped stick or wireframe. Selected bond lengths (Å) and angles (°) for **3(m*TP*^{m})** are given in Table 2-4.

Parameter	[{U(*m*TP^{m})}$_2$]·3benzene
U(1)–O(1)	2.108(2)
U(1)–O(2)	2.137(2)
U(1)–O(3)	2.140(2)
U(1)–O(4)	2.126(2)
U(1)–C(2)	2.857(3)
U(1)–C(7)	3.050(3)
O(1)–U(1)–O(2)	87.16(8)
O(3)–U(1)–O(4)	84.76(8)
O(3)–U(1)–O(1)	141.00(8)
O(2)–U(1)–O(3)	131.05(8)
C(2)–U(1)–C(7)	84.76(8)

Table 2-3 Selected bond lengths and angles for **3(*m*TP^{m})**.

Each uranium(IV) centre has an approximately trigonal bipyramidal geometry. Four coordination sites are occupied by two aryloxides from each ligand, while the remaining site supports the π-interaction. This interaction is most accurately described as η^3 in nature with

a 2.826 Å distance between the calculated C(3)–C(2)–C(7) centroid and U(1). U(IV)–arene interactions are very rare, but in this case it is thought that the low coordination number of the metal, in addition to the ligand geometry impose this interaction. Enforced by this interaction, one benzylic proton (on each ligand) now points out of the cavity whilst the other benzylic C–H bond remains directed towards the internal space, in contrast to the structures of **2(*m*TP)**, in which all four benzylic C–H bonds are directed towards the internal space, Figure 2-7.

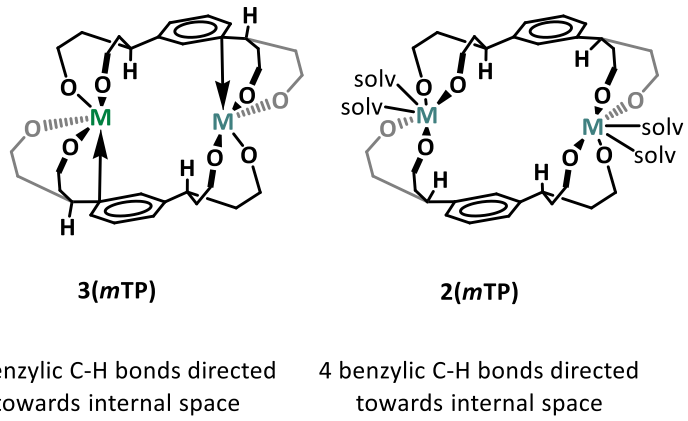

Figure 2-7 Schematic showing contrasting geometries of **3(*m*TP)** and **2(*m*TP)**.

The U–U distance is significantly reduced from 9.3076(7) Å and 9.497(7) Å in **2(*m*TP^{t})** and **2(*m*TP^{m})** respectively, to 6.573 Å. The average U–O bond distance is 2.13(2) Å, shorter than in **2(*m*TP)**, but still within the usual range of U(IV)–O aryloxides.[21–23] In the equatorial plane of U(1), the O(3)–U(1)–O(1) angle (141.00(8) °) is significantly greater than the O(2)−U(1) −O(3) and O(1) −U(1) −O(2) angles (131.05(8) ° and 87.16(8) °), resulting in an open, sterically accessible U face, pointing towards the inside of the cavity. By comparison, the O−U−O angles in the related homoleptic U(IV) aryloxide complex, [U(ODtbp)$_4$], are close to tetrahedral and more evenly distributed- 110.23(12) ° and 107.96(23) °.[18]

These sites (on U(1) and U(1')) appear readily available for substrate binding and potential activation chemistry.

In addition to the U–U distance (6.5732(5) Å), it is interesting to note the volume of the internal cavity, which is apparent on inspection of a space-filling model of the atoms surrounding the cavity, Figure 2-8.

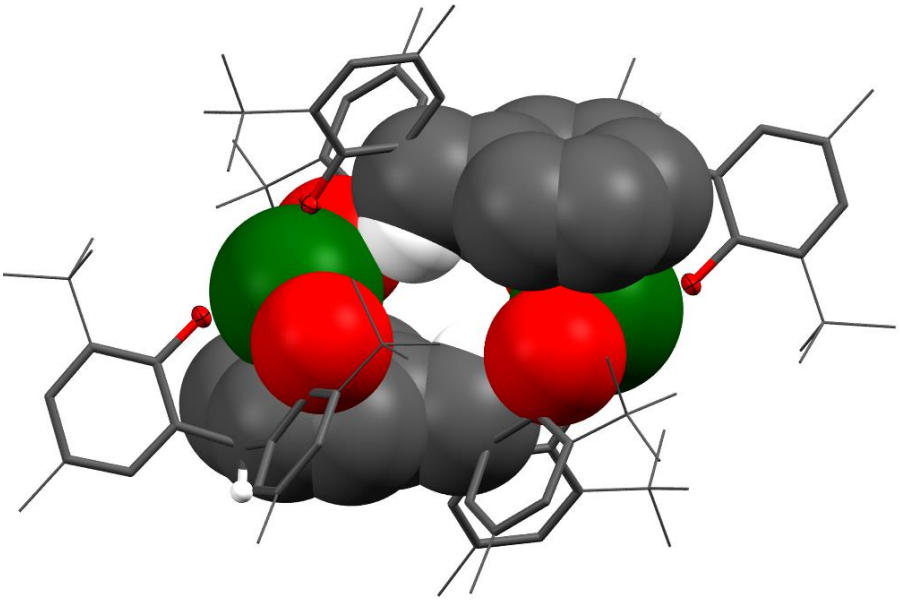

Figure 2-8 Solid-state structure of **3(*m*TP^{m})·3benzene**. For clarity, all hydrogen atoms and lattice solvent molecules are omitted. Selected oxygen atoms are shown as displacement ellipsoids drawn at 50 % probability. The atoms surrounding the internal cavity are shown as space-filling spheres to highlight the empty space. The remaining atoms and bonds are shown as capped stick or wire frame.

The approximate volume can be calculated by placing a dummy atom in the centre of the space and modelling it to fill the available volume (Figure 2-9). A volume of 8.7 Å^3 is suggested by an atom with a radius of 1.3 Å.[1] This value suggests that it should be possible for small diatomic or triatomic molecules to enter the cavity by diffusion.

[1] Calculation by Dr. Stephen Moggach, Edinburgh University, School of Chemistry.

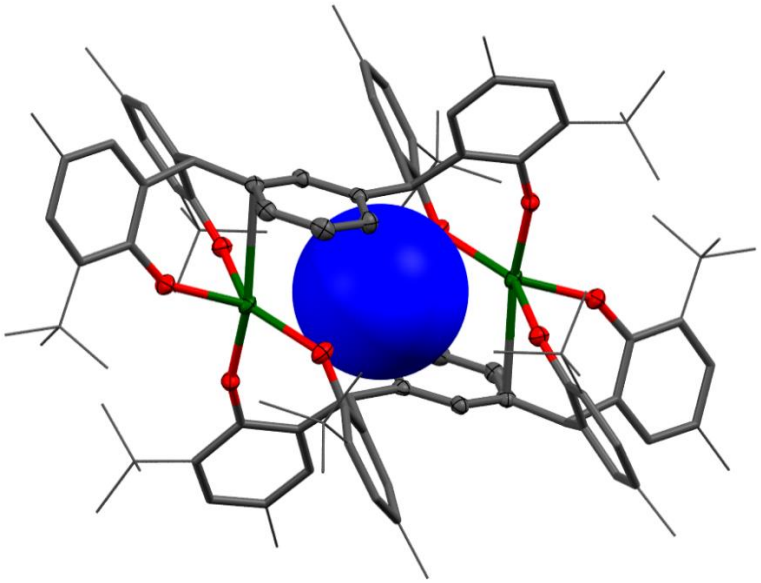

Figure 2-9 Solid-state structure of **3(*m*TP^{m})·3benzene**. For clarity, all hydrogen atoms and lattice solvent molecules are omitted. Uranium, oxygen, and selected carbon atoms are shown as displacement ellipsoids drawn at 50 % probability. The remaining atoms and bonds are shown as capped stick or wire frame. The dummy atom in the centre of the calculated space is shown in blue.

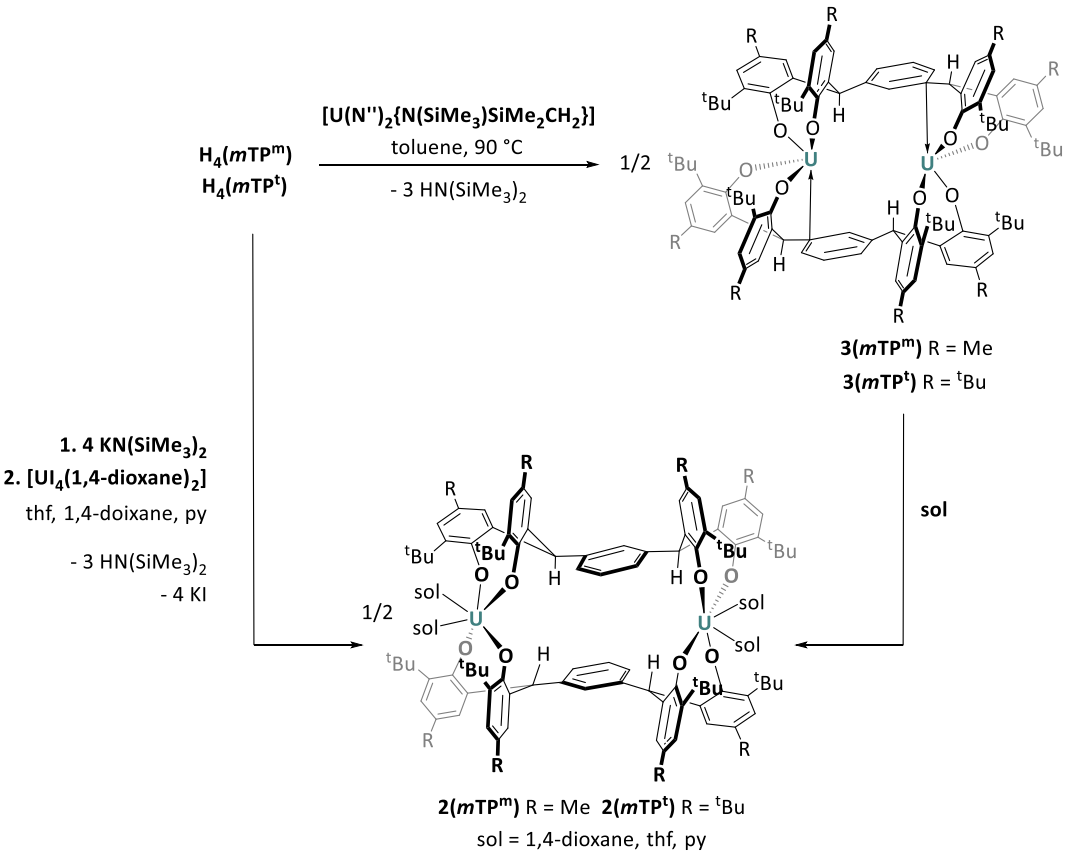

Scheme 2-7 Conversion of **3(*m*TP^{m})** to **2(*m*TP^{m})** *via* solvent coordination.

Exposure of **3(*m*TP^{m})** complexes to coordinating solvents thf, 1,4-dioxane or pyridine results in coordination and loss of the metal–arene interaction to yield **2(*m*TP^{m})** (Scheme 2-7).

In contrast to **2(*m*TP^{m})**, the two ligands in **3(*m*TP^{m})** are symmetrically inequivalent in the solid-state and in solution, and accordingly two sets of ligand resonances can be identified by ^{1}H NMR spectroscopy, affording the spectrum shown in Figure 2-10.

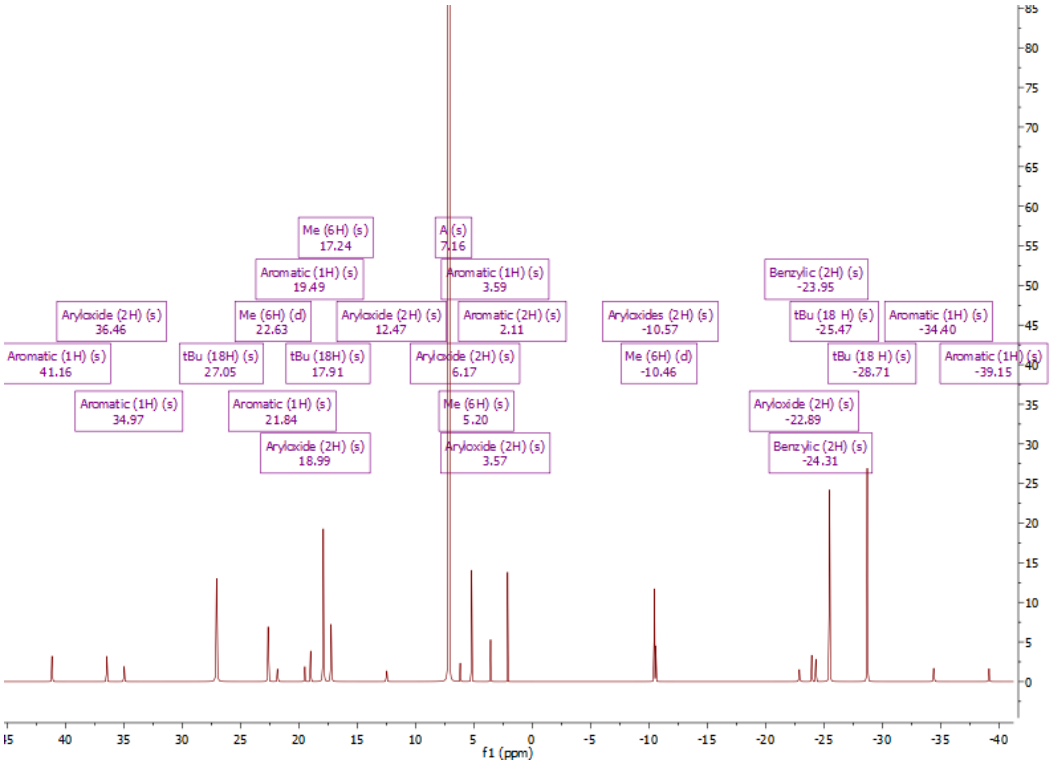

Figure 2-10 ^{1}H NMR spectrum of **3(m*TP^{m}*)** (C_6D_6), showing two sets of ligand resonances.

Diffusion ordered NMR spectroscopy (DOSY) was used to confirm that the dimeric structure does not dissociate into monomeric units in solution, and the measured diffusion coefficient of –9.325 log m^2 s was used to calculate a hydrodynamic radius of 7.638 Å using the Stokes-Einstein equation.[2]

The UV-Vis spectra of **3(*m*TP^{m})** and **3(*m*TP^{t})** solutions in toluene show absorption maxima at 286 nm (ε = 28237 dm mol^{-1} cm^{-1}) and 292 nm (ε = 21978 dm mol^{-1} cm^{-1}), respectively, shown in Figure 2-11. These are assigned as ligand based π-π transitions. A second, broad peak is present at approximately 400 nm (ε = 4409 dm mol^{-1} cm^{-1} for **3(*m*TP^{m})**) assigned as a charge

[2] DOSY HdRC Tools v2, P. Symmers, University of Edinburgh, 2012

transfer band. A similar charge transfer band may be present in the spectrum of **3(*m*TP^{t})**, although this is significantly broadened.

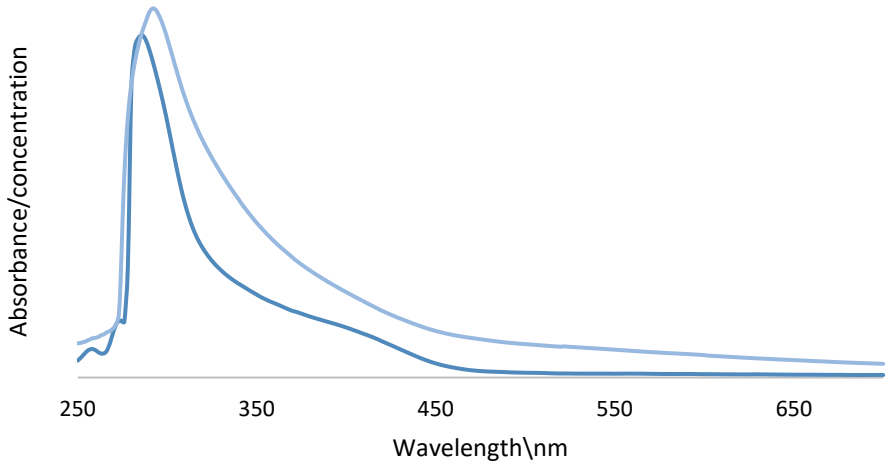

Figure 2-11 Overlaid UV-Vis spectra of **3(*m*TP^{m})** in dark blue and **3(*m*TP^{t})** in light blue.

The solution magnetic moment of **3(*m*TP^{m})** was calculated as 3.58 μ_B using Evans' Method[24] (see Appendix 1). This value is consistent with the $^{3}H_4$ ground state of U(IV).

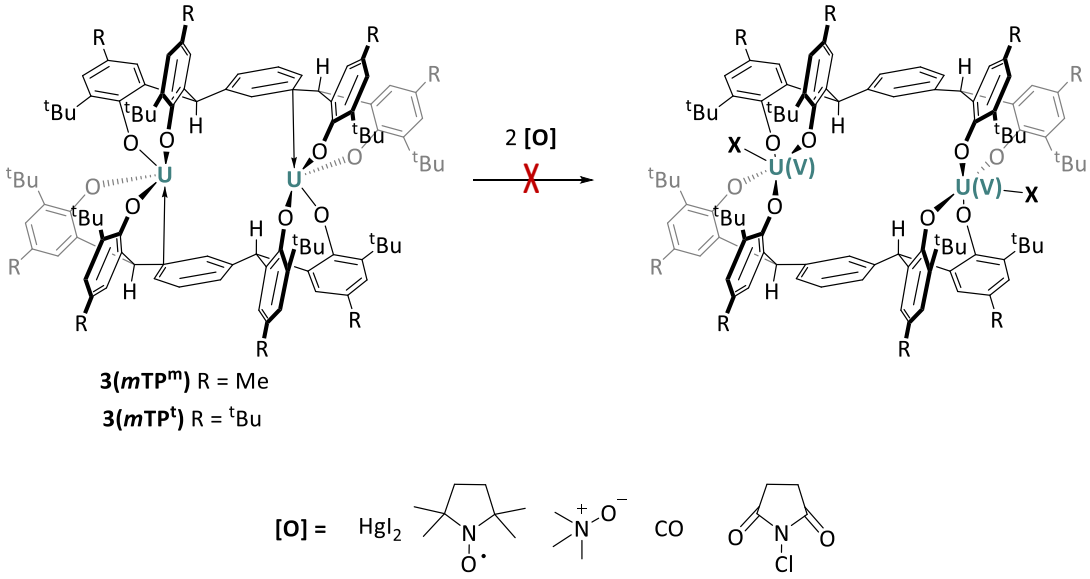

Scheme 2-8 Attempted oxidations of **3(*m*TP^{m})**.

Attempts to oxidise **2(*m*TP^{m})** and **3(*m*TP^{m})** using HgI_2, NCS (N-chlorosuccinimide), TEMPO ((2,2,6,6-tetramethylpiperidin-1-yl)oxyl), CO and trimethylamine N-oxide were not successful (Scheme 2-8). However, reactions with reducing agents have been successful and are presented below.

2.8 Reduction of 3(*m*TP^{m}) to [K_4{U(*m*'TP)(NH)}$_2$], and N_2 activation

The U(IV)/(III) redox couple typically ranges from −2.78 to −1.83 V versus ferrocene.[25–27] The reduction of **3(*m*TP)** with two equivalents of KC_8 was attempted under a variety of reaction conditions. Under atmospheres of argon or nitrogen, and at either ambient or high temperatures.

^{1}H NMR spectra of reaction mixtures are challenging to interpret but indicated incomplete consumption of **3(*m*TP)** and formation of at least one new product. Single crystals of a new product were obtained on one occasion but XRD data was not of sufficient quality to allow unambiguous assignment of the compound. The data show significant electron density in the centre of the cavity, which was tentatively assigned as a bound N_2 ligand.

This product could be reproducibly synthesised when four, instead of two equivalents of KC_8 in toluene were added to a solution of **3(*m*TP)** at −30 ° C (Scheme 2-9). Over several hours, the change from a bright green suspension to dark orange solution indicates increased solubility of the product relative to **3(*m*TP)** and ^{1}H NMR spectroscopy confirms complete consumption of **3(*m*TP)**. Following removal of insoluble graphite from the reaction mixture, a dark orange powder was obtained when the toluene was removed under reduced pressure. Washing with hexane yielded **4(*m'*TP)** as an orange powder in good yield (64 %).

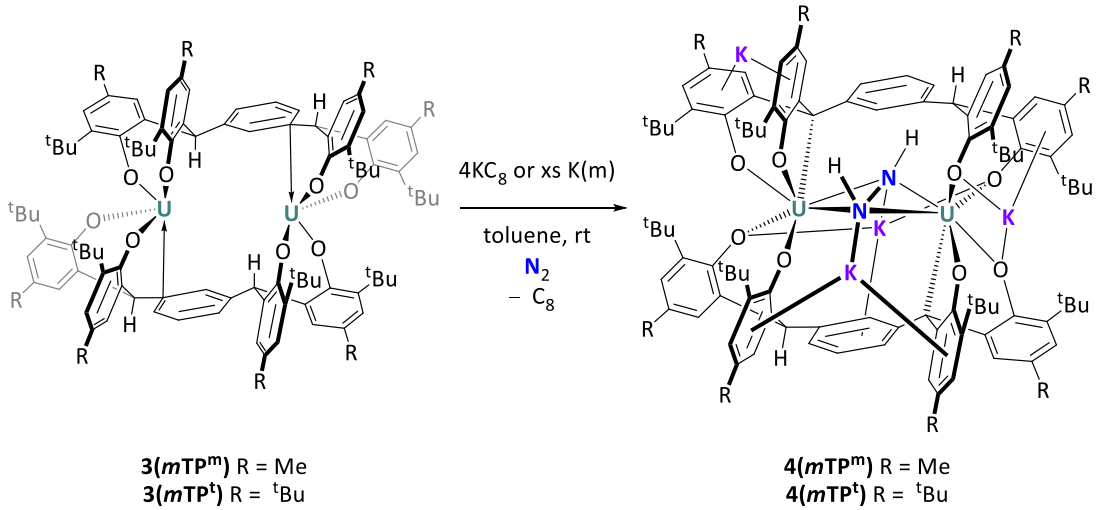

3(*m*TP^{m}) R = Me
3(*m*TP^{t}) R = ^{t}Bu

4(*m*TP^{m}) R = Me
4(*m*TP^{t}) R = ^{t}Bu

Scheme 2-9 Reduction of **3(*m*TP)** to give **4(*m*'TP)**.

Analysis by single crystal XRD revealed the molecular structure of **4(*m*'TP^{m})**, showing the binding of atmospheric dinitrogen. The solid-state structure of **4(*m*'TP^{m})·6toluene** is shown below (Figure 2-12).

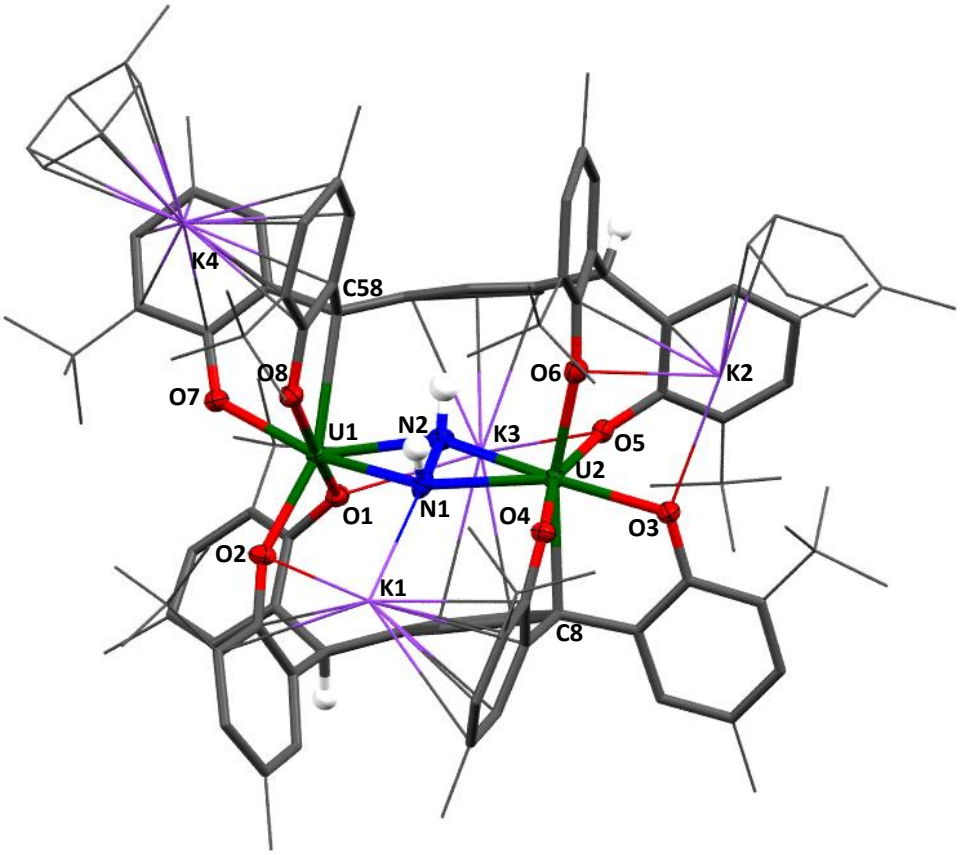

Figure 2-12 Solid-state structure of **4(*m*'TP^{m})·6toluene**. For clarity, all backbone hydrogen atoms and lattice solvent molecules are omitted. Nitrogen, uranium, oxygen and benzylic and diazenido hydrogen atoms are

shown as displacement ellipsoids drawn at 50 % probability. The remaining atoms and bonds are shown as capped stick or wireframe. Selected bond lengths (Å) and angles (°) for **4(*m*'TP^{m})** are given in Table 2-4.

Parameter	[K$_4${U(*m*'TP^{m})(NH)}$_2$].6toluene
U(1)–N(1)	2.432(4)
U(1)–N(2)	2.472(4)
U(1)–O(1)	2.389(3)
U(1)–O(2)	2.230(3)
U(1)–O(7)	2.275(3)
U(1)–O(8)	2.305(3)
U(1)–C(58)	2.557(4)
U(2)–N(1)	2.370(4)
U(2)–N(2)	2.550(4)
U(2)–O(3)	2.282(3)
U(2)–O(4)	2.223(3)
U(2)–O(5)	2.292(3)
U(2)–O(6)	2.214(3)
U(2)–C(8)	2.733(4)
N(1)–U(1)–N(2)	35.4(1)
N(1)–U(2)–N(2)	35.0(1)

Table 2-4 Selected bond lengths and angles for **4(*m*'TP^{m})**.

The dimeric structure of **3(*m*TP)** is retained, with incorporation of four potassium cations into the ligand framework. A side-on hydrazido $[N_2H_2]^{2-}$ ligand bridges U(1) and U(2), which are 4.6420 Å from each other. The pseudo-pyramidal nitrogen atoms create a 14.93 ° puckering of the U–diazenido–U core (determined by measuring the angle between U(1), a centroid between N(1) and N(2), and U(2), then subtracting from 180 °). The N–N distance is 1.492(5) Å, which is consistent with reduction of dinitrogen to $[N_2H_2]^{2-}$ and is the same within standard uncertainty as the bond length in hydrazine (1.47(2) Å) and very close to the corresponding N–N bond in the related zirconium complex $[(\eta^5\text{-}\ C_5Me_4H)_2Zr(C{\equiv}C(C_6H_5)]_2(\mu^2,\eta^2,\eta^2\text{-}N_2H_2)$, 1.454(2) Å.[28] The core of the molecule is asymmetric with two short (2.432(4) Å and 2.370(4) Å) and two long (2.472(4) Å and 2.550(4) Å) U–N bonds, consistent with the Lewis structure shown in Figure 2-13.

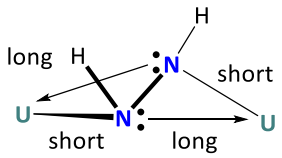

Figure 2-13 Lewis structure of diazenido ligand binding.

One benzylic C–H in each ligand has been activated, resulting in ligand functionalisation **(*m*'TP^{m})** and two new 2.645(4) Å (avg) U–C bonds. The two uranium–aryloxide ligand planes are staggered by an angle of 42.1 °, presumably to minimise steric interactions between the aryloxide substituents. Arene interactions with potassium cations K(2) and K(4) anchor two toluene molecules to **4(*m*'TP^{m})**.

The ^{1}H NMR spectrum of **4(*m*'TP)** contains 32 resonances**,** suggesting that the potassium–ligand arene interactions seen in the solid state are retained in solution and render almost every single proton unique. **4(*m*'TP)** was further characterised by elemental microanalysis, as well as by atmospheric pressure photoionization mass spectrometry (APPI), giving a measured mass of 2160.86246 m/z, in good agreement with the calculated value of 2160.89216 m/z.

The UV-Vis spectrum of **4(*m*'TP^{m})** in toluene is shown in Figure 2-14, overlaid with the spectrum of **3(*m*TP^{m})** in toluene. The absorption maximum (296 nm, ε = 33209 dm mol^{-1} cm^{-1}) assigned as a ligand based π-π transition, shows a slight bathochromic shift relative to **3(*m*TP^{m})**. A shoulder at 280 nm (ε = 29023 dm mol^{-1} cm^{-1}) is also present with an extinction coefficient characteristic of another ligand based π-π transition.

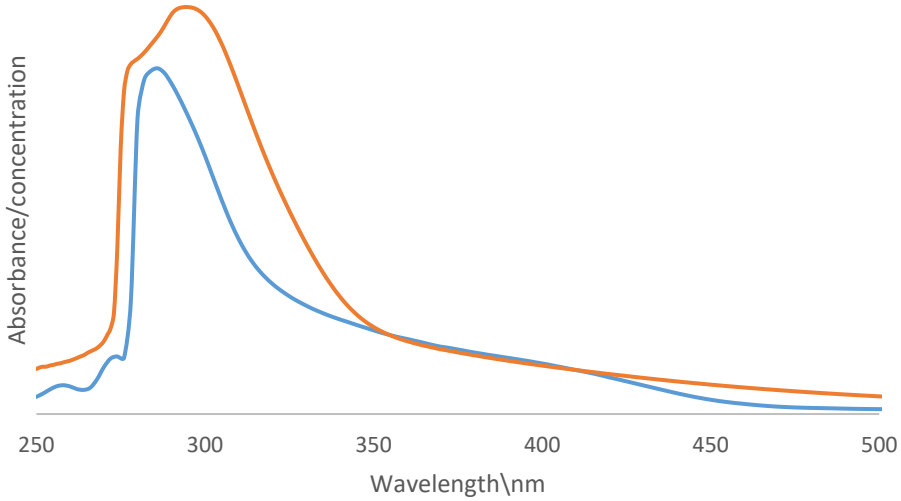

Figure 2-14 UV-Vis spectra of **3(*m*TP^{m})** (blue) and **4(*m*'TP^{m})** (orange) in toluene. Normalised with respect to concentration.

Solid-state FTIR spectroscopy (KBr, nujol mull) was used to verify the formation of N–H bonds, the spectrum of **4(*m*'TP^{m})** is shown in Figure 2-15.

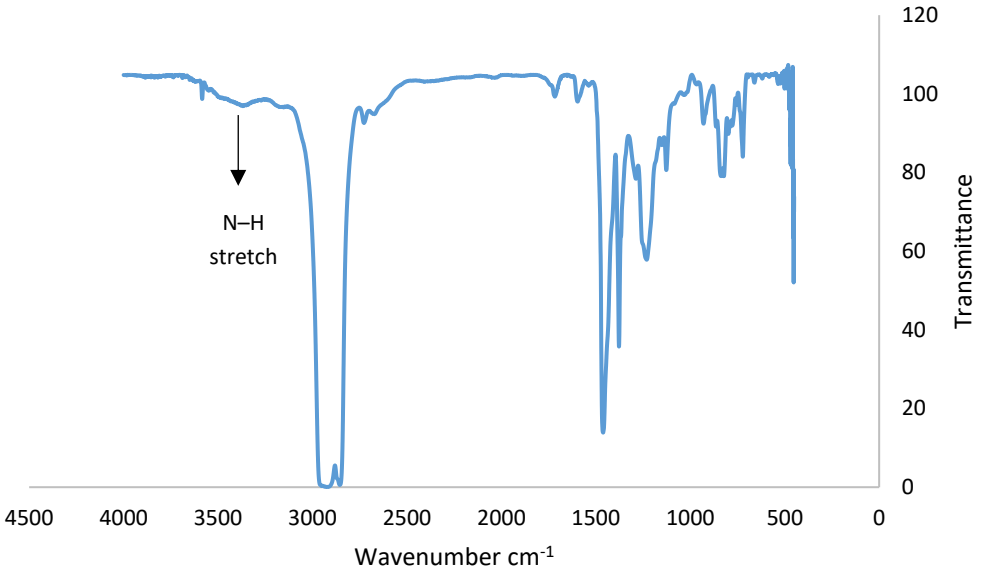

Figure 2-15 Solid-state IR spectrum of **4(*m*'TP^{m})**.

The broad peak at 3382 cm^{-1} arises from **4(*m*'TP^{m})** and is tentatively assigned as an N–H stretch. This is in good agreement with reported IR data for [(η^5- $C_5Me_4H)_2ZrR]_2(\mu^2,\eta^2,\eta^2$-$N_2H_2$)

(R = CMe_3, C_6H_5, $(CH_2)_3CH_3$), where broad peaks ranging from 3297 cm^{-1} to 3582 cm^{-1} are attributed to N–H stretches as R is varied.[28]

In contrast to the N–H bonds, the N–N bond is symmetric and the stretching frequency cannot be characterised by IR spectroscopy. The sample was sealed inside a glass capillary (glass thickness approximately 120 µm) and Raman spectra were recorded at an excitation wavelength of 785 nm (Figure 2-16).

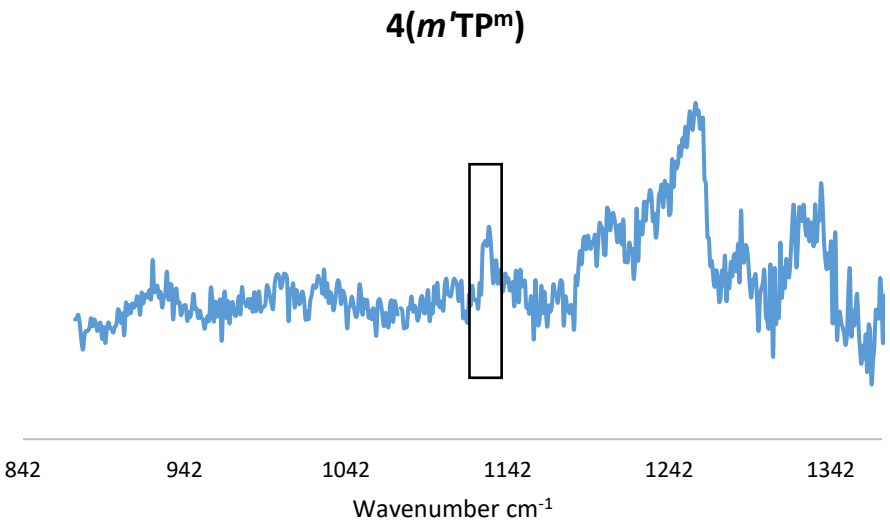

Figure 2-16 Raman spectrum of **4(*m'*TP^m)** (powder in glass capillary, wall thickness 120 µm, 785 nm laser, 5 % power, 15 seconds acquisition time, 20 accumulations).

The peak at 1138 cm^{-1} is assigned as an N−N stretch. This is in good agreement with the only known uranium bound $[N_2]^{4-}$ complex[29] (1100 cm^{-1}) and is much closer to the stretching frequency in hydrazine (1111 cm^{-1}) than free dinitrogen (2331 cm^{-1}).[30]

Using the harmonic oscillator model, the force constant of the $^{14}N–^{14}N$ bond, k, was calculated using Equation 2-1, where μ is the reduced mass of the atoms connected by the bond, m_1 and m_2 are the masses of each atom, (Equation 2-2) and ϑ is the stretching frequency of the bond.

$$\vartheta = \frac{1}{2\pi}\sqrt{\frac{k}{\mu}}$$

Equation 2-1 Hooke's Law

$$\frac{1}{\mu} = \frac{1}{m_1} + \frac{1}{m_2}$$

Equation 2-2 Reduced mass equation

Based on the stretching frequency of 1138 cm^{-1}, and reduced mass of 7, *k* is calculated as $3.529x10^8$.

In order to unambiguously assign the N–N stretch by Raman spectroscopy, the ^{15}N analogue of **4(*m'*TP^m)** is required. Using the calculated force constant of $3.529x10^8$ along with a reduced mass of 7.5, the stretching frequency of the corresponding ^{15}N–^{15}N bond was calculated to be 1092 cm^{-1}.

2.9 Synthesis of ^{15}N-4(*m'*TP^m), [K_4{U(m'TP^m)(^{15}NH)}$_2$]

The procedure detailed in Scheme 2-9 was repeated using $^{15}N_2$. To exclude atmospheric $^{14}N_2$ from the reaction, 10 ml of toluene was degassed before being transferred *via* vacuum distillation into an ampoule containing **3(*m*TP^m)** and KC_8. The headspace was refilled using $^{15}N_2$. The reaction was stirred overnight before filtration to remove the graphite from the dark orange solution. The volatiles were removed under reduced pressure to provide a dark red powder which was washed several times with hexane to yield orange **^{15}N-4(*m'*TP^m)**. The sample was sealed inside a glass capillary and Raman spectra were recorded at an excitation wavelength of 785 nm (Figure 2-17).

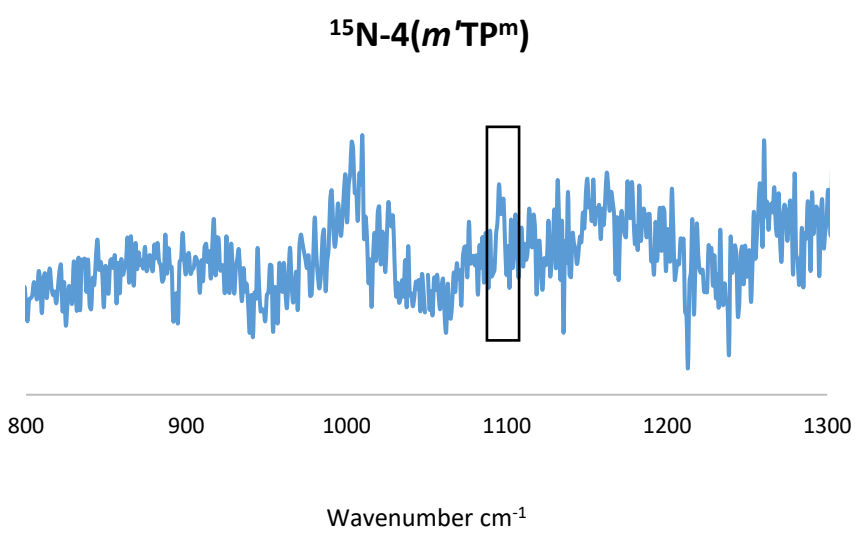

Figure 2-17 Raman spectrum of **^{15}N-4(*m'*TP^{m})** (powder in glass capillary, wall thickness 120 µm, 785 nm laser, 5 % power, 15 seconds acquisition time, 20 accumulations).

It was more difficult to obtain a well-resolved Raman spectrum for **^{15}N-4(*m'*TP^{m})** (loss of resolution in ^{15}N-labelled spectra has also been observed by other authors).[31] The substrate peak is weak relative to the signal from the surface of the glass capillary, resulting in a low signal:noise ratio. Increasing laser power leads to increased intensity of this glass signal, and a relative loss of intensity of the product peaks. Low laser power, long exposure times and high numbers of acquisitions were used to optimise the ^{15}N–^{15}N stretching peak.

Although poorly resolved, a peak at 1097 cm^{-1} is clearly visible in Figure 2-17. This peak is not present in spectra of the clean glass surface. This experimentally observed value corresponds very well to the calculated stretch for the ^{15}N–^{15}N bond, 1092 cm^{-1}. It was also observed that for both **4(*m'*TP^{m})** and **^{15}N-4(*m'*TP^{m})**, no thermal decomposition occurred following several scans with 5 % laser power, focused on the same position.

The concentration of the I=1/2 ^{15}N nucleus in natural dinitrogen (0.37%) is not sufficiently high that NMR spectra can be observed under normal experimental conditions. It was however possible to measure the nitrogen resonance in the ^{15}N NMR spectrum of **^{15}N-4(*m'*TP^{m})**.

The only uranium dinitrogen complex to have been characterised by ^{15}N NMR spectroscopy is $[U\{OSi(Mes)_3\}_3]_2(\mu\text{-}\eta^2\text{:}\eta^2\text{-}N_2)$, **BI**, giving rise to a resonance at +4213.5 ppm.[31] $\{(C_5Me_4H)_2Ln(thf)\}_2(\mu\text{-}\eta^2\text{:}\eta^2\text{-}N_2))$ (Ln = Ce, Pr) were the first paramagnetic lanthanide

complexes to be analysed by ^{15}N NMR spectroscopy, showing ^{15}N resonances at +1001 ppm and +2383 ppm respectively.[32] These reports demonstrate that the chemical shift of ^{15}N resonances is highly dependent on the identity of the paramagnetic metal. The {^{1}H}^{15}N NMR spectrum of **^{15}N-4(*m'*TP^{m})** (Figure 2-18) shows a resonance at −4060 ppm.

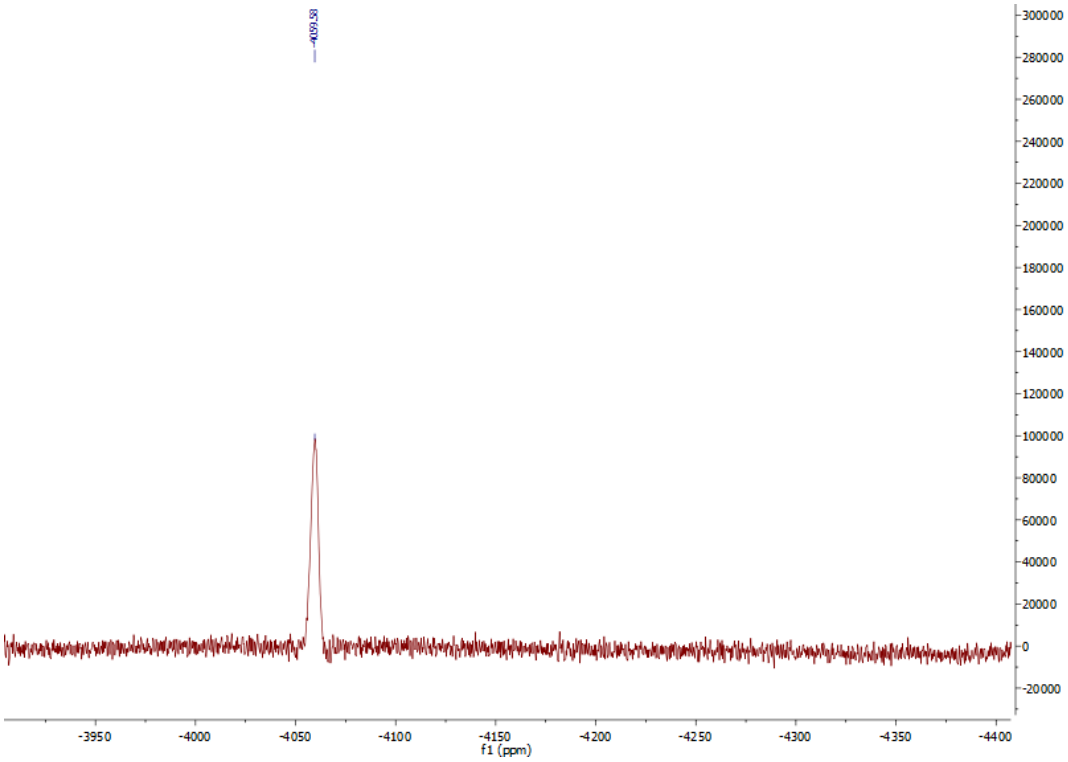

Figure 2-18 {^{1}H}^{15}N NMR spectrum of **^{15}N-4(*m'*TP^{m})**.

This result represents the lowest recorded ^{15}N signal for any lanthanide or actinide dinitrogen complex, and also confirms the stability of **^{15}N-4(*m'*TP^{m})** when stored in solution for a number of weeks.

The full set of characterisation data including multinuclear NMR spectroscopy, mass spectrometry, UV-Vis spectroscopy, Raman spectroscopy, IR spectroscopy, X-ray crystallography and elemental microanalysis are all consistent with the proposed structure of **4(*m'*TP^{m})**, containing bound $[N_2H_2]^{2-}$ following an intramolecular reaction of an activated N_2 fragment with benzylic C−H bonds provided by the ligand.

2.10 DFT Computational analysis of the mechanism of nitrogen activation

A possible reaction pathway was determined at the DFT (B3PW91) level for the activation and functionalisation of N_2 by **3(*m*TP)**.[3] The reaction pathway, schematic representations of computed intermediates with associated energies and energy barriers are shown in Figure 2-19. Drawings of the computed transition states are shown in Figures 2-20 and 2-21. It should be noted that such calculations are not routine as two uranium centres and more than 250 atoms are involved.

Given that the thorium(IV) analogue of **4(*m'*TP^m)** has been prepared within the Arnold group and it also demonstrates nitrogen activation in the presence of potassium reducing agents, and that thorium(IV) is not easily reduced to Th(III) in organic solvents by potassium (, the calculations were carried out with the assumption that the metal oxidation state is fixed during the course of the reaction.

[3] The computational analyses described in this section were performed by our collaborator Professor Laurent Maron at Université Toulouse, Laboratoire de Physique et Chimie des Nano-objets, Institut National des Sciences Appliquées, France.

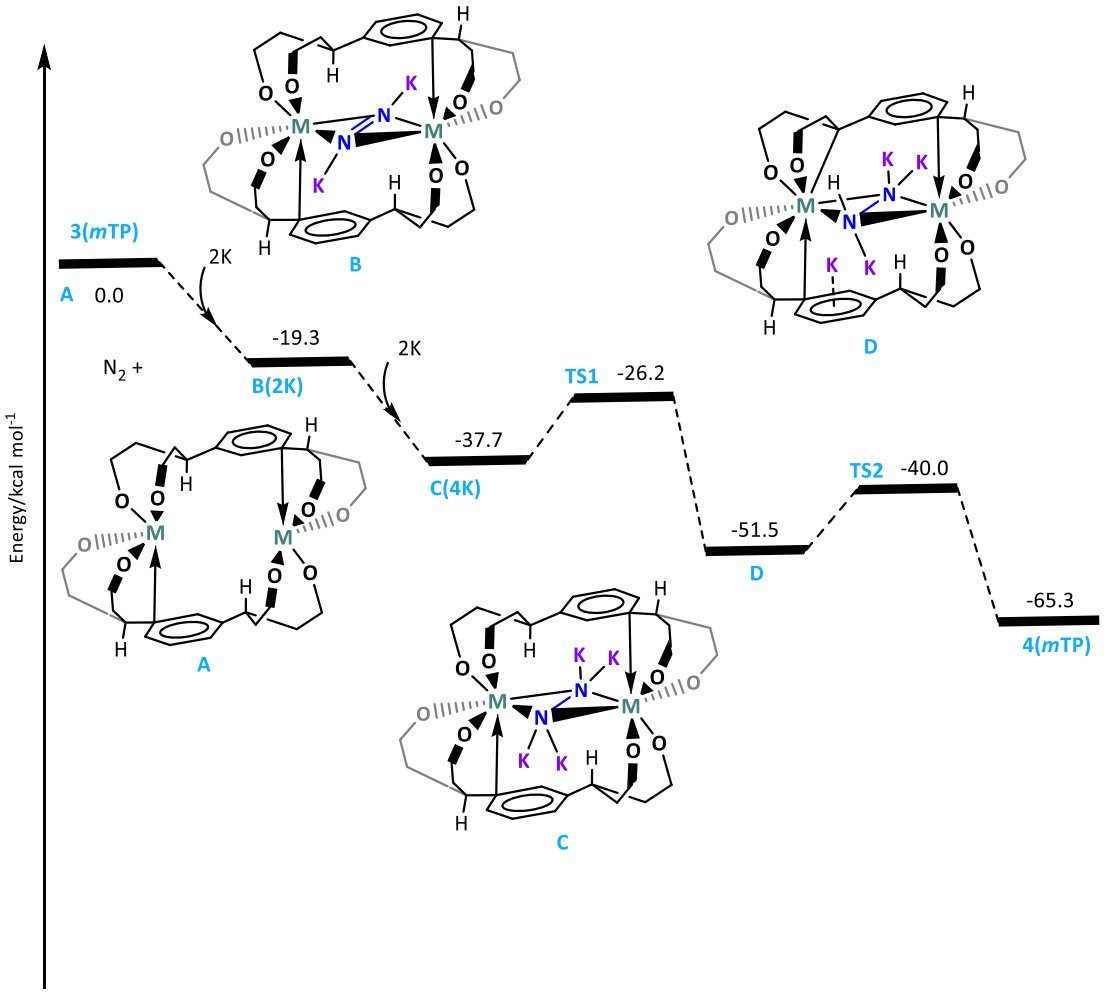

Figure 2-19 Computed enthalpy pathway at room temperature for the activation and functionalisation of N_2.

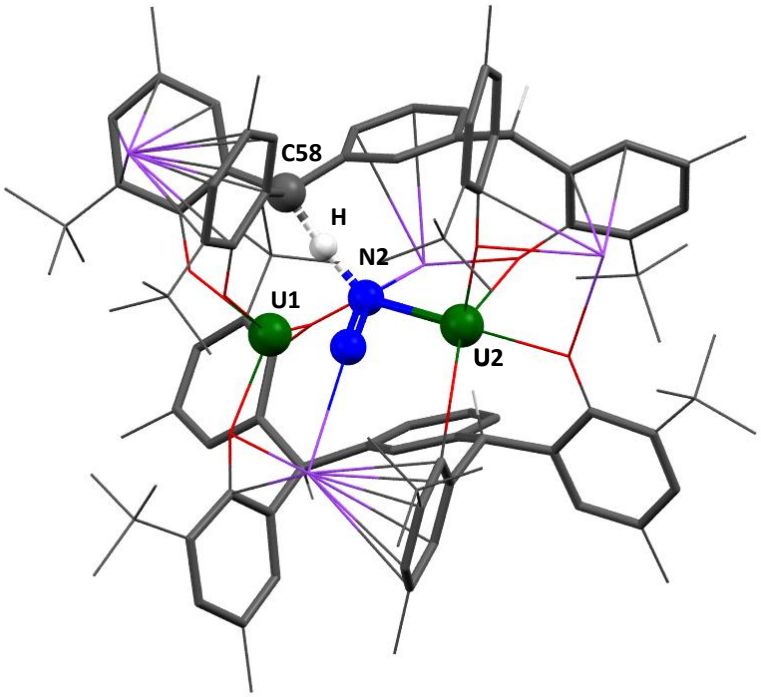

Figure 2-20 Computed structure of **Transition state 1,** showing proton transfer from C(58) to N(2).

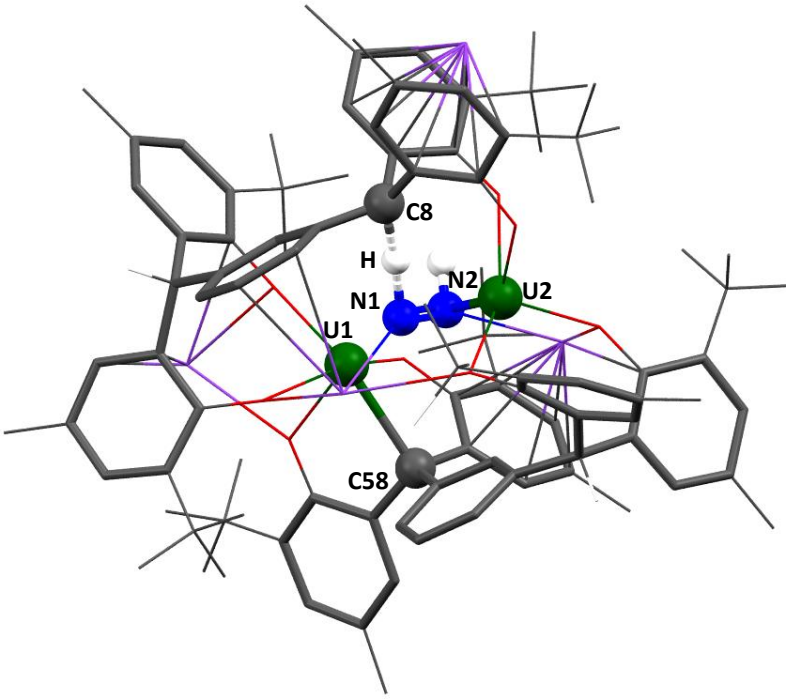

Figure 2-21 Computed structure of **Transition state 2**, showing proton transfer from C(8) to N(1).

The addition of N_2 and two equivalents of a potassium source to **[{U(*m*TP^m)}$_2$]**, **3(*m*TP^m)** is computed to be exothermic by 19.3 kcal mol^{-1} to provide intermediate **B**. The N−N bond length in **B** (1.25 Å) is significantly longer than that of free dinitrogen (1.098 Å) and is consistent with a double bond. A similar intermediate was computed by Holland and coworkers, showing coordination of two potassium cations to the N−N bond in L^{R}FeNNFeL^R (L^R = *β*-diketiminate; R = Me, ^{t}Bu). This study is discussed in more detail below.[33] Schematics of intermediates **B** and **C** are shown in Figure 2-19.

The addition of the further two equivalents of potassium to **B** is exothermic by 18.4 kcal mol^{-1} and yields computed intermediate **C** at −37.7 kcal mol^{-1}. The N−N bond length in **C** (1.53 Å) is consistent with reduction to a single bond. For comparison, the N−N bond length in hydrazine is 1.48 Å. Each nitrogen atom in **C** has a *pseudo* planar geometry, with a π-lone pair in an orbital orthogonal to the plane formed by the U−N bonds. These lone pairs are oriented towards the benzylic C−H bonds, with one pointing upwards from the plane and one pointing downwards to avoid a destablising 4e$^-$ π-interaction. The other three valence electron pairs on each nitrogen atom in **C** are involved in bonding to the uranium centres or potassium cations.

The energy barrier for the formation of Transition state 1 (TS1) is low (11.5 kcal mol^{-1}). The orientation of the N lone pairs in intermediate **C** allow proton transfer. The computed structure for TS1 is drawn in Figure 2-20 and shows no involvement of the uranium centres. Proton transfer between C(58) and N(2) is almost linear and bond breaking (C−H bond = 1.40 Å) and bond formation (N−H bond = 1.41 Å) are shown as dashed lines.

Proton transfer is complete in intermediate **D**, and the deprotonated benzylic carbon, C(58) is bound to U(1). Intermediate **D** is stabilised by 13.8 kcal mol^{-1} relative to intermediate **C**. The energy barrier for the formation of Transition state 2 (TS2), in which the second proton transfer takes place, is identical to that of TS1, 11.5 kcal mol^{-1}. The experimentally observed complex, **[K$_4${U(*m*'TP^m)(NH)}$_2$], 4(*m*'TP)** lies 11.8 kcal mol^{-1} below intermediate **D**.

The mechanism is consistent with the experimental observation that addition of four equivalents of crown-ether 18-c-6 to a reaction mixture containing **[{U(*m*TP)}$_2$]**, **3(*m*TP^m)**, and four equivalents of KC_8 appears to prevent nitrogen activation. The dark red product recovered from the reaction could not be fully characterised owing to its insolubility in

organic solvents but further reactions with electrophiles did not yield nitrogen-containing products. It is proposed that the binding of K^+ by the crown-ether prevents formation of intermediate **B**, thereby preventing N_2 reduction.

The ability to bind potassium ions within the ligand framework, in close proximity to the dinitrogen ligand, is also a feature of **BI**, $[K_3\{[U(OR)_3]_2(\mu\text{-}N)(\mu\text{-}\eta^2\text{:}\eta^2\text{-}N_2)\}]$, the only other uranium complex reported to reduce N_2 by a total of four electrons (see Chapter 1). Work by Holland and coworkers has also examined the role of potassium and other alkali metal cations in the reduction of nitrogen by iron complexes.[34,35] When the bis-iron dinitrogen complex $L^RFeNNFeL^R$ (L^R = *β*- diketiminate; R = Me, ^{t}Bu) is treated with two equivalents of KC_8, the potassium cations coordinate to the bridging N_2 and the aryl rings of the ligand. Although the extent of the dinitrogen reduction is not clear from Raman spectroscopy, the experimental N−N bond length (1.215(6) Å) is consistent with reduction to a double bond from the triple bond present in $L^RFeNNFeL^R$. As in this case, experimental attempts by Holland to remove the potassium cations from the complex led to decomposition. Computational studies implied that the iron was reduced by the alkali metal, weakening the N−N bond, but also that the coordination of the potassium cations to the weakened N−N bond was responsible for further dinitrogen reduction. This work demonstrates further evidence that the incorporation of reducing alkali metals could be an important feature in the design of future complexes for nitrogen activation.

Different Group 1 reductants were tested for the synthesis of **4(*m*′TP^m)**. Unsurprisingly, it was found that an excess of potassium metal also yielded **4(*m*′TP^m)**. Excess potassium was added as a single small lump to a toluene solution of **[{U(*m*TP)}$_2$]**, **3(*m*TP^m)**, at −30 ° C. Overnight, the reaction mixture changed from green to dark red in colour and **4(*m*′TP^m)** was recovered in 65 % yield.

Addition of caesium metal (Cs/Cs^+ potential = −3.026 V vs. SHE)[36] (excess) to a toluene solution of **[{U(*m*TP)}$_2$]**, **3(*m*TP^m)**, yields a dark red solid, insoluble in toluene or other hydrocarbon solvents, preventing full characterisation. Interestingly, Mazzanti noted that potassium reductants resulted in greater solubility of **BI** and its precursor complexes compared to the analogous caesium compounds, allowing for more controlled reactivity.[19]

Another feature **4(*m*′TP^m)** has in common with **BI** is the side-on bridging manner in which the N_2 is bound. As discussed in Chapter 1, the nucleophilicity of bound dinitrogen, and

accordingly its availability for further reactions, is determined by the manner in which it is coordinated. Whilst it has already been established that side-on bridging N_2 complexes of early transition metals are nucleophilic,[37] these early examples prove that the same is true for uranium, particularly given the direct protonation of activated N_2 in this case. To date, direct functionalisation of N_2 by any *f*-element compound is unprecedented, and the intramolecular C−H activation observed in this case is unique.

2.11 Further N_2 functionalisation

As explained above, this unique reactivity results from the migration of H atoms from the ligand to the Lewis basic N_2 during the course of the reduction. More commonly, external electrophiles are added to nitrogen complexes to afford functionalisation. In many cases the functionalised nitrogen ligand remains bound to the metal complex, but judicious choice of reagents can completely quench M−N bonds with the release of new organonitrogen products. Several examples of N−H[19,38–40] and N−Si[41–44] bond formation are known, whilst N−C bond formation remains more challenging.[45–47] Reactions of **[K_4{U(*m*'TP)(NH)}$_2$], 4(*m*'TP^m)**, to target further N_2 functionalisation are presented below.

2.11.1 N–H bond formation

The formation of N−H bonds to give N_xH_y products, most commonly ammonia, represents the most fundamental target of dinitrogen functionalisation. Industrially, the number of moles of ammonia produced exceeds that of any other compound.[48]

In almost all cases N−H bond formation from metal dinitrogen complexes is proposed to proceed *via* a series of electron and proton transfer steps rather than *via* H atom transfer from a hydrogen atom source known as proton-coupled electron transfer (PCET).[49,50]

Both routes were investigated to target N−H bond formation from **4(*m*'TP^m)**.

2.11.1.1 N–H bond formation *via* electron and proton transfer

Mazzanti and coworkers were able to liberate NH_3 as (NH_4Cl) from [K_3{[U(OR)$_3$]$_2$(μ-N)(μ-η^2:η^2-N_2)}], **BI**, (R = Si(O^{t}Bu)$_3$) in 25 % - 42 % yield using excess [PyH]Cl as a proton source.[19]

20 equivalents of [PyH]Cl was added to an orange toluene solution of **4(*m*'TP^{m})** at room temperature and stirred for half an hour. A pale-yellow supernatant was isolated from a colourless solid *via* filtration. The solid was washed three times with thf to remove unreacted [PyH]Cl, and then dried and dissolved in d_6-DMSO (Scheme 2-10).

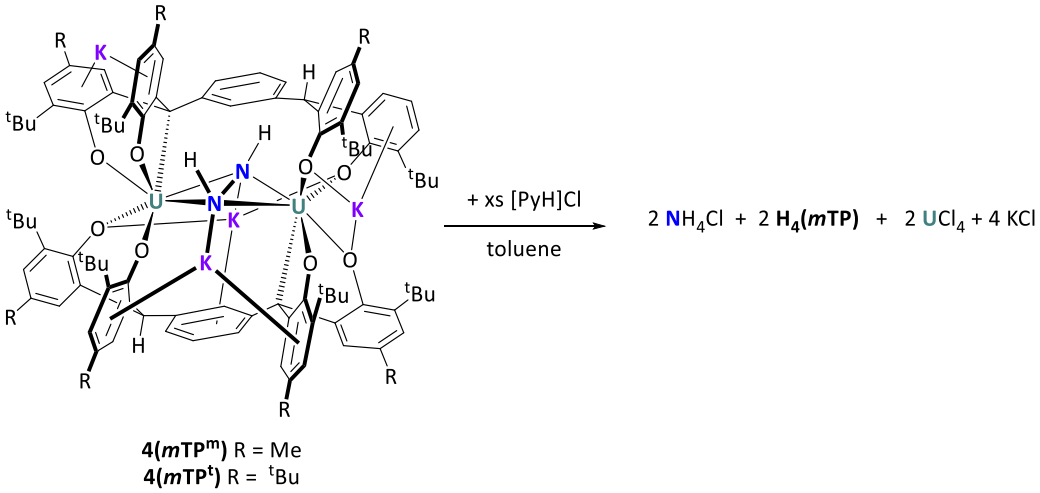

Scheme 2-10 Quenching of **4(*m*'TP^{m})** to yield NH_4Cl.

Analysis by ^{1}H NMR spectroscopy shows free pyridine, and a 1:1:1 triplet resonance at 7.42 ppm ($^{1}J_{NH}$ = 51 Hz). This signal is assigned to NH_4Cl with the splitting pattern consistent with the N nuclear spin, I(^{14}N), equal to one. This quenching reaction was repeated using **^{15}N-4(*m*'TP^{m})**, to yield $^{15}NH_4Cl$, observed by ^{1}H NMR spectroscopy as a doublet at 7.42 ppm ($^{1}J_{NH}$ = 73 Hz, I(^{15}N) = 0.5). The spectra are overlaid in Figure 2-22.

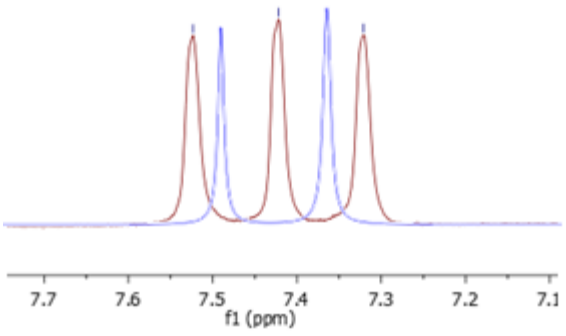

Figure 2-22 ^{1}H NMR spectra (500 MHz, d_6-DMSO) red: [PyH]Cl quenched sample of **4(*m*'TP^{m})** showing a triplet resonance at 7.42 ppm ($^{1}J_{NH}$ = 51 Hz, I(^{14}N) =1) for NH_4Cl, blue: [PyH]Cl quenched sample of **^{15}N-4(*m*'TP^{m})**, showing a doublet at 7.42 ppm ($^{1}J_{NH}$ = 73 Hz, I(^{15}N) =0.5) for $^{15}NH_4Cl$.

The yield of ammonium chloride was determined from several independent reactions using quantitative NMR spectroscopy with dimethylsulfone as an internal standard and was found to vary between 43 % and 11 % per uranium centre. It is proposed that the additional electron required to cleave the N−N single bond comes from the reductive disproportionation of the N_2H_2 ligand, (3 N_2H_2 → 2 N_2 + 2 NH_3). This would limit the maximum yield of NH_4Cl to 66 %. This procedure was repeated using **4(*m*'TP^t)**, yielding NH_4Cl in a 52 % yield.

In order to determine the origin of the NH_4Cl protons, the quenching reaction was repeated using [PyD]Cl (Scheme 2-11). Assuming that one of the protons originates from the N−H bond in **4(*m*'TP)** and the three remaining protons are provided by the added acid to yield NHD_3Cl, the expected ^{1}H NMR spectrum according to 2nI + 1, (I(^{2}H) = 1, I(^{14}N) =1), should contain a triplet of septets and the expected ^{2}H (I(^{1}H) = ½) spectrum should contain a triplet of doublets. Unfortunately, poorly resolved multiplets at 7.12 ppm are observed in both spectra, making conclusions difficult.

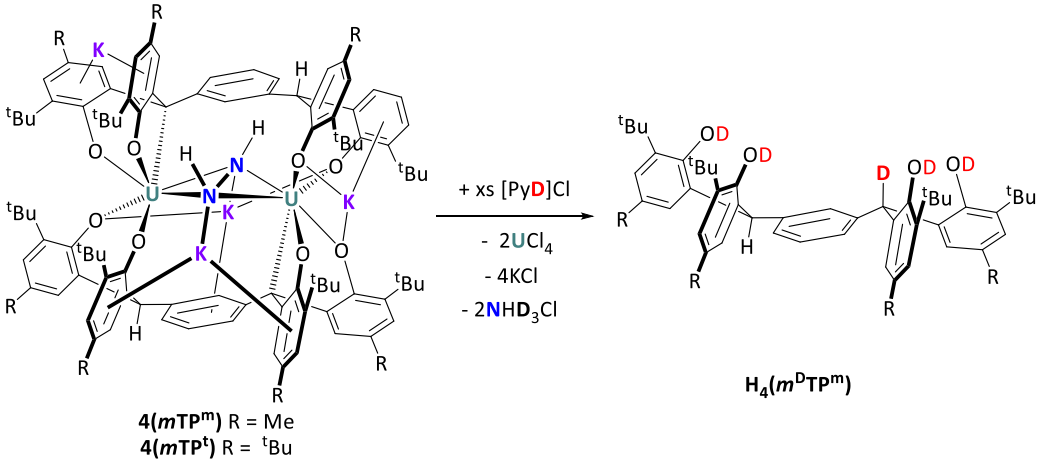

Scheme 2-11 Quenching of **4(*m*'TP^m)** to yield NHD_3Cl and **H$_4$(*m*^{D}TP^m)**.

The supernatant was analysed by ^{1}H and ^{2}H NMR spectroscopy which showed free ligand with complete substitution of the phenol protons for deuterium, and partial substitution of the benzylic protons for deuterium. This result is consistent with a 50 % conversion to **H$_4$(*m*^{D}TP^m)** (Scheme 2-11) indicating that the U−C bonds in **4(*m*'TP)** are quenched during the reaction, reinstating the benzylic H/D atom.

Although the release of NH_4Cl is promising, the decomposition of **4(*m*'TP)** into its constituent ligands makes catalytic turnover impossible. Accordingly, a weaker proton source allowing

ammonia generation from **4(*m*'TP)** whilst leaving the parent **3(*m*TP)** intact for further reductions was sought.

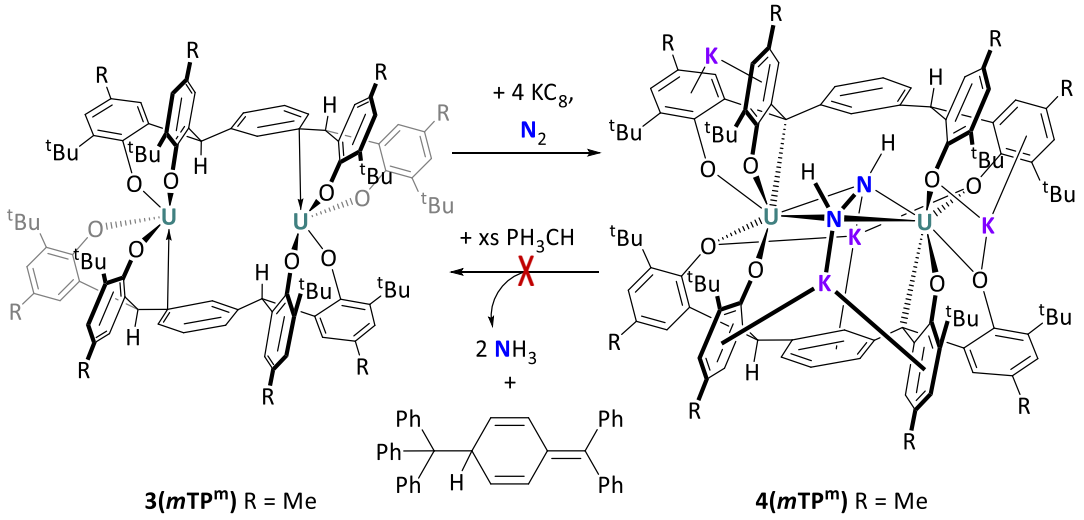

Scheme 2-12 Reaction to target release of NH_3 and Gomberg's dimer *via* treatment of **4(*m*'TP^m)** with PH_3CH.

Ph_3CH (pK_a = 33) was investigated as a source of protons. A toluene solution of **4(*m*'TP^m)** was treated with 20 equivalents of Ph_3CH (Scheme 2-12). No reaction was observed after an hour at room temperature but a new paramagnetic species was observed by ^{1}H NMR spectroscopy after two weeks at 60 °C. No NH_3 was observed in ^{1}H NMR spectra and no evidence of Gomberg's dimer,[51] which would indicate formation of triphenylmethyl radicals during the course of the reaction, was seen. The paramagnetic species has not been isolated or characterised, but it indicates that **3(*m*TP)** is not being reformed in the reaction.

Et_3NHBPh_4 (pK_a = 9) has been known to afford selective and well-defined reprotonation to reverse ligand metalation by Th(IV) in [M(L^{-2H})U(R)] (M = Th, R = CH_2Ph, L = *trans*-calix[2]benzene[2]pyrrolide) to yield [(L)Th(R)][BPh_4].[52] Ten equivalents of Et_3NHBPh_4 were added to a solution of **4(*m*'TP)** in toluene at –30 °C (Scheme 2-13). A slow colour change from dark red to green was observed, and the reaction mixture was allowed to stir overnight before being filtered. The ^{1}H NMR spectrum of the green filtrate revealed regeneration of **3(*m*TP)**. The ^{1}H NMR spectrum of the remaining colourless solid in d_6-dmso is consistent with unreacted Et_3NHBPh_4. No NH_4BPh_4 was present in the isolated solids or in solution, and it was therefore assumed that the bound nitrogen had been protonated and liberated as ammonia gas, NH_3. NH_3 is partially soluble in toluene and may be seen by ^{1}H NMR spectroscopy,[53]

although in this case, no quadrupolar NH_3 resonance could be clearly resolved in solution due to the broad paramagnetic resonances resulting from **3(*m*TP)** and trace **4(*m'*TP).**

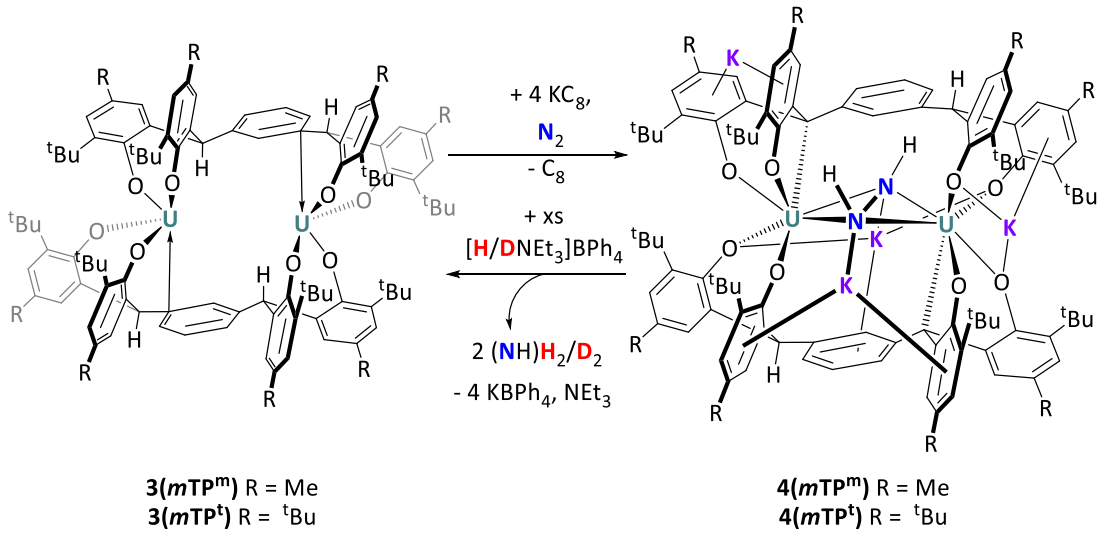

Scheme 2-13 Synthesis of NH_3 /NHD_2 and NH_4Cl from **4(*m'*TP)**.

To assist in detection of NH_3 by NMR spectroscopy, the deuterated acid, $Et_3N\mathbf{D}BPh_4$, was synthesised. NHD_2 was clearly visible by ^2H NMR spectroscopy as a broad resonance with unresolved splitting at −0.06 ppm when the reaction was repeated using $Et_3N\mathbf{D}BPh_4$. C_6D_6 was added as an internal standard so that the NHD_2 yield could be measured. The yield was calculated as 14 % (per U), increasing to 27 % (per U) when excess K metal instead of KC_8 was used as the reductant, in the presence of 30 equivalents of $Et_3N\mathbf{D}BPh_4$. These experiments provide confirmation of the production of ammonia but are not thought to represent actual yields due to the low solubility of ammonia in toluene and the significant broadening effects of the quadrupolar ^{14}N nucleus on NH_3 ^1H resonances.

As a more accurate method of measuring NH_3 yield, the gas was vacuum transferred into a solution of 2M HCl to yield solid NH_4Cl. The yield was calculated 64 % per U as an average of the yield calculated gravimetrically and by quantitative NMR spectroscopy.

Whilst a 64 % yield of ammonia is competitive with other stoichiometric processes,[19] a growing number of systems have accomplished catalytic conversion of dinitrogen to NH_3, and recently TONs in excess of 100 have been reported using a dinitrogen-bridged dimolybdenum complex, [{Mo(N_2)$_2$(Me-Bim-PCP)}$_2$(μ-N_2)] (**AS**), as described in Chapter 1, Scheme 2-14.[54]

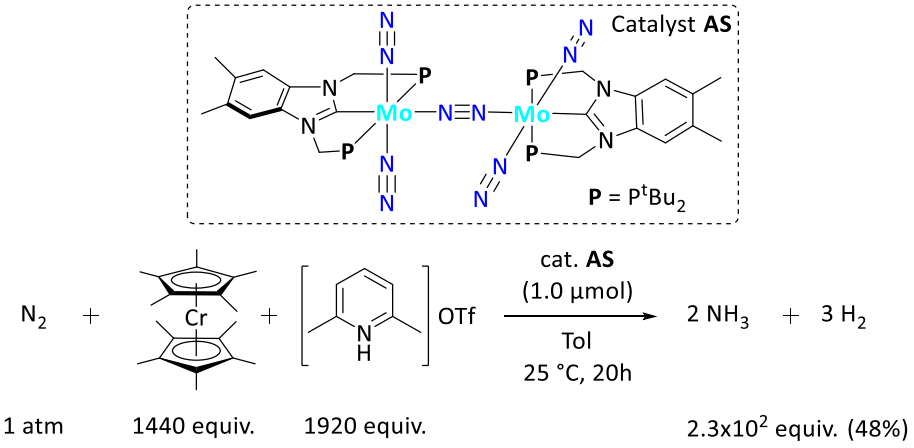

Scheme 2-14 Catalytic NH_3 production using [{Mo(N_2)$_2$(Me-Bim-PCP)}$_2$(µ-N_2)], **AS**.[54]

In the present case, despite Et_3NHBPh_4 closing a catalytic cycle by returning **3(*m*TP)** from **4(*m*'TP)**, the system cannot turnover as control reactions have shown that Et_3NHBPh_4 reacts with the reductants KC_8 and K metal at room temperature in organic solvents to evolve hydrogen gas and form $KNEt_3BPh_4$.

Nishibayashi and coworkers used lutidinium triflate as a proton source for NH_3 generation from [{Mo(N_2)$_2$(Me-Bim-PCP)}$_2$(µ-N_2)] (Scheme 2-14).[54] Therefore, lutidinium was investigated as source of protons. This reaction was carried out by Dr Rory Kelly in the Arnold group. Treatment of **4(*m*'TP)** with 20 equivalents of [lutH][BPh_4] failed to regenerate **3(*m*TP)** and no NH_4Cl was present in ^{1}H NMR spectra following acidification of the volatiles with 2M HCl. To date no compatible reductant and proton source have been found and turnover of NH_3 from **4(*m*'TP)** has not been achieved.

Table 2-5 summarises results of the reduction and proton transfer reactions described in Section 2.11.1.1, and includes reactions performed by Dr Tatsumi Ochiai in the Arnold group on the analogous throrium compounds **3Th(*m*TP^m)** and **3Th(*m*TP^t)** for comparison (entries 9 and 10).

Entry	Compound	Reduct-ant[a]	Solvent	Acid (equivs)	Major products[b]	Comment
1	**3(*m*TP^m)**	KC_8	benzene	[PyH]Cl (20)	NH_3 (as NH_4Cl), 11 - 43 %	NH_3 release by addition of strong acids decomposes the complex.
2	**3(*m*TP^m)**	KC_8	benzene	$[HNEt_3][BPh_4]$ (10)	**3(*m*TP^m)** (quant.), NH_3, 64 %	Shows catalytic turnover is possible since NH_3 can be released with weak acid and the metal complex reformed.
3	**3(*m*TP^m)**	KC_8	toluene	$[DNEt_3][BPh_4]$ (10)	**3(*m*TP^m)** (quant.), ND_2H[c,d] 14%	Confirms the source of each proton.
4	**3(*m*TP^m)**	K	benzene-d_6	$[DNEt_3][BPh_4]$ (10)	**3(*m*TP^m)** (quant.), ND_2H[c,d] 27 %	Confirms that one hydrogen derives from the ligand benzylic groups.
5	**3(*m*TP^t)**	KC_8	toluene	[PyH]Cl (6)	**3(*m*TP^t)** (quant.), NH_3 (as NH_4Cl), 52 %	Shows that ligand modification has little effect on reactivity.
6	**3(*m*TP^t)**	Na	benzene	$[HNEt_3][BPh_4]$ (40)	No NH_3 production.	Shows that K ions are important in **4(*m*′TP)** structure.
7	**3(*m*TP^m)**	KC_8	toluene	Ph_3CH (20)	New unknown product.	Shows that Ph_3CH does not release NH_3.
8	**3(*m*TP^m)**	KC_8	toluene	$[lutH][BPh_4]$ (20)	No NH_3 production.	Shows $[lutH][BPh_4]$ is not a suitable proton source.
9	**3Th(*m*TP^t)**	KC_8	toluene	[PyH]Cl (6)	NH_3 (as NH_4Cl), 57 %	Confirms generality of metal/ligand architecture.
10	**3Th(*m*TP^m)**	KC_8	toluene	[PyH]Cl (6)	NH_3 (as NH_4Cl), 45 %	Confirms generality of metal/ligand architecture.

[a] Present in excess, as solid. [b] Yield measured gravimetrically (for NH_3 as ammonium salt), and by integration of NMR spectra against an added, internal standard. [c] deuterium-incorporated analogue. [d] Quoted yield is artificially low as only NH_3/ND_2H dissolved in toluene was measured in the NMR sample.

Table 2-5 Summary of results from Section 2.11.1.1.

2.11.1.2 N–H bond formation *via* hydrogen atom transfer (HAT)

It was recently reported by Mock and coworkers that ammonia formation from the chromium complex, $[Cr(N_2)_2(PPh_4NBn_4)]$, could be achieved through reaction with the hydrogen atom donor, TEMPO-H (2,2,6,6-tetramethyl-1-hydroxypiperidine).[49] Under the right experimental conditions, a hydrogen atom donor provides the concerted transfer of protons and electrons, i.e. proton coupled electron transfer (PCET). Peters and coworkers have fond that the performance of their Fe catalyst, P_3BFe^+ (P_3B = tris(*o*-diisopropylphosphinophenyl)-borane) for ammonia production from N_2 can be improved when $[Cp^*_2Co]$ and $[Ph_2NH_2][OTf]$ are used as the reductant and proton source respectively (TONs up to 84).[55] Previous reports had employed stronger reductants and acids (KC_8 and $[H(OEt_2)_2][BAr^F_4]$) and had achieved lower TONs (up to 64) for the same catalyst[56]. This result was rationalised by experimental and computational studies suggesting that protonated decamethylcobaltocene acts as discrete PCET reagent during the catalytic cycle, increasing the efficiency of the system. This led Peters to suggest that PCET pathways may be operative in other previously reported N_2 reduction systems in which metallocene reductants have been used.[38,54,57]

The PCET pathway, which has the potential to deliver NH_3 from dinitrogen using much lower chemical overpotentials, is in contrast to the separated electron transfer and proton transfer (ET-PT) that has been widely suggested in mechanistic studies of almost all other stoichiometric and catalytic N–H bond forming reactions.

Given that the use of protic reagents as described in Section 2.11.1.1 was shown to prevent catalytic turnover through unwanted reactivity with reducing species, N–H bond formation by hydrogen atom transfer may present a useful alternative strategy to target catalytic turnover.

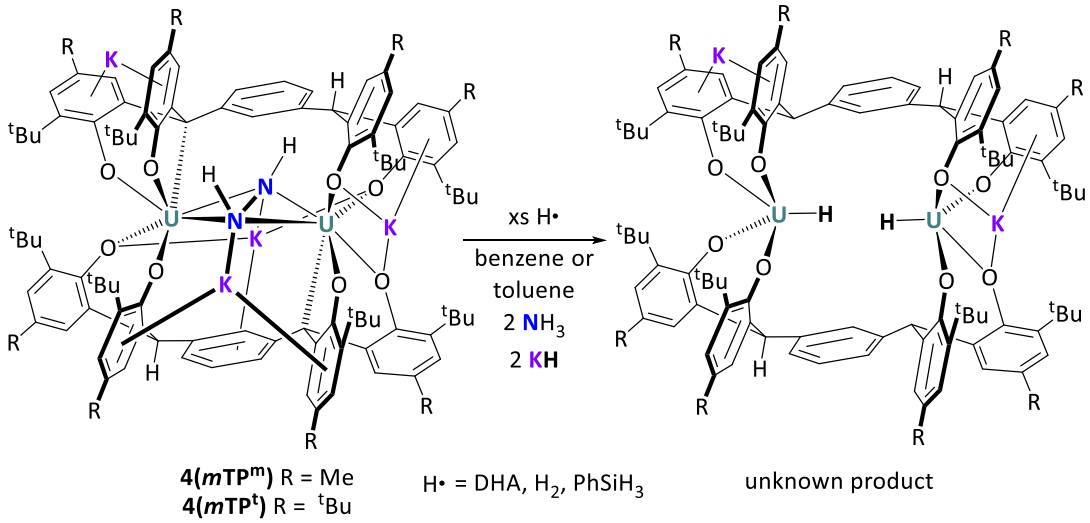

Scheme 2-15 Reactions to target catalytic NH_3 production *via* hydrogen atom transfer to **4(*m*'TP)**.

The reactivity of **4(*m*'TP^m)** with the hydrogen atom donor DHA (9,10-dihydroanthracene) was investigated. The bond dissociation energy of the aliphatic carbon–hydrogen bonds in DHA is 77 Kcal mol^{-1} (cf 105 kcal mol^{-1} for the aliphatic C–H bond in methane), with the release of H_2 providing stable, aromatic anthracene.[58] To a toluene or benzene solution of **4(*m*'TP^m)**, 100 equivalents of DHA were added at room temperature and the resulting suspension was stirred overnight in a sealed ampoule. Vacuum transfer of the resulting volatiles onto a 1.25 M HCl solution provided a colourless precipitate of NH_4Cl in 24 % yield (from C_6H_6) or 25 % (from toluene) which was measured independently by quantitative ^{1}H NMR spectroscopy using dimethylsulfone as an internal standard. The substoichiometric yield of ammonia indicates that **4(*m*'TP^m)** is not catalytically active under these conditions.

To investigate H_2 as a hydrogen atom source a mixture of 5% H_2 in N_2 was added to a benzene solution of **3(*m*TP^m)** containing an excess of potassium metal**.** The reaction mixture was immediately frozen and degassed before the ampoule was charged with one atmosphere of the gas mixture (approximately ten molar equivalents of H_2 per **3(*m*TP^m)** from the ideal gas law). After stirring overnight at room temperature, and transfer of the volatiles onto HCl, the yield of NH_4Cl (49 %) was determined using the procedure described above. Reactions were attempted using higher pressures of 5% H_2/N_2 (2 bar, 10 bar) along with excess reductants to target catalytic turnover. Yields of 23 % and 24 % were determined by acidification to yield NH_4Cl, indicating that **4(*m*'TP^m)** is not catalytically active under these conditions and the higher pressures may in fact be detrimental to NH_3 yield.

The absence of catalytic turnover indicates that following release of NH_3, **4(*m*'TP^m)** forms a new species which is not susceptible to further reduction and release of NH_3. A hydride species is proposed in Scheme 2-15, although attempts to characterise this species were not successful, and the mechanism by which it forms remains unclear. It is noted however, that all yields reported in Table 2-6 are under 50 %, suggesting that reductive disproportionation of the bound $[N_2H_2]^{2-}$, giving equimolar quantities of N_2 and NH_3, could be a key step in the mechanism of NH_3 release.

Table 2-6 summarises hydrogen transfer reactions of **4(*m*TP)**.

Entry	Compound	Reductant	Solvent	H reagent (equivs)	Major products[a]	Comment
1	**4(*m*'TP^m)**		benzene	DHA (100)	NH_3, 47%	Shows that H atom transfer can provide NH_3.
2	**4(*m*'TP^m)**		toluene	DHA (100)	NH_3, 25%	Shows that choice of solvent is not important.
3	**3(*m*TP^m)**	K	benzene	H_2 [b]	NH_3, 49 %	Shows that H_2 gas can act as H atom source to provide NH_3.
4	**3(*m*TP^m)**	K	benzene	H_2 [c]	NH_3, 23 %	Shows that higher pressures of H_2 gas may be detrimental to yield.
5	**4(*m*'TP^m)**		toluene	$PhSiH_3$	**4(*m*'TP^m)**	**4(*m*'TP^m)** does not react with $PhSiH_3$.

[a] Yield of measured gravimetrically (for NH_3 as ammonium salt), and by integration of NMR spectra against an added, internal standard. [b] one atm, 5% in N_2. [c] 2 bar, 5% in N_2.

Table 2-6 Summary of results from Section 2.11.1.2.

2.11.2 Reactions to target N–C bond formation

A well-understood mechanism for catalytic N–C bond formation from a well-defined molecular dinitrogen complex has not yet been reported, despite attempts from the groups of Hidai, Holland, Chirik and others.[45,59,60] Frequently, C-electrophiles can be bonded to activated dinitrogen, but cleavage and catalyst regeneration remain challenging.

For example, as described in Chapter 1, Holland and coworkers have reported the treatment of the iron nitride complex **AZ,** $[(L_3Fe_3N_2)(\mu\text{-}KCl)_2(FeL)]$ (L = 2,4-bis(2,6-dimethylphenylimido)-3-methylpentyl) with MeOTs to form a new N–CH_3 bond in $[(LFe^{III})_2(LFe^{II})(\mu\text{-}N)(NCH_3)]$, **BB**. Further alkylation of the N atom to liberate $N(R)_3$ from the metal complex however was not achieved.[45]

The reactivity of **4(*m*'TP^m)** with electrophilic carbon reagents was therefore investigated. Reactions with methyl and *tert*-butyl iodide or triflate provided new paramagnetic products cleanly according to analysis by ^{1}H NMR spectroscopy, with no **4(*m*'TP^m)** remaining. No new products were observed in the diamagnetic region, however, indicating that if dinitrogen has been alkylated, the new organonitrogen products remain bound to the paramagnetic uranium complex, even in the presence of up to six equivalents of electrophile. Single crystals of the paramagnetic products could not be obtained from the reactions. To investigate the identity of the complexes, the reactions were quenched with excess HCl to yield free ligand. Isolation of the ligand and analysis by ^{1}H NMR spectroscopy indicates that alkylation of the benzylic position of **H_4(*m*TP)** had been afforded *via* quenching of the U–C bonds in **4(*m*'TP^m)** (Scheme 2-16).

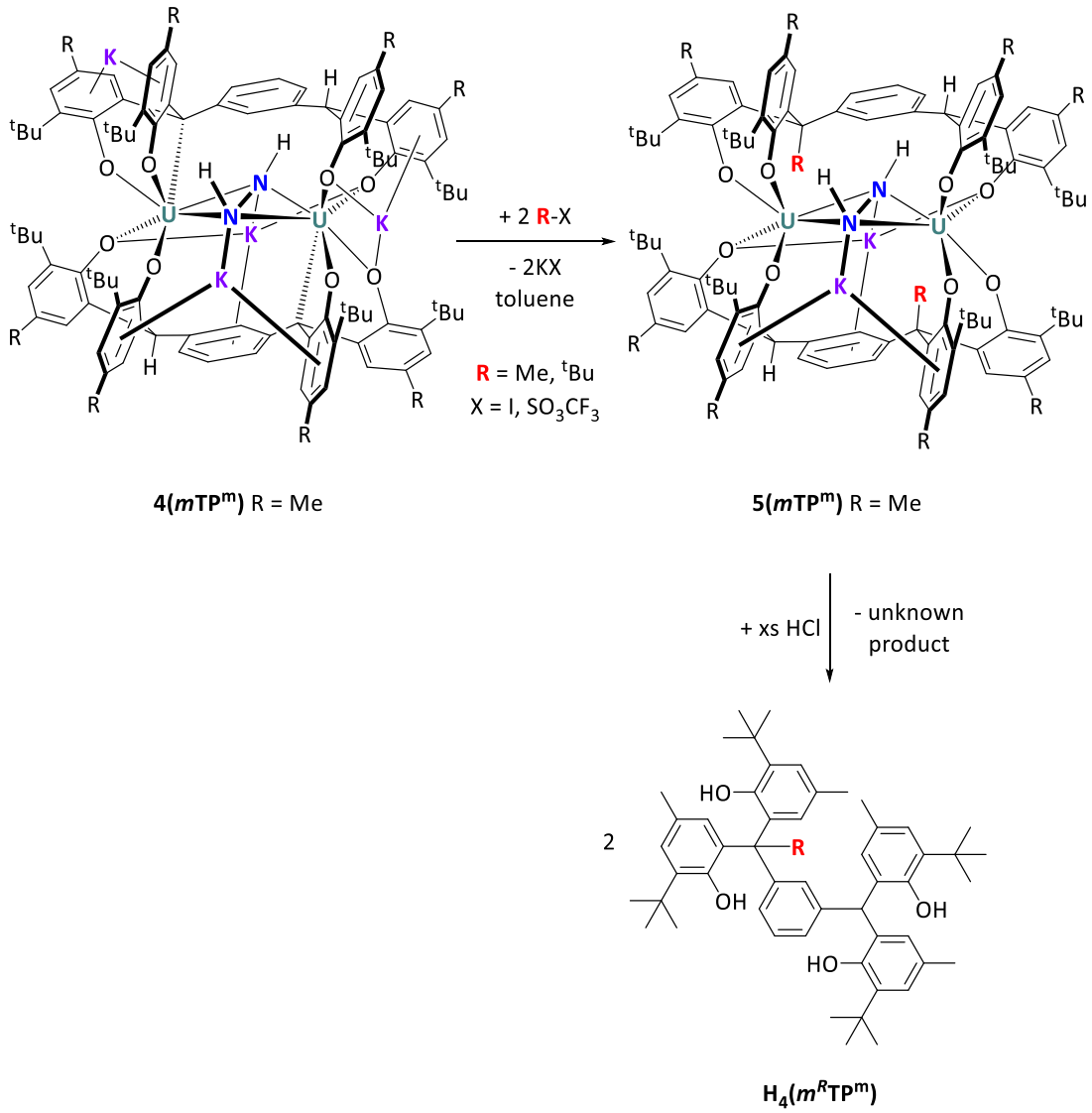

Scheme 2-16 Akylation of ligand benzylic positions.

Given that electrophilic carbon reagents appear to preferentially alkylate the ligand framework, reactivity with unsaturated nucleophilic reagents was investigated.

In a seminal study, Fryzuk reported a series of N–C bond forming reactions exploiting the reactivity of terminal alkynes with a dinuclear zirconium side-on bound dinitrogen complex. $([P_2N_2]Zr)_2(\mu\text{-}\eta^2\text{:}\eta^2\text{-}N_2)$ (where $[P_2N_2]$ = $PhP(CH_2SiMe_2NSiMe_2CH_2)_2PPh$) was treated with a slight excess of phenylacetylene. After one week the reaction yielded the functionalised product $([P_2N_2]Zr)_2(\mu\text{-}\eta_2\text{:}\eta_2\text{-}N_2CCPh)(\mu\text{-}CCPh)$ in which one equivalent of acetylide bridges between the two zirconium centres *via* the terminal carbon atom, and a second equivalent is bound to one of the nitrogen atoms. This transformation was proposed to proceed *via* an initial cycloaddition of alkyne across a Zr–N bond to provide a zircona-aza-cyclobutene

intermediate that subsequently undergoes cleavage of the Zr−C bond by protonation with the second equivalent of alkyne (Scheme 2-17).[61]

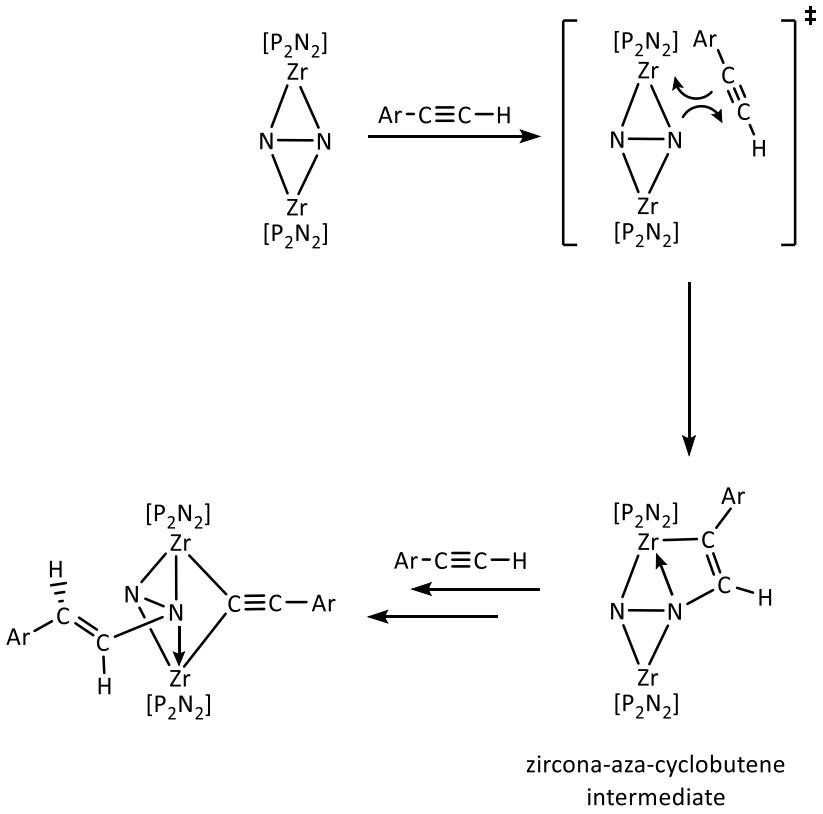

Scheme 2-17 Proposed mechanism of reaction between phenylacetylene and $([P_2N_2]Zr)_2(\mu\text{-}\eta^2\text{:}\eta^2\text{-}N_2)$.[61]

4(*m*'TP^m) was reacted with six equivalents of phenyacetylene to target N−C bond formation. A mixture of paramagnetic products were observed by ^{1}H NMR spectroscopy. These were not successfully isolated or characterised. It is proposed that the sterically protected cavity in which N_2 is bound within **4(*m*'TP^m)** may prevent the initial cycloaddition step from proceeding cleanly.

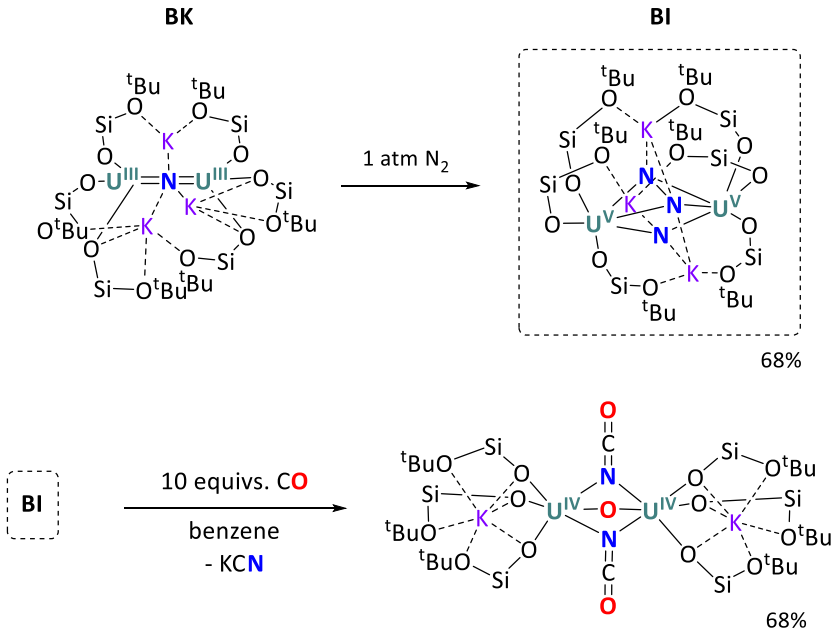

Scheme 2-18 Reaction of **BI** with CO to yield $[K_2\{[U(OR)_3]_2(\mu\text{-}O)(\mu\text{-}NCO)_2\}]$, ligand OR groups emitted for clarity.[29]

Mazzanti and coworkers reported formation of N−C bonds *via* reaction of $[K_3\{[U(OR)_3]_2(\mu\text{-}N)(\mu\text{-}\eta^2\text{:}\eta^2\text{-}N_2)\}]$, **BI**, with ten equivalents of CO at room temperature to afford the U(IV)/U(IV) oxo/cyanate complex $[K_2\{[U(OR)_3]_2(\mu\text{-}O)(\mu\text{-}NCO)_2\}]$ (R = $Si(O^tBu)_3$) in 68 % yield. Insertion of a bridging oxo between the two uranium centres in addition to N−CO bond formation was confirmed by XRD as well as NMR analysis (Scheme 2-18).

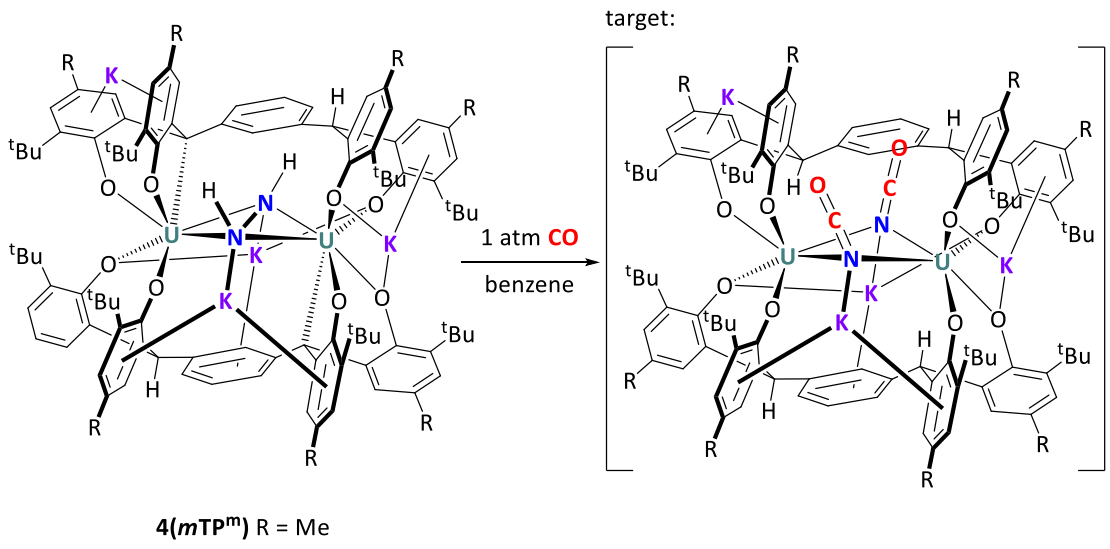

4(*m*TP^m) R = Me

Scheme 2-19 Reaction to target cyanate formation *via* treatment of **4(*m*'TP^m)** with CO.

4(*m*'TP^{m}) was dissolved in benzene and exposed to one atmosphere of CO. No colour change was observed but ^{1}H NMR spectroscopy indicated complete consumption of **4(*m*'TP^{m})** and formation of a new paramagnetic product. The small scale of the reaction prevented the collection of further characterisation data, so the identity of the product, shown in Scheme 2-19 as the proposed double cyanate complex, cannot be unambiguously assigned.

2.11.3 N–Si bond formation

As described in Chapter 1, a bound –N=NSiMe$_3$ fragment was formed, following N_2 silylation mediated by the Fe complex, Si(PhP^{i}Pr$_2$)$_3$Fe–N_2, **AW**, described by Peters and co-workers.[62] Additionally, several Mo and Co complexes have been shown to afford catalytic silylation of dinitrogen, yielding the silylamine, N(SiMe$_3$)$_3$, achieving turnover numbers of over 100. These are described in detail in Section 1.5.2.[43,57,63]

Stoichiometric reactions of **4(*m*'TP^{m})** with Me$_3$SiI (six equivalents), did not result in any new Si-containing products according to ^{29}Si(INEPT) NMR spectra (entry 1, Table 2-7). When this reaction was repeated using Me$_3$SiCl, partial conversion to a new product was observed by ^{29}Si(INEPT) NMR, with a singlet resonance at 2.01 ppm. Corresponding to a resonance in the ^{1}H NMR spectrum at 0.06 ppm, this product was assigned as HN(SiMe$_3$)$_2$, resulting from the silylation of the diazenido $[N_2H_2]^{2-}$ ligand in **4(*m*'TP^{m})**, and cleavage of the N−N bond affording an overall hydrosilylation of dinitrogen to give the secondary amine (Scheme 2-20) (entry 2, Table 2-7). This unprecedented reactivity is enabled by the initial transfer of hydrogen atoms from ligand C–H bonds to the activated N_2 fragment described in Section 2.6.

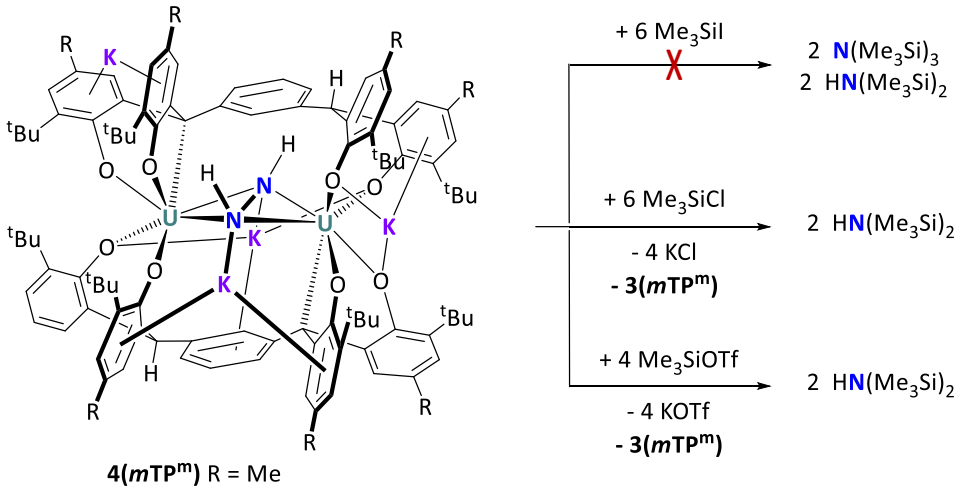

Scheme 2-20 Hydrosilylation of dinitrogen mediated by **4(*m*'TP^{m})**.

Reactions of a large excess of Me_3SiX (X = Cl, I) (40 equivalents) and KC_8 (40 equivalents) with **3(*m*TP^m)** were carried out to target catalytic silylation of nitrogen *via* **4(*m'*TP^m)** (entry 3, Table 2-7). The reactions were monitored over 14 days but in both cases the only Si containing product observed was identified as $(Me_3Si)_2$ by ^{29}Si(INEPT) and ^{1}H NMR spectroscopy and GCMS. Several previous reports of this product describe how generation of $SiMe_3$ radicals in solution by alkali metal reductants (Scheme 1-18) can lead to such homocoupled (Si−Si) products, competing kinetically with nitrogen silylation processes.[49] A control reaction between KC_8 and Me_3SiI was carried out and confirmed that the coupling reaction was observed in the absence of **3(*m*TP^m)** (control reaction, Table 2-7). Other authors, including Nishibayashi and coworkers, have shown experimentally and theoretically that Me_3SiX slowly generates disilane $Me_3SiSiMe_3$ in the presence of K and Na metals, even in the absence of any other metal complexes.[57]

In order to slow down the competing radical coupling reaction, an excess of potassium metal was used instead of 40 equivalents of the reductant KC_8. Additionally, reactions were carried out at –30 °C. Although providing the same reduction potential, the reduced surface area and the insolubility of a single lump of potassium metal provides a greater kinetic barrier to reaction. Treatment of **3(*m*TP^m)** with potassium metal and Me_3SiCl or Me_3SiI (40 equivalents) (entries 4 and 5, Table 2-7) over two days afforded substochiometric amounts of $HN(SiMe_3)_2$ in addition to smaller quantities of the homocoupling product $(Me_3Si)_2$. The volatiles from these reactions were isolated by vacuum transfer and the yield of $HN(SiMe_3)_2$ was measured by integration of the ^{1}H NMR spectra against an added standard of 1,3,5-tri-*tert*-butylbenzene.

With promising stoichiometric hydrosilylation, but no catalytic turnover evident for Me_3SiX where X = Cl or I, the more reactive Me_3SiOTf (OTf = $CF_3SO_3^-$) was investigated (entry 6, Table 2-7). Again, stoichiometric reactions with **4(*m'*TP^m)** yielded $HN(SiMe_3)_2$ in addition to the silyl ether $(Me_3Si)_2O$, which is presumably formed by radical coupling reactions of Me_3SiOTf. Integration of the ^{1}H NMR spectrum against an internal standard of 1,3,5-tri-*tert*-butylbenzene confirms that the two products are present in 33 % ($HN(SiMe_3)_2$) and 11 % ($(Me_3Si)_2O$) yields per metal in the **4(*m'*TP^m)** starting material.

The results from Section 2.11.3 are summarised in Table 2-7.

Entry	Compound	Reductant (equivs)	Solvent	Electrophile (equivs)	Major products (yield) [b]	Comment
1	**4(*m'*TP^m)**		toluene-d_8	$SiMe_3I$ (6)	None	No new Si-containing products.
2	**4(*m'*TP^m)**		toluene-d_8	$SiMe_3Cl$ (6)	$HN(SiMe_3)_2$	Overall hydrosilylation of N_2.
3	**3(*m*TP^m)**	KC_8 (40)	toluene-d_8	$SiMe_3Cl$ (40)	$(SiMe_3)_2$	Radical homocoupling reaction kinetically favourable.
4	**3(*m*TP^m)**	K (xs)	toluene-d_8	$SiMe_3Cl$ (40)	$HN(SiMe_3)_2$ (15 %) $(SiMe_3)_2$	Competing radical homocoupling reaction is now slower.
5	**3(*m*TP^m)**	K (xs)	toluene-d_8	$SiMe_3I$ (40)	$HN(SiMe_3)_2$ (51 %) $(SiMe_3)_2$	Competing radical homocoupling reaction is now slower. $SiMe_3I$ is better than $SiMe_3Cl$
6	**4(*m'*TP^m)**		toluene-d_8	Si Me_3OTf (6)	$HN(SiMe_3)_2$ (33 %) $(SiMe_3)_2O$ (11 %)	
Control 1		KC_8 (40)	toluene-d_8	$SiMe_3I$ (40)	$(SiMe_3)_2$	Product is from homocoupling of $SiMe_3$ radicals.

Table 2-7 Summary of stoichiometric silylation mediated by **4(*m'*TP^m).**

Reactions to target catalytic silylation using Me_3SiOTf were investigated. **3(*m*TP^m)** was treated with 40 equivalents of Me_3SiOTf in the presence of excess potassium metal in toluene and stirred at room temperature for two days. Integration of the resonance at 0.06 ppm in ^{1}H NMR spectra against added 1,3,5-tri-*tert*-butylbenzene suggests that $HN(SiMe_3)_2$ has been formed in 734 % yield per uranium (seven turnovers of **3(*m*TP^m)**), shown in Figure 2-23.

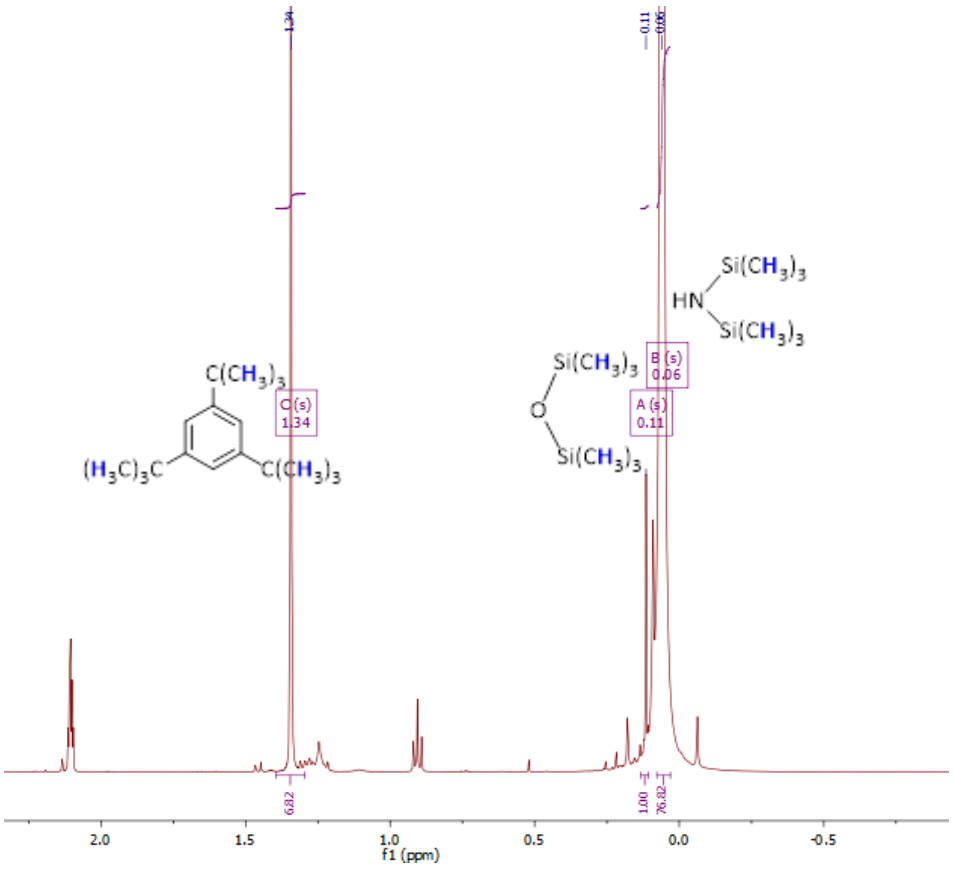

Figure 2-23 ^{1}H NMR spectrum (500 MHz, d_8-toluene) of the $HN(SiMe_3)_2$ formed from reduction of **3(*m*TP^{m})** in the presence of excess K, diamagnetic region only. Resonances are 1.34 internal standard; 0.06 $HN(SiMe_3)_2$; 0.11 $(Me_3Si)_2O$ by-product.

It is noted that whist the resonance at 0.06 ppm is coincident with that of $HN(SiMe_3)_2$, other reactions detailed in Appendix 2, Table A3, that were analysed by quantitative NMR in this way, suggest up to 15 turnovers per metal in **3(*m*TP^{m})**. The maximum number of turnovers possible based on 40 equivalents of $SiMe_3OTf$ is 10. It must therefore be concluded that other side-products have similar NMR spectra and it is not possible to distinguish them unambiguously by ^{1}H NMR spectroscopy. Whilst ^{29}Si INEPT NMR spectroscopy was used to confirm the presence of $HN(SiMe_3)_2$, integration of Si resonances does not correspond to concentration of material in solution because signal intensity is enhanced by polarisation transfer from ^{1}H nuclei. Attempts to corroborate the NMR yields and characterise side-products by GCMS were not successful as the amines were found to hydrolyse in the GC column. There is therefore insufficient evidence at this time to propose catalytic turnover.

Turnover of $HN(SiMe_3)_2$ in the absence of an external proton or radical hydrogen source could be possible if the relatively weak methyl C–H bond of toluene, (experimental bond dissociation energy (25 °C) = 89.9 kcal mol^{-1}, p*K*a = 42 in DMSO)[64,65] present in vast excess as solvent, was able to regenerate the ligand benzylic C–H bond. Regeneration of this C–H bond would allow **3(*m*TP)** to reform so that subsequent equivalents of nitrogen could be reduced and activated by the intramolecular C–H bond, and then react with the incoming $SiMe_3$ radicals, yielding the secondary amine catalytically (Scheme 2-21). Control experiments indicate that **4(*m'*TP)** is stable in toluene at room temperature but possible mechanisms for regeneration of **3(*m*TP)** from toluene in the presence of a reductant and a source of $SiMe_3$ are discussed in Section 2.11.3.1.

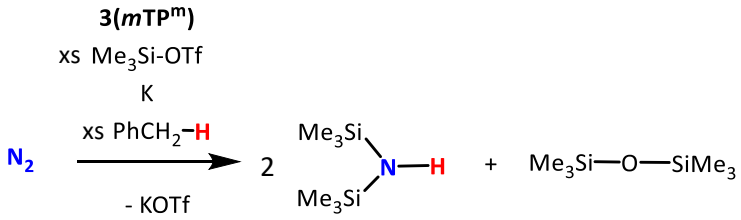

Scheme 2-21 Nitrogen functionalisation by reduction then silylation of **3(*m*TP^m)**.

To investigate the role of toluene, silylation reactions were repeated in C_6D_6. **3(*m*TP)** was dissolved in C_6D_6 and treated with excess potassium metal and 40 equivalents of $SiMe_3OTf$. The reaction mixtures were stirred at room temperature and monitored over 10 days. The homocoupled $Me_3SiOSiMe_3$ was now formed as the major product, with only trace quantities of $HN(SiMe_3)_2$. These reactions were repeated with an added H atom source (DHA, 100 equivalents or H_2, one atmosphere) (Scheme 2-22). $HN(SiMe_3)_2$ was now observed in much larger quantities (~10 turnovers by quantitative ^{1}H NMR spectroscopy) although as explained above, these yields should be treated with caution.

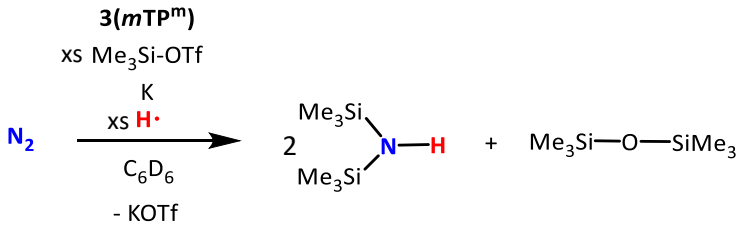

H· = H_2, (1 atmosphere) or DHA (100 equivalents)

Scheme 2-22 Nitrogen functionalisation by reduction then silylation of **3(*m*TP^m)** in C_6D_6.

2.11.3.1 DFT Computational analysis of the mechanism of silylation

Possible mechanisms for the experimentally observed reactivity were investigated. Figure 2-24 shows a computed enthalpy pathway for the silylation of dinitrogen mediated by **4(*m'*TP^m)**.[4]

[4] The computational analyses described in this section were performed by our collaborator Professor Laurent Maron at Université Toulouse, Laboratoire de Physique et Chimie des Nano-objets, Institut National des Sciences Appliquées, France.

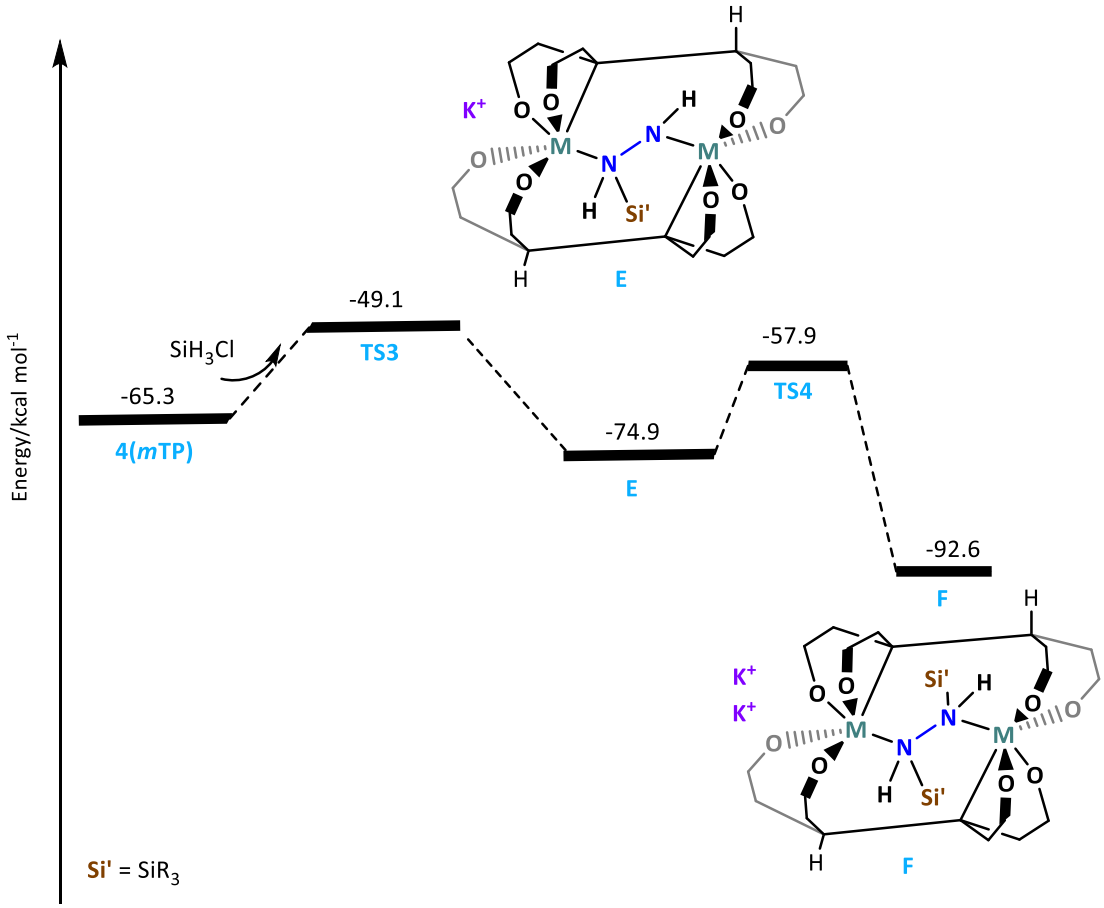

Figure 2-24 Computed enthalpy pathway at room temperature for the silylation of dinitrogen mediated by **4(*m*'TP^{m}).**

The silylation step was computed from complex **4(*m*'TP)**, using SiH_3Cl as a model to reduce the size of the calculation. A transition state was located for the addition of one equivalent of SiH_3Cl to **4(*m*'TP)**, showing the formation of the N(1)–Si(1) bond. The activation barrier was calculated as 16.2 kcal mol^{-1}.

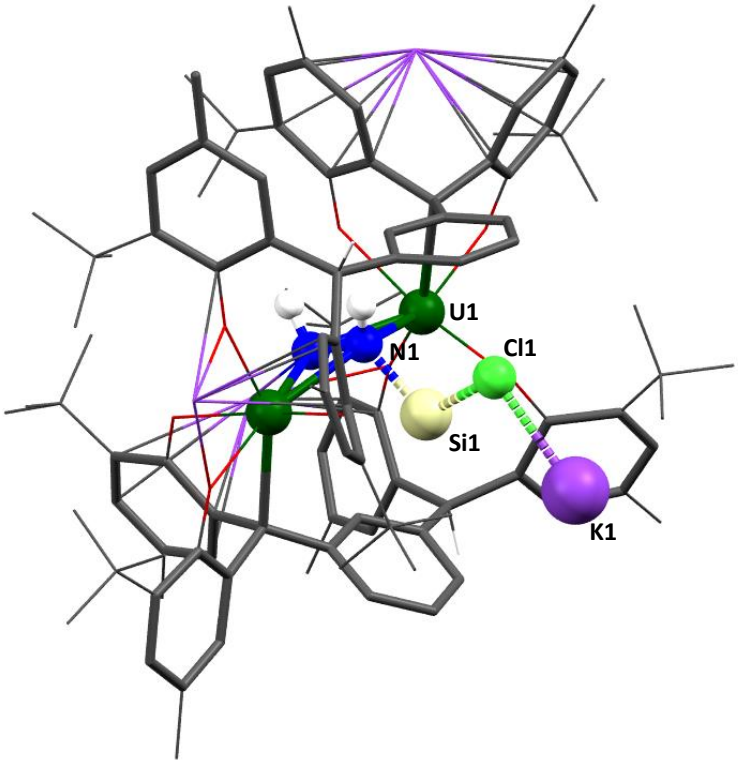

Figure 2-25 Computed structure of **Transition state 3**, showing formation of an N(1)─Si(1) bond.

Transition state 3 is drawn in Figure 2-25 and shows nucleophilic substitution with the bond breaking (Si−Cl bond = 2.20 Å) and bond formation (N−Si bond = 1.90 Å) drawn as dashed lines. The coordination geometry of Si(1) is trigonal bipyramidal with the apical Si−Cl bond being displaced by the equatorial Si−N bond. A potassium chloride interaction with K(1) helps to stabilise the chloride leaving group (K−Cl distance = 2.82 Å), a feature that was also observed in the uranium mediated nitrogen activation chemistry reported by Mazzanti.[29] Completion of the Si−N bond formation provides intermediate **E**.

From intermediate **E**, the second silylation proceeds *via* Transition state 4, (TS4) with an activation barrier of 17.0 kcal mol^{-1}. As in TS3, K(3) now helps to stabilise the departing Cl(2), allowing nucleophilic substitution to yield intermediate **F**. In intermediate **F**, both nitrogen atoms are silylated and the N−N bond remains intact.

If the system is to be rendered catalytic, **3(*m*TP)** must be regenerated. To reform **3(*m*TP)** from **F**, there are two possibilities. In the first possible mechanism (Scheme 2-23), **F** abstracts H from the solvent to yield **G**, in which the benzylic position is reprotonated and the N−N

bond is cleaved. **G** can then react with Me_3SiCl to liberate KCl and $HN(SiR_3)_2$, reforming **3(*m*TP)**.

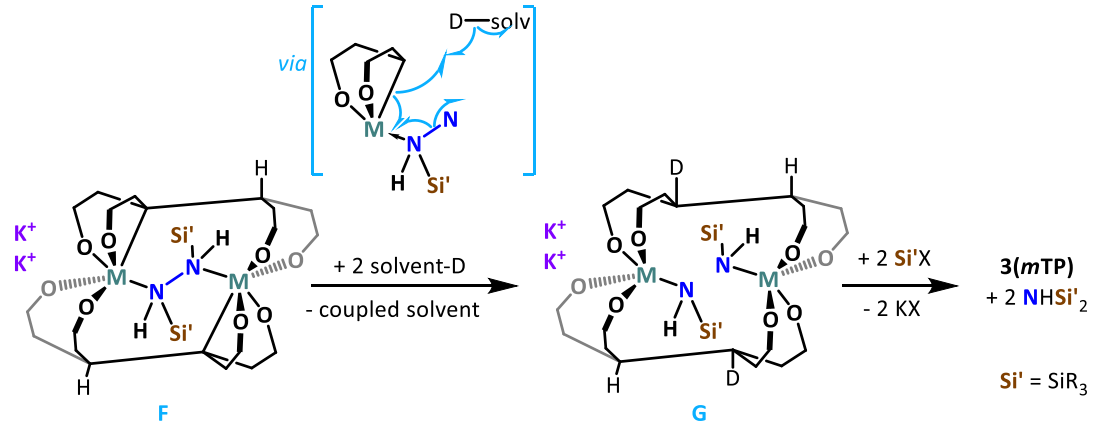

Scheme 2-23 Possible mechanism for the liberation of $HN(SiMe_3)_2$ from intermediate **F** and reformation of **3(*m*TP)**.

Alternatively, **F** may react with two ·SiR_3 radicals (formed from reaction of K and $ClSiR_3$) to yield **I**, in which the U–C bond is conserved and $HN(SiR_3)_2$ acts as a donor to the metal. $HN(SiR_3)_2$ is released either before or after **I** abstracts the final two hydrogen atoms from the solvent to yield K-solvent, and reform **3(*m*TP)** (Scheme 2-24).

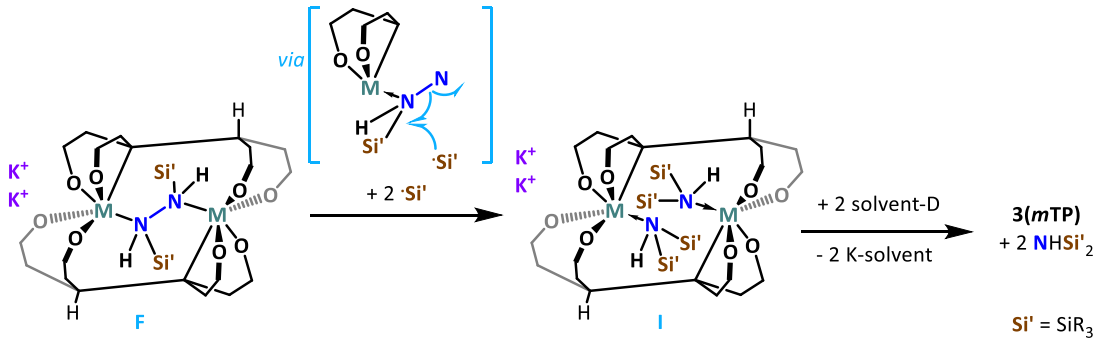

Scheme 2-24 Possible mechanism for the liberation of $HN(SiMe_3)_2$ and reformation of **3(*m*TP)**.

Unfortunately, attempts to confirm the operative mechanism by identifying side products (bibenzyl from solvent radical coupling or potassium benzyl from toluene deprotonation) were not conclusive.

2.12 Synthesis of $[K(thf)_6][U_2(mTP^m)_2K(thf)_2]$, 6(*m*'$TP^m$)

Having identified the mechanistic importance of the benzylic C–H bonds to the reactions described in Sections 2.8–2.11, the independent reactivity of the benzylic hydorgens in the

3(*m*TP) precursors, **H_4(*m*TP)** and **K_4(*m*TP)** was investigated. The pK_a of the benzylic protons in **H_4(*m*TP)** is expected to be close to 30 (pk_a Ph_3CH = 30 in DMSO).[66]

Attempts to functionalise the benzylic positions of **H_4(*m*TP)** or **K_4(*m*TP)** using the strong nucleophilic bases MeLi and BuLi resulted in complex product mixtures. On the other hand, the synthesis of **4(*m*'TP)** demonstrated that the two inward facing benzylic C–H bonds of **3(*m*TP)** can be deprotonated by a nitrogen based lone pair, suggesting that within the 'letterbox' complex, these benzylic hydrogen atoms may become more susceptible to nucleophilic attack.

Potassium benzyl, $C_6H_5CH_2K$ (KBn) should be sufficiently basic to deprotonate these benzylic C–H bonds (p*K*a toluene = 42 in DMSO).[66] Despite this, it has been demonstrated within the Arnold group that the closely related Ce(III) complex **[K(thf)$_6$][Ce$_2$(*p*TP^m)$_2$K(thf)$_4$]** synthesised from the (*p*TP^m) ligand, reacts with KBn (four equivalents in thf) to yield the addition product **[K(thf)$_6$][K$_3$(*p*TP^m)$_2$Ce$_2$Bn$_2$(thf)$_4$]** in 72 % yield rather than affording deprotonation (Scheme 2-25).[67]

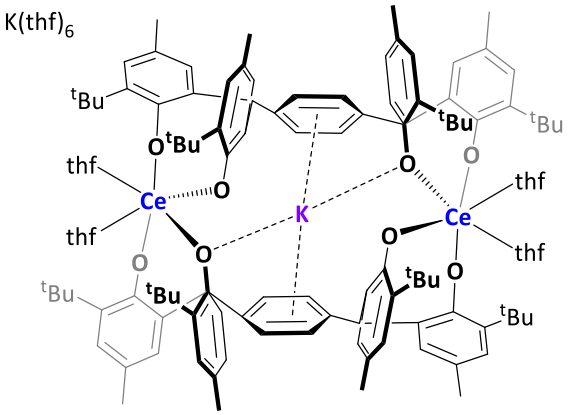

[K(thf)$_6$][Ce$_2$(*p*TP^m)$_2$K(thf)$_4$]

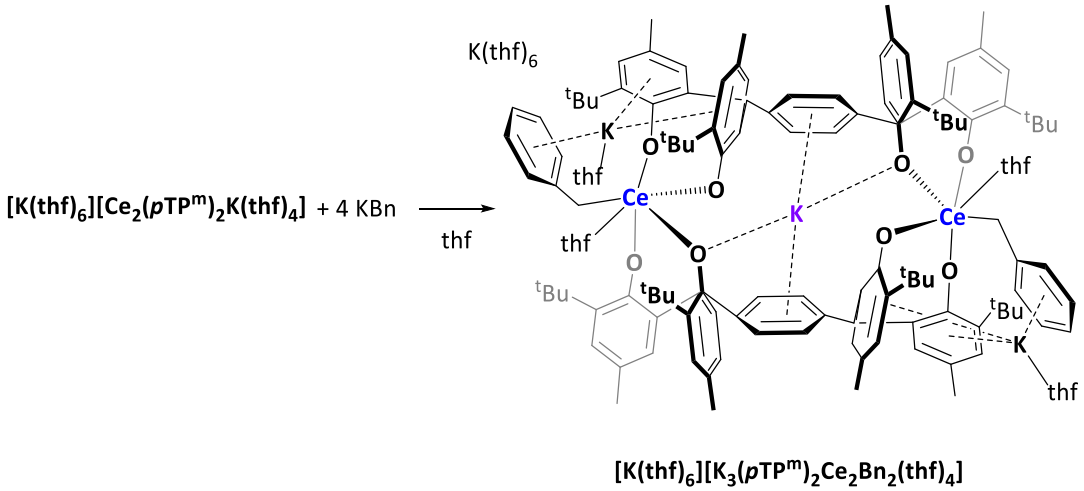

[K(thf)$_6$][K$_3$(*p*TP^m)$_2$Ce$_2$Bn$_2$(thf)$_4$]

Scheme 2-25 Synthesis of **[K(thf)$_6$][K$_3$(*p*TP^m)$_2$Ce$_2$Bn$_2$(thf)$_4$]** *via* treatment of **[K(thf)$_6$][Ce$_2$(*p*TP^m)$_2$K(thf)$_4$]** with KBn.

The reactivity of **3(*m*TP)** with KBn was investigated. KBn (2.5 equivalents) was dissolved in thf and added dropwise to a suspension of **3(*m*TP^m)** in thf at –30 °C (Scheme 2-26). The resulting orange suspension was allowed to warm slowly to room temperature and stirred for 16 hours to provide a dark red solution which was concentrated and cooled to –30 °C. **[K(thf)$_6$][U$_2$(*m'*TP^m)$_2$K(thf)$_2$]**, **6(*m'*TP^m)** was isolated as a dark red crystalline material in moderate yield (22 %) from this solution. ^{1}H NMR spectroscopy indicates that the remaining solution still contains **6(*m'*TP^m)** as the major product, but material isolated *via* removal of all volatiles from this solution contains impurities not present in the isolated crystalline material.

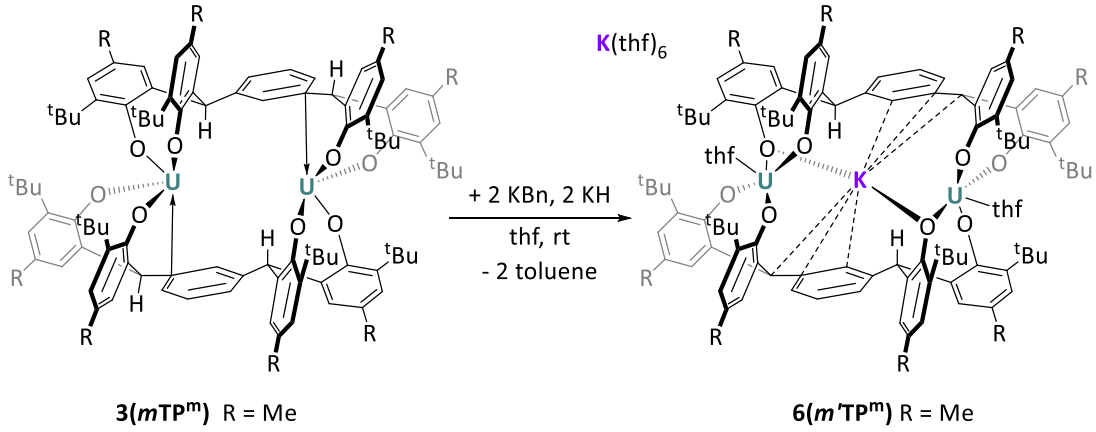

Scheme 2-26 Synthesis of **6(*m'*TP^{m})**.

Two equivalents of toluene are generated from protonation of the benzyl anion and its formation can be observed by ^{1}H NMR monitoring of the reaction. **6(*m'*TP^{m})** can also be obtained by using the strong base KH, with evolution of H_2 gas observed as the reaction proceeds.

The ^{1}H NMR spectrum of the product, **6(*m'*TP^{m})**, shows 20 distinct resonances at room temperature, arising from the inequivalence of all hydrogen atoms around each ligand. Bulk purity of **6(*m'*TP^{m})** was confirmed by elemental microanalysis.

X-ray quality single crystals of **6(*m'*TP^{m})** could be readily obtained from storing the filtered thf reaction mixture at –30 °C and confirm deprotonation of two benzylic positions (one on each ligand), with one potassium counter-ion confined within the internal cavity and one externally coordinated by six molecules of thf (Figure 2-26).

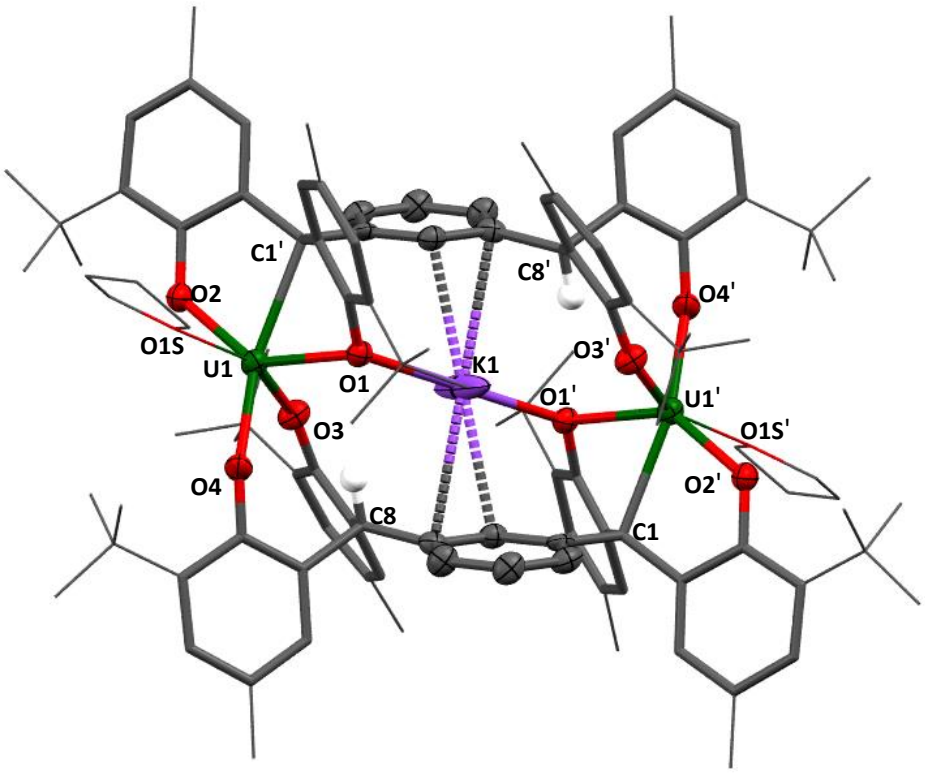

Figure 2-26 Solid-state structure of the anion of **6(*m'*TP^{m})·2thf**. For clarity, all backbone hydrogen atoms and lattice solvent molecules are omitted. Potassium, uranium, selected oxygen and carbon, and benzylic hydrogen atoms are shown as displacement ellipsoids drawn at 50% probability. The remaining atoms and bonds are shown as capped stick or wireframe. Selected bond lengths (Å) and angles (°) for **6(*m'*TP^{m})** are given in Table 2-8.

Parameter	[K(thf)$_6$][U$_2$(*m'*TP^{m})$_2$K(thf)$_2$] ·2thf
U(1)–O(1)	2.162(5)
U(1)–O(2)	2.192(5)
U(1)–O(3)	2.256(5)
U(1)–O(4)	2.207(5)
U(1)–C(8)	2.592(8)
U(1)–O(1S)	2.569(6)
U(1)–K(1)	4.1134(3)
K(1)–O(3)	2.650(5)
O(1)–U(1)–O(2)	83.5(2)
O(1)–U(1)–O(4)	96.3(2)
O(3)–U(1)–O(1)	93.7(2)
O(4)–U(1)–O(3)	139.0(2)
O(2)–U(1)–O(3)	93.4(2)
O(2)–U(1)–O(4)	127.2(2)
O(1)–U(1)–C(8)	102.8(2)

O(3)–U(1)–C(8)	69.5(2)
O(4)–U(1)–C(8)	69.5(2)

Table 2-8 Selected bond lengths and angles for **6(*m'*TP^{m})**.

Figure 2-26 shows the solid-state structure of **[K(thf)$_6$][U$_2$(*m'*TP^{m})$_2$K(thf)$_2$]·2thf**. Uranium(IV) adopts a distorted octahedral geometry, coordinated by four ligand aryloxide moieties, one thf molecule and one deprotonated benzylic carbon on the ligand backbone. The mean U–aryloxide oxygen distance is 2.204(5) Å, shorter than the U–O(1)S bond to thf, 2.569(6) Å, but longer than typical literature U(IV)−OAr bonds such as those in [U(ODtbp)$_4$] (2.135(4) Å),[68] [U(ODtbp)$_3$(NEt$_2$)] (2.140 Å)[69] and [U(ODtbp)$_3$(I)] (2.091 Å).[70] The uranium alkyl U(1)–C(8) distance is 2.592(8) Å, lying between the two corresponding U–C bond lengths in **4(*m'*TP^{m})**. Although no other Ar$_3$C–U or Ar$_2$C–U bonds exist for direct comparison, the length is similar to those found in typical U(IV)–benzyl complexes.[71–75] The deprotonation of the benzylic carbons C(1) and C(1'), and stabilisation of the resulting carbanion through resonance delocalisation leads to ligand desymmetrisation with double bond character shortening the C(8)–C(4) bond relative to the C(1)–C(2) bond (1.486(1) Å compared to 1.521(1) Å). One potassium cation is octahedrally coordinated by six solvent thf molecules and is not associated with the molecular anion. The other potassium cation is in an approximately square planar geometry, bound to two ligand aryloxides at 2.650(5) Å and to the central ligand arene in an η^3 fashion. The distance between K(1) and the C(1)–C(2)–C(3) centroid is 2.968 Å.

Attempts to deprotonate the remaining benzylic carbons were not successful; **6(*m'*TP^{m})** was always formed even when an excess of four equivalents of base were used. This suggests that deprotonation of C(1) may increase the pK_a of the C(8)–H bond.

It was anticipated that the potassium cations may allow further reactivity of **6(*m'*TP^{m})** through salt elimination reactions. However, interaction with the ligand arenes in addition to phenoxide binding evidently results in very strong coordination of the centrally caged K^+, and no attempts to displace it were successful. Scheme 2-27 shows some of the reactions carried out to target further functionalisation of **6(*m'*TP^{m})**.

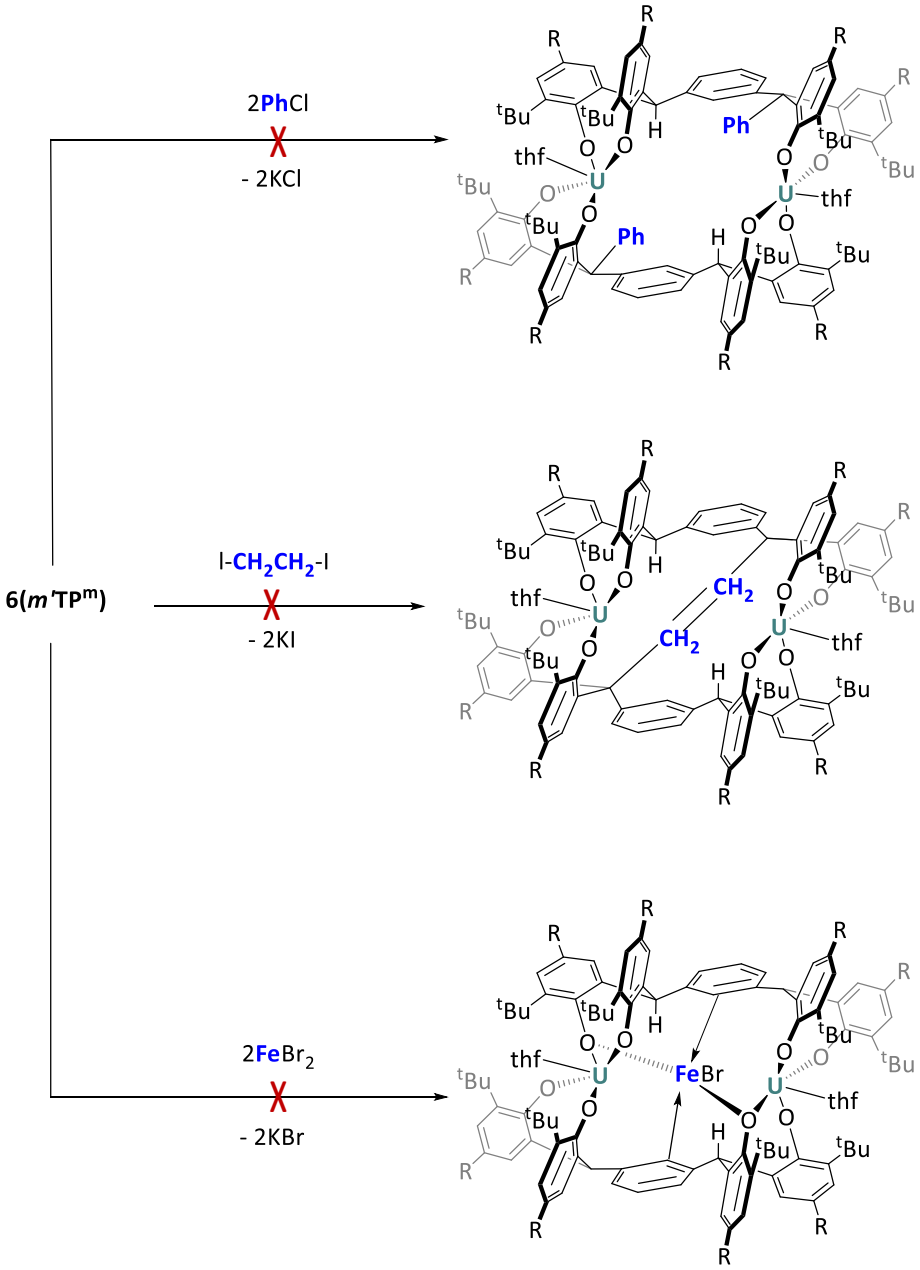

Scheme 2-27 Reactions to target salt metathesis of **6(*m'*TP^{m})**.

6(*m'*TP^{m}) was also treated with hydrazine, targeting the insertion of a diazenido unit yielding an analogue of **4(*m'*TP^{m})**. This reaction did not give the desired product, only a mixture of products that proved challenging to separate. It is proposed that the significant conformational change brought about by the binding of thf solvent molecules to uranium in **6(*m'*TP^{m})** relative to **3(*m*TP^{m})**, and the associated increase in the metal–metal distance (discussed in section 2.5 with respect to **3(*m*TP^{m})** and **2(*m*TP)**), precludes coordination

between the two metal centres. It is also thought that the four potassium cations in **4(*m*'TP^m)** play an important role in stabilising the diazenido ligand. The stabilising effect of K^+ on reduced dinitrogen ligands has been reported by several other authors including Holland[34,35] and Mazzanti.[19]

2.13 Synthesis of [(U(*m*TP))$_2$(NaOSiMe$_3$)$_3$], 7(*m*TP^m)

In Chapter 1, monomeric uranium poly(aryloxide) [UL] complexes were discussed and their CO_2 functionalisation[15] and H_2O reduction[13] chemistry was described. Our group has demonstrated that 1:1 protonolysis reactions of **[U(N")$_2$(N{SiMe$_3$}SiMe$_2$CH$_2$)]** with the *para*-functionalised arene tetraphenol ligand precursor, **H$_4$(*p*TP)**, yield monometallic [U(*p*TP)] complexes which are highly reactive towards Lewis bases such as CNXyl.[76]

The synthesis of monometallic [U(*m*TP)] analogues of the bimetallic complexes described in this chapter was targeted. Initially, reactions to target the direct synthesis of [U(*m*TP)] were investigated. Protonolysis reactions of **[U(N")$_2$(N{SiMe$_3$}SiMe$_2$CH$_2$)]** with **H$_4$(*m*TP)** (in a 1:1 stoichiometry) in hexane, toluene and benzene and 1:1 salt metathesis reactions of **K$_4$(*m*TP)** with U(IV) iodide or chloride in a range of solvents were carried out. These reactions all yielded solvated **2(*m*TP)** or solvent-free **3(*m*TP)**, [U$_2$(*m*TP)$_2$] structures.

The protonolysis reaction of **[U(N")$_2$(N{SiMe$_3$}SiMe$_2$CH$_2$)]** with **H$_4$(*m*TP)** in thf yielded an unknown product. ^{1}H NMR spectra of this product do not match those of **2(*m*TP)** or **3(*m*TP)** and are not sufficient to propose a structure. A sample of **3(*m*TP)** was added to an NMR tube containing a benzene solution of this product. DOSY NMR spectroscopy was used to confirm that both products have diffusion coefficients of −9.33 log m^2 s (calculated hydrodynamic radius = 7.64 Å), and the new product is not a monoarene analogue, which would be expected to have a larger diffusion coefficient. Monoarenes synthesised by Francis Lam in the Arnold group have been analysed by DOSY NMR spectroscopy and have diffusion coefficients of −9.21 log m^2 s, corresponding to a hydrodynamic radius of 5.83 Å.

[U(*m*TP)] complexes were therefore targeted *via* treatment of **3(*m*TP^m)** with Group 1 salts according to Scheme 2-28.

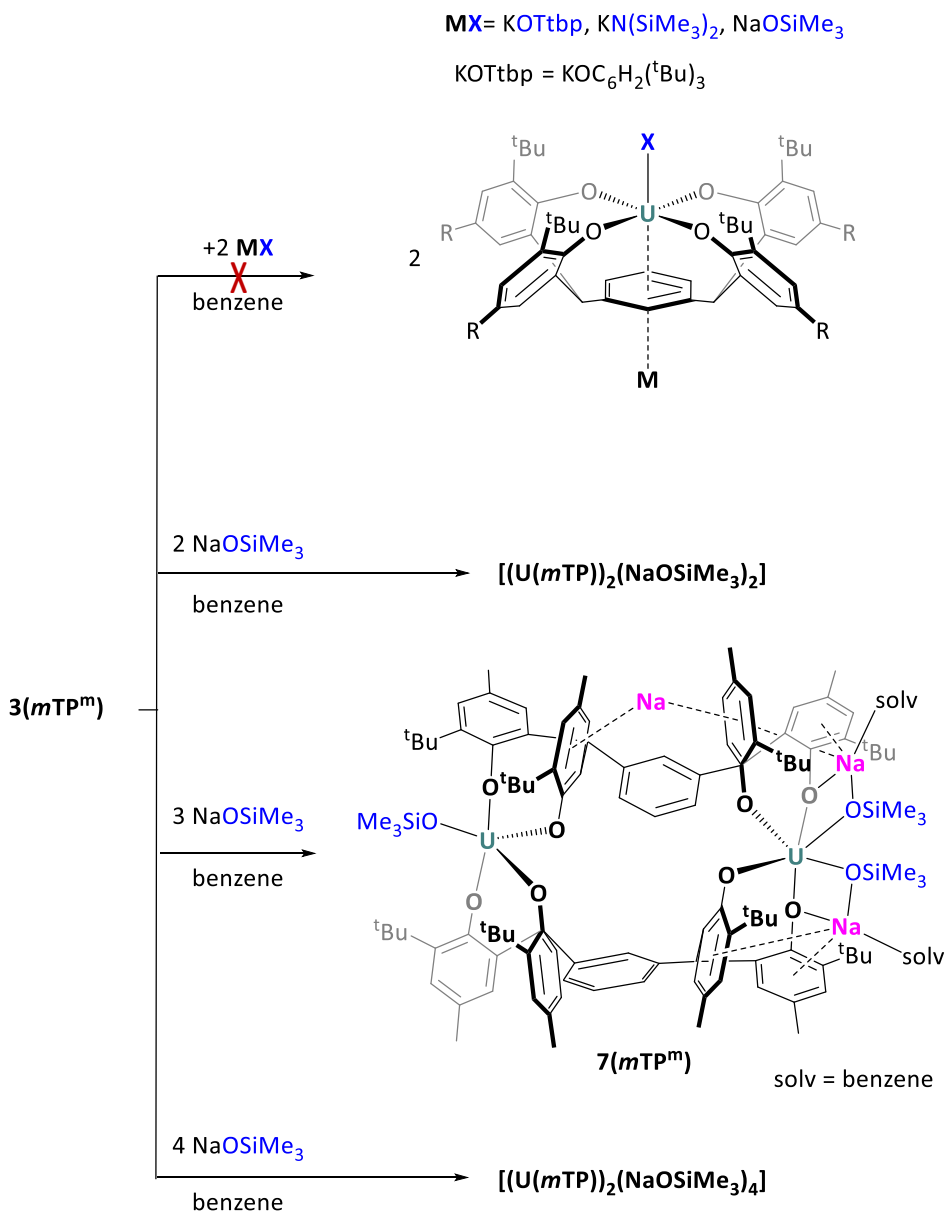

Scheme 2-28 Reactions of **3(*m*TP^{m})** with Group 1 salts.

Reactions with potassium 2,4,6-tri-*tert*-butylphenoxide, [KN(SiMe$_3$)$_2$] and NaOSiMe$_3$ did not yield the targeted monomers. It is proposed that for complexes of (*m*TP), the dimeric structure is a thermodynamic sink, and once formed, the U−O bonds are not easily broken, making rearrangement unfavourable.

From a reaction with 2.5 equivalents of NaOSiMe$_3$ in C_6H_6, a small number of pale blue crystals of **7(*m*TP^{m})** were obtained. Single crystal XRD showed that 3 $SiMe_3O^-$ units had

coordinated to the uranium centres with incorporation of three Na^+ ions into the retained dimeric structure to achieve charge balance.

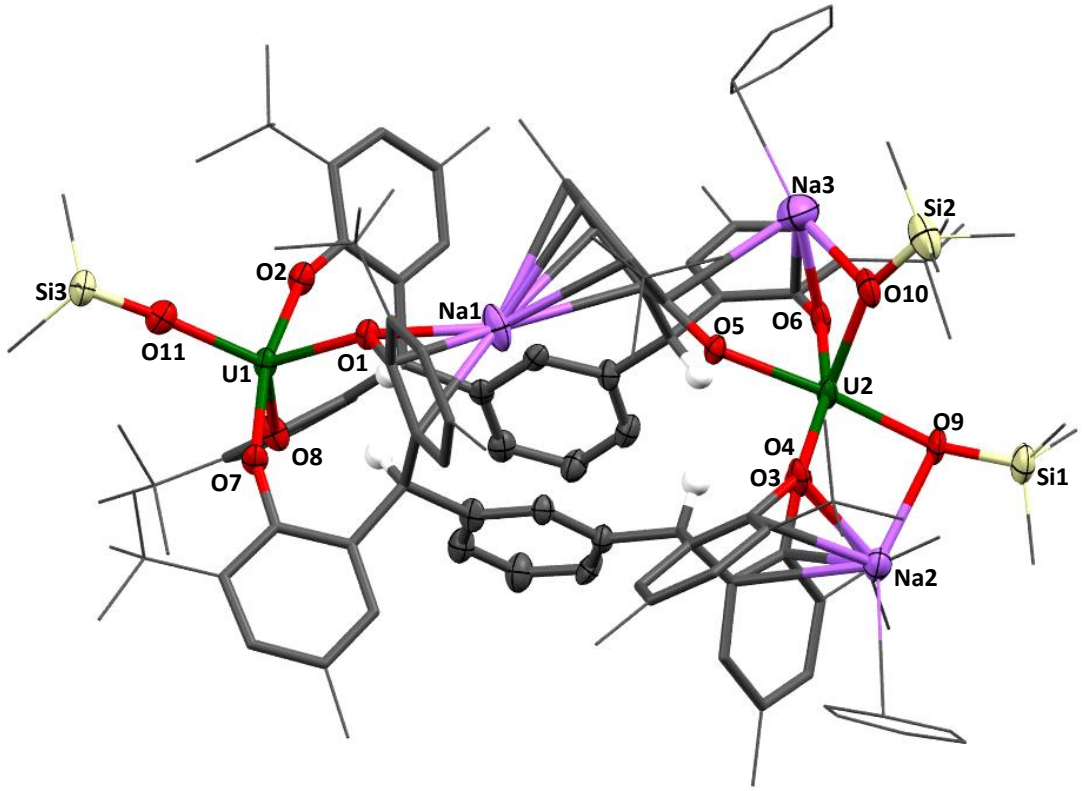

Figure 2-27 Solid-state structure of **7(*m*TP^m).6benzene.** For clarity, all backbone hydrogen atoms and lattice solvent molecules are omitted. Sodium, silicon, oxygen, uranium and benzylic hydrogen atoms are shown as displacement ellipsoids drawn at 50 % probability. The remaining atoms and bonds are shown as capped stick or wireframe. Selected bond lengths (Å) and angles (°) for **7(*m*TP^m)** are given in Table 2-8.

Parameter	[(U(*m*TP^m))$_2$(NaOSiMe$_3$)$_3$]·6benzene
U(1)–O(1)	2.282(6)
U(1)–O(2)	2.150(6)
U(2)–O(3)	2.231(7)
U(2)–O(4)	2.247(6)
U(2)–O(5)	2.254(6)
U(2)–O(6)	2.258(7)
U(1)–O(7)	2.160(7)
U(1)–O(8)	2.150(7)
U(2)–O(9)	2.241(7)
U(2)–O(10)	2.264(8)

U(1)–O(11)	2.162(7)
O(9)–Si(1)	1.624(7)
O(10)–Si(2)	1.632(8)
O(11)–Si(3)	1.618(8)
O(2)–U(1)–O(1)	88.3(2)
O(4)–U(2)–O(5)	83.1(2)

Table 2-8 Selected bond lengths and angles for **7(*m*TP^{m})**.

Figure 2-27 shows the solid-state structure of **[(U(*m*TP^{m}))$_2$(NaOSiMe$_3$)$_3$]·6benzene**. U(1) adopts a distorted square pyramidal geometry (τ_5 = 0.75) to coordinate four aryloxide ligand moieties and one O–SiMe$_3$, whereas U(2) has a distorted octahedral geometry, coordinating an additional O–SiMe$_3$. The mean U(1)–O(aryloxide) bond distance is 2.186(7) Å, with the U(1)–O(1) bond significantly longer than the others as a result of the O(1)–Na(1) interaction. Around U(2), the mean U(2)–O(aryloxide) bond distance is significantly longer, 2.248(7) Å, reflecting the increased uranium coordination number. Similarly, U(1)–O(11) is shorter than the mean U(2)–O(SiMe$_3$) bond length. Reported U(IV)−OSiR$_3$ bonds range from 2.096 Å to 2.161 Å,[31,77] demonstrating that U(2)−O(9) and U(2)−O(10) are significantly elongated by the greater coordination number of the metal. 10.3369(6) Å separates the two U(IV) centres, which is more than double the corresponding distance in **4(*m*′TP^{m})** (4.6476(7) Å), demonstrating the robust yet highly flexible nature of the ligand framework.

7(*m*TP^{m}) was fully characterised by elemental analysis and ^{1}H and ^{29}Si NMR spectroscopy. The 30 distinct resonances in the ^{1}H NMR spectrum are accounted for by the high degree of asymmetry retained in solution. Si(1) and Si(2) appear as a single resonance in ^{29}Si NMR spectra, resulting in only two ^{29}Si NMR resonances.

The synthesis of **7(*m*TP^{m})** can be reproduced rationally, by using three equivalents of NaOSiMe$_3$. Reactions with two and four equivalents appeared to give the expected **[(U(*m*TP))$_2$(NaOSiMe$_3$)$_2$]** and **[(U(*m*TP))$_2$(NaOSiMe$_3$)$_4$]** products respectively, which have been identified by multinuclear NMR spectroscopy but not further characterised.

This reactivity, although not yielding the targeted [U(*m*TP)] product, indicates that the dimeric [U$_2$(*m*TP)$_2$] unit is inert to rearrangement into monomers and can demonstrate an unexpected degree of flexibility to facilitate the retention of both metals.

2.14 Summary and conclusions for Chapter 2

The *meta*-functionalised arene tetraphenol ligand precursors **H_4(*m*TP^m)** and **H_4(*m*TP^t)** have been prepared and used to synthesise the solvated bimetallic uranium(IV) complexes, **2(*m*TP^m)** and **2(*m*TP^t)**, *via* salt metathesis of the potassium salt **[K_4(*m*TP)]** with U(IV) iodide. The solvent-free analogues, **3(*m*TP^m)** and **3(*m*TP^t)**, have been prepared *via* protonolysis with **[U(N")$_2$(N{SiMe$_3$}SiMe$_2$CH$_2$)]**. Complexes **2(*m*TP)** and **3(*m*TP)** share an unusual **'**letterbox' geometry, with an internal rectangular-shaped cavity formed by the ligand framework. The uranium centres in **3(*m*TP)** are sterically unsaturated and form an arene interaction with the ligand backbone.

Reduction of **3(*m*TP)** under an atmosphere of dinitrogen yields **4(*m*′TP). 4(*m*′TP)** contains bound $[N_2H_2]^{4-}$ following dinitrogen reduction and H abstraction from the benzylic positions on the ligand backbone. This reduction is thought to proceed without change in the metal oxidation state, with the electrons provided by the potassium source. Quenching reactions with acids yield NH_3, and reactions with silyl electrophiles afforded an overall hydrosilylation to provide $HN(SiMe_3)_2$. Calculations suggest that the potassium cations play a key role in stabilising the transition state in this transformation.

Control reactions show that it is possible to deprotonate the benzylic positions in **3(*m*TP^m)** using an external base to yield **6(*m*′TP^m)**, but reactions designed to split the **3(*m*TP^m)** dimer into its constituent [U(*m*TP)] monomers were not successful.

Even in the absence of catalytic turnover, **3(*m*TP)** represents the first uranium system to mediate the silylation of dinitrogen, and only the second to enable the protonation of dinitrogen. Furthermore, although molecular systems for the silylation and protonation of dinitrogen exist independently, this is the first time the two have been combined in a single system, to provide secondary amines.

The unique 'letterbox' geometry of the complexes is proposed to be important for several reasons: the initial capture of N_2 between two metals; the incorporation of potassium ions which are required for the reduction of N_2; providing access to the benzylic C−H bonds for the initial functionalisation of N_2; and in stabilising the transition states in reactions with added electrophiles.

2.15 References for Chapter 2

(1) Tang, L.; Wasserman, E. P.; Neithamer, D. R.; Krystosek, R. D.; Cheng, Y.; Price, P. C.; He, Y.; Emge, T. J. *Macromolecules* **2008**, *41* (20), 7306–7315.

(2) Christiansen, A.; Franke, R.; Fridag, D.; Hess, D.; Kreidler, B.; Vogt, D.; Bini, L.; Janssen, M.; Hamers, B. Organophosphorus Compounds Based on Tetraphenol Substituted Structures, 2012, patent number: US9000220B2.

(3) Zhang, J.; Jian, C.; Gao, Y.; Wang, L.; Tang, N.; Wu, J. *Inorg. Chem.* **2012**, *51* (24), 13380–13389.

(4) Al-Khafaji, Y.; Sun, X.; Prior, T. J.; Elsegood, M. R. J.; Redshaw, C. *Dalton Trans.* **2015**, *44* (27), 12349–12356.

(5) Mobinikhaledi, A.; Moghanian, H.; Deinavizadeh, M. *Comptes Rendus Chim.* **2013**, *16* (11), 1035–1041.

(6) La Pierre, H. S.; Scheurer, A.; Heinemann, F. W.; Hieringer, W.; Meyer, K. *Angew. Chem. Int. Ed.* **2014**, *53* (28), 7158–7162.

(7) Inman, C. J.; Frey, A. S. P.; Kilpatrick, A. F. R.; Cloke, F. G. N.; Roe, S. M. *Organometallics* **2017**, *36* (23), 4539–4545.

(8) Breslow, R.; Chu, W. *J. Am. Chem. Soc.* **1970**, *92* (7), 2165–2165.

(9) Kumar, D.; Jaikumar, V. *Des. Monomers Polym.* **2015**, *18* (3), 295–302.

(10) Tang, L.; Wasserman, E. P.; Neithamer, D. R.; Krystosek, R. D.; Cheng, Y.; Price, P. C.; He, Y.; Emge, T. J. *Macromolecules*, **2008**, *41* (20), 7306–7315.

(11) Tanner, P. S.; Burkey, T.P.; Hanusa, T. P. *Polyhedron.* **1995**, *14* (2), 331-333.

(12) He, X.; Noll, B. C.; Beatty, A.; Mulvey, R. E.; Henderson, K. W. *J. Am. Chem. Soc.* **2004**, *126* (24), 7444–7445.

(13) Halter, D. P.; Heinemann, F. W.; Bachmann, J.; Meyer, K. *Nature* **2016**, *530* (7590), 317–321.

(14) La Pierre, H. S.; Kameo, H.; Halter, D. P.; Heinemann, F. W.; Meyer, K. *Angew. Chem. Int. Ed.* **2014**, *53* (28), 7154–7157.

(15) Inman, C. J.; Frey, A. S. P.; Kilpatrick, A. F. R.; Cloke, F. G. N.; Roe, S. M. *Organometallics* **2017**, *36* (23), 4539–4545.

(16) Lewis, A. J.; Williams, U. J.; Carroll, P. J.; Schelter, E. J.; Roy, P. *Inorg. Chem.* **2013**, *52*, 7326–7328.

(17) Arnold, P. L.; Mansell, S. M.; Maron, L.; McKay, D. *Nat. Chem.* **2012**, *4* (8), 668–674.

(18) Berg, J. M.; Clark, D. L.; Huffman, J. C.; Morris, D. E.; Sattelberger, A. P.; Streib, W. E.; Van der Sluys, W. G.; Watkin, J. G. *J. Am. Chem. Soc.* **1992**, *114* (27), 10811–10821.

(19) Falcone, M.; Chatelain, L.; Scopelliti, R.; Živković, I.; Mazzanti, M. *Nature* **2017**, *547* (7663), 332–335.

(20) Dormond, A.; El Bouadili, A.; Aaliti, A.; Moise, C. *J. Organomet. Chem.* **1985**, *288* (1), C1–C5.

(21) Wells, J. A. L.; Seymour, M. L.; Suvova, M.; Arnold, P. L. *Dalton Trans.* **2016**, *45* (40), 16026–16032.

(22) Mansell, S. M.; Kaltsoyannis, N.; Arnold, P. L. *J. Am. Chem. Soc.* **2011**, *133* (23), 9036–9051.

(23) Van Der Sluys, W. G.; Sattelberger, A. P.; Streib, W. E.; Huffman, J. C. *Polyhedron* **1989**, *8*(9), 1247–1249.

(24) Evans, D.F., *J. Chem. Soc.* **1959,** 400, 2003-2005.

(25) Arnold, P. L. *Chem. Commun.* **2011**, *47* (32), 9005.

(26) Morris, D. E.; DaRe, R. E.; Jauntuen, K. C.; Castro-Rodriguez, I.; Kiplinger J. L. *Organometallics*, **2004**, 23 (22), 5142–5153.

(27) Vallat, A.; Laviron, E.; Dormond, A. *J. Chem. Soc. Dalton Trans.* **1990**, (3), 921.

(28) Bernskoetter, W. H.; Pool, J. A.; Lobkovsky, E.; Chirik, P. J. *J. Am. Chem. Soc.*, **2005**, 127 (21), 7901–7911.

(29) Falcone, M.; Chatelain, L.; Scopelliti, R.; Živković, I.; Mazzanti, M. *Nature* **2017**, *547* (7663), 332–335.

(30) Cohen, J. D.; Mylvaganam, M.; Fryzuk, M. D.; Loehr, T. M. *J. Am. Chem. Soc.*, **1994**, 116 (21), 9529–9534.

(31) Mansell, S. M.; Farnaby, J. H.; Germeroth, A. I.; Arnold, P. L. *Organometallics* **2013**, *32* (15), 4214–4222.

(32) Evans, W. J.; Rego, D. B.; Ziller, J. W. *Inorg. Chem.* **2006**, *45* (26), 10790–10798.

(33) Smith, J. M.; Sadique, A. R.; Cundari, T. R.; Rodgers, K. R.; Lukat-Rodgers, G.; Lachicotte, R. J.; Flaschenriem, C. J.; Vela, J.; Holland, P. H. *J. Am. Chem. Soc. Soc.* **2006**, *128* (3), 756–769.

(34) Grubel, K.; Brennessel, W. W.; Mercado, B. Q.; Holland, P. L. *J. Am. Chem. Soc.* **2014**, *136* (48), 16807–16816.

(35) Smith, J. M.; Sadique, A. R.; Cundari, T. R.; Rodgers, K. R.; Lukat-Rodgers, G.; Lachicotte, R. J.; Flaschenriem, C. J.; Vela, J.; Holland, P. L. *J. Am. Chem.*

Soc., **2006**, *128* (3), 756–769.

(36) Lewis, R.; Evans, W. *Chemistry*; Macmillan International Higher Education, 2011.

(37) Burford, R. J.; Fryzuk, M. D. *Nat. Rev. Chem.* **2017**, *1* (4), 1-13.

(38) Yandulov, D. V.; Schrock, R. R. *Science*. **2003**, *301* (5629), 76-78.

(39) Eizawa, A.; Arashiba, K.; Tanaka, H.; Kuriyama, S.; Matsuo, Y.; Nakajima, K.; Yoshizawa, K.; Nishibayashi, Y. *Nat. Commun.* **2017**, *8*, 14874.

(40) Rittle, J.; Peters, J. C. *J. Am. Chem. Soc.* **2016**, *138* (12), 4243–4248.

(41) Tanaka, H.; Sasada, A.; Kouno, T.; Yuki, M.; Miyake, Y.; Nakanishi, H.; Nishibayashi, Y.; Yoshizawa, K. *J. Am. Chem. Soc.* **2011**, *133* (10), 3498–3506.

(42) Mori, M. *Journal of organometallic chemistry*, **2004**, 689(24), 4210-4227.

(43) Komori, K.; Oshita, H.; Mizobe, Y.; Hidai, M. *J. Am. Chem. Soc.* **1989**, *111* (5), 1939–1940.

(44) Lee, Y.; Mankad, N. P.; Peters, J. C. *Nat. Chem.* **2010**, *2* (7), 558–565.

(45) MacLeod, K. C.; Menges, F. S.; McWilliams, S. F.; Craig, S. M.; Mercado, B. Q.; Johnson, M. A.; Holland, P. L. *J. Am. Chem. Soc.* **2016**, *138* (35), 11185–11191.

(46) Hori, M.; Mori, M. *J. Org. Chem.* **1995**, *60* (6), 1480–1481.

(47) Kupfer, T.; Schrock, R. R. *J. Am. Chem. Soc.* **2009**, *131* (35), 12829–12837.

(48) Facts & Figures for the Chemical Industry, *Chem. Eng. News* **1997**, *75* (25), 38–79.

(49) Kendall, A. J.; Johnson, S. I.; Bullock, R. M.; Mock, M. T. *J. Am. Chem. Soc.* **2018**, *140 (7)*, 2528-2563

(50) Chalkley, M. J.; Del Castillo, T. J.; Matson, B. D.; Roddy, J. P.; Peters, J. C. *ACS Cent. Sci.* **2017**, *3* (3), 217–223.

(51) Bienfait, A. M.; Wolf, B. M.; Törnroos, K. W.; Anwander, R. *Inorg. Chem.* **2018**, *57* (9), 5204–5212.

(52) Suvova, M.; O'Brien, K. T. P.; Farnaby, J. H.; Love, J. B.; Kaltsoyannis, N.; Arnold, P. L. *Organometallics* **2017**, *36* (23), 4669–4681.

(53) Protchenko, A. V.; Bates, J. I.; Saleh, L. M. A.; Blake, M. P.; Schwarz, A. D.; Kolychev, E. L.; Thompson, A. L.; Jones, C.; Mountford, P.; Aldridge, S. *J. Am. Chem. Soc.* **2016**, *138* (13), 4555–4564.

(54) Eizawa, A.; Arashiba, K.; Tanaka, H.; Kuriyama, S.; Matsuo, Y.; Nakajima, K.; Yoshizawa, K.; Nishibayashi, Y. *Nat. Commun.* **2017**, *8*, 14874.

(55) Chalkley, M. J.; Del Castillo, T. J.; Matson, B. D.; Roddy, J. P.; Peters, J. C. *ACS Cent. Sci.* **2017**, *3* (3), 217–223.

(56) Del Castillo, T. J.; Thompson, N. B.; Peters, J. C. *J. Am. Chem. Soc.* **2016**, *138* (16), 5341–5350.

(57) Tanaka, H.; Sasada, A.; Kouno, T.; Yuki, M.; Miyake, Y.; Nakanishi, H.; Nishibayashi, Y.; Yoshizawa, K. *J. Am. Chem. Soc.* **2011**, *133* (10), 3498–3506.

(58) McMillen, D. F.; Golden, D. M. *Annu. Rev. Phys. Chem.* **1982**, *33* (1), 493–532.

(59) Ishii, Y.; Ishino, Y.; Aoki, T.; Hidais, M. *J. Am. Chem. Soc.* **1992**, *114*, 5429–5430.

(60) Knobloch, D. J.; Lobkovsky, E.; Chirik, P. J. *Nat. Chem.* **2010**, *2* (1), 30–35.

(61) Morello, L.; Love, J. B.; Patrick, B.; Fryzuk, M. D. *J. Am. Chem. Soc.*, **2004**, 126 (31), 9480–9481.

(62) Lee, Y.; Mankad, N. P.; Peters, J. C. *Nat. Chem.* **2010**, *2* (7), 558–565.

(63) Siedschlag, R. B.; Bernales, V.; Vogiatzis, K. D.; Planas, N.; Clouston, L. J.; Bill, E.; Gagliardi, L.; Lu, C. C. *J. Am. Chem. Soc.* **2015**, *137* (14), 4638–4641.

(64) Ellison, G. B.; Davico, G. E.; Bierbaum, V. M.; DePuy, C. H. *Int. J. Mass Spectrom. Ion Process.* **1996**, *156* (1–2), 109–131.

(65) Michiue, K.; Jordan, R. F. *J. Mol. Catal. A Chem.* **2008**, *282* (1–2), 107–116.

(66) Dicks, A. P. *J. Chem. Educ.* **2003**, *80* (11), 1322.

(67) Wang, K. *PhD Thesis,* Characterisation and Reactivity Study of Rare Earth Metal Complexes, **2017**, Univeristy of Edinburgh.

(68) Berg, J. M.; Clark, D. L.; Huffman, J. C.; Morris, D. E.; Sattelberger, A. P.; Streib, W. E.; Van der Sluys, W. G.; Watkin, J. G. *J. Am. Chem. Soc.* **1992**, *114* (27), 10811–10821.

(69) Hitchcock, P. B.; Lappert, M. F.; Singh, A.; Taylor, R. G.; Brown, D. *J. Chem. Soc. Chem. Commun.* **1983**, (10), 561.

(70) Avens, L. R.; Barnhart, D. M.; Burns, C. J.; McKee, S. D.; Smith, W. H. *Inorg. Chem.* **1994**, *33* (19), 4245–4254.

(71) Matson, E. M.; Franke, S. M.; Anderson, N. H.; Cook, T. D.; Fanwick, P. E.; Bart, S. C. *Organometallics*, **2014**, *33* (8), 1964–1971

(72) Kraft, S. J.; Fanwick, P. E.; Bart, S. C. *J. Am. Chem. Soc.* **2012**, *134* (14), 6160–6168.

(73) Pool, J.; Scott, B.; Kiplinger, J. L. *J. Am. Chem. Soc.*, **2005**, 127 (5), 1338–1339.

(74) Arnold, P. L.; Hollis, E.; White, F. J.; Magnani, N.; Caciuffo, R.; Love, J. B. *Angew. Chem. Int. Ed.* **2011**, *123* (4), 917–920.

(75) Kiplinger, J.; Morris, D.; Scott, B.; Burns, C. J. *Organometallics*, **2002**, 21 (26), 5978–5982.

(76) Wells, J. A. L. *PhD Thesis,* Bimetallic actinide complexes for small molecule

activation, **2018**, University of Edinburgh.

(77) Fortier, S.; Kaltsoyannis, N.; Wu, G.; Hayton, T. W. *J. Am. Chem. Soc.* **2011**, *133* (36), 14224–14227.

Chapter 3: Uranium Half Letterbox Complexes for Nitrogen Activation and Functionalisation

3.1 Introduction and aims for Chapter 3

Chapter 2 describes multiple uranium complexes in which two equivalents of **(*m*TP)** bind to two metal centres to yield complexes with a 'letterbox' geometry. Reports by Wu and co-workers indicate that a single tetraphenolate ligand can bind multiple alkali metals when supported by neutral donors (such as thf molecules) as ancillary ligands (Scheme 3-1).[1] Additionally, previous work in the Arnold group has successfully demonstrated the synthesis of bimetallic uranium complexes supported by a single equivalent of Wu's *para*-tetraphenolate **(*p*TP)** arene ligand,[2] but solid-state structures of all complexes of **(*p*TP)** indicate that the two metals occupy opposite faces of the ligand.[1,2] In the U/U complexes, the metal metal separation distance in the solid-state was between 11.537 and 11.887 Å, depending on the aryl substituents and ancillary ligands, and no evidence of nitrogen activation by these complexes has been observed. We proposed that the 'letterbox' geometry of the complexes in Chapter 2, in which the two uranium centres occupy the central cavity with a separation distance of just 6.5732(5) Å is key to allowing the two metals to react in a cooperative manner to reduce dinitrogen.

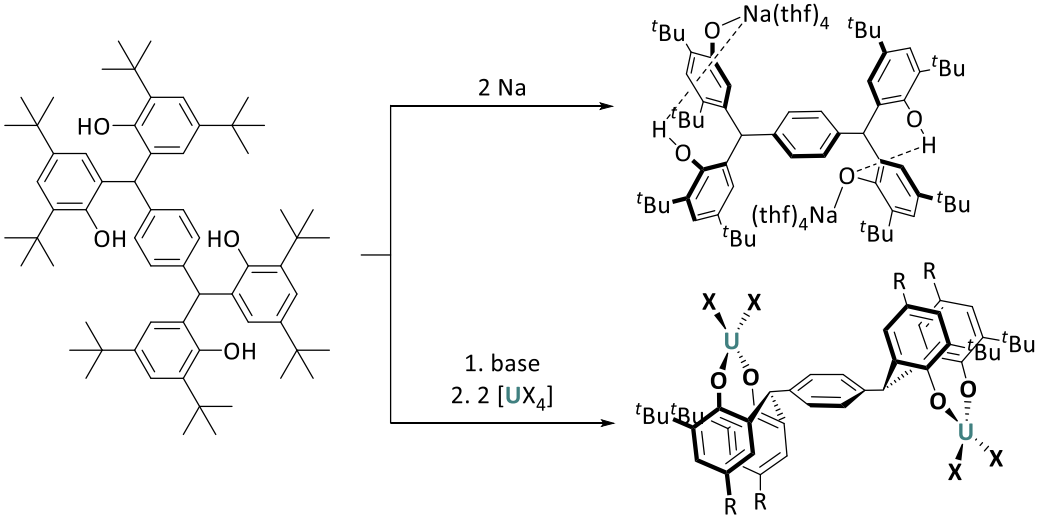

Scheme 3-1 Synthesis of a disodium[3] and bimetallic uranium complexes[2] supported by **(*p*TP)** ligands.

The work described in this chapter pertains to the synthesis of bimetallic uranium complexes supported by one *meta*-tetraphenol arene: **H_4(*m*TP^m)** or **H_4(*m*TP^t)**, to target complexes which retain a short U−U distance and geometry pre-organised for small molecule binding, as seen in the letterbox complexes described in Chapter 2. These ***U_2X_4*(*m*TP)** complexes are termed 'half-letterbox' complexes.

3.2 Halides as ancillary ligands

[K_4(*m*TP)] undergoes salt metathesis with **[UI_4(1,4-dioxane)$_2$]** to yield **[{U(*m*TP)(solv)$_2$}$_2$]** (solv = thf or 1,4-dioxane) complexes (see Chapter 2), eliminating KI as a by-product. An analogous metathesis reaction was attempted in a 1:2 stoichiometry.

Ligand precursors **H_4(*m*TP^m)** and **H_4(*m*TP^t)** were reacted *via* potassium salts, **[K_4(*m*TP)]**, which were treated *in situ* with two equivalents of uranium(IV) halide: **[UCl_4]** or **[UI_4(1,4-dioxane)$_2$]** (Scheme 3-2). In all cases the target complexes **[U_2I_4(*m*TP^m)(thf)$_4$], 8(*m*TP^m), [U_2I_4(*m*TP^t)(thf)$_4$], 8(*m*TP^t)**, **[U_2Cl_4(*m*TP^m)(thf)$_4$], 9(*m*TP^m)** and **[U_2Cl_4(*m*TP^t)(thf)$_4$], 9(*m*TP^t)** were obtained in excellent yields (79 - 96 %). KCl or KI salt by-products were formed as precipitates and removed from the reaction mixtures by filtration, to yield the products as green or pale brown powders following removal of volatiles under reduced pressure.

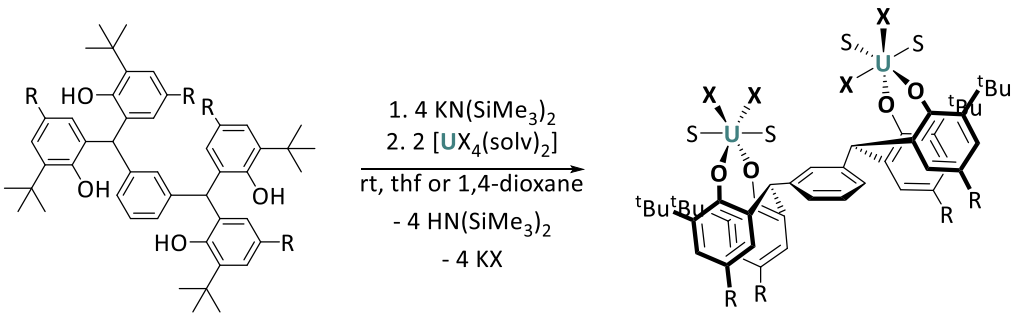

H_4(*m*TP^m) R = Me
H_4(*m*TP^t) R = ^{t}Bu

X = I, solv = (1,4-dioxane)
X = Cl, solv = none

8(*m*TP^m) R = Me, X = I, S = thf, diox
9(*m*TP^m) R = Me, X = Cl, S = thf, diox
8(*m*TP^t) R = ^{t}Bu, X = I, S = thf, diox
9(*m*TP^t) R = ^{t}Bu, X = Cl, S = thf, diox

Scheme 3-2 Synthesis of compounds **8(*m*TP)** and **9(*m*TP)** *via* salt metathesis.

Complexes **8(*m*TP)** and **9(*m*TP)** have been characterised by ^{1}H NMR spectroscopy and elemental analysis which are consistent with the molecular compositions proposed. The ^{1}H NMR spectra of **8(*m*TP)** and **9(*m*TP)** are similar to those obtained for the **[{U(*m*TP)(solv)$_2$}$_2$]** complexes described in Section 2.4, indicating C_2 symmetry in solution, and a total of eight

resonances. Figure 3-1 shows the ^{1}H NMR spectrum of **[U_2Cl_4(*m*TP^{m})(thf)$_4$], 9(*m*TP^{m})**, (in thf-d_8) which exhibits paramagnetism as expected for a U(IV) complex but has a relatively narrow paramagnetic range of 13.91 to 0.13 ppm, compared to 34.60 to −13.43 ppm for **[{U(*m*TP^{m})(1,4-dioxane)$_2$}$_2$], 2(*m*TP^{m})**. The benzylic hydrogen resonances in spectra of **8(*m*TP)** and **9(*m*TP)** are typically the most negative, appearing at 0.13 ppm in the spectrum of **9(*m*TP^{m})**.

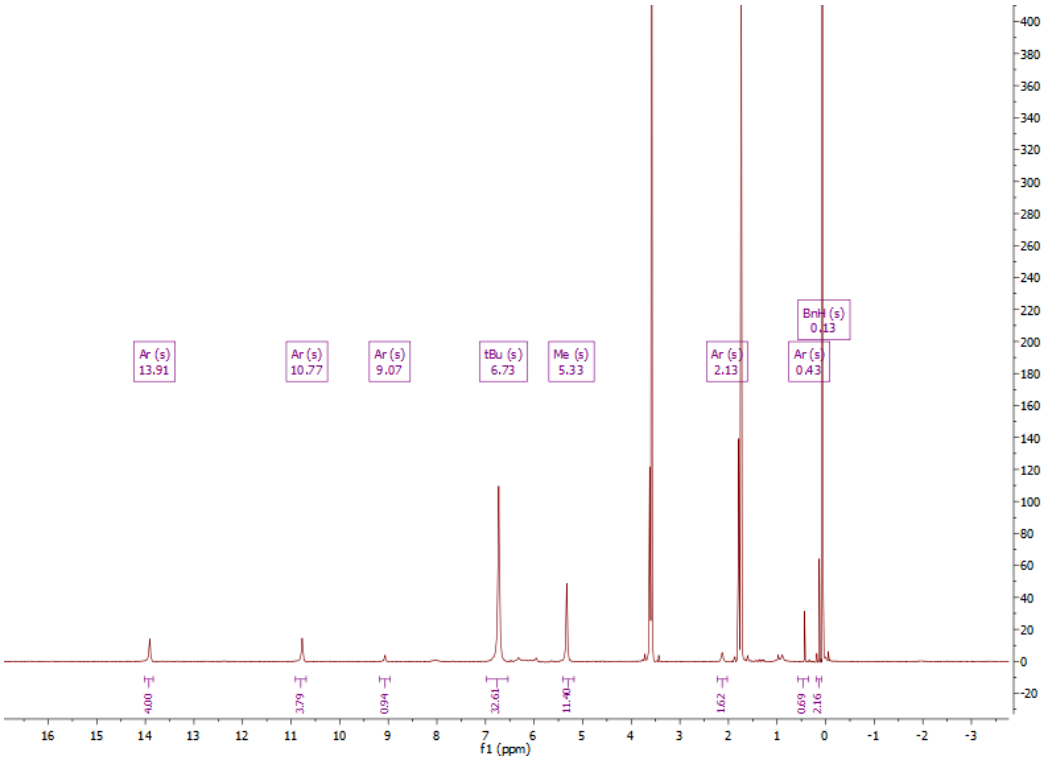

Figure 3-1 ^{1}H NMR (500 MHz) spectrum of **[U_2Cl_4(*m*TP^{m})(thf)$_4$], 9(*m*TP^{m})**, in thf-d_8.

The iodide complexes **8(*m*TP^{m})** and **8(*m*TP^{t})** have also been characterised by single crystal XRD. Salt incorporation (to provide **[(U_2Cl_4{*m*TP}{thf}$_4$)$_2$(KCl)]**) has been observed in single crystals of the chloride complexes studied by single crystal XRD, but following steps to remove this incorporated KCl, bulk purity has been confirmed by elemental analysis.

Free rotation about the Ar_2C–Ar bond in solution can be inferred from the C_2 symmetry observed in the ^{1}H NMR spectra of complexes **8(*m*TP)** and **9(*m*TP)**. However, a comparison of the crystal structures of **8(*m*TP^{m})** and **8(*m*TP^{t})** indicates that in the solid-state the additional steric bulk provided by **(*m*TP^{t})** has a dramatic effect on molecular conformation. The methyl groups on **(*m*TP^{m})** are all pointing downwards relative to the plane of the central

arene ring, allowing both metals to sit on the same face of the ligand opposite to these methyl substituents, with a U–U separation of 9.387 Å, Figure 3-2. This geometry is proposed to be favoured by the generation of a dipole moment across the molecule. In contrast, the bulkier *tert*-butyl groups of **(*m*TP^{t})** give rise to a conformer that is rotated by 180 ° around one Ar_2C–Ar single bond, likely due to steric congestion. This results in the metals now occupying opposite faces of the ligand, with a greater U–U separation of 11.628 Å, Figure 3-3.

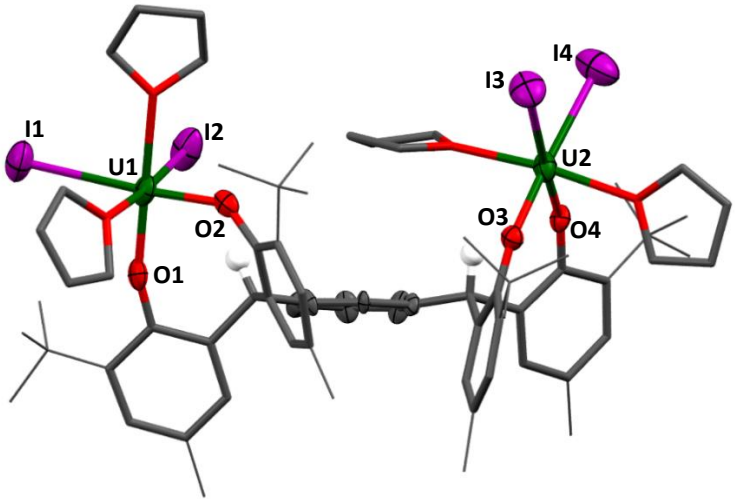

Figure 3-2 Solid-state structure of **[U_2I_4(*m*TP^{m})(thf)$_4$]·3thf, 8(*m*TP^{m}).** For clarity, all backbone hydrogen atoms and lattice solvent molecules are omitted. The benzylic hydrogen, uranium, iodine and selected carbon and oxygen atoms are displayed as displacement ellipsoids drawn at 50 % probability. The remaining atoms and bonds are shown as capped stick or wireframe. Selected bond lengths (Å) and angles (°) for **8(*m*TP^{m})** are given in Table 3-1.

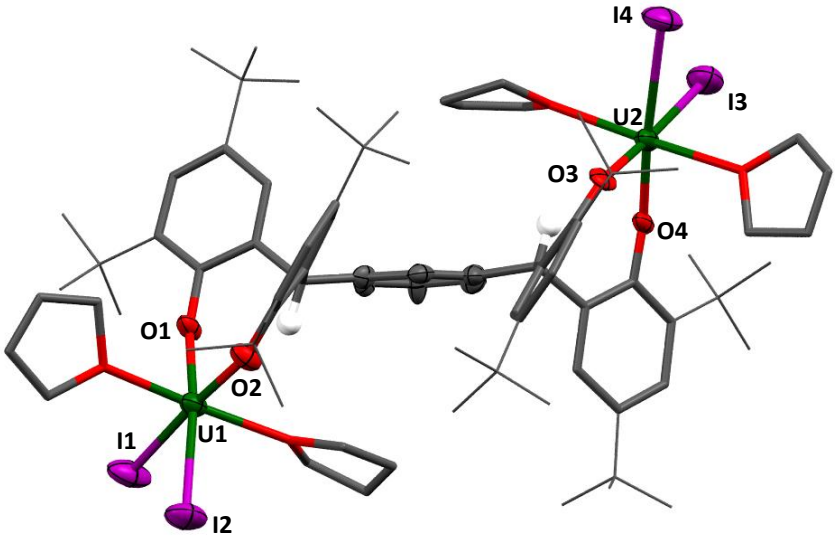

Figure 3-3 Solid-state structure of **[U_2I_4(*m*TP^t)(thf)$_4$]·1.5toluene, 8(*m*TP^t)**. For clarity, all backbone hydrogen atoms and lattice solvent molecules are omitted. The benzylic hydrogen, uranium, iodine and selected carbon and oxygen atoms are displayed as displacement ellipsoids drawn at 50 % probability. The remaining atoms and bonds are shown as capped stick or wireframe. Selected bond lengths (Å) and angles (°) for **8(*m*TP^t)** are given in Table 3-1.

Parameter	[U_2I_4(*m*TP^m)(thf)$_4$]·3thf, 8(*m*TP^m)	[U_2I_4(*m*TP^t)(thf)$_4$]·1.5tol, 8(*m*TP^t)
U(1)–O(1)	2.08(1)	2.10(1)
U(1b)–O(1b)		2.10(1)
U(1)–O(2)	2.13(1)	2.12(1)
U(1b)–O(2b)		2.10(1)
U(1)–I(1)	3.064(2)	3.041(2)
U(1b)–I(1b)		3.046(2)
U(1)–I(2)	2.986(1)	3.036(2)
U(1b)–I(2b)		3.019(2)
U(2)–O(3)	2.12(9)	2.12(1)
U(2b)–O(3b)		2.11(1)
U(2)–O(4)	2.13(1)	2.11(1)
U(2b)–O(4b)		2.10(2)
U(2)–I(3)	3.011(2)	3.036(2)
U(2b)–I(3b)		3.037(2)
U(2)–I(4)	3.056(1)	3.055(2)
U(2b)–I(4b)		3.036(2)
O(1)–U(1)–O(2)	94.1(4)	90.9(4)
O(1b)–U(1b)–O(2b)		90.6(4)
O3–U2–O4	91.5(4)	91.5(4)
O3b–U2b–O4b		91.7(5)

Table 3-1 Selected bond lengths and angles for **[U_2I_4(*m*TP^m)(thf)$_4$]·3thf**, **8(*m*TP^m)** and **[U_2I_4(*m*TP^t)(thf)$_4$]·1.5toluene**, **8(*m*TP^t)**.

The solid-state structure of **[U_2I_4(*m*TP^m)$(thf)_4$]·3thf, 8(*m*TP^m)** is displayed in Figure 3-2. The coordination environment of the two uranium centres differs. Whilst both metal centres adopt a *pseudo*-octahedral geometry, the aryloxide and iodide ligands occupy the equatorial plane about U(2) with the axial positions occupied by thf donor molecules in a *trans* arrangement. The coordinated thf molecules about U(1) are mutually *cis*, occupying one axial and one equatorial position. This surprising feature results in different bond lengths and angles. The U(1)–O(1) bond length is shorter than the average of the three other U–O(aryloxide) bond lengths. The overall average U–O(aryloxide) bond distance is 2.11(5) Å, which is shorter than the average U–O(aryloxide) bond distances in the **[U_2(*m*$TP)_2$]** complexes **2(*m*TP)** and **3(*m*TP)** and the dinitrogen complex **4(*m*TP)**. Perhaps most notable is the distortion of the U(1)–O(1)–C_{ipso} angle of 138.7(9)° compared to the other three angles, 157.0(9)° (avg). This bend in the C_{ipso} angles is similar to the corresponding angles in the homoleptic uranium(IV) complex $U(ODtbp)_4$ (154.04(8))°.[4] This is unusual, as the U–O–C_{ipso} bond angles of other complexes of the type $UI_2(OAr)_2$ fall within the range 166.2(8)° to 176.9(8)°, but is ascribed to the constraints imposed by the multidentate ligand framework.

Figure 3-3 shows the solid-state structure of **[U_2I_4(*m*TP^t)$(thf)_4$]·1.5tol, 8(*m*TP^t).** There are two non-identical molecules of **8(*m*TP^t)** in the asymmetric unit cell, which are very similar to the bimetallic uranium complexes synthesised from the *para*-tetraphenol arene ligand in the Arnold group.[5] Both uranium(IV) centres have a *pseudo*-octahedral geometry. The equatorial plane of each uranium is occupied by two iodides and two aryloxide ligands, with two coordinating thf donors in the axial positions. The average U–O(aryloxide) bond distance (2.11(1) Å) is identical to **8(*m*TP^m)**, but longer than the corresponding bond lengths in the related uranium(IV) bisaryloxo-diiodo complexes $[I_2U(ODtbp)_2(thf)]$ (2.076 Å avg),[6] and $[I_2U(OAr)_2(thf)_3]$ (Ar = O-4-^{t}BuC_6H_4) (2.068(8) Å avg).[7] Additionally, the mean U–O–C_{ipso} bond angle in **[U_2I_4(*m*TP^t)$(thf)_4$]·1.5tol, 8(*m*TP^t)** is slightly greater than in **[U_2I_4(*m*TP^m)$(thf)_4$]·3thf, 8(*m*TP^m)** (154.83°).

3.2.1 Reaction to target deprotonation of [U_2I_4(*m*TP^m)$(thf)_4$], 8(*m*TP^m)

The pK_a of the benzylic protons in **8(*m*TP^m)** is expected to be close to 30 (pK_a Ph_3CH = 30 in DMSO).[8] It was demonstrated in Chapter 2 that two of the hydrogen atoms in the benzylic positions of the ligand in **[{U(*m*TP^m)}$_2$]**, **3(*m*TP^m)** are susceptible to abstraction by potassium

benzyl (p*K*a toluene = 42 in DMSO),[8] yielding the potassium incorporated product **[K(thf)$_6$][U$_2$(*m*TP^m)$_2$K(thf)$_2$]**, **6(*m*'TP^m)**. When **8(*m*TP^m)** was treated with potassium benzyl however, multiple products were formed. By-product formation was assumed to be the result of KI elimination with benzyl coordination to the uranium centres, but clean isolation of these species was unsuccessful (Scheme 3-3).

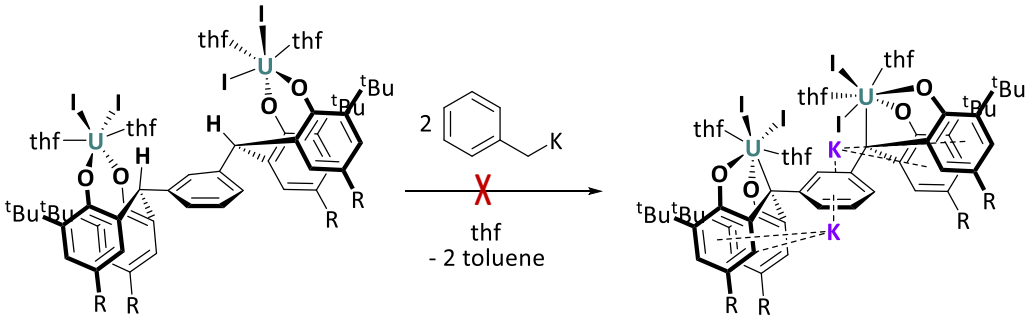

8(*m*TP^m) R = Me

Scheme 3-3 Reaction to target deprotonation of the ligand backbone of **8(*m*TP^m)**.

3.2.2 Ancillary ligand substitution and synthesis of [(UI{OTtbp})$_2$(*m*TP^m)], 10(*m*TP^m)

The potassium salt of the bulky aryloxide 2,4,6-tri-*tert*-butylphenoxide (KOTtbp) is prepared from 2,4,6-tri-*tert*-butylphenol and [KN(SiMe$_3$)$_2$] in Et$_2$O according to a literature procedure.[9] A solution of **[U$_2$I$_4$(*m*TP^m)(thf)$_4$]**, **8(*m*TP^m)** in toluene was added to a suspension of 2.1 equivalents of KOTtbp in toluene and stirred overnight. The precipitated KI and excess KOTtbp were removed by filtration, and the solvent was removed under reduced pressure to provide **[(UI{OTtbp})$_2$(*m*TP^m)]**, **10(*m*TP^m)** as a dark green solid in 73 % yield.

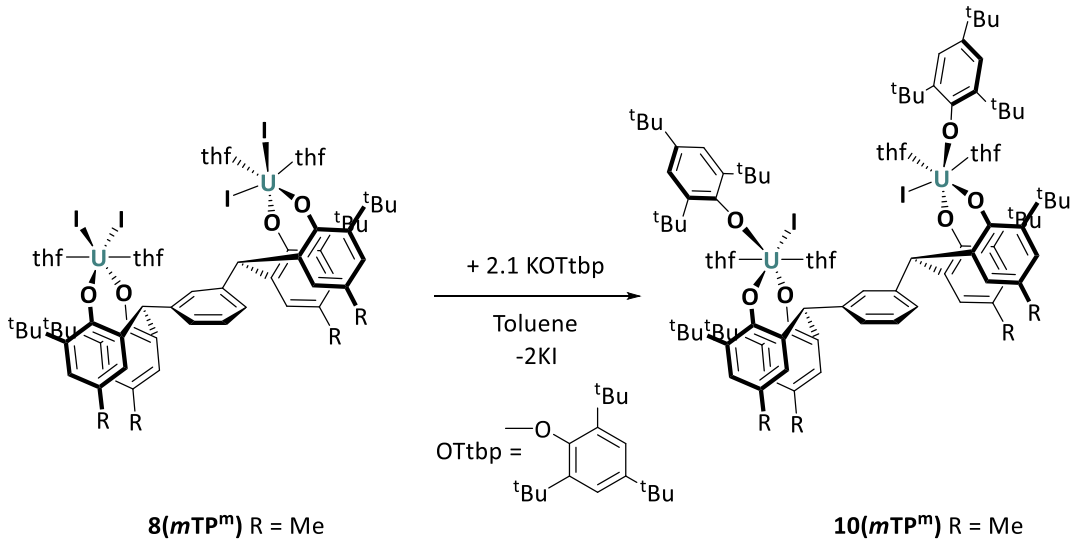

Scheme 3-4 Synthesis of **10(m*TP*^{m})**.

The ^{1}H NMR spectrum of a benzene solution of **10(*m*TP^{m})** contains eight resonances within the range 14 ppm to −1 ppm. These are significantly shifted relative to the corresponding resonances in the ^{1}H NMR spectrum of the parent tetraiodide complex and include three new proton resonances consistent with the pendent aryloxide ligand. Elemental microanalysis was consistent with the proposed structure.

8(*m*TP^{m}) was also treated with 4,4'-bipyridine and potassium or lithium salts of several other aryloxides and substituted anilines (Scheme 3-5) in attempts to generate a series of substituted complexes for further studies. Whilst there is evidence for the formation of new substitution products, these have not been isolated cleanly. Attempts to generate uranium alkyls by reacting **8(*m*TP^{m})** with MeLi were also unsuccessful.

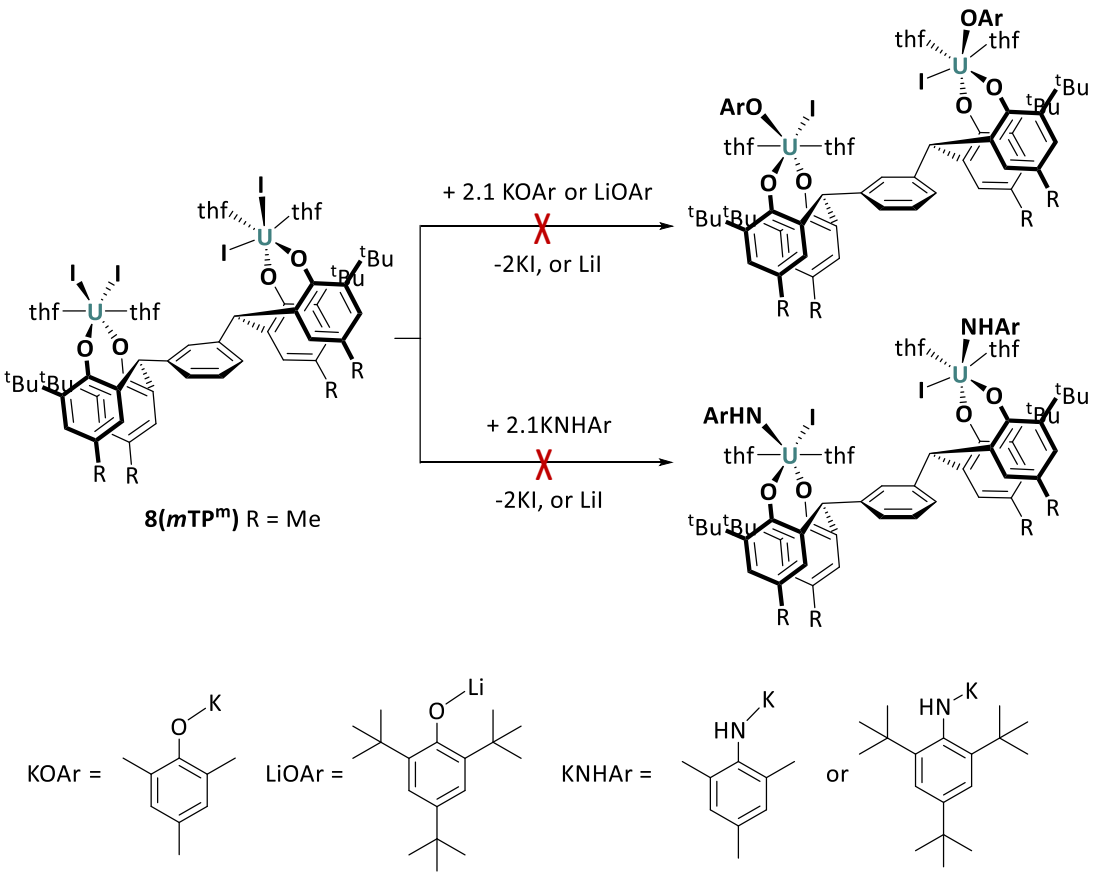

Scheme 3-5 Reactions of **8(*m*TP^{m})** to target further substitution products.

Authors including Tanaka and coworkers have exploited redox active bridging ligands in novel catalyst design. 1,8-Bis(2,2′:6′,2″-terpyridyl)anthracene (btpyan), for example, was used to bridge two ruthenium centres providing the water oxidation catalyst $[Ru^{III}_2(O)_2(3,6\text{-}{}^{t}Bu_2qui)_2(btpyan)]^{4+}$ (qui = 1,2-benzoquinone) with an efficiency of 91% (21 turnovers).[10] Substitution of an iodo co-ligand on each U in **8(*m*TP^{m})** for a conjugated bidentate ligand (Scheme 3-6) was attempted to target insertion of a redox active bridge between the two metals.

The mean O–O separation of 4,4′-dihydroxybiphenoxide fragments in structures available in the Cambridge Structural Database (CSD) was found to be 9.782 Å (771 structures, range = 8.648 - 10.242 Å). The U–U separation distance in **8(*m*TP^{m})** in the solid-state is 9.387 Å, suggesting that 4,4′-dihydroxybiphenoxide should be an appropriate lengthed bridge.

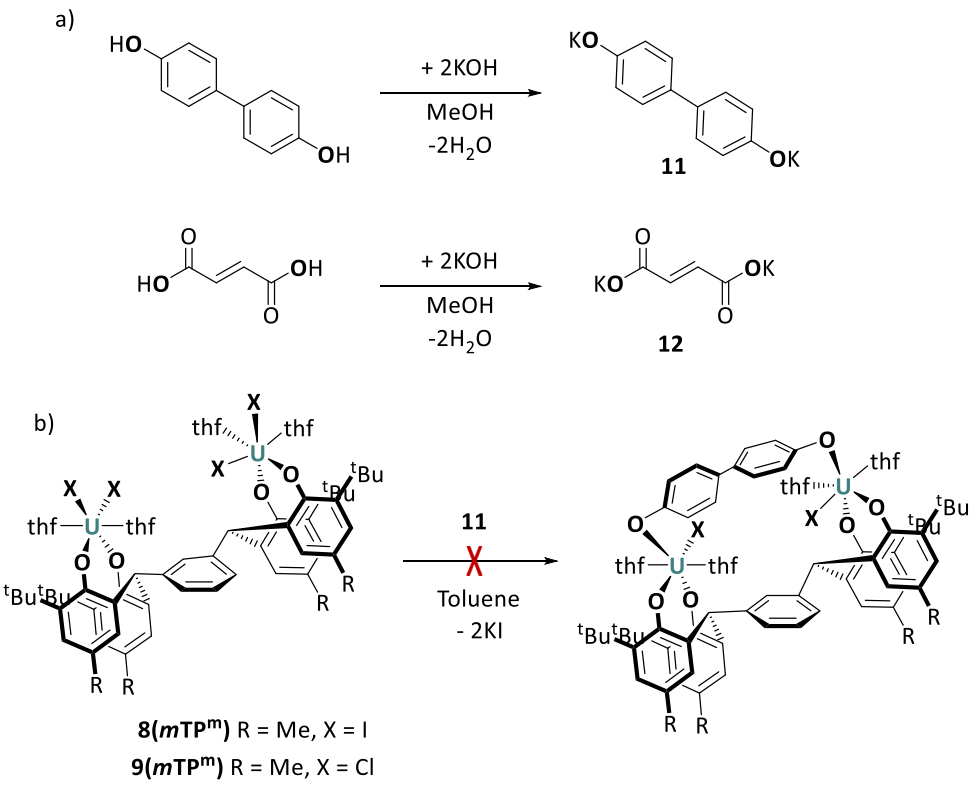

8(*m*TP^{m}) R = Me, X = I
9(*m*TP^{m}) R = Me, X = Cl

Scheme 3-6 a) Synthesis of **11** and **12** and b) reactions to target synthesis of **[(UX)$_2$(μ-OR)(*m*TP^{m})]**.

The dipotassium salt of 4,4'-dihydroxybiphenol (**11**) was prepared by treatment with KOH in methanol, yielding an off-white solid in 66 % yield, but metathesis with **8(*m*TP^{m})** was not successful (Scheme 3-6).

The shorter aliphatic analogue, dipotassium *trans*-butenedioate (**12**), was obtained *via* deprotonation of *trans*-butenedioic acid with KOH (Scheme 3-6) and reacted with both **8(*m*TP^{m})** and **9(*m*TP^{m})**. In both cases, new paramagnetically shifted resonances were observed in the ^{1}H NMR spectra but the products could not be cleanly isolated and were not further characterised.

3.2.3 Reduction of [U$_2$X$_4$(*m*TP)(solv)$_4$]

Attempts to directly synthesise U(III) 'half-letterbox' complexes from UI_3 and **H$_4$(*m*TP^{m})** *via* salt metathesis reactions were not successful, instead disproportionation was observed to yield U and U(IV) products. Reduction of the U(IV) complex **8(*m*TP^{m})** was therefore targeted. The U(IV)/(III) redox couple is known to range from −2.78 to −1.83 V versus Fc/Fc^{+} depending on the ligand environment.[11–13] Cyclic voltammetry measurements indicate that **8(*m*TP^{m})** has

one reduction at −2.0289 V (vs. Fc/Fc^+) (peak **1**) attributed to the single electron reduction of both metal centres at the same time, confirming the absence of U(IV)/U(IV) electronic communication through the ligand (Figure 3-4). The small feature at −1.7 V (peak **2**) varies in size during repeated experiments and is not associated with the complex. Cyclic voltammetry measurements are discussed in more detail in Section 3.4 (*vide infra*).

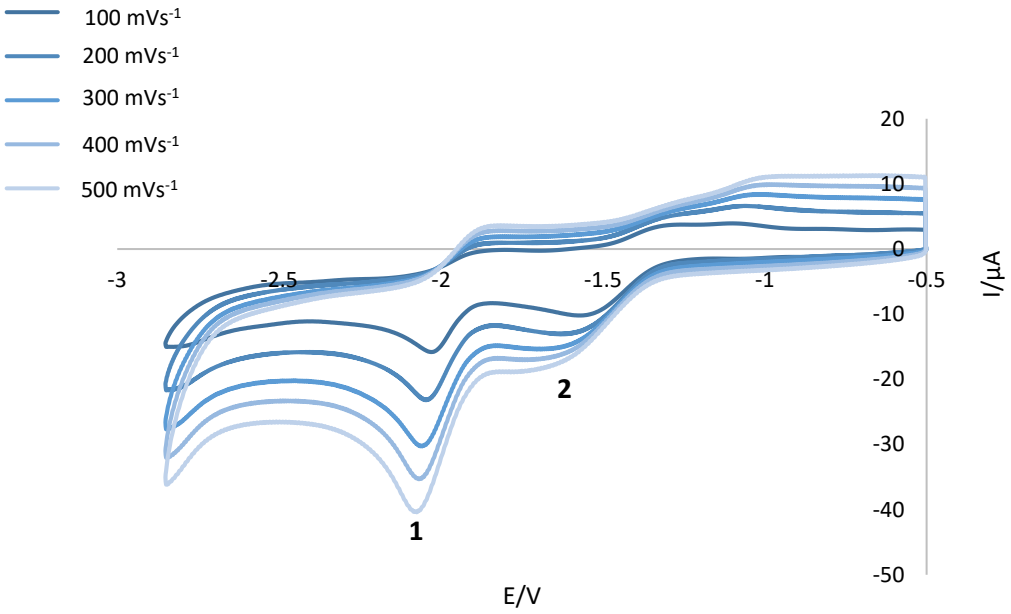

Figure 3-4 Cyclic voltammogram of **[U_2I_4(*m*TP^m)(thf)$_4$]**, **8(*m*TP^m)** at varying scan rates, thf /0.1 M [^{n}Bu$_4$N][BPh_4].

The U(III) analogue should therefore be chemically accessible *via* reaction with potassium reductants (K/K^+ potential = −2.9 V vs. SHE). Despite this, multiple attempts at the reduction of **8(*m*TP^m)** with two equivalents (or a slight excess) of KC_8 in both coordinating and non-coordinating solvents failed to provide the target complex. Despite colour changes to dark brown from green, ^{1}H NMR spectra indicated that no new paramagnetic products were formed.

Reduction of **[(UI{OTtbp})$_2$(*m*TP^m)]**, **10(*m*TP^m)** on the other hand, was more successful. Although it was anticipated that the additional steric congestion provided by the bulky pendant aryloxide ligand may favour reduction to U(III) by providing a steric driving force for the loss of the remaining iodide, the reduction potential of **10(*m*TP^m)**, as determined by cyclic voltammetry is −2.5068 V, which is 0.478 V more negative than that of **8(*m*TP^m)**. The reaction of **10(*m*TP^m)** with two equivalents of KC_8 in 1,4-dioxane proceeded within two hours, yielding

a dark brown suspension. Following filtration to remove graphite and KI by-products, the brown solution was dried under reduced pressure to yield a pale brown solid, which was extracted into benzene. The volatiles were removed under reduced pressure to yield **[U_2(*m*TP^m)(OTtbp)$_2$(solv)$_4$]**, **13(*m*TP^m)** as a brown solid (62%).

Attempts to grow single crystals of **13(*m*TP^m)** have not been successful, but the ^{1}H NMR spectrum is consistent with the clean isolation of **[U_2(*m*TP^m)(OTtbp)$_2$(solv)$_4$]**; eight resonances corresponding to ligand protons are present, along with three additional resonances attributed to the coordinated aryloxide. The resonances are significantly shifted relative to the U(IV) precursor, **10(*m*TP^m)**, consistent with the proposed uranium reduction (Scheme 3-7).

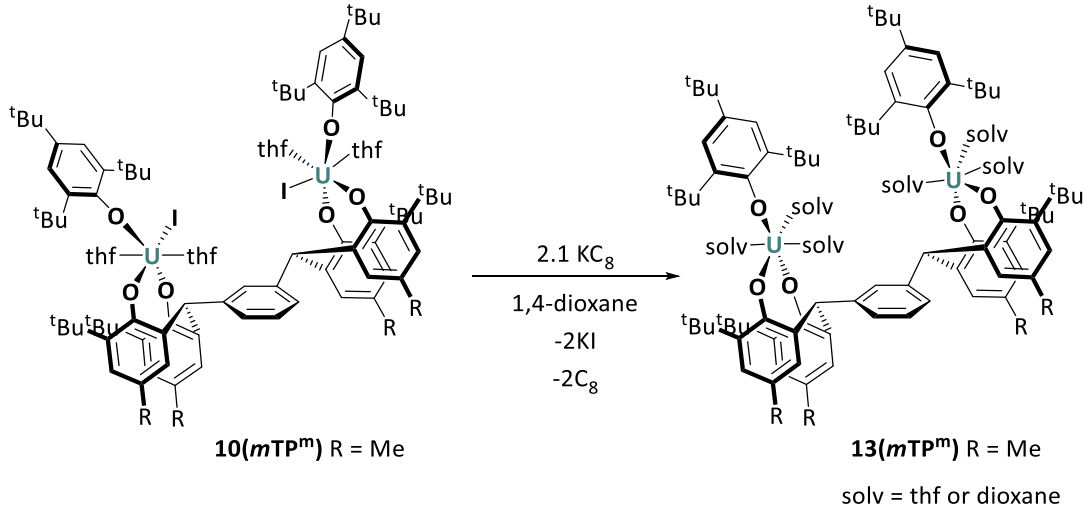

Scheme 3-7 Reduction of **[(UI{OTtbp})$_2$(*m*TP^m)]**, **10(*m*TP^m)** to yield **[U_2I_2(*m*TP^m)(OTtbp)$_2$(solv)$_4$], 13(*m*TP^m).**

3.2.4 Reactivity of [U_2(*m*TP^m)(OTtbp)$_2$(solv)$_4$], 13(*m*TP^m)

The related U(III) aryloxide complex [U(OTtbp)$_3$] (OTtbp = tri-*tert*-butylphenol) (described in Chapter 1) was reported to reductively insert CO_2 at ambient pressures, albeit only at elevated temperatures and with ligand dissociation and a significant structural reorganisation to provide **AK**, U_2(OTtbp)$_4$(μ-O)(μ-η^1:η^1-$O_2COC_6H_2$-^{t}Bu$_3$-2,4,6)$_2$ (Scheme 3-8).[14] It was anticipated that the incorporation of the more robust, chelating tetraphenol ligand framework (*m*TP) around a U(III)−OTtbp bond may prevent ligand rearrangement and allow for more well-defined, well-controlled CO_2 activation chemistry.

The reaction of **[U_2(*m*TP^m)(OTtbp)$_2$(solv)$_4$]**, **13(*m*TP^m)** with CO_2 was carried out to target reductive insertion, but the addition of one bar of CO_2 to a frozen solution of **13(*m*TP^m)** in d_6-benzene lead an immediate colour change upon thawing to dark brown and a complete loss of sharp resonances in the ^{1}H NMR spectrum of the reaction mixture, suggesting oxidative decomposition of the compound (Scheme 3-8).

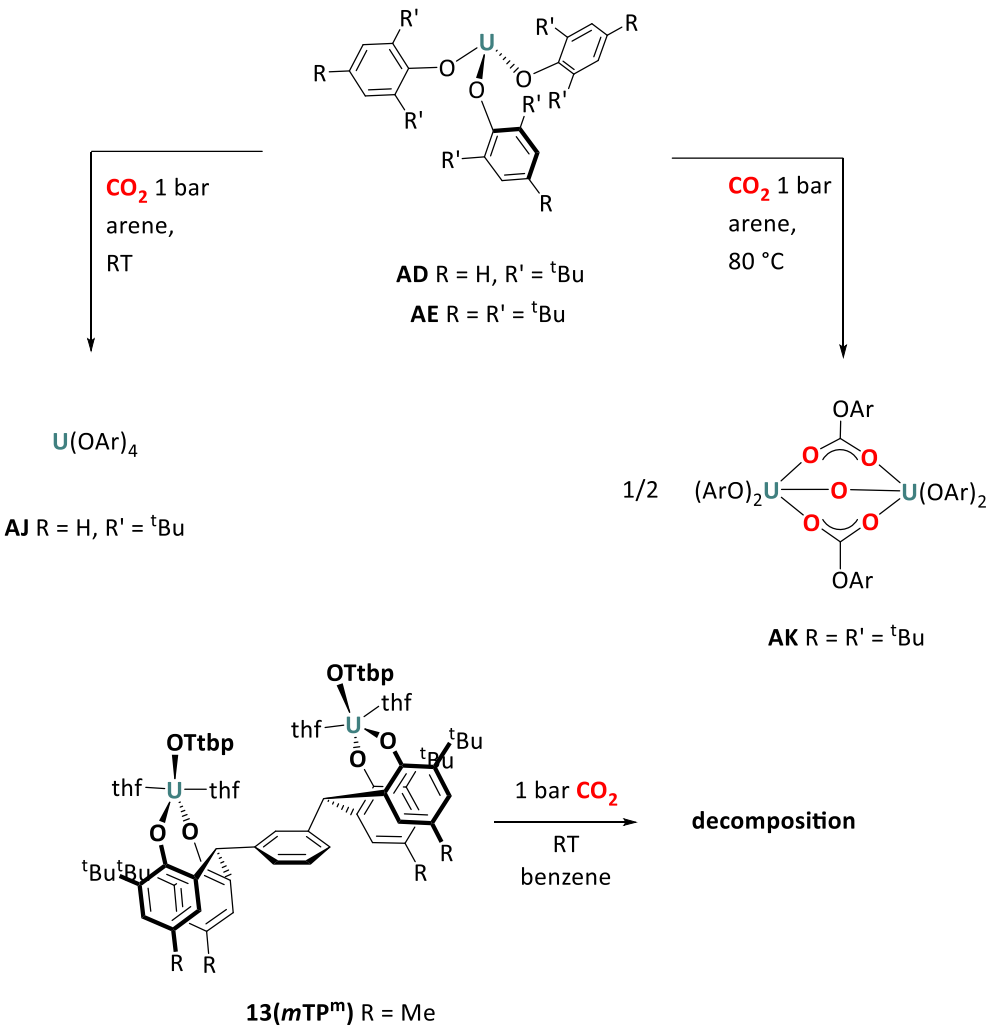

Scheme 3-8 Reaction to target CO_2 insertion into **13(*m*TP^m)** and reported CO_2 insertion chemistry of [U(OTtbp)$_3$].[14]

Reactions of **13(*m*TP^m)** with CO and xylyl isocyanide were also carried out but the target insertion products were not isolated.

3.2.5 Dinitrogen activation mediated by $[U_2I_4(mTP)(thf)_4]$, 8(mTP^m)

Section 3.2.3 describes the reduction of **[(UI{OTtbp})$_2$(*m*TP^m)]**, **10(*m*TP^m)** with two equivalents of KC_8 to yield **[U$_2$(*m*TP^m)(OTtbp)$_2$(solv)$_4$]**, **13(*m*TP^m)**, and the treatment of **[U$_2$I$_4$(*m*TP^m)(thf)$_4$]**, **8(*m*TP^m)** with two equivalents of KC_8 which showed the formation of no new paramagnetic products.

The two uranium centres in **8(*m*TP^m)** and **8(*m*TP^t)** are considerably further apart (9.387 Å (*m*TP^m), 11.628 Å (*m*TP^t) in the solid-state) than observed in **3(*m*TP)**, **[{U(*m*TP^m)}$_2$]**, (6.573 Å), and the siloxide bridged structures described by Mazzanti and co-workers (4.234 Å in the nitride bridged $[K_3\{[U(OR)_3]_2(\mu\text{-}N)\}]$, **BK**, Chapter 1).[15] There is no literature precedent that suggests a bimetallic uranium complex with such a long metal-metal separation distance should be able to support metal based cooperative reactivity, but results presented in this and previous chapters suggest that the ligand backbone demonstrates considerable flexibility and that in solution **8(*m*TP^m)** and **8(*m*TP^t)** exhibit free rotation around the ligand $Ar_2C–Ar$ single bonds. The reactivity of **8(*m*TP^m)** and **8(*m*TP^t)** with excess reductant was therefore investigated to target N_2 binding.

8(*m*TP^m) was treated with six equivalents of KC_8 in toluene at −30 °C under an atmosphere of N_2 and stirred overnight (Scheme 3-9). The resulting dark brown reaction mixture was filtered to remove graphite and KI by-products and the volatiles were removed under reduced pressure. The isolated dark brown powder was washed several times with hexane to yield a new product, **14(*m*TP^m)**, in modest yield (27 %). Whilst no molecular structure has been found by XRD, elemental microanalysis is consistent with a chemical formula of $C_{68}H_{94}I_2K_4N_2O_8U_2$, which corresponds to incorporation of a single molecule of N_2, coordination of four potassium cations and the loss of two iodide ligands yielding **[K$_4$][U$_2$I$_2$(*m*TP^m)(N$_2$)(thf)$_4$]** (Scheme 3-9). This formulation is supported by ^{1}H NMR spectroscopy of the product which shows a loss of symmetry (15 resonances over a range of 56 ppm) relative to the parent **8(*m*TP^m)**, consistent with binding of potassium cations to the ligand arenes.

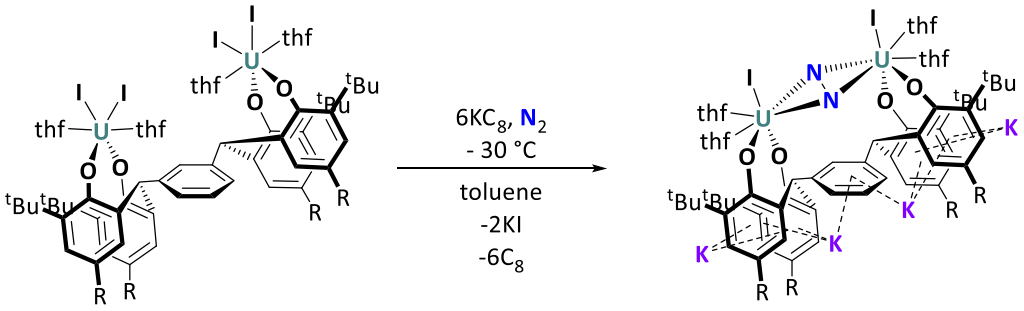

8(*m*TP^{m}) R = Me
8(*m*TP^{t}) R = ^{t}Bu

14(*m*TP^{m}) R = Me
14(*m*TP^{t}) R = ^{t}Bu

Scheme 3-9 Reduction of **8(*m*TP)** under dinitrogen to yield **14(*m*TP)**.

The proposed molecular structure is most likely to correspond to two U(III) centres and a $[N_2]^{4-}$ ligand. Collection of magnetic moment, single crystal XRD and Raman spectroscopy data would help to confirm this assignment.

In Chapter 2, quenching reactions and characterisation of the resulting products were used to help confirm the identity of complex **4(*m'*TP^{m})**. **14(*m*TP^{m})** and **14(*m*TP^{t})** were therefore reacted with acids and electrophiles in reactions targeting the release of functionalised nitrogen products.

20 equivalents of [PyH]Cl were added to solutions of **14(*m*TP^{m})** and **14(*m*TP^{t})** in benzene, respectively, and stirred for approximately 30 minutes to yield colourless suspensions. In each case the colourless solid was collected by filtration, washed with thf and dried under reduced pressure. The solid was dissolved in d_6-dmso and an internal standard was added (dimethylsulfone). In both cases, protonation of the N_2 ligand provided NH_4Cl in moderate yields (17–24 %) (Scheme 3-10), as determined by quantitative ^{1}H NMR spectroscopy.

In order to establish the origin of each proton in the NH_4Cl product, the quench reaction was repeated using [PyD]Cl. A sample of **[K$_4$][U$_2$I$_2$(*m*TP^{m})(N$_2$)(thf)$_4$]**, **14(*m*TP^{m})** was prepared in toluene-d_8 and added to 20 equivalents of [PyD]Cl. After 30 minutes the colourless solid was collected by filtration. ^{1}H NMR spectroscopy of the solid confirmed the absence of N*H*$_4$Cl. ^{2}H NMR spectroscopy, on the other hand, showed a broad triplet at 7.55 ppm. This was assigned as N*D*$_4$Cl, confirming that in this case the (*m*TP) ligand is not providing any protons. In Chapter 2, the unusual positioning of the benzylic C–H bonds within the 'letterbox' cavity enabled direct functionalisation of N_2 to yield bound $[N_2H_2]^{2-}$ in complex **4(*m'*TP^{m})**. It is suggested that

the more open structure of the 'half-letterbox' geometry allows the benzylic C–H bonds to remain intact, preventing the direct protonation.

As described in Chapter 2, **4(*m'*TP^m)** mediates the overall hydrosilylation of N_2 *via* initial C–H activation of the (*m*TP) ligand followed by reactions with external Si electrophiles. The deuterium labelled quenching experiment described above suggests that in this case, C–H activation of the (*m*TP) ligand does not take place during the reduction step. Therefore, if it is possible to quench the product to provide N–Si bonds, reactions with Si electrophiles are expected to provide $N(SiMe_3)_3$ rather than $HN(SiMe_3)_2$. Complete silylation of dinitrogen by external Si electrophiles to afford $N(SiMe_3)_3$ is more typical.[16–18]

14(*m*TP^m) and **14(*m*TP^t)** were treated with six equivalents of Me_3SiOTf (Scheme 3-10). ^{29}Si INEPT NMR spectra of the resulting reaction mixture indicated no release of N–Si products in either case, but rather only two products assigned as the homocoupled $Me_3Si–SiMe_3$ and an iodine incorporated analogue $IMe_2Si\text{-}SiMe_2I$, formed *via* abstraction of iodide ligands, as well as unreacted Me_3SiOTf.

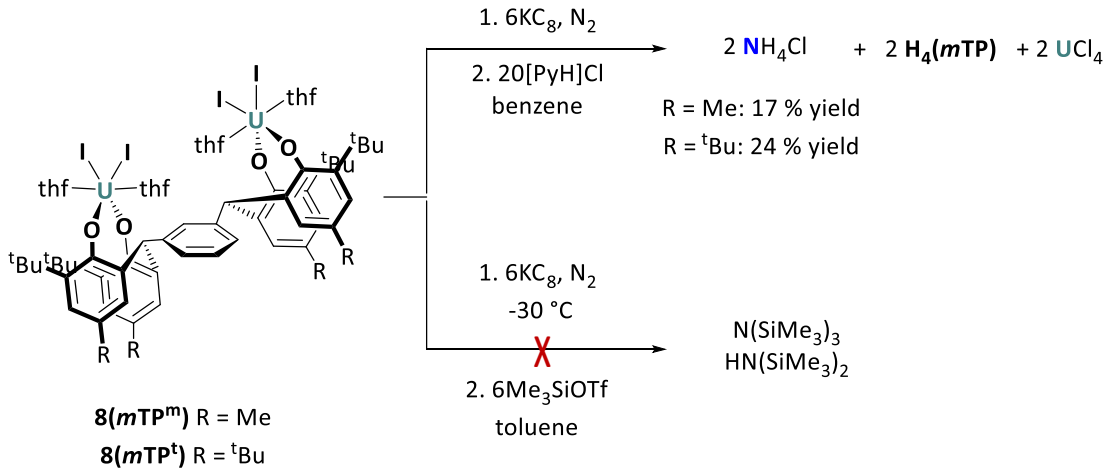

Scheme 3-10 N_2 functionalisation mediated by **8(*m*TP).**

Whilst it was anticipated that the coordinatively unsaturated uranium centres in **4(*m'*TP)** (Chapter 2) may mediate N_2 binding under reducing conditions, N_2 activation mediated by the coordinatively saturated uranium centres in **8(*m*TP^m)** and **8(*m*TP^t)** is more surprising, especially given the relatively long U–U distances (9.387 Å **8(*m*TP^m)**, 11.628 Å **8(*m*TP^t)**) in the solid-state.

Moreover, the reactivity demonstrated by **8(*m*TP^t)**, (Scheme 3-10) indicates that the solid-state geometry and 'pre-organisation' of the metals on the same face of the ligand may be less important than previously suggested. In solution, there is a very low energy barrier for rotation around the Ar_2C–Ar single bond, allowing cooperative reactivity of the metals regardless of the most favourable conformer in the solid-state. This result is also consistent with NMR spectra of **8(*m*TP^t)** which show C_2 symmetry in solution, and the synthesis of 'letterbox' type complexes from **H$_4$(*m*TP^t)** in Chapter 2, in which the templating effect of the second ligand equivalent allowed the metals to align on the same ligand face.

3.3 Silylamido ancillary ligands

The synthesis of silylamido coordinated half-letterbox complexes was targeted *via* protonolysis with the U(IV) metallacycle **[U(N")$_2$(N{SiMe$_3$}SiMe$_2$CH$_2$)]**. **H$_4$(*m*TP^m)** or **H$_4$(*m*TP^t)** were dissolved in a minimum amount of hexane and added slowly to a concentrated solution of **[U(N")$_2$(N{SiMe$_3$}SiMe$_2$CH$_2$)]** (two equivalents) in hexane. The solutions were stirred overnight at room temperature to yield the target complexes **[U$_2$(*m*TP^m)(N{SiMe$_3$}$_2$)$_4$]**, **15(*m*TP^m)** and **[U$_2$(*m*TP^t)(N{SiMe$_3$}$_2$)$_4$]**, **15(*m*TP^t)** respectively, in good yields (54 - 65 %). **15(*m*TP^m)** was isolated by filtration as a pale-yellow powder which formed as a precipitate from the reaction mixture. The bulkier substituents around **15(*m*TP^t)** rendered the complex soluble in hexane at room temperature. This product was isolated as a yellow crystalline solid following storage of the hexane reaction mixture at −30 ° C overnight (Scheme 3-11).

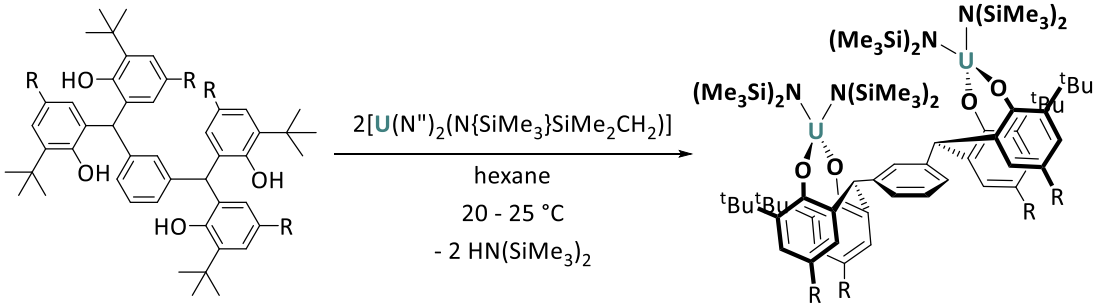

H$_4$(*m*TP^m) R = Me
H$_4$(*m*TP^t) R = ^{t}Bu

15(*m*TP^m) R = Me
15(*m*TP^t) R = ^{t}Bu

Scheme 3-11 Synthesis of complexes **15(*m*TP^m)** and **15(*m*TP^t)** *via* protonolysis.

^{1}H and ^{29}Si INEPT NMR spectroscopy, elemental analysis and single crystal XRD are consistent with the proposed molecular formulations of **15(*m*TP^{m})** and **15(*m*TP^{t})**, however attempts to characterise these complexes by MALDI (Matrix Assisted Laser Desorption Ionization) mass spectrometry were not successful. ^{1}H NMR spectra show C_2 symmetry in solution, with nine discrete resonances over a paramagnetic range of 65 ppm.

The ^{29}Si INEPT NMR spectra of **15(*m*TP^{m})** and **15(*m*TP^{t})** each contain a single resonance close to −230 ppm, indicating only one Si environment, consistent with C_2 symmetry. Si chemical shifts have been shown to correlate with through-space uranium–silicon distances in complexes of $[N(SiMe_3)_2]^-$.[19] Most U(IV) complexes with Si-containing ligands show Si chemical shifts between 0 and −150 ppm, but the related U(III) complex $U[N(SiMe_3)_2]_3$ has a ^{29}Si NMR chemical shift of −220 ppm and complexes containing cyclometalated silicon-containing ligands such as $[(\eta^5{:}\eta^1\text{-}C_5Me_4SiMe_2CH_2)_2U]$, (which have uranium(IV)–silicon distances comparable to those in **15(*m*TP^{m})** and **15(*m*TP^{t})**), have given rise to ^{29}Si NMR resonances shifted as far as −255 ppm.[19]

Recrystallisation of **15(*m*TP^{m})** by either slow diffusion of hexanes into a concentrated 1,4-dioxane solution or slow diffusion of benzene into a concentrated hexane solution, provided yellow crystals suitable for single crystal XRD. Crystals of **15(*m*TP^{t})** could be obtained by storing the crude hexane reaction mixture at −30 °C overnight. Solid-state structures of **15(*m*TP^{m})** and **15(*m*TP^{t})** are shown in Figures 3-5 and 3-6, respectively, and show that in analogy with the halide complexes, (*m*TP^{t}) forces the metals to opposite faces of the ligand, whereas (*m*TP^{m}) favours the co-facial conformer.

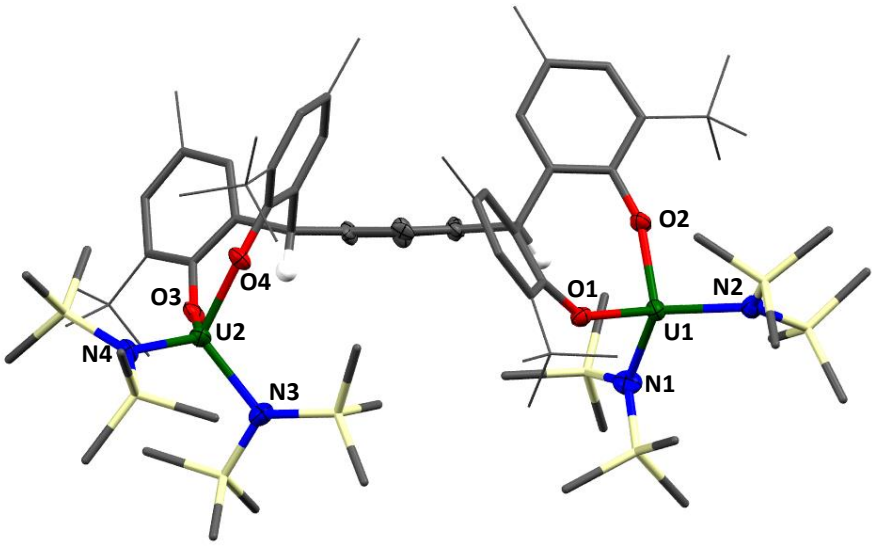

Figure 3-5 Solid-state structure of **[U_2(*m*TP^m)(N{$SiMe_3$}$_2$)$_4$]·hex, 15(*m*TP^m).** For clarity, all backbone hydrogen atoms and lattice solvent molecules are omitted. The benzylic hydrogens, uranium, nitrogen, oxygen and selected carbon atoms are displayed as displacement ellipsoids drawn at 50 % probability. The remaining atoms and bonds are shown as capped stick or wireframe. Selected bond lengths (Å) and angles (°) for **15(*m*TP^m)** are given in Table 3-2.

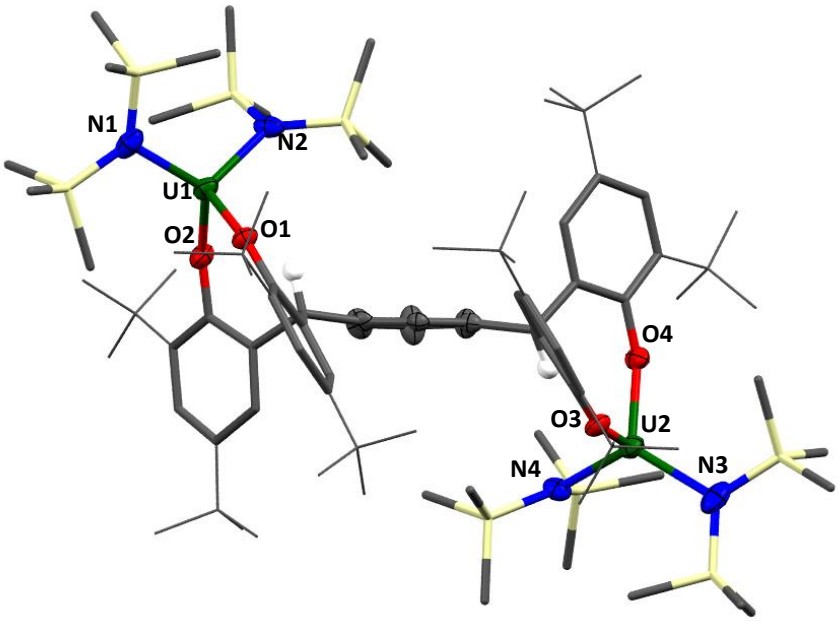

Figure 3-6 Solid-state structure of **[U_2(*m*TP^t)(N{$SiMe_3$}$_2$)$_4$], 15(*m*TP^t).** For clarity, all backbone hydrogen atoms and lattice solvent molecules are omitted. The benzylic hydrogens, uranium, nitrogen, oxygen and selected carbon atoms are displayed as displacement ellipsoids drawn at 50 % probability. The remaining atoms and bonds are shown as capped stick or wireframe. Selected bond lengths (Å) and angles (°) for **15(*m*TP^t)** are given in Table 3-2.

Parameter	$[U_2(mTP^m)(N\{SiMe_3\}_2)_4]\cdot$hex, 15($mTP^m$)	$[U_2(mTP^t)(N\{SiMe_3\}_2)_4]$, 15($mTP^t$)
U(1)–O(1)	2.130(4)	2.098(5)
U(1)–O(2)	2.110(4)	2.142(5)
U(1)–N(1)	2.265(5)	2.264(7)
U(1)–N(2)	2.254(6)	2.260(7)
U(2)–O(3)	2.139(5)	2.118(5)
U(2)–O(4)	2.112(4)	2.134(5)
U(2)–N(3)	2.228(5)	2.255(7)
U(2)–N(4)	2.264(6)	2.269(6)
O(1)–U(1)–O(2)	97.46(2)	98.6(2)
N(1)–U(1)–N(2)	117.0(2)	121.8(3)
O(3)–U(2)–O(4)	98.81(2)	99.7(2)
N(3)–U(2) –N(4)	113.4(2)	115.4(3)

Table 3-2 Selected bond lengths and angles for **$[U_2(mTP^m)(N\{SiMe_3\}_2)_4]\cdot$hex**, **15($mTP^m$)** and **$[U_2(mTP^t)(N\{SiMe_3\}_2)_4]$**, **15($mTP^t$)**.

The crystal structures of **$[U_2(mTP^m)(N\{SiMe_3\}_2)_4]\cdot$hexane**, **15($mTP^m$)** and **$[U_2(mTP^t)(N\{SiMe_3\}_2)_4]$**, **15($mTP^t$)**, are closely related to those of **8(mTP^m)** and **8(mTP^t)**. The $[N(SiMe_3)_2]^-$ ligand is more sterically demanding than the iodide ligands in **8(mTP^m)** and **8(mTP^t)**, resulting in a four-coordinate distorted tetrahedral metal geometry (τ_4(U1,U2) = 0.82,0.81 for **8(mTP^m)** and 0.83,0.84 for **8(mTP^t)**) in contrast to the six coordinate uranium centres provided by the coordination of two solvent molecules to each metal in **8(mTP^m)** and **8(mTP^t)**.

Each metal in **$[U_2(mTP^m)(N\{SiMe_3\}_2)_4]\cdot$hexane, 15($mTP^m$)** is coordinated by two aryloxide ligand moieties and two silylamido ligands. The average O–U–O angle is 98.14(2)°, which is more acute than the average N–U–N angle (115.20(2)°). This asymmetry is thought to be due to the steric bulk of the $N(SiMe_3)_2$ groups. The average U–O bond distance is 2.123(4) Å, which is shorter than the corresponding distance in **3(mTP^m)** but similar to that of $[U(ODtbp)_4]$ (ODtbp = O-2,6-$^tBu_2C_6H_4$), as well as the *pseudo*-tetrahedral mixed aryloxo-amido uranium(IV) complexes $[Et_2NU(ODtbp)_3]$ and $[\{N(SiMe_3)_2\}_3U(ODtbp)]$.[20–22] The mean U–N bond distance in **15(mTP^m)** (2.260(6) Å) is significantly longer than the U–N distance of 2.161(5) Å exhibited by $[Et_2NU(ODtbp)_3]$, but is similar to the U–N bond distances in $[\{N(SiMe_3)_2\}_3U(ODtbp)]$.

Compared to **8(*m*TP^{m})**, the metal-metal separation distance is significantly longer at 10.4404(5) Å, compared to 9.387(1) Å. The mean through-space U–Si distance is only 3.418(3) Å, which is consistent with the very negative value of the ^{29}Si NMR chemical shift.

The solid-state structure of **8(*m*TP^{t})** is very similar. The average U–O (2.123(5) Å) and U–N (2.262(7) Å) bond distances are identical to those in **8(*m*TP^{m})**. The two uranium(IV) cations occupy coordination sites on opposite faces of the ligand with a diagonal U–U distance of 11.2365(8) Å. Key metrics are almost identical to those in the *para*-tetraphenol arene supported analogue, [U$_2$(*p*TP^{m})(N{SiMe$_3$}$_2$)$_4$], synthesised previously in the Arnold group.[5]

Attempts to directly synthesise U(III) analogues of **15(*m*TP^{m})** and **15(*m*TP^{t})** using **[U{N(SiMe$_3$)$_2$}$_3$]** were not successful and instead yielded U(IV) products, as a result of disproportionation. Reduction of the U(IV) centres to yield U(III) products was therefore targeted.

3.3.1 Reduction of [U$_2$(*m*TP)(N{SiMe$_3$}$_2$)$_4$], 15(*m*TP)

Cyclic voltammetry measurements identify a reduction potential of −1.995 V (*vs*. Fc/Fc^{+}) for **15(*m*TP^{m})**, assigned to the independent U(IV)→U(III) reduction of both metal centres. The cyclic voltammogram is discussed in more detail in Section 3.4 (*vide infra*). The U(III)/U(III) complex observed electrochemically was targeted chemically.

A solution of **15(*m*TP^{m})** in toluene was treated with two equivalents of KC_8 and stirred overnight at room temperature, providing a dark purple solution (Scheme 3-12). The volatiles were then removed under reduced pressure, and the product was recrystalised from heptane. The product was dried under reduced pressure to yield a dark purple solid in good yield (74 %), which was characterised by elemental analysis and ^{1}H and ^{29}Si NMR spectroscopy.

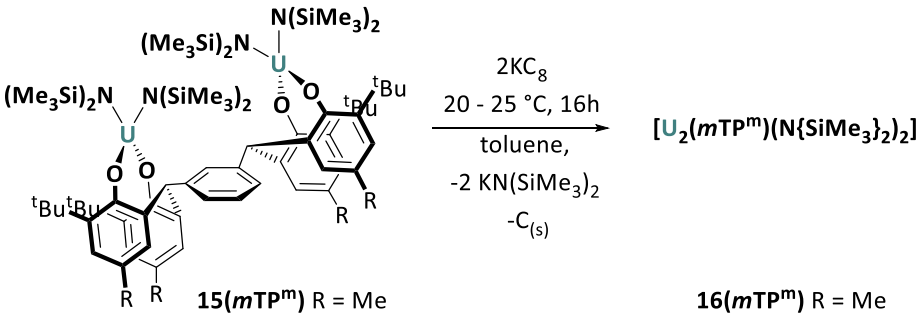

Scheme 3-12 Reduction of **15(*m*TP^{m})** with KC_8 to afford **16(*m*TP^{m})**.

All characterisation data are consistent with the loss of one equivalent of $KN(SiMe_3)_2$ per metal centre to yield the trivalent complex **[U_2(*m*TP^m)(N{$SiMe_3$}$_2$)$_2$]**, **16(*m*TP^m)**, as shown in Scheme 3-12. The single resonance present in ^{29}Si INEPT NMR spectra, which is assigned to the $N(SiMe_3)_2$ groups, is shifted downfield (−100 ppm) relative to the corresponding signal in **15(*m*TP^m)**, (−231 ppm). No evidence of N_2 incorporation was observed in samples of **16(*m*TP^m)**.

3.3.2 Reactions to target dinitrogen activation mediated by [U_2(*m*TP)(N{$SiMe_3$}$_2$)$_4$], 15(*m*TP)

Reduction of **[U_2(*m*TP)X_4]** with two equivalents of KC_8 yields U(III) **[U_2(*m*TP^m)X_2]** compounds for complexes with both halide and silylamido ancillary ligands. In Chapter 2, and Section 3.2.4, four or more equivalents of reductant were required to isolate the dinitrogen-bound complexes **4(*m*TP^m)**, **4(*m*TP^t)**, **14(*m*TP^m)** and **14(*m*TP^t)**. The reduction of **15(*m*TP^m)** and **15(*m*TP^t)** with four equivalents of reductant was therefore investigated.

Unlike the reactions of **8(*m*TP)** described in previous sections in which the only possible source of nitrogen in the organonitrogen products is N_2 incorporated during the reduction step, here silylamido ligands are present in **15(*m*TP)** prior to reduction, and $KNSiMe_3$ may be eliminated during the course of the reduction. It should therefore be noted that in the absence of ^{15}N labelling experiments, it cannot be confirmed that the source of the organonitrogen products is N_2 and not the $N(SiMe_3)_2$ ligands. Preliminary results are described below but further work is required to confirm N_2 activation.

The addition of four equivalents of KC_8 in toluene to a solution of **15(*m*TP^m)** or **15(*m*TP^t)** under an N_2 atmosphere yielded a dark red solution after stirring for several hours. Quenching reactions with [PyH]Cl yield NH_4Cl (50 % yield per U from **15(*m*TP^m)**, 93 % yield per U from **15(*m*TP^t)**). Given that yields of quenching reactions for the other complexes described have not exceeded 64 % for NH_4Cl production, an NH_4Cl yield of 93 % based on **15(*m*TP^t)** seems unlikely to be representative of nitrogen functionalisation alone and should not be considered reliable evidence of N_2 conversion.

When four equivalents of $SiMe_3OTf$ were added to the reduced intermediate derived from **15(*m*TP^m)** at low temperature (−30 °C) the dark red colour turned to orange and a colourless

solid began to form over a period of 1-2 hours, consistent with the formation of KOTf as a salt elimination product. ^{1}H and ^{29}Si INEPT NMR spectroscopy indicated partial conversion of $SiMe_3OTf$ to $N(SiMe_3)_3$. The NMR yield was quantified against an added internal standard of tri-*tert*-butylbenzene and calculated as 63 % $N(SiMe_3)_3$ per U in **15(*m*TP^{m})**. The major by-product was $(SiMe_3)_2O$, derived from the reaction of $SiMe_3$ radicals with $SiMe_3OTf$, which is proposed to be the kinetically favoured reaction. No nitrogen-containing products could be observed following the $SiMe_3OTf$ reaction of the reduced intermediate derived from **15(*m*TP^{t})** (Scheme 3-13). This contrasting reactivity between the two complexes would be unlikely if simple U−$N(SiMe_3)_2$ bond cleavage was responsible for the $N(SiMe_3)_3$ production and is suggestive of N_2 functionalisation.

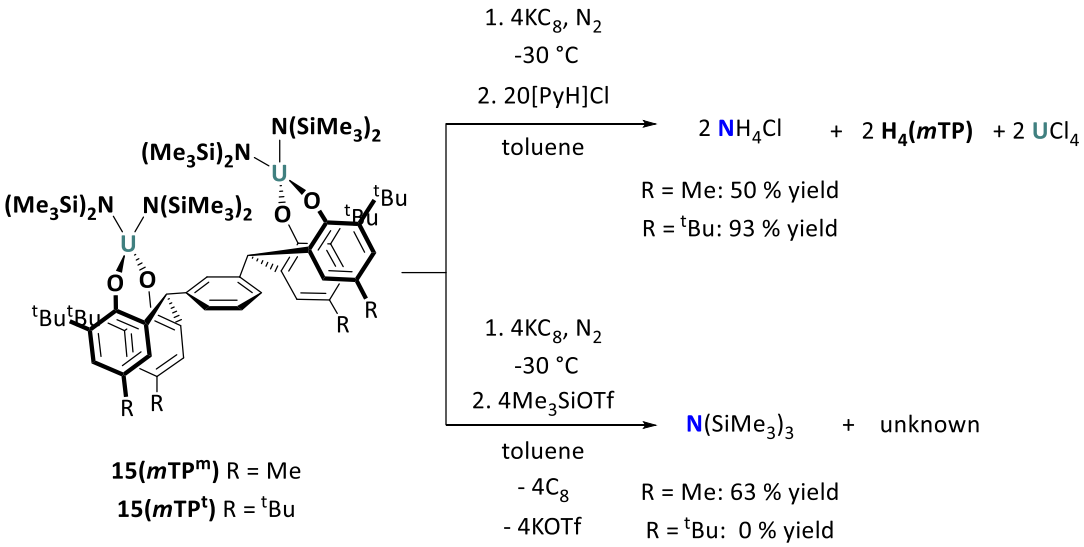

Scheme 3-13 Nitrogen activation by **15(*m*TP^{m})** and **15(*m*TP^{t})**.

Despite this, without characterisation of an N_2 bound intermediate (the proposed product of the initial reduction step) there is currently insufficient evidence to support N_2 reduction by this system and attempts to isolate and fully characterise the intermediate have not yet been successful. The crude ^{1}H NMR spectra contain more resonances with a wider chemical shift range than those of the isolated U(III) complex, **[U_2(*m*TP^{m})(N{$SiMe_3$}$_2$)$_2$]**, **16(*m*TP^{m})**, discussed in the Section 3.3.1, suggesting desymmetrisation and possible incorporation of potassium cations within the ligand arene framework.

3.4 Cyclic Voltammetry Experiments

To ensure that the reductions observed in the cyclic voltammograms of **15(*m*TP^{m})** and **8(*m*TP^{m})** discussed in the above sections were correctly assigned to metal-based and not ligand-based transformations, **(*m*TP^{m})** was also studied by CV. The sparing solubility of **H$_4$(*m*TP)** in thf resulted in poorly resolved voltammograms, however the **K$_4$(*m*TP^{m})** salt is sufficiently soluble to allow collection of meaningful data. The redox inactive K^+ is assumed not to affect the redox behaviour.

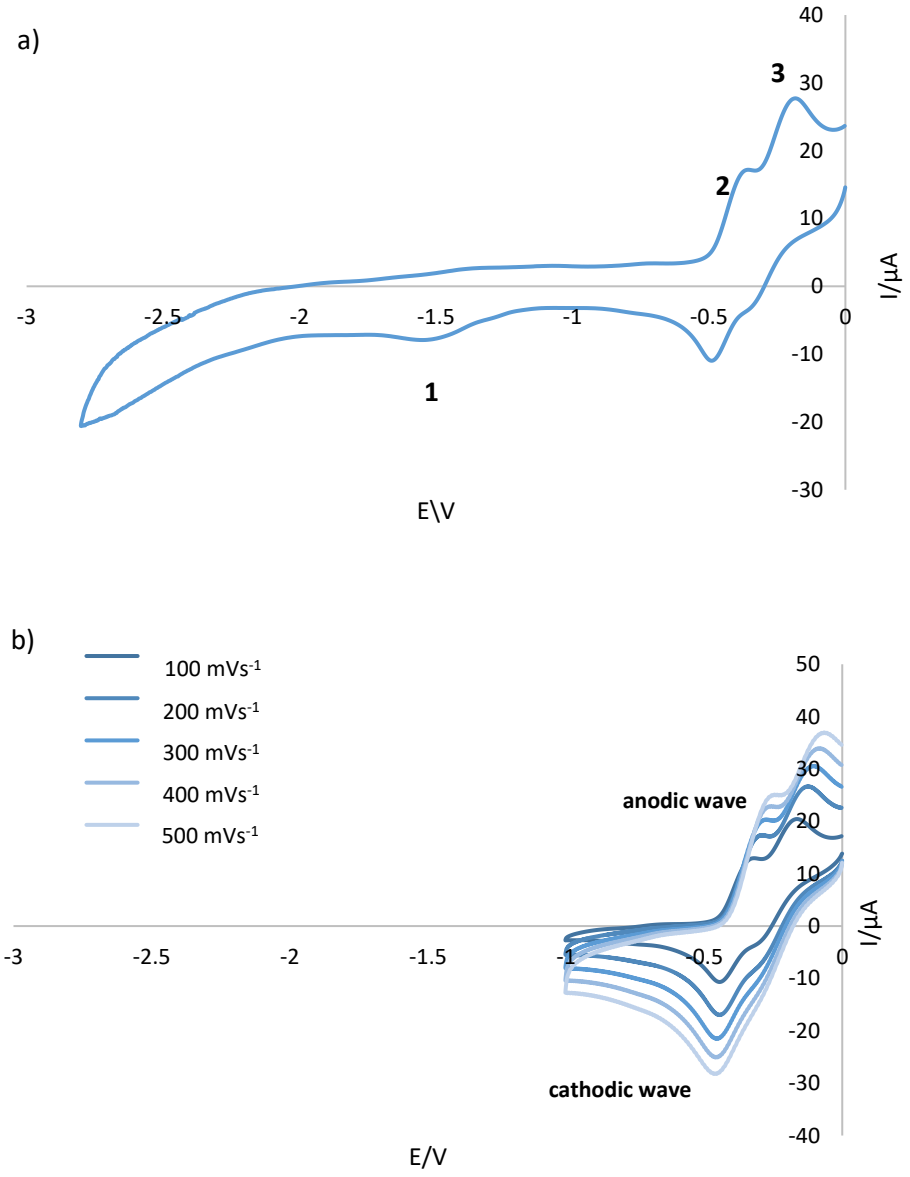

Figure 3-7 Cyclic voltammogram of **K$_4$(*m*TP^{m})**. a) at 100 mV s^{-1} scan rate across the full electrochemical window provided by thf/[^{n}Bu$_4$N][BPh$_4$], b) oxidative region only at varying scan rates.

The scan across the full electrochemical window provided by thf/[^{n}Bu$_4$N][BPh$_4$] shows two peaks (peak **2** and peak **3**) at the more positive end of the window (Figure 3-7a). Integration of these peaks shows that their areas in the anodic wave are larger than their areas in the cathodic wave, so both peaks are assigned as (partially reversible) oxidations. The small feature (peak **1**) at −1.5 V varies in size during repeated experiments and is absent in scans of the reductive region only. This suggests that it can be ascribed to the formation of a decomposition product at higher potentials and is not associated with the complex itself.

The absence of visible redox processes in the 1.995 - 2.029 V region of spectra of **K$_4$(*m*TP^{m})** suggests that the reductions seen in the cyclic voltammograms of complexes **15(*m*TP^{m})** and **8(*m*TP^{m})** are due to the redox active metal and not any ligand-based reduction. This is consistent with the chemical reductions discussed in Sections 3.2.2 and 3.3.1. Figure 3-8 shows a scan of the reductive region of **K$_4$(*m*TP^{m})** at 100 mVs^{-1}, overlaid on the voltammogram of **8(*m*TP^{m})** in the same region.

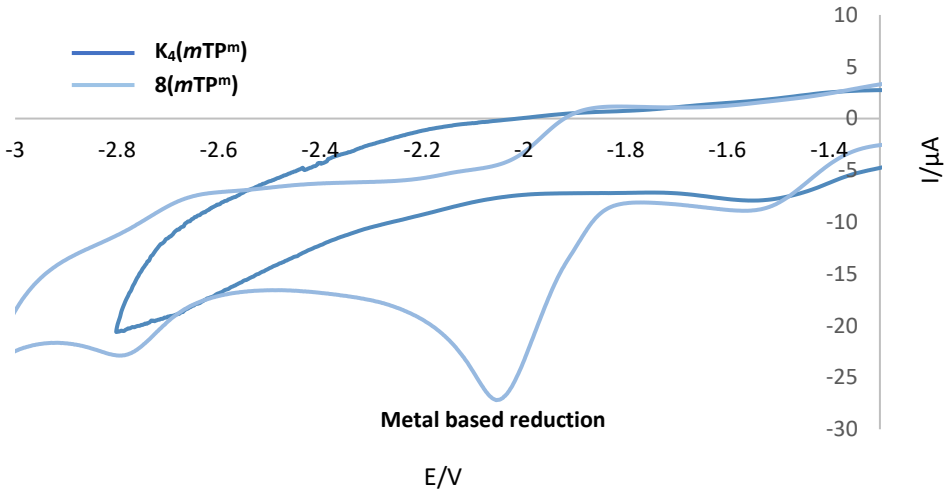

Figure 3-8 The reductive region of **K$_4$(*m*TP^{m})** at 100 mVs^{-1} (dark blue) overlaid with reductive region of **8(*m*TP^{m})** (pale blue).

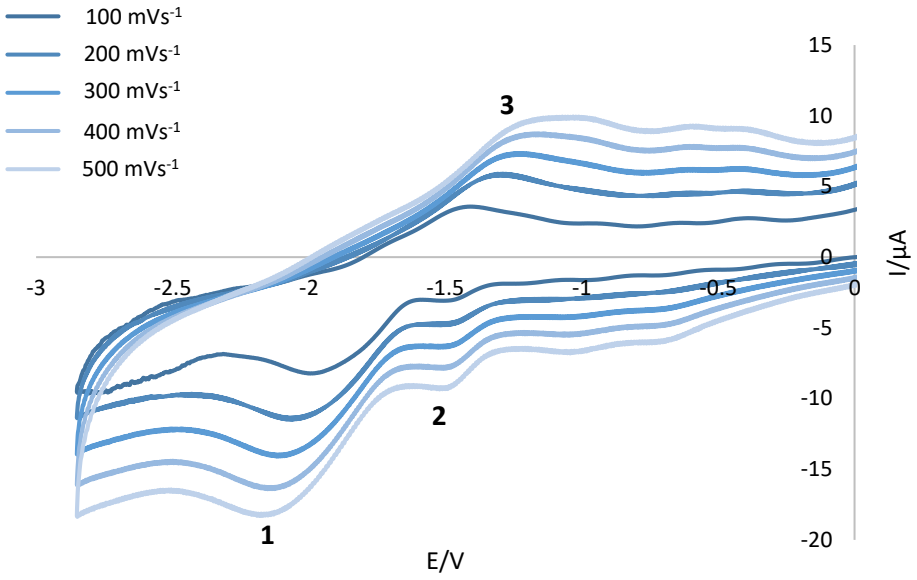

Figure 3-9 Cyclic voltammogram of **15(*m*TP^{m})** at varying scan rates, thf /0.1 M [^{n}Bu$_4$N][BPh$_4$].

Figure 3-9 shows the cyclic voltammogram of **15(*m*TP^{m}).** The reduction at −1.995 V (vs. Fc/Fc^{+}) (peak **1**) is assigned to the independent U(IV)→U(III) reduction of both metal centres. Peaks **2** and **3** are related. They vary in size during repeated experiments and are not associated with the complex.

Although no literature electrochemical studies of complexes of this class of arene bridged tetraphenolate ligand exist for comparison, the U(IV) complex of the closely related mesitylene bridged trisaryloxide ligand, ({^{Ad,Me}ArO}$_3$mes), (Figure 3-10) (see also Section 1.4) has been investigated as an electrocatalyst for the production of dihydrogen from water. No redox events were observed in the cyclic voltammogram of [U(OH)({^{Ad,Me}ArO}$_3$mes)] in thf with 0.1 M NBu$_4$PF$_6$ but the square-wave voltammogram showed two reduction peaks. The first broad peak centred at –1.9 V *vs.* Fc^{+}/Fc was assigned as the metal based U(IV)/U(III) reduction of the complex, whilst a second peak at –2.2 V was attributed to the U(III)/U(II) redox couple.[23] The U(IV)/U(III) reduction occurs at a very similar potential to **8(*m*TP^{m})** (−2.0289 V) and **15(*m*TP^{m})** (−1.995 V) measured in this study.

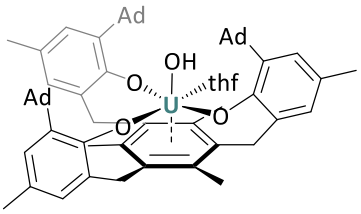

[U(OH)({^{Ad,Me}ArO}$_3$mes)]

Figure 3-10 [U(OH)({^{Ad,Me}ArO}$_3$mes)], the closely related monoarene analogue to the complexes discussed in this chapter.

3.5 Summary and Conclusions for Chapter 3

Straightforward syntheses of the dinuclear U(VI) complexes **[U_2Cl_4(*m*TP^m)$(thf)_4$]**, **9(*m*TP^m)**, **[U_2Cl_4(*m*TP^t)$(thf)_4$]**, **9(*m*TP^t)**, **[U_2I_4(*m*TP^m)$(thf)_4$]**, **8(*m*TP^m)**, and **[U_2I_4(*m*TP^t)$(thf)_4$]**, **8(*m*TP^t)**, are possible *via* salt metathesis reactions using two different tetraphenolate ligands in which an aryl backbone provides a strong yet flexible support to the two metal centres. In the solid-state the methyl substituted ligand **(*m*TP^m)** appears to favour the coordination of both metals on the same side of the central arene bridge, whereas the more sterically demanding tertiary butyl substituted **(*m*TP^t)** favours a conformer with metal coordination on opposite sides of the central arene. The presence of halide ancillary ligands allows ligand exchange to afford the heteroleptic aryloxide complex **[{UI(OTtbp)}$_2$(*m*TP^m)]**, **10(*m*TP^m)**. These are the first reported examples of *O*-donor compounds containing two discrete U(IV) centres in a single molecule, in geometries pre-organised for small molecule binding

Protonolysis of the tetraphenolate ligand precursors with **[U(N")$_2$(N{$SiMe_3$}$SiMe_2CH_2$)]** affords **[U_2(*m*TP^m)(N{$SiMe_3$}$_2$)$_4$], 15(*m*TP^m)** and **[U_2(*m*TP^t)(N{$SiMe_3$}$_2$)$_4$]**, **15(*m*TP^t)**, in which again **(*m*TP^m)** displays same side metal binding whereas **(*m*TP^t)** favours the opposite side conformer in the solid-state.

Whist direct syntheses of U(III) analogues of 'half-letterbox' type complexes were not successful; cyclic voltammetry identified reduction potentials between −2.5068 V and −1.995 V, which were characterised as single electron reductions of both metal centres at the same time, confirming the absence of U(IV)/U(IV) electronic communication through the ligand. Chemical reductions using two equivalents of the one electron reductant KC_8 yielded the two U(III)/U(III) complexes **[U_2(*m*TP^m)$(OTtbp)_2$], 13(*m*TP^m)** and **[U_2(*m*TP^m)(N{$SiMe_3$}$_2$)$_2$]**, **16(*m*TP^m)** which were isolated and characterised without N_2 binding.

Reduction of **[U_2I_4(*m*TP)(thf)$_4$], 8(*m*TP)** with six equivalents of KC_8 yields the N_2 activation product **14(*m*TP)**. Whilst these intermediates have not yet been fully characterised, quenching with the acid [PyH]Cl liberates the reduced N_2 as NH_4Cl. Labelling studies confirm that all of the NH_4Cl protons are derived from the added acid, and not intramolecular ligand deprotonations.

This work confirms that the derivatisable, tetraaryloxide ligand framework affords a powerful platform to harness the multi-electron reductive capacity of two uranium centres. Future work should aim to fully characterise all intermediates involved in the N_2 activation step in order to clarify mechanistic details and investigate catalytic reactivity to target turnover of N_2 into functionalised products.

3.6 References for Chapter 3

(1) Zhang, J.; Jian, C.; Gao, Y.; Wang, L.; Tang, N.; Wu, J. *Inorg. Chem.* **2012**, *51* (24), 13380–13389.

(2) Wells, J. A. L.; Seymour, M. L.; Suvova, M.; Arnold, P. L. *Dalton Trans.* **2016**, *45* (40), 16026–16032.

(3) Zhang, J.; Jian, C.; Gao, Y.; Wang, L.; Tang, N.; Wu, J. *Inorg. Chem.* **2012**, *51* (24), 13380–13389.

(4) Berg, J. M.; Clark, D. L.; Huffman, J. C.; Morris, D. E.; Sattelberger, A. P.; Streib, W. E.; Van Der Sluys, W. G.; Watkin, J. G. *J. Am. Chem. Soc*. **1992**, 114, 10811-10821.

(5) Wells, J. A. L. *PhD Thesis*, Bimetallic actinide complexes for small molecule activation, **2018**, University of Edinburgh.

(6) Avens, L. R.; Barnhart, D. M.; Burns, C. J.; McKee, S. D.; Smith, W. H. *Inorg. Chem.* **1994**, *33* (19), 4245–4254.

(7) Schnaars, D. D.; Wu, G.; Hayton, T. W. *Dalton Trans.* **2009**, (19), 3681.

(8) Dicks, A. P. *J. Chem. Educ.* **2003**, *80* (11), 1322.

(9) Michiue, K.; Jordan, R. F. *J. Mol. Catal. A Chem.* **2008**, *282* (1–2), 107–116.

(10) Wada, T.; Tsuge, K.; Tanaka, K. *Inorg. Chem.* **2001**, *40* (2), 329–337.

(11) Arnold, P. L. *Chem. Commun.* **2011**, *47* (32), 9005.

(12) Morris, D. E.; DaRe, R. E.; Jauntuen, K. C.; Castro-Rodriguez, I.; Kiplinger J. L. *Organometallics*, **2004**, *23* (22), 5142–5153.

(13) Vallat, A.; Laviron, E.; Dormond, A. *J. Chem. Soc. Dalton Trans.* **1990**, *0* (3), 921.

(14) Mansell, S. M.; Kaltsoyannis, N.; Arnold, P. L. *J. Am. Chem. Soc.* **2011**, *133* (23), 9036–9051.

(15) Falcone, M.; Chatelain, L.; Scopelliti, R.; Živković, I.; Mazzanti, M. *Nature* **2017**, *547* (7663), 332–335.

(16) Siedschlag, R. B.; Bernales, V.; Vogiatzis, K. D.; Planas, N.; Clouston, L. J.; Bill, E.; Gagliardi, L.; Lu, C. C. *J. Am. Chem. Soc.* **2015**, *137* (14), 4638–4641.

(17) Oshita, H.; Mizobe, Y.; Hidai, M. *J. Organomet. Chem.* **1993**, *456* (2), 213–220.

(18) Shiina, K. *J. Am. Chem. Soc.* **1972**, *94* (26), 9266–9267.

(19) Windorff, C. J.; Evans, W. J. *Organometallics* **2014**, *33* (14), 3786–3791.

(20) Berg, J. M.; Clark, D. L.; Huffman, J. C.; Morris, D. E.; Sattelberger, A. P.; Streib, W. E.; Van der Sluys, W. G.; Watkin, J. G. *J. Am. Chem. Soc.* **1992**, *114* (27), 10811–10821.

(21) Hitchcock, P. B.; Lappert, M. F.; Singh, A.; Taylor, R. G.; Brown, D. *J. Chem. Soc., Chem. Commun.*, **1983**, 561-563.

(22) Lewis, A. J.; Mullane, K. C.; Nakamaru-Ogiso, E.; Carroll, P. J.; Schelter, E. J. *Inorg. Chem.* **2014**, *53* (13), 6944–6953.

(23) Halter, D. P.; Heinemann, F. W.; Bachmann, J.; Meyer, K. *Nature* **2016**, *530* (7590), 317–321.

Chapter 4: Cerium Letterbox Complexes

4.1 Introduction to Chapter 4

4.1.1 Fundamentals of Cerium Chemistry

Group III of the periodic table contains the rare earth elements (RE) and includes scandium, yttrium, and the fifteen lanthanide metals. In recent years, organometallic RE complexes have received much attention as homogeneous catalysts and in small molecule transformation chemistry.[1–4] Cerium is the most abundant rare earth element and is of particular interest due to its unusual redox chemistry.

Cerium has two common oxidation states: Ce(III) and Ce(IV), although Ce(II) is also known. Ce(IV) is the most stable non-trivalent RE ion in aqueous solution. The closed shell electron configuration [Xe]4f^0 affords a unique stability and has allowed isolation of many molecular cerium(IV) complexes.[5–8] These complexes can be highly oxidising and are widely used in synthesis and catalysis as one-electron oxidants.[9] The Ce(IV)/Ce(III) reduction potential however, is extremely dependent on ligand environment, with a range of over 3.5 V (from +1.63 V to −1.83 V vs. SCE),[10] meaning that in a strongly donating ligand environment, Ce(III) can act as an effective reductant.

Compared to uranium and the other actinide metals, the smaller radial extent of the lanthanide 4*f* orbitals relative to the more diffuse 5*f* orbitals has implications in covalent bonding (see Section 1.1). Increased orbital overlap results in a higher degree of covalency in Ac–E (where E is any element) bonds compared to Ln–E bonds. Ln–E multiple bonds accordingly remain very rare, in contrast to the expanding number of multiply bonded uranium complexes.[11–15] These differences in electronic structure are of industrial importance, allowing separation of lanthanides and actinides in spent nuclear fuels.[16]

These differences also account for the contrasting small molecule activation chemistry of cerium with respect to uranium, some aspects of which will be discussed in the following sections.

4.1.2 Nitrogen activation by rare earth complexes

Dinitrogen binding is more common amongst the rare earth elements than the actinides, although it should be taken into account that the organometallic chemistry of the actinides

in general has been far less explored. With the exceptions of radioactive promethium, europium and ytterbium, dinitrogen complexes are known and have been crystallographically characterised for all elements in the lanthanide series,[17–21] including cerium.

Reactions of LnX_3 compounds (where X is a one electron donor ligand) with strong reductants yield side-on bridging dinitrogen complexes **BN**–**BP**, in which N_2 is formally reduced to $[N_2]^{2-}$; these complexes are summarised in Figure 4-1.

BN **BO** **BP**

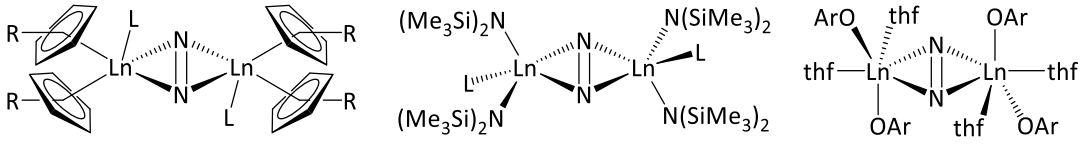

OAr = 2,6-di^{t}butylphenolate

BN[19,22–33]

Ln	L	Cp^R
Sc		C_5Me_4H
Y		C_5Me_5
	thf	C_5Me_4H, $SiMe_3$-C_5H_4
La	thf	C_5Me_5, C_5Me_4H
Ce	thf	C_5Me_5, C_5Me_4H
Pr	thf	C_5Me_5, C_5Me_4H
Nd		1,2,4-^{t}Bu-C_5H_2
	thf	C_5Me_4H
Sm		C_5Me_5
Dy		C_5Me_5, $SiMe_3$-C_5H_4
Tm		C_5Me_5, 1,3-$SiMe_3$-C_5H_3
	thf	$SiMe_3$-C_5H_4
Lu		C_5Me_5
	thf	C_5Me_4H

BO[24,34–40]

Ln	L
Y	thf, PhCN, C_5H_5N, 4-NMe_2-C_5H_4N, Ph_3PO, Me_3NO
La	thf
Nd	thf
Gd	thf
Tb	thf
Dy	thf
Ho	thf
Er	thf
Tm	thf
Lu	thf

BP[34,36,37]

Ln
Nd
Dy

Figure 4-1 Summary of $[N_2]^{2-}$ rare earth complexes.

The N–N bond lengths in **BN**–**BP** range from 1.172(6) Å in $[(Cp^*)_2Y]_2(\mu\text{-}\eta^2\text{:}\eta^2\text{-}N_2)$ to 1.305(6) Å in $[(Me_3SiN)_2(thf)Dy]_2(\mu\text{-}\eta^2\text{:}\eta^2\text{-}N_2)$, consistent with a bond order of two. Calculations suggest that for $[(Cp^*)_2Sc]_2(\mu\text{-}\eta^2\text{:}\eta^2\text{-}N_2)$, reduction is afforded by electron donation from an occupied metal 3*d*-orbital to an antibonding π* dinitrogen orbital that is coplanar with the M–$(\mu\text{-}\eta^2\text{:}\eta^2\text{-}N_2)$–M axis, as shown in Figure 4-2.[26] This bonding scheme can likely be extended for all compounds **BN**–**BP**, with the donor *nd* orbital varying with the metal centre.[41]

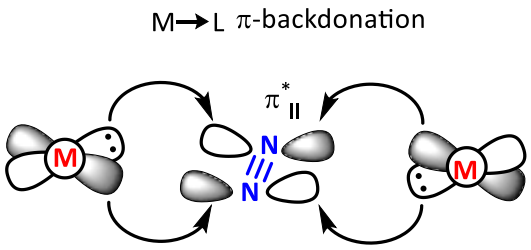

Figure 4-2 Bonding description of RE $[N_2]^{2-}$ complexes.

Although less common, a number of complexes exist in which side-on bound dinitrogen has been reduced by rare earth metals to $[N_2]^{3-}$, and even $[N_2]^{4-}$. Reduction to $[N_2]^{3-}$ requires additional M–L backdonation, with the out-of-plane antibonding π* dinitrogen orbital now also being occupied by a single electron.

Examples are provided by **BQ** and **BR**, see Figure 4-3. Reduction to $[N_2]^{4-}$ requires more complex multidentate ligands and electron donation from more than two metal centres, as seen in the tetrametallic samarium dipyrrolide complexes $[\{R_2C(C_4H_3N)_2\}Sm(thf)]_4(\mu_4\text{-}\eta^1{:}\eta^1{:}\eta^2{:}\eta^2\text{-}N_2)$ (R = Ph, Cy, Et).[42–44]

BQ

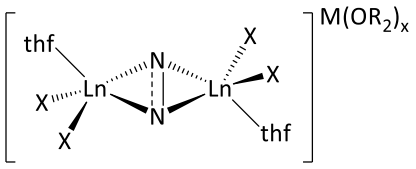

BR

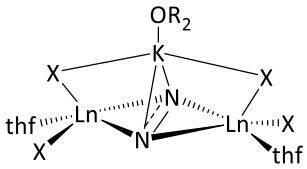

BQ[34,38,39,45]

Ln	X	M	$(OR_2)_x$
Y	$N(SiMe_3)_2$	K	thf_6
	$N(SiMe_3)_2$	K	thf_2; 18-crown-6
	$N(SiMe_3)_2$	Na	thf_6
La	$N(SiMe_3)_2$	K	thf_6
Gd	$N(SiMe_3)_2$	K	thf_2; 18-crown-6
Tb	$N(SiMe_3)_2$	K	thf_2; 18-crown-6
Dy	$N(SiMe_3)_2$	K	thf_2; 18-crown-6
	O-2,6-^{t}Bu-C_6H_3	K	thf_6
Ho	$N(SiMe_3)_2$	K	thf_2; 18-crown-6
Er	$N(SiMe_3)_2$	K	thf_2; 18-crown-6
		Na	thf_6
Lu	$N(SiMe_3)_2$	K	thf_6

BR[38,39,46,47]

Ln	X	OR_2
Y	$N(SiMe_3)_2$	
Gd	$N(SiMe_3)_2$	
Tb	$N(SiMe_3)_2$	
Dy	$N(SiMe_3)_2$	
	O-2,6-^{t}Bu-C_6H_3	thf

Figure 4-3 Summary of $[N_2]^{3-}$ rare earth complexes.

The wealth of examples of RE dinitrogen complexes has helped to build a detailed understanding of the bonding involved in such systems. In contrast to uranium however, dinitrogen cleavage and functionalisation have not been reported for RE complexes to date, with N_2 dissociation frequently observed instead.[48–51]

It was seen in Chapter 1 that for analogous uranium complexes, in addition to donation from *d*-orbitals into the 'in plane' N_2 antibonding orbitals, which is typical of RE dinitrogen complexes, backdonation into N_2 π* orbitals can occur *via* the radially diffuse 5*f* orbitals into the out of plane N_2 π* orbitals (δ bonding, Figure 4-4) which prevents dissociation by strengthening the M–N bonds. Subtle differences in the molecular orbital model arising from participation of 5*f* orbitals are likely responsible for the ability of side on bound N_2 ligands in uranium complexes to undergo functionalisation and cleavage reactions unprecedented for RE systems,[52] but these effects are complex and not well understood.

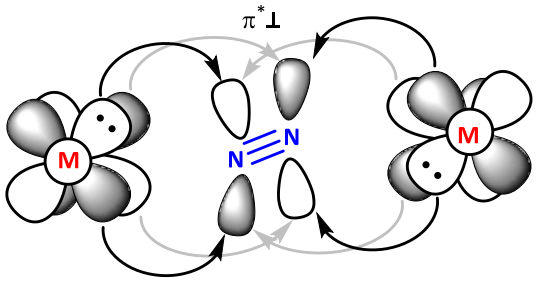

Figure 4-4 Bonding description of RE $[N_2]^{3-}$ complexes.

4.1.3 Ce(III) aryloxide complexes and redox chemistry

The application of Ce(IV) reagents as single electron oxidants is widespread and usually exploits electron deficient ligand systems to stabilise the Ce(III) oxidation state. Electron-rich ligands that stabilise the oxidising Ce(IV) oxidation state however, have been less thoroughly investigated.

The first simple Ce(III) aryloxide complexes were characterised 30 years ago when Kang and coworkers reported the synthesis of $Ce(ODtbp)_3$, **BS** *via* protonolysis of $Ce[N(SiMe_3)_2]_3$, and its reactivity towards the Lewis bases thf and ^{t}BuNC (to provide **BT**) as shown in Scheme 4-1.[53] More recently, Boyle and coworkers have presented the insertion of a single equivalent of CO_2 (per Ce) into $Ce(ODtbp)_3$ to provide $[Ce(\mu_c\text{-}O_2C\text{-}ODtbp)(ODtbp)_2]_2$, **BU.**[54]

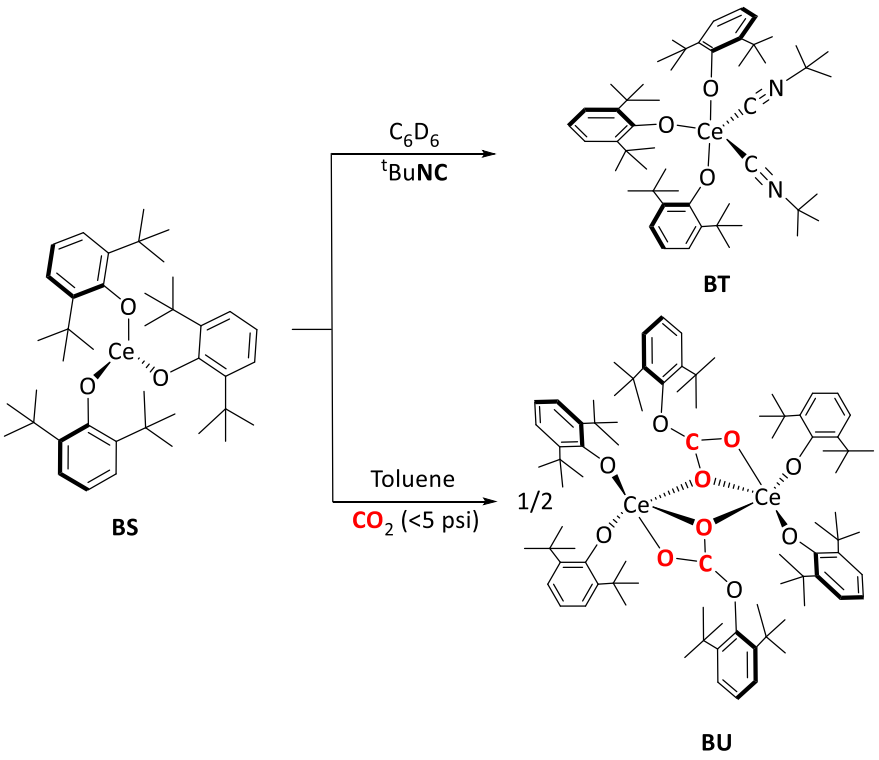

Scheme 4-1 The reactivity of Ce(ODtbp)$_3$, **BS**.[53,54]

In contrast to the wealth of well-characterised U(III)→U(IV) transformations, the oxidation chemistry of cerium(III) complexes remains poorly understood. The use of molecular Ce(III) complexes as reductants requires well-controlled oxidation reactivity and there is a growing interest in exploring the subtle effects of ligand reorganisation and sterics as well as thermodynamics on the oxidation of organometallic Ce(III).[55]

Schelter and coworkers used a simple *(S)*-binolate ligand to synthesise a series of Ce(III) complexes with coordination of alkali metals (Li, Na and K) within their secondary coordination sphere. The identity of the alkali metal cation not only had a significant effect on the measured potential of the oxidation, but was also shown to control the nature of the chemical oxidation achieved by reaction with one equivalent of Ph_3CCl (Scheme 4-2).[55]

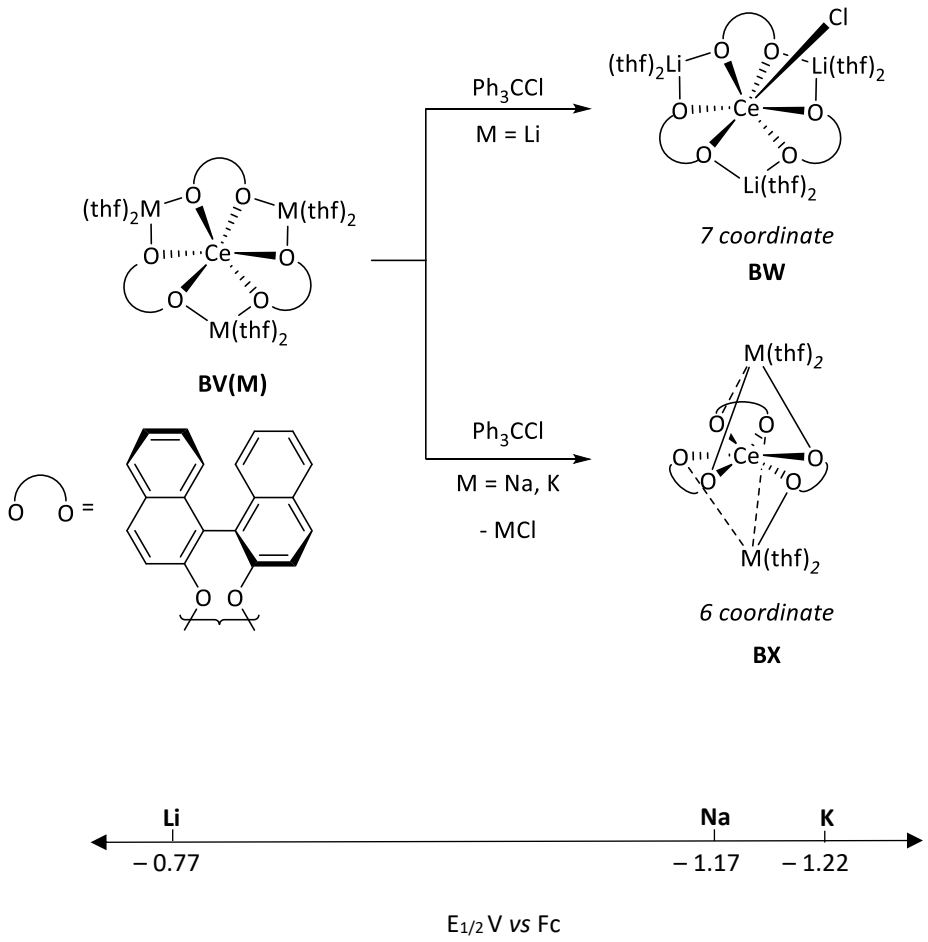

Scheme 4-2 Selective oxidation of **BV(M)** and $E_{1/2}$ of **BV(Li), BV(Na) and BV(K),** measured by cyclic voltammetry in thf:CH_3CN (1:6) using a 3 mm diameter glassy carbon working electrode; v = 50 mV/s; [Ce] ≈ 1 mM; [NPr_4][$BArF_4$] ≈ 100 mM.

BV(Na) and **BV(K)** have similar redox potentials of −1.17 and −1.22 respectively as measured by cyclic voltammetry; whereas the smaller Li cation results in a much less negative potential, −0.77 V. The oxidation of **BV(M)** proceeds *via* chlorination at Ce for **BV(Li)** or *via* elimination of one equivalent of MCl for the heterobimetallic complexes **BV(Na)** and **BV(K)**. A significant structural rearrangement was found to accompany the salt elimination route, resulting in the migration of the alkali metal ions to two axial positions and the aryloxide moieties adopting an octahedral coordination environment around the Ce(IV) centre. This selectivity is rationalised by considering the 0.14 Å reduction in ionic radius going from Ce(III) (1.01 Å) to Ce(IV) (0.87 Å). The predominantly ionic nature of bonding in 4*f* systems means that coordination environment is highly influenced by sterics rather than orbital overlap.[56] The seven-coordinate geometry becomes unstable for the larger alkali metals (Na and K),

resulting in a geometric rearrangement, MCl elimination and reduction in coordination number to provide **BX**. The salt elimination provides the extra enthalpy needed for the structural rearrangement, leading Schelter to conclude that as well as an electron-donating ligand environment at Ce(III), the heterobimetallic framework may be key to carrying out well controlled oxidation reactions.[55]

In more recent work, Schelter and coworkers have shown that in addition to Ph_3CCl, **BV(Li)** is susceptible to inner-sphere functionalisation by a large range of one electron group-transfer oxidants, Scheme 4-3.[57]

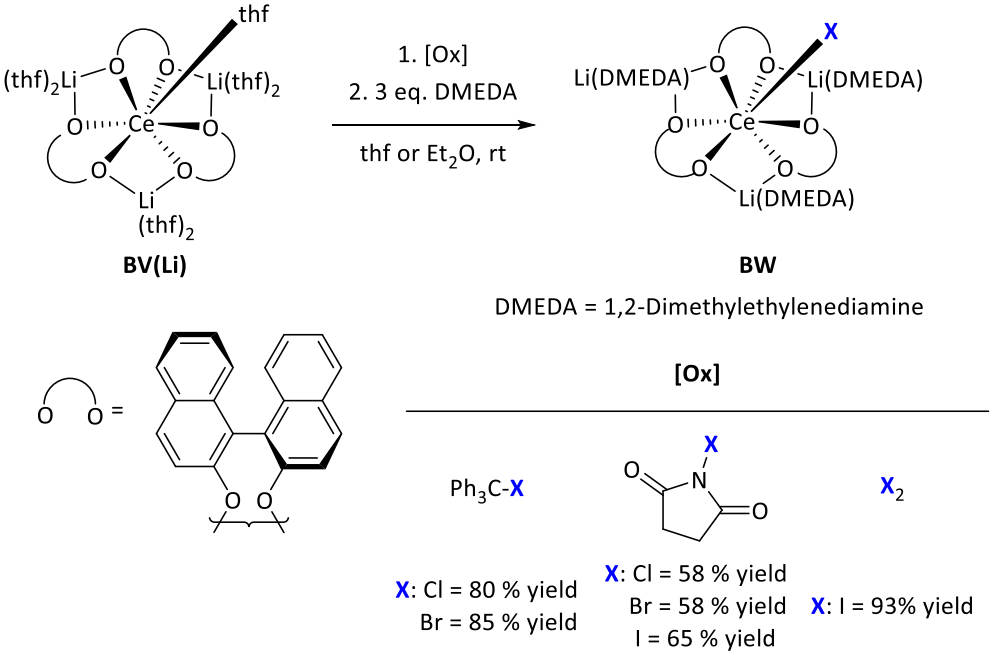

Scheme 4-3 Oxidation of **BV(Li)** by a range of oxidants.

Additionally, when a Cl group-transfer oxidant is used (N-Chlorosuccinimide (NCS), Ph_3CCl), the resulting Ce(IV)−Cl bond can be further functionalised *via* salt metathesis reactions to afford rare terminal Ce(IV)−OAr, $-N_3$ and –NCS bonds in **BW**.[57]

4.2 Chapter 4 Aims

The above discussion has highlighted that a flexible, yet well defined, electron-rich ligand that accommodates variable alkali metal binding within a secondary coordination sphere is well placed for developing controlled Ce(III) oxidation systems. In turn, such platforms may

contribute to the rational design of molecular cerium reagents for various redox applications, including use in reductive small molecule activation reactions.

The synthesis of **6(*m'*TP^{m})**, **[K(thf)$_6$][U$_2$(*m'*TP)$_2$K(thf)$_2$]**, and the isolation of **1(*m*TP^{m})**, **[K$_3$(*m*TP^{m})H(thf)$_6$]**, as described in Chapter 2 demonstrates that **(*m*TP)** can accommodate potassium binding within the framework provided by the multiple arene rings. Furthermore, work by Wu and coworkers has shown that Li and Na also readily coordinate to the arenes of closely related tetraphenolate ligands in various stoichiometries and geometries.[58]

Despite Ce complexes finding widespread use in catalysis,[9] bimetallic cerium complexes remain rare. Unpublished work within the Arnold group has already successfully demonstrated that **(*p*TP)** can provide a flexible ligand framework for two Ce(III) or Ce(IV) centres.[59] As described in Chapter 2 however, complexes afforded by the closely related *para*- and *meta*- tetraphenolate arene ligands can show surprising variation in their composition and further reactivity.

The work discussed in this chapter aims to exploit the flexible, electron-rich nature of the *meta*-tetraphenol arene ligand, **(*m*TP^{m})**, and apply analogous synthetic routes to those used in Chapter 2 to target Ce(III) complexes of **(*m*TP)** with and without coordinated alkali metal cations. These complexes will be compared to those supported by **(*p*TP)** and their redox chemistry and potential reactivity towards small molecule substrates will be explored.

4.3 Synthesis of [K(solv)$_n$][Ce$_2$(*m*TP^{m})$_2$K(solv)$_4$], 18(*m*TP^{m})

Having successfully demonstrated that **K$_4$(*m*TP)** undergoes salt metathesis with uranium(IV) halides in Chapter 2, yielding **[{U(*m*TP)(solv)$_2$}$_2$]** complexes and eliminating KI as a byproduct, an analogous route using $CeCl_3(thf)_n$ was targeted. Pyridine was used in order to solubilise $CeCl_3(thf)_n$ which is poorly soluble in the ether solvents typically used in the metathesis reactions with actinide salts.

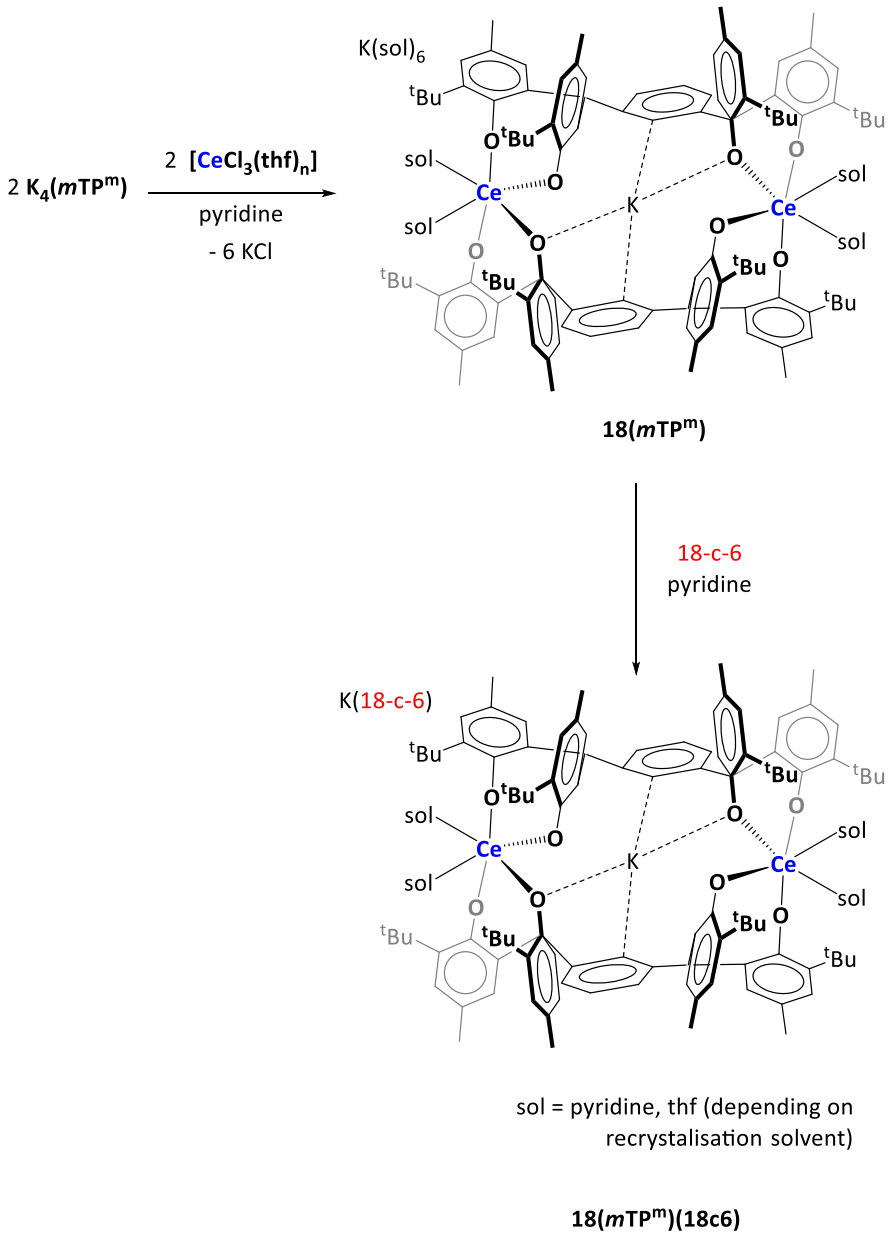

Scheme 4-4 Synthesis of **18(*m*TP^{m})** by salt metathesis.

K$_4$(*m*TP^{m}) was prepared *in situ* by mixing **H$_4$(*m*TP^{m})** and [KN(SiMe$_3$)$_2$] in pyridine. One equivalent of **CeCl$_3$(thf)$_n$** was dissolved in pyridine and added to the solution. The yellow solution was stirred overnight and then precipitated KCl was removed by filtration. **[K(py)$_6$][Ce$_2$(*m*TP^{m})$_2$K(py)$_4$], 18(*m*TP^{m})(py),** was isolated as a yellow powder, in good yield (73 %) following removal of volatiles under reduced pressure.

Yellow crystals of **18(*m*TP^{m})(py)** suitable for single crystal XRD were grown from a concentrated solution of pyridine at −30 °C. Alternatively, recrystallisation of **18(*m*TP^{m})** in

thf gives the mixed solvate **[K(thf)$_6$][Ce$_2$(*m*TP^m)$_2$K(py)$_2$(thf)$_2$]·5thf**, **18(*m*TP^m)(thf)**, and the addition of one equivalent of a potassium-selective crown ether (18-crown-6) (in pyridine, at room temperature) gives the analogous **[K(18-c-6)][Ce$_2$(*m*TP^m)$_2$K(py)$_4$]·7py**, **18(*m*TP^m)(18c6)**. All three complexes have been characterised independently by single crystal XRD, and are shown in Figures 4-5, 4-6 and 4-7.

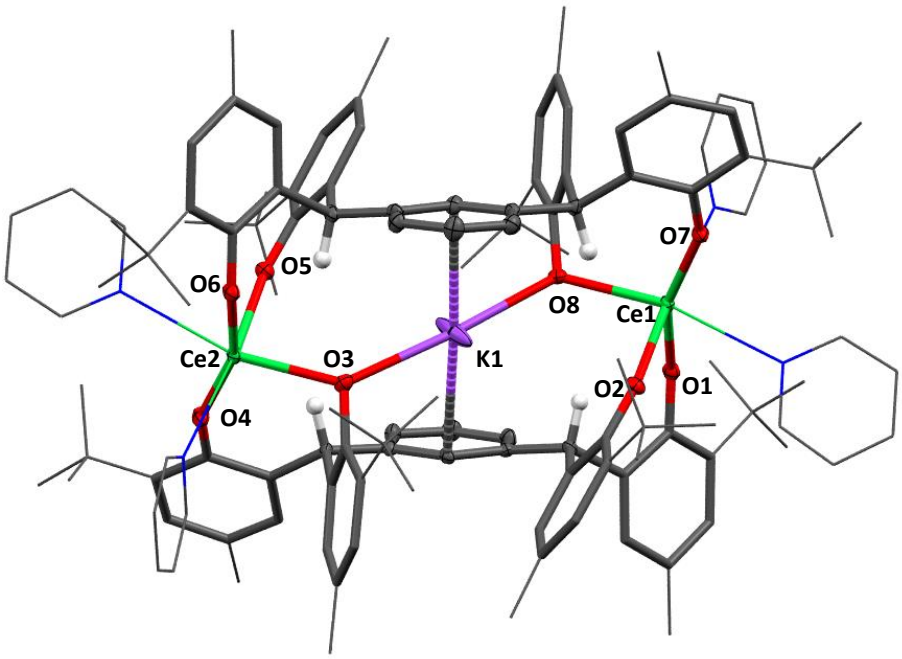

Figure 4-5 Solid-state structure of the anion of **[K(py)$_6$][Ce$_2$(*m*TP^m)$_2$K(py)$_4$]·7py, 18(*m*TP^m)(py).** For clarity, all backbone hydrogen atoms and lattice solvent molecules are omitted. Cerium, potassium, oxygen, benzylic hydrogen and carbon atoms on the central arene rings are displayed as displacement ellipsoids drawn at 50 % probability. The remaining atoms and bonds are shown as capped stick or wireframe. Selected bond lengths (Å) and angles (°) for **18(*m*TP^m)(py)** are given in Table 4-1.

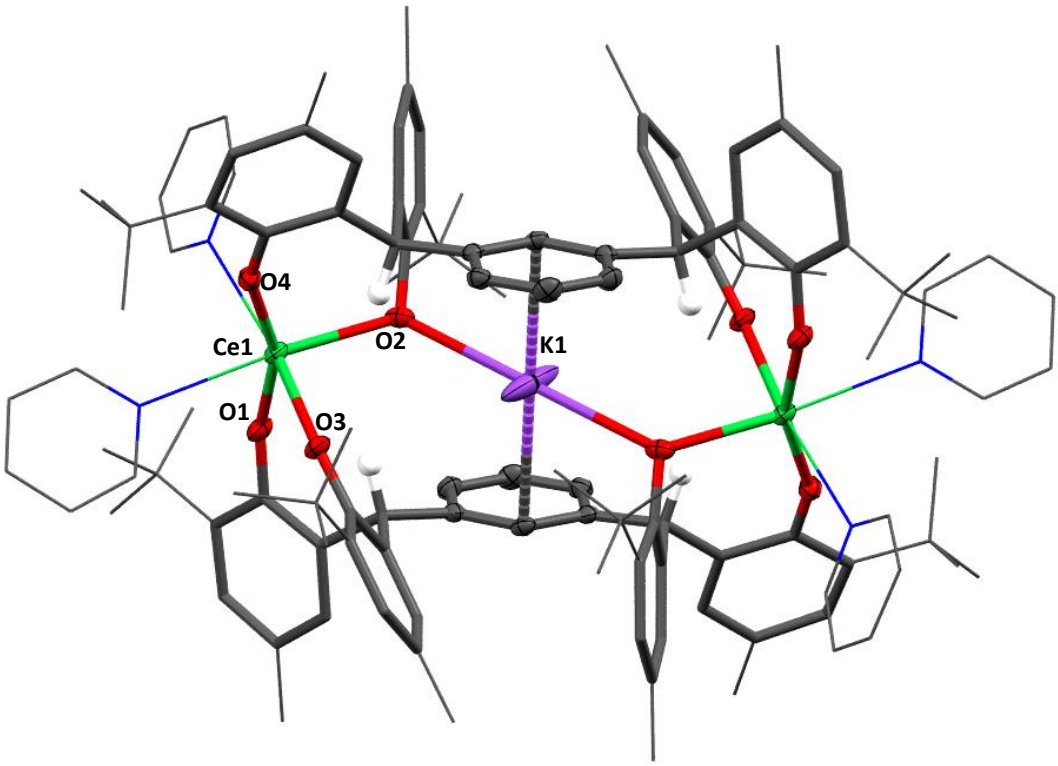

Figure 4-6 Solid-state structure of the anion of **[K(18-c-6)][Ce$_2$(*m*TP^m)$_2$K(py)$_4$]·7py, 18(*m*TP^m)(18c6).** For clarity, all backbone hydrogen atoms and lattice solvent molecules are omitted. Cerium, potassium, oxygen, benzylic hydrogen and carbon atoms on the central arene rings are displayed as displacement ellipsoids drawn at 50 % probability. The remaining atoms and bonds are shown as capped stick or wireframe. Selected bond lengths (Å) and angles (°) for **18(*m*TP^m)(18c6)** are given in Table 4-1.

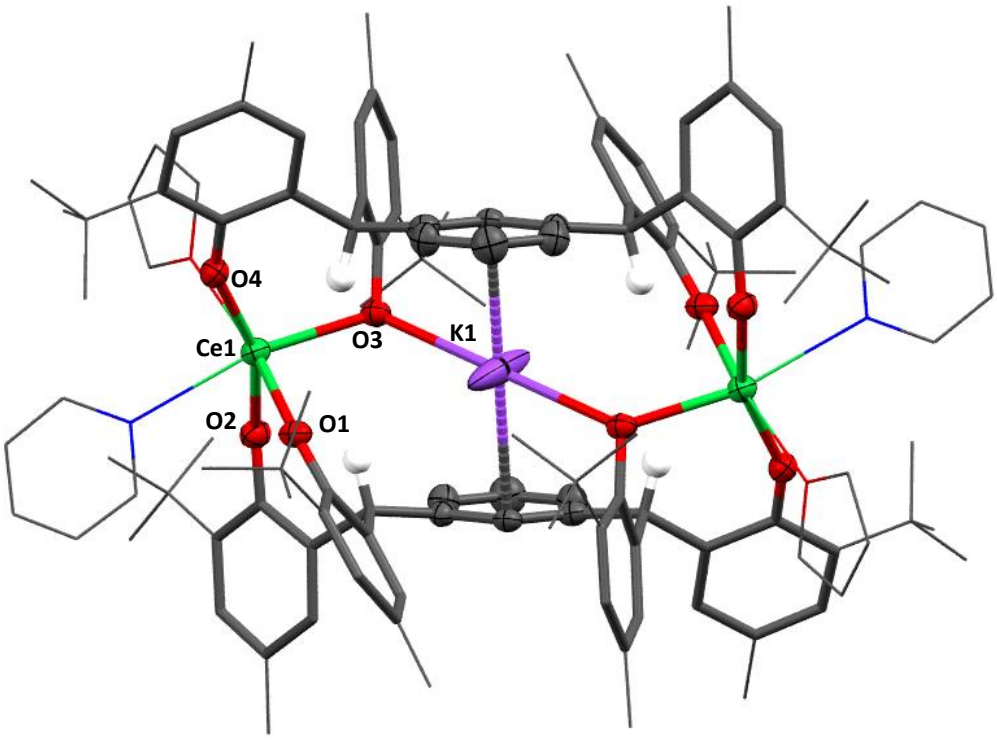

Figure 4-7 Solid-state structure of the anion of **[K(thf)$_6$][Ce$_2$(*m*TP^m)$_2$K(py)$_2$(thf)$_2$]·5thf, 18(*m*TP^m)(thf).** For clarity, all backbone hydrogen atoms and lattice solvent molecules are omitted. Cerium, potassium, oxygen, benzylic hydrogen and carbon atoms on the central arene rings are displayed as displacement ellipsoids drawn at 50 % probability. The remaining atoms and bonds are shown as capped stick or wireframe. Selected bond lengths (Å) and angles (°) for **18(*m*TP^m)(thf)** are given in Table 4-1.

Parameter	[K(py)$_6$] [Ce$_2$(*m*TP^m)$_2$K(py)$_4$]·7py	[K(18-c-6)] [Ce$_2$(*m*TP^m)$_2$K(py)$_4$]·7py	[K(thf)$_6$] [Ce$_2$(*m*TP^m)$_2$K(py)$_2$(thf)$_2$]·5thf
Ce(1)–O(1)	2.317(3)	2.319(2)	2.242(3)
Ce(1)–O(2)	2.246(3)	2.250(2)	2.332(3)
Ce(1)– O(3)	(2.294(3))	2.401(2)	2.378(3)
Ce(1)– O(4)	(2.372(3))	2.306(2)	2.305(3)
Ce(2)–O(3)	2.377(3)		
Ce(2)–O(4)	2.293(3)		
Ce(2)–O(5)	2.240(3)		
Ce(2)–O(6)	2.316(3)		
K(1)–O(3)	2.672(4)	2.782(2)	2.748(3)
K(2)–O(8)	2.648(3)		
K(1)···C(7)	3.100(4)	3.058(2)	3.103(3)
K(1)···C(52)	3.113(4)		
Ce(1)–O(8)–K(1)	131.4(1)		
Ce(1,2)–O(3)–K(1)	(135.7(2))	129.23(9)	128.7(1)
O(8)–K(1)–O(3)	175.2(1)		

Table 4-1 Selected bond lengths (Å) and angles (°) for **[K(py)$_6$][Ce(*m*TP^m)$_2$K(py)$_4$]·7py, [K(18-c-6)][Ce$_2$(*m*TP^m)$_2$K(py)$_4$]·7py** and **[K(thf)$_6$][Ce$_2$(*m*TP^m)$_2$K(py)$_2$(thf)$_2$]·5thf.**

The solid-state structure of **[K(py)$_6$][Ce$_2$(*m*TP^m)$_2$K(py)$_4$]·7py** is displayed in Figure 4-3**.** Both cerium(III) cations possess *pseudo*-octahedral geometry; four coordination sites are occupied by aryloxide ligands, and the remaining two by coordinated pyridine solvent molecules. A 'caged' potassium ion occupies the internal cavity of the structure, bridging oxygen atoms O(3) and O(8). The potassium binding elongates the Ce−O(3) and Ce−O(8) bonds to 2.375(3) Å (avg) relative to the remaining Ce−O bonds, (2.284(3) Å (avg)). This is comparable to the analogous complex synthesised from **(*p*TP^m)** within the Arnold group, where the Ce−O bond lengths range from 2.235(5) Å to 2.394(5) Å,[59] and to literature Ce(III) bis-aryloxy complexes such as [Li(thf)$_2$Ce(MBP)$_2$(thf)$_2$] (BMP = 2,2'-methylenebis(6-*tert*-butyl-4-methylphenolate)) with a mean Ce-O bond length of 2.3570 Å.[60]

K(1) is capped by two ligand arene rings *via* η^1 interactions with C(7) and C(52), as shown in Figure 4-8. The K(1)···C(52) distance, 3.113(4) Å and the K(1)···C(7) distance, 3.100(4) Å, are not statistically different. Potassium arene interactions are common in related systems but are typically of a higher hapticity. In the [K$_2$H$_2$(*p*TP^t)] system reported by Wu for example, the two potassium atoms participate in η^3 and η^6 interactions with the central arene,[58] and in the

para-analogue of **18(*m*TP^{m})(py)** prepared within the Arnold group, K(1) is fully encapsulated by the two phenyl-linkers through η^{6} coordination.[59] It is proposed that the relative under coordination of K(1) in **18(*m*TP^{m})(py)** results from the offset of the two phenyl rings relative to each other, which is enforced by the ligand geometry (Figure 4-8).

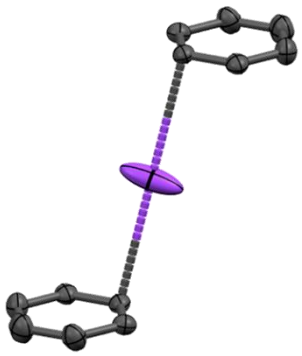

Figure 4-8 Solid state structure of **[K(py)$_6$][Ce$_2$(*m*TP^{m})$_2$K(py)$_4$]·7py, 18(*m*TP^{m})(py).** K(1) and arene rings displayed as displacement ellipsoids drawn at 50% probability. All other atoms are hidden.

The second potassium cation, K(2), is octahedrally coordinated by six pyridine solvent molecules and lies 10.530 Å from the centre of the molecular anion. The counterion has been omitted from Figures 4-5, 4-6, 4-7 and 4-8 for clarity.

In the solid-state, **[K(18-c-6)][Ce$_2$(*m*TP^{m})$_2$K(py)$_4$]·7py, 18(*m*TP^{m})(18c6)** (Figure 4-6) has two identical Ce(III) cations. K(2) is bound by a single molecule of 18-crown-6. The key bond lengths and parameters of the molecular anion are not dramatically altered from those in **18(*m*TP^{m})(py)**. The molecular anion of **18(*m*TP^{m})(thf)** is isostructural with that of **18(*m*TP^{m})(18c6)**. One pyridine solvent molecule and one thf solvent molecule are now coordinated to Ce, and K(2) is solvated by six thf molecules.

The ^{1}H NMR spectra for **18(*m*TP^{m})** are only narrowly paramagnetically shifted, with resonances located between 10.60 and −4.37 ppm in d_8-thf, but are consistent with the proposed molecular composition. Elemental microanalysis was used to confirm the bulk purity of **18(*m*TP^{m})**.

The successful synthesis and isolation of **18(*m*TP^{m})** shows that **(*m*TP)** provides a suitable structural framework that can be applied to both the lanthanides (Ce) and the actinides (U). The incorporation of two potassium cations to provide heterometallic complexes is advantageous because it may allow alkali metal-mediated redox chemistry similar to that

observed for Schelters's heterobimetallic complexes.[55,57] Redox reactions are discussed in Section 4.5.

4.4 EPR studies on $[K(py)_6][Ce_2(mTP^m)_2K(py)_4]$, 18($mTP^m$)

The f^2 (S = 1) electron configuration of U(IV) leads to very large spin-orbit coupling dominated zero-field splitting, which means any measurable electron paramagnetic resonance (EPR) transitions lie outside the commonly accessible range of magnetic fields. Line broadening due to very fast relaxation rates make even high frequency/high field EPR experiments very difficult. In contrast, Ce(III) has only one unpaired *f* electron (S = ½). It may therefore be informative to use EPR spectroscopy to study the magnetic properties of complexes containing Ce(III) cations.

A preliminary EPR study was carried out on **18(mTP^m)(py)**. It is expected that the unpaired electrons should be localised in a 4*f* orbital on each Ce(III) centre. The solid-state structure of **18(mTP^m)(py)** shows that each cerium ion has an approximately octahedral geometry. An isotropic spectrum is therefore expected, but the distortion from ideal octahedral angles could give rise to an axial or rhombic signal.

Cerium has a nuclear spin of 0, so no hyperfine coupling is expected. Each cerium is directly bonded to four O atoms and two N atom. The nuclear spin of ^{16}O is 0, so no superhyperfine coupling to oxygen is expected. ^{14}N has a non-zero nuclear spin (I = 1), so according to *2nI +1*, superhyperfine coupling to the N atom of the coordinated pyridine could split the 4*f* electron into five EPR lines. Each Ce(III) centre is just two bonds and approximately 4.6 Å from the centrally caged K. ^{39}K (I = 3/2) could result in a further splitting into four lines.

Existing EPR data on molecular cerium complexes remains rare. One example studied the magnetic behaviour of $[Li(thf)_4][Ce(cot)_2]$ (cot = (η^8-C_8H_8) and indicates an axial complex with $g_\perp$ = 2.272 and $g_{||}$ = 1.123.[61] More commonly, Ce(III) doped crystals have been studied to determine the symmetry of the crystal site occupied by the metal. For example, an isotropic signal for 1 % Ce(III) doped Cs_2NaYCl_6 at |g| = 1.266 was used to suggest the octahedral symmetry of the cerium sites within the crystal.[62]

No EPR signal could be detected in solution (10 mM) at room temperature or 100 K, which was attributed to low spin density in solution. Solid state measurements, however, revealed a temperature dependent EPR signal.

At room temperature, a rhombic signal was observed. The g values g_x = 2.0097, g_y = 1.9964 and g_z = 2.0356 were obtained from the simulated spectrum, Figure 4-9.[1]

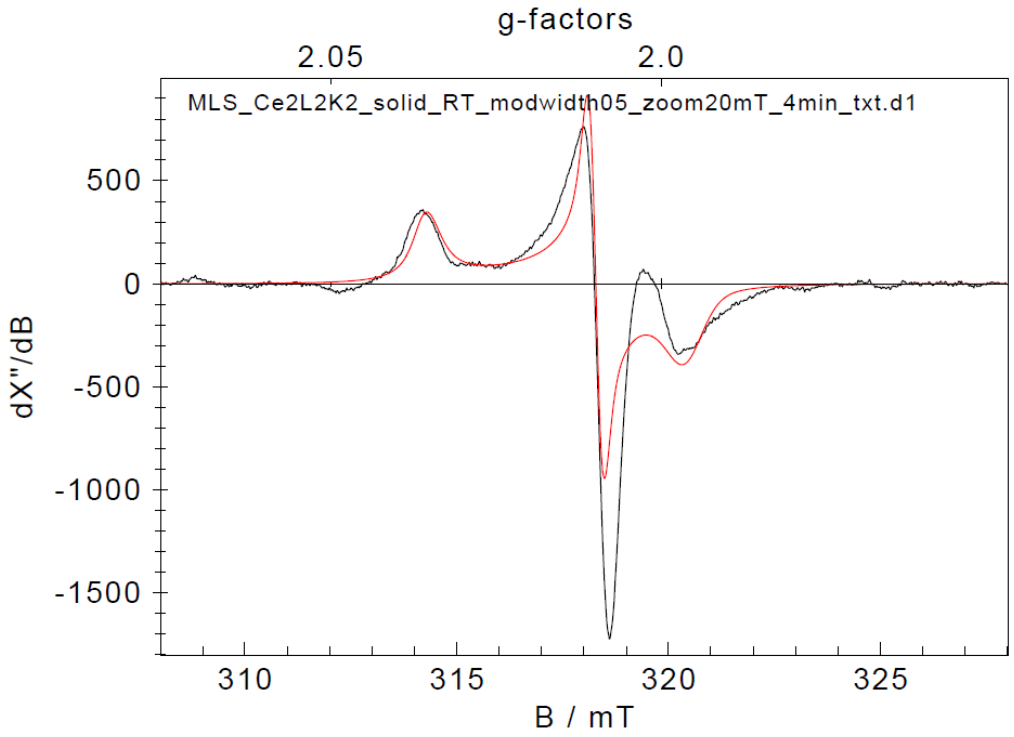

Figure 4-9 Solid-state EPR spectrum of **18(*m*TP^m)(py)** at room temperature, 0.50 G modulation. Black: experimental. Red: simulated spectrum.

At 86 K a broad isotropic signal was seen with g = 1.5241, Figure 4-10. This result is consistent with magnetically independent unpaired *f* electrons on each octahedral Ce(III) centre. The rhombic signal is present as a feature on the isotropic wave, and a narrowed sweep over the 300 mT region at 86 K showed that this secondary signal was almost identical to the room temperature signal shown in Figure 4-9. In this case, the g values were simulated as g_x = 2.0093, g_y = 1.9927 and g_z = 2.0388, Figure 4-11.

[1] EPR spectra were visualised and simulated using eView4W and eSimX 1.1, written by Eckhard Bill, Max-Planck-Instutut für Chemische Energiekonversion, Mülheim, December 2016

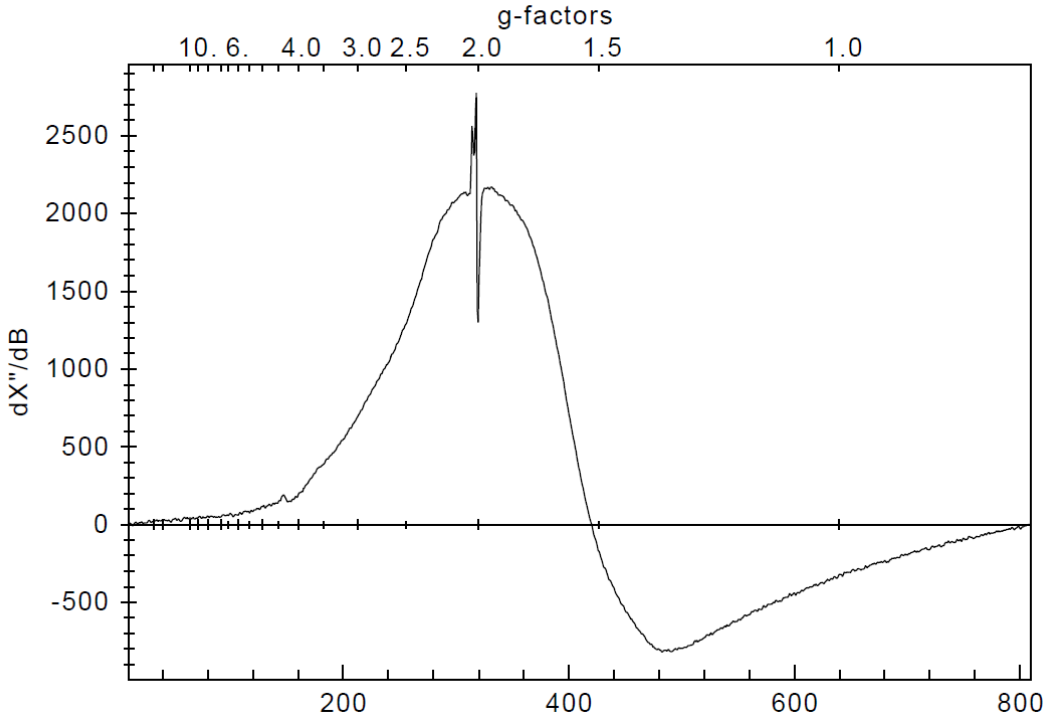

Figure 4-10 Full width solid-state EPR spectrum of **18(*m*TP^{m})(py)** at 86 K. Black: experimental. Red: simulated spectrum.

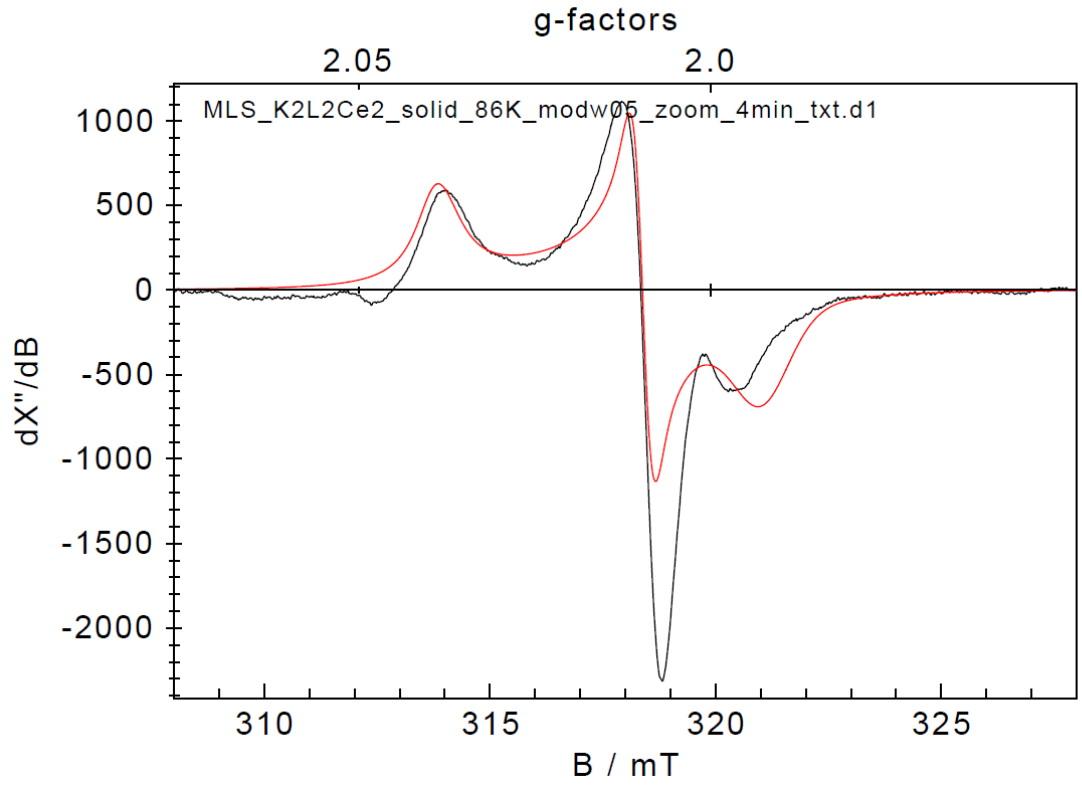

Figure 4-11 300- 330 mT sweep, solid-state EPR spectrum of **18(*m*TP^{m})(py)** at 86 K. Black: experimental. Red: simulated spectrum.

The simple isotropic signal in Figure 4-10 indicates that there is no coupling interaction between the unpaired electrons on the respective cerium centres. No superhyperfine coupling is observed, possibly due to minimal ligand overlap with the contracted 4*f* orbitals. The origin of the signal simulated as rhombic is more difficult to explain, and no similar studies exist for comparison. No *f* electron signal is expected at room temperature, or with a *g* value so close to g_e (2.0023), so this signal is most likely to arise from an organic radical or an impurity not associated with the complex. It is noted however that an identical signal was measured for the analogous complex of **(*p*TP)**, and tentatively suggested that coupling of the *f* electron to the caged K^+ ion may allow an observable signal at room temperature.[59] Further studies on the magnetic behaviour of this complex are required before meaningful conclusions can be drawn.

4.5 Reactivity of [K(solv)$_n$][Ce$_2$(*m*TP^{m})$_2$K(solv)$_4$], 18(*m*TP^{m})

Frequently, bright yellow **18(*m*TP^{m})** proved difficult to isolate and manipulate, readily forming dark-purple decomposition products that are assigned as Ce(IV) compounds formed *via* oxidation/hydrolysis by the presence of trace quantities of oxygen or moisture. It is suggested that the strongly electron-donating tetraphenolate ligand favours Ce(IV) over Ce(III), but the exact identity of these spontaneous oxidation/hydrolysis products remains unclear. The rational oxidation of the Ce(III) centres was therefore targeted.

Novel, mixed-valent Ce cluster compounds (such as the trinuclear [{(Ce(OBu^{t})$_2$}$_2$(μ-OBu^{t})$_3$(μ$_3$-OBu^{t})$_2${Ce(OBu^{t})(NO$_3$)}]) have recently been suggested to have potential in the field of *f*-electron molecular switches.[63] The molecular structure of **18(*m*TP^{m})** (Figures 4-5, 4-6, 4-7) shows that K(2) is located outside the coordination sphere of the metal ions and is solvated by donor solvents or bound by crown ether. It may therefore be possible to affect an outer sphere oxidation by abstracting K(2) to yield a Ce(III)/Ce(IV) mixed oxidation state complex. The single electron oxidant MoO_3 is known to act as a 'potassium sponge', forming insoluble K*x*[MnO_3]*y* 'molybdenum blues'.[64] Attempts to abstract this single K^+ counter ion in one electron oxidation reactions were not successful. Reacting yellow **18(*m*TP^{m})(py)** with one equivalent of MoO_3 in pyridine or thf yielded a dark purple solution. Following slow diffusion of hexanes into this solution, yellow crystals of **18(*m*TP^{m})(py)** were obtained. This result suggested that instead of the desired oxidation to Ce(III)/Ce(IV), half an equivalent of **18(*m*TP^{m})(py)** had been fully oxidised to a Ce(IV)/Ce(IV) species, **19(*m*TP^{m})(py)** (Scheme 4-5). This result is consistent with other unsuccessful attempts to yield mixed valence cerium species *via* oxidation of bimetallic precursors.[59]

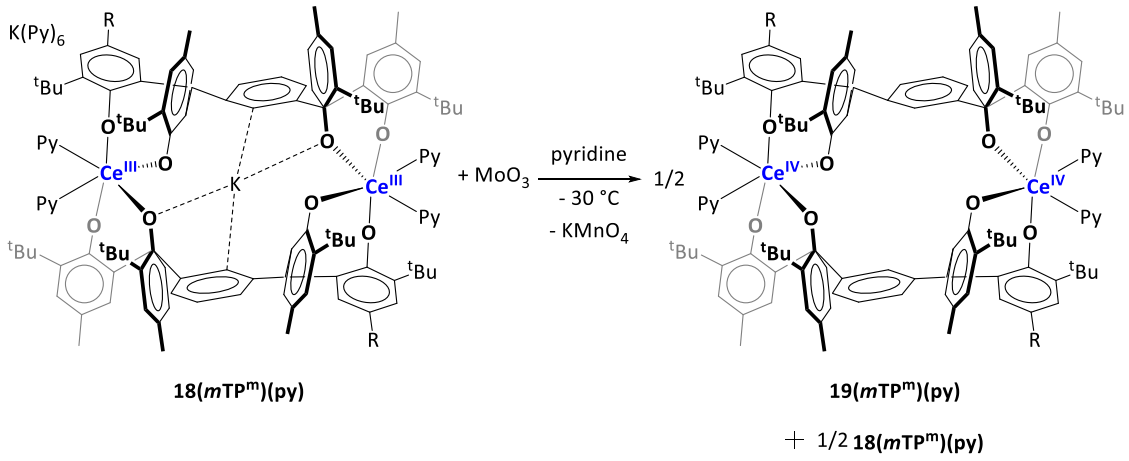

Scheme 4-5 Oxidation of **18(*m*TP^{m})(py)** by MoO_3.

Although the resulting ^{1}H NMR provided evidence of a new diamagnetic product in addition to the signals assigned as **18(*m*TP^{m})(py)**, these signals were broad and could not be fully assigned.

Oxidations to target the mixed valence Ce(III)/Ce(IV) species and to rationally synthesise the fully oxidised Ce(IV)/Ce(IV) complex, **19(*m*TP^{m})(py)** were also investigated with a range of other reagents, shown in Table 4-2.

Entry	Oxidant	Equivalents	Solvent	Temperature	Result
1	$[Cp_2Fe][OTf]$	2	toluene	− 30 ° C	Broad, diamagnetic ^{1}H NMR
2	$[Cp_2Fe][OTf]$	1	toluene	− 30 ° C	^{1}H NMR shows **18(*m*TP^{m})(py)** & diamagnetic species matching Entry 1.
3	I_2	1	thf	− 30 ° C	Dark blue insoluble solid
4	$[Cu(OTf)_2]$	2	toluene	− 30 ° C	Broad, diamagnetic NMR, with some unreacted $[Cu(OTf)_2]$
5	$[Cu(OTf)_2]$	1	toluene	− 30 ° C	Lilac solution with broad, diamagnetic ^{1}H NMR
6	HgI_2	2	thf, toluene	− 30 ° C	Broad, diamagnetic ^{1}H NMR, signal shift in ^{199}Hg NMR

Table 4-2 Reactions to target oxidation of **18(*m*TP^{m})(py)**.

Of the oxidations targeting the fully oxidised Ce(IV)/Ce(IV), (Entries 1, 3, 4 and 6) the reactions with two equivalents of $[Cp_2Fe][OTf]$ and $[Cu(OTf)_2]$ yielded dark purple solutions with diamagnetic ^{1}H NMR spectra, indicating complete oxidation of all paramagnetic Ce(III) centres. Spectra were however broad and poorly resolved, making characterisation difficult. Entry 2 shows the reaction with one equivalent of the one electron oxidant $[Cp_2Fe][OTf]$. A mixture of products was observed by ^{1}H NMR spectroscopy, including some unreacted **18(*m*TP^{m})**, and a diamagnetic product matching the ^{1}H NMR spectrum described for Entry 1, indicating that half of the Ce(III)/Ce(III) **18(*m*TP^{m})(py)** had been fully oxidised to yield the Ce(IV)/Ce(IV) species, **19(*m*TP^{m})(py)** consistent with the results of the initial MoO_3 reaction.

Reactions with KBn were also investigated to target deprotonation of the benzylic ligand hydrogens in analogy to the reactions discussed in Chapter 2 (Scheme 4-6), but no evidence of deprotonation or further K incorporation was observed in this case.

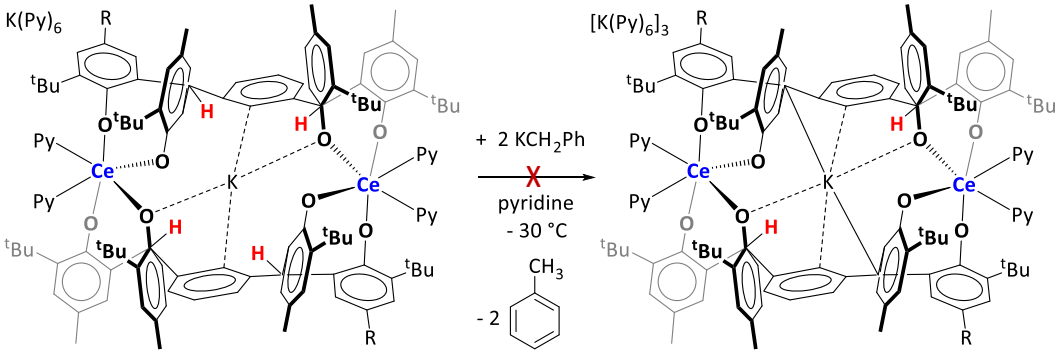

18(*m*TP^{m})

Scheme 4-6 Reaction to target deprotonation of **18(*m*TP^{m})** using KBn.

4.6 Summary and Conclusions for Chapter 4

H$_4$(*m*TP^{m}) has been used to prepare a heterometallic Ce(III) complex, **18(*m*TP^{m})**, *via* salt metathesis. Two inequivalent potassium cations are incorporated within the structure of **18(*m*TP^{m})**, but attempts to selectively remove one in outer sphere oxidation reactions to provide mixed valance Ce(III)/Ce(IV) complexes were not successful. Evidence of oxidation to Ce(IV)/Ce(IV) species is more promising.

Low temperature EPR measurements suggest octahedral symmetry and indicate that there is no electronic communication between the two 4*f*^{1} centres. Room temperature EPR spectra show a rhombic signal which is not fully understood.

These results show that whilst **H$_4$(*m*TP^{m})** provides a structural framework suited to the isolation of heterometallic complexes of lanthanide metals, it remains more challenging to access well-controlled redox reactivity for cerium than for the actinides discussed in Chapter 2.

Further studies could examine the electrochemical redox behaviour of **18(*m*TP^{m})** and investigate the effect of using sodium or lithium cations in place of potassium, as well as targeting small molecule reductions.

4.7 References for Chapter 4

(1) Yin, H.; Carroll, P. J.; Schelter, E. J. *Chem. Commun.* **2016**, (52), 9813–9816.

(2) Evans, W. J.; Fujimoto, C. H.; Ziller, J. W. *Organometallics,* **2001,** 20, (22), 4529-4536

(3) Zhang, J.; Cai, R.; Weng, L.; Zhou, L. *Organometallics,* **2003**, 22 (26), 5385–5391

(4) Li, H.; Yao, Y.; Shen, Q.; Weng, L. *Organometallics*, **2002**, 21 (12), 2529–2532

(5) Levin, J. R.; Cheisson, T.; Carroll, P. J.; Schelter, E. J. *Dalton Trans.* **2016**, *45* (38), 15249–15258.

(6) Solola, L. A.; Carroll, P. J.; Schelter, E. J. *J. Organomet. Chem.* **2018**, *857*, 5–9.

(7) So, Y.-M.; Wang, G.-C.; Li, Y.; Sung, H. H.-Y.; Williams, I. D.; Lin, Z.; Leung, W.-H. *Angew. Chem. Int. Ed.* **2014**, *53* (6), 1626–1629.

(8) Friedrich, J.; Schneider, D.; Bock, L.; Maichle-Mössmer, C.; Anwander, R. *Inorg. Chem.* **2017**, *56* (14), 8114–8127.

(9) Riley, D. P.; Smith, M. R.; Correa, P. E. *J. Am. Chem. Soc.* **1988**, *110* (1), 177–180.

(10) Piro, N. A.; Robinson, J. R.; Walsh, P. J.; Schelter, E. J.; Roy, P. *Coord. Chem. Rev.* **2014**, *260*, 21–36.

(11) Fox, A. R.; Arnold, P. L.; Cummins, C. C. *J. Am. Chem. Soc.* **2010**, *132* (10), 3250–3251.

(12) La Pierre, H. S.; Meyer, K. *Inorg. Chem.* **2013**, *52* (2), 529–539.

(13) Fox, A. R.; Arnold, P. L.; Cummins, C. C. *J. Am. Chem. Soc.* **2010**, *132* (10), 3250–3251.

(14) Cooper, O. J.; Mills, D. P.; McMaster, J.; Moro, F.; Davies, E. S.; Lewis, W.; Blake, A. J.; Liddle, S. T. *Angew. Chem. Int. Ed.* **2011**, *123* (10), 2431–2434.

(15) Fox, A. R.; Cummins, C. C. *J. Am. Chem. Soc.* **2009**, *131* (16), 5716–5717.

(16) Lukens, W. W.; Speldrich, M.; Yang, P.; Duignan, T. J.; Autschbach, J.; Kögerler, P. *Dalton Trans.* **2016**, *45*.

(17) Evans, W. J.; Lee, D. S.; Lie, C.; Ziller, J. W. *Angew. Chem. Int. Ed.* **2004**, *43* (41), 5517–5519.

(18) Evans, W.; Rego, D.; Ziller, J. W. *Inorg. Chem.*, **2006**, *45* (26), 10790–10798

(19) Evans, W. J.; Ulibarri, T. A.; Ziller, J. W. *J. Am. Chem. Soc.* **1988**, *110* (20), 6877–6879.

(20) Evans, W. J.; Lee, D. S.; Ziller, J. W. *J. Am. Chem. Soc.*, **2004**, *126* (2), 454–455

(21) Evans, W. J.; Lee, D. S.; Rego, D.; Perotti, J. M.; Kozimor, S. A.; Moore, E. K.; Ziller, J. W. *J. Am. Chem. Soc.*, **2004**, *126* (44), 14574–14582

(22) Jaroschik, F.; Momin, A.; Nief, F.; Le Goff, X.-F.; Deacon, G. B.; Junk, P. C. *Angew. Chem. Int. Ed.* **2009**, *48* (6), 1117–1121.

(23) Evans, W. J.; Lee, D. S.; Lie, C.; Ziller, J. W. *Angew. Chem. Int. Ed.* **2004**, *43* (41), 5517–5519.

(24) Evans, W. J; Lee, D. S; Ziller, J. W. *J. Am. Chem. Soc.*, **2004**, *126* (2), 454–455

(25) Evans, W. J; Lee, D. S; Johnston, M. A.; Ziller, J. W. *Organometallics*, **2005**, *24* (26), 6393–6397

(26) Demir, S.; Lorenz, S. E.; Fang, M.; Furche, F.; Meyer, G.; Ziller, J. W.; Evans, W. J. *J. Am. Chem. Soc.* **2010**, *132* (32), 11151–11158.

(27) Demir, S.; Siladke, N. A.; Ziller, J. W.; Evans, W. J. *Dalton Trans.* **2012**, *41* (32), 9659.

(28) Schmiege, B. M.; Ziller, J. W.; Evans, W. J. *Inorg. Chem.* **2010**, *49* (22), 10506–10511.

(29) Evans, W. J.; Allen, N. T.; Ziller, J. W. *Angew. Chem. Int. Ed.* **2002**, *41* (2), 359.

(30) Evans, W. J.; Allen, N. T.; Ziller, J. W. *J. Am. Chem. Soc.* **2001**, 123, (32), 7927-7928

(31) Mueller, T. J.; Fieser, M. E.; Ziller, J. W.; Evans, W. J. *Chem. Sci.* **2011**, *2* (10), 1992.

(32) Evans, W. J.; Rego, D.; Ziller, J. W. *Inorg. Chem.* **2006**, *45* (26), 10790–10798.

(33) MacDonald, M. R.; Ziller, J. W.; Evans, W. J. *J. Am. Chem. Soc.* **2011**, *133* (40), 15914–15917.

(34) Fang, M.; Bates, J. E.; Lorenz, S. E.; Lee, D. S.; Rego, D. B.; Ziller, J. W.; Furche, F.; Evans, W. J. *Inorg. Chem.* **2011**, *50* (4), 1459–1469.

(35) Evans, W. J.; Lee, D. S.; Rego, D.; Perotti, J. M.; Kozimor, S. A.; Moore, E. K.; Ziller, J. W. *J. Am. Chem. Soc.*, **2004**, *126* (44), 14574–14582

(36) Evans, W. J.; Zucchi, G.; Ziller, J. W. *J. Am. Chem. Soc.*, **2003**, *125* (1), 10–11

(37) Evans, W. J.; Fang, M.; Zucchi, G.; Furche, F.; Ziller, J. W.; Hoekstra, R. M.; Zink, J. I. *J. Am. Chem. Soc.* **2009**, *131* (31), 11195–11202.

(38) Rinehart, J. D.; Fang, M.; Evans, W. J.; Long, J. R. *Nat. Chem.* **2011**, *3* (7), 538–542.

(39) Rinehart, J. D.; Fang, M.; Evans, W. J.; Long, J. R. *J. Am. Chem. Soc.* **2011**, *133* (36), 14236–14239.

(40) Corbey, J. F.; Farnaby, J. H.; Bates, J. E.; Ziller, J. W.; Furche, F.; Evans, W. J. *Inorg. Chem.* **2012**, *51* (14), 7867–7874.

(41) Turner, Z. *Inorganics* **2015**, *3* (4), 597–635.

(42) Bérubé, C. D.; Yazdanbakhsh, M.; Gambarotta, S.; Yap, G. P. A. O*rganometallics*, **2003**, *22* (18), 3742–3747

(43) Dubé, T.; Ganesan, M.; Conoci, S.; Gambarotta, S.; Yap, G. P. A. *Organometallics*, **2000**, *19* (18), 3716–3721

(44) Dubé, T.; Conoci, S.; Gambarotta, S.; Yap, G. P. A.; Vasapollo, G. *Angew. Chem. Int.*

Ed. **1999**, *38* (24), 3657–3659.

(45) Meihaus, K. R.; Corbey, J. F.; Fang, M.; Ziller, J. W.; Long, J. R.; Evans, W. J. *Inorg. Chem.* **2014**, *53* (6), 3099–3107.

(46) Zhang, Y.-Q.; Luo, C.-L.; Wang, B.-W.; Gao, S. *J. Phys. Chem. A* **2013**, *117* (42), 10873–10880.

(47) Rajeshkumar, T.; Rajaraman, G. *Chem. Commun.* **2012**, *48* (63), 7856.

(48) Evans, W. J.; Lee, D. S.; Ziller, J. W.; Kaltsoyannis, N. *J. Am. Chem. Soc.*, **2006**, *128* (43), 14176–14184

(49) Corbey, J. F.; Fang, M.; Ziller, J. W.; Evans, W. J. *Inorg. Chem.* **2015**, *54* (3), 801–807.

(50) Evans, W. J.; Fang, M.; Bates, J. E.; Furche, F.; Ziller, J. W.; Kiesz, M. D.; Zink, J. I. *Nat. Chem.* **2010**, *2* (8), 644–647.

(51) Lorenz, S. E.; Schmiege, B. M.; Lee, D. S.; Ziller, J. W.; Evans, W. J. *Inorg. Chem.* **2010**, *49* (14), 6655–6663.

(52) Falcone, M.; Chatelain, L.; Scopelliti, R.; Živković, I.; Mazzanti, M. *Nature* **2017**, *547* (7663), 332–335.

(53) Kang, B. S.; Weng, L. H.; Wu, D. X.; Wang, F.; Guo, Z.; Huang, L. R.; Huang, Z. Y.; Liu, H. Q. *Inorg. Chem.* **1988**, *27* (12), 1130–1132.

(54) Steele, L. A. M.; Boyle, T. J.; Kemp, R. A.; Moore, C. *Polyhedron* **2012**, *42* (1), 258–264.

(55) Robinson, J. R.; Carroll, P. J.; Walsh, P. J.; Schelter, E. J. *Angew. Chem. Int. Ed.* **2012**, *51* (40), 10159–10163.

(56) Cotton, S. A. John Wiley & Sons. *Lanthanide and actinide chemistry*; Wiley, 2006.

(57) Robinson, J. R.; Gordon, Z.; Booth, C. H.; Carroll, P. J.; Walsh, P. J.; Schelter, E. J. *J. Am. Chem. Soc.*, **2013**, *135* (50), 19016–19024

(58) Zhang, J.; Jian, C.; Gao, Y.; Wang, L.; Tang, N.; Wu, J. *Inorg. Chem.* **2012**, *51* (24), 13380–13389.

(59) Wang, K. Synthesis, *PhD Thesis*, Characterisation and Reactivity Study of Rare Earth Metal Complexes, **2017**, Univeristy of Edinburgh.

(60) Evans, W.; Rego, D.; Ziller, J. W. *Inorg. Chem.*, **2006**, *45* (26), 10790–10798

(61) Walter, M. D.; Booth, C. H.; Lukens, W. W.; Andersen, R. A. *Organometallics*, **2009**, *28* (3), 698–707

(62) Schwartz, R. W.; Hill, N. J. *J. Chem. Soc., Faraday Trans. 2***, 1974**, 70**,** 124-131

(63) Gun'ko, Y. K.; Elliott, S. D.; Hitchcock, P. B.; Lappert, M. F. *J. Chem. Soc. Dalton Trans.*

2002, (8), 1852–1856.

(64) Chakarawet, K.; Davis-Gilbert, Z. W.; Harstad, S. R.; Young, V. G.; Long, J. R.; Ellis, J. E. *Angew. Chem.* **2017**, *129* (35), 10713–10717.

Chapter 5: Experimental Details

5.1 General Procedures and Techniques

All moisture and air sensitive materials were manipulated through the use of standard Schlenk-line techniques and stored in dinitrogen filled MBraun gloveboxes. All gases were supplied by BOC gases UK, apart from $^{15}N_2$ which was purchased from Cambridge Isotope Laboratories. All glassware was dried in a 160 °C oven overnight, cooled under vacuum and purged with nitrogen before use. All cannulae and Fisherbrand 1.2 μm retention glass microfibre filters were dried in a 160 °C oven overnight prior to use.

Tetrahydrofuran, acetonitrile, methanol, toluene and hexane were collected from a Vac Atmospheres solvent purification system, degassed and stored over activated 4 Å molecular sieves under dinitrogen. Prior to collection the solvent was cycled over a drying column containing molecular sieves for 12 hours. 1,4-Dioxane was refluxed over sodium for three days, distilled and collected into an ampoule containing 4 Å molecular sieves. Toluene-d_8, benzene-d_6 and tetrahydrofuran-d_8 were degassed, refluxed over potassium for 24 hours and distilled by trap to trap distillation under static vacuum prior to use. All solvents were purchased from Sigma-Aldrich or Fisher Scientific.

^{1}H, ^{2}H (77 MHz), $^{15}N\{^{1}H\}$ (51 MHz), $^{13}C\{^{1}H\}$ (126 MHz), DOSY and ^{29}Si (99 MHz) NMR spectra were recorded on Bruker AVA400, AVA500, or PRO500 spectrometers at 298 K unless otherwise specified. Chemical shifts are reported in parts per million, δ. All ^{1}H NMR and $^{13}C\{^{1}H\}$ NMR spectra were referenced relative to external $SiMe_4$ at 0 ppm, relative to internal residual solvent H atoms; benzene-d_6 (7.16 ppm); toluene-d_8 (7.09, 7.00, 6.98. 2.09 pm) pyridine-d_5 (8.74, 7.58, 7.22 ppm) for ^{1}H NMR. ^{15}N and ^{29}Si NMR spectra were referenced using an external standard of CH_3NO_2 (0.0 ppm) and $SiMe_4$ (0.0 ppm), respectively. Raman data were recorded on a Renishaw InVia Raman microscope. Raman sample were prepared by adding a small amount of solid to a glass capillary tube and sealing the end. Infrared spectra were recorded on a Perkin Elmer Spectrum 65 FT-IR spectrometer as nujol mulls between NaCl disks. Elemental analyses were performed by Mr Stephen Boyer at London Metropolitan University. Mass spectrometry and GC-MS were performed on Bruker Ultraflex MALDI TOF TOF and ThermoElectron MAT 900. Samples were prepared by filtering dilute solutions into 9mm screw top vials.

Variable temperature EPR measurements were recorded using a JEOL JES-FA200 continuous wave spectrometer equipped with an X-band high-power, low-noise Dual-Gunn oscillator bridge and a high sensitivity cylindrical mode cavity and a nitrogen/helium cryostat. UV-vis-NIR absorption spectra were recorded at room temperature (typically 288 K) on a Jasco V-670 spectrophotometer in a 10 mm quartz cuvette fitted with a teflon tap.

Cyclic voltammograms were recorded for quiescent solutions at variable scan rates between 100 and 500 mV s^{-1} in thf using 0.1 M $[^{n}Bu_4N][BPh_4]$ as the supporting electrolyte. A glassy carbon working electrode, platinum gauze counter electrode and a silver-wire quasi-reference were used throughout. The voltammograms were first calibrated against decamethylcobaltocene ($CoCp^*_2$), previously dissolved in a small volume of toluene, and measured under the same conditions. They were then calibrated against the ferricenium/ferrocene (Fc+/Fc = 0 V) couple by comparison of the $E_{1/2}$ potentials of $[CoCp^*_2]^+/CoCp^*_2$ and Fc^+/Fc, measured in thf against the saturated calomel electrode (SCE) taken from a different study.[1]

5.2 Preparation of Reagents

1,3-diacetylbenzene, 1,3-phenylbenzene, 3-methylisopthaldehyde, benzene-1,2-dicarboxaldehyde, 2,4-di*tert*butylphenol, N-chlorosuccinimide, TEMPO, trimethylamine-N-oxide, HgI_2, HgI_2, Et_3N, $NaBPh_4$, 2M HCl in ethanol, dimethylsulfone, DHA, 2-iodo-2-methylpropane, $SiMe_3OTf$, tri-*tert*butylbenzene, KOH, 1-diphenyl-4,4'-diol, [PyH]Cl, MoO_3, $[Cp_2Fe]OTf$, I_2, $[Cu(OTF)_2]$, potassium metal, caesium metal, sodium metal, 2-*tert*-butyl-4-methylphenol, *p*-toluenesulfonic acid, isophtalaldehyde, 1'-biphenyl-4,4'-diol and 2,4,6-tri-*tert*butylphenol are commercially available and were purchased from Sigma-Aldrich, Alfa Aesar or other commercial suppliers. DCl in D_2O was purchased from Magnisolv. $CeCl_3 \cdot 7H_2O$ was purchased from Sigma-Aldrich and stirred with excess $SiMe_3Cl$ to yield anhydrous $CeCl_3(thf)_n$. The number of coordinated thf molecules was determined by quantitative ^1H NMR spectroscopy.

All commercially available solid reagents for use in air sensitive reaction were dried under vacuum for a minimum of 18 hours or used as received for air stable reactions. Liquid reagents for use with air- and moisture-sensitive reactions were either dried with alkali metal or activated molecular sieves, as appropriate, and purified by trap to trap vacuum distillation.

$K[N(SiMe_3)_2]$,[2] $[UI_4(dioxane)_2]$,[3] $[UI_3(dioxane)_{1.5}]$,[3] $[U[N(SiMe_3)_2]_3]$,[3] $[UN''_2(N(SiMe_3)SiMe_2CH_2)]$,[4] $[Ca[N(SiMe_3)_2]_2]$,[5] $[Mg[N(SiMe_3)_2]_2]$,[5] $Na[N(SiMe_3)_2]$,[2] KC_8,[6] and UCl_4[7] were synthesised according to literature procedures, in some cases with slight modifications.

5.3 Synthetic procedures for Chapter 2

5.3.1 Synthesis of H_4(*m*TP^m)

A two necked 250 cm^3 round bottomed flask was charged with 2-^{t}butyl-4-methylphenol (26.94 g, 161 mmol), isophthalaldehyde (5.0 g, 37 mmol) and *p*-toluenesulfonic acid (0.71 g, 3.8 mmol), and equipped with a stirrer bar and an oil bubbler. The flask was placed under a flow of nitrogen, stirred and heated to 110 °C. The solids melted to yield a yellow liquid. After 2 hours, the reaction mixture turned into a clear red solid. 30 cm^3 of MeCN was added to the solid and sonicated. The resulting beige suspension was filtered to provide **H_4(*m*TP^m)** as a colourless solid which was collected and washed with MeCN (20 cm^3). The resulting colourless solid was dried under reduced pressure at 65 °C overnight and stored in a glove box.

Yield 22.9 g (82 %).

^{1}H NMR (500 MHz, Benzene-d_6) δ 7.09 (s, aryloxide-*H*, 4H), 7.06-6.96 (m, aromatic-*H*, 4H), 6.68 (s, aryloxide-*H*, 4H), 5.47 (s, Ar_3CH, 2H), 4.90 (s, aryloxide-*H*, 4H), 2.05 (s, Me*H*, 12H), 1.43 (s, ^{t}Bu*H*, 36H).

^{13}C NMR (126 MHz, Benzene-d_6) δ 151.11 (aryloxide-*C*) , 141.77 (aromatic-*C*) , 137.57 (aryloxide-*C*) , 130.67 (aryloxide-*C*) , 129.64 (aryloxide-*C*) , 128.42 (aromatic-*C*), 127.95 (aryloxide-*C*), 47.55 (Ar_3C), 34.53 (aryloxide-*C*), 31.57 (aryloxide-*C*) , 29.61 (^{t}Bu*C*) , 22.65 (Me_3C), 20.73 (Me*C*) , 13.94 (Aromatic-*C*).

Elemental Analysis: C 82.71 %, H 8.81 % calculated. C 82.83 %, H 8.92 % found.

HRMS-ESI (*m/z*): $[H_4(mTP)+Na]^+$ calcd for $C_{52}H_{66}NaO_4$ 777.59; found, 777.4850.

5.3.2 Reaction to target H_4(*m*TP^a)

2-*t*butyl-4-methylphenol (1.5 g, 9.13 mmol), 1,3-diacetylbenzene (0.34 g, 2.08 mmol) and an acid catalyst (see Table 5-1) were added to a glass microwave vial with a stirrer bar. The reaction mixture was heated to 110 °C inside the microwave reactor for 1 hour. The resulting thick orange tacky solid was dissolved in MeCN and GC-MS and ^{1}H NMR spectroscopy were used to confirm that only starting materials and decomposition products were present.

Table 5-1 Acid catalysts used in reactions to target **H_4(*m*TP[a])**

methanesulfonic acid	0.9 equivalents	179 mg	1.87 mmol
concentrated HCl	1 equivalent	0.5 g	2.08 mmol

5.3.3 Reaction to target H_4(*m*TP[b])

A two necked 250cm^3 round bottomed flask was charged with 2-*t*butyl-4-methylphenol (1.26 g, 7.68 mmol), 1,3-phenylbenzene (0.5 g, 1.75 mmol) and *p*-toluenesulfonic acid (33 mg, 0.175 mmol), and equipped with a stirrer bar and an oil bubbler. The flask was placed under a flow of nitrogen, stirred and heated to 100 °C. The solids melted to yield a yellow liquid. After heating overnight, the resulting tacky yellow solid was dissolved in MeCN. Addition of a mixture of H_2O and MeOH resulted in precipitation of a white powder which was characterised as a mixture of unreacted starting materials.

5.3.4 Reaction to target H_4(*m*TP[c])

A two necked 250 cm^3 round bottomed flask was charged with 2-*t*butyl-4-methylphenol (20.06 g, 122 mmol), 3-methylisopthaldehyde (5.0 g, 27.8 mmol) and *p*-toluenesulfonic acid (0.53 g, 2.78 mmol), and equipped with a stirrer bar and an oil bubbler. The flask was placed under a flow of nitrogen, stirred and heated to 110 °C. The solids melted to yield a yellow liquid. After heating overnight, TLC (9:1 hexane: ethyl acetate) and ^{1}H NMR indicated no conversion of the starting materials.

5.3.5 Reaction to target H_4(*o*TP[d])

A two necked 250 cm^3 round bottomed flask was charged with 2-*t*butyl-4-methylphenol (5.39 g, 32.8 mmol), benzene-1,2-dicarboxaldehyde (1.0 g, 7.46 mmol) and an acid catalyst (see Table 5-2), and equipped with a stirrer bar and an oil bubbler. The flask was placed under a flow of nitrogen, stirred and heated to 110 °C. The solids melted to yield a yellow liquid. After

heating for several hours a colour change to red was observed. Crude ^{1}H NMR spectroscopy indicated multiple minor products, but predominantly unreacted starting materials.

Table 5-2 Acid catalysts used in reactions to target **H_4(*o*TP^d)**

p-toluenesulfonic acid	0.1 equivalents	0.14 g	0.75 mmol
p-toluenesulfonic acid	0.5 equivalents	0.70 g	3.75 mmol

Via microwave synthesis:

2-^{t}butyl-4-methylphenol (1.5 g, 9.13 mmol), benzene-1,2-dicarboxaldehyde (0.38 g, 2.08 mmol) and *p*-toluenesulfonic acid (39.5 mg, 0.21 mmol) were added to a glass microwave vial with a stirrer bar. The reaction mixture was heated to 110 °C inside the microwave reactor for 1 hour. The resulting thick brown tacky solid was dissolved in MeCN and washed three times with saturated aqueous $NaHCO_3$. The resulting dark brown solution was cooled to 0 °C to yield a colourless crystalline material. This solid was isolated by filtration and characterised as unreacted benzene-1,2-dicarboxaldehyde.

5.3.6 Synthesis of H_4(*m*TP^t)

A two necked 250 cm^3 round bottomed flask was charged with 2,4-di^{t}butylphenol (6.77 g, 3.28 mmol), isophthalaldehyde (1.0 g, 0.746 mmol) and *p*-toluenesulfonic acid (0.14 g, 0.075 mmol), and equipped with a stirrer bar and an oil bubbler. The flask was placed under a flow of nitrogen, stirred and heated to 110 °C. The solids melted to yield a yellow liquid. After 2 hours, the reaction mixture had turned into a clear red solid. 20 cm^3 of MeCN was added to the solid and sonicated. The resulting beige suspension was filtered to provide a colurless solid which was collected by filtration and washed with MeCN (20 cm^3). The resulting colourless solid was dried under reduced pressure at 65 °C overnight and stored in a glove box.

Yield 5.44 g (79 %).

^{1}H NMR (500 MHz, Benzene-d_6) δ 7.48 (s, aryloxide-*H*, 4H), 7.08 – 6.99 (m, aromatic-*H*, 4H), 6.93 (s, aryloxide-*H*, 4H), 5.50 (s, Ar$_3$*H*, 2H), 4.86 (s, ArO*H*, 4H), 1.51 (s, ^{t}Bu*H*, 36H), 1.23 (s, ^{t}Bu*H*, 36H).

Elemental Analysis: C 83.25 %, H 9.82 % calculated. C 83.06 %, 10.01 % found.

HRMS-ESI (*m/z*): $[H_4(mTP^t)+Na]^+$ calculated for $C_{64}H_{90}NaO_4$ 945.67; found, 945.6689.

5.3.7 General procedure for attempted synthesis of Group 1 and 2 salts of H_4(*m*TP)

One equivalent of **H_4(*m*TP)** was dissolved in C_6D_6 and added to a Young's tap NMR tube. A solution of $M[N(SiMe_3)_2]_n$ (M = Ca, Mg: 2 equivalents; M = Na, K: 4 equivalents) in C_6D_6 was added to the NMR tube and allowed to react at room temperature.

5.3.8 Synthesis of K_4(*m*TP^m), 1(*m*TP^m)

A Schlenk flask was charged with **H_4(*m*TP)** (2.00 g, 2.65 mmol) and $[KN(SiMe_3)_2]$ (2.11 g, 10.60 mmol) and equipped with a stirrer bar. Thf was added and the yellow solution was stirred for 1 hour at RT. **K_4(*m*TP^m)** was usually reacted *in situ* without purification. The product could however be precipitated as a colourless powder by the addition of hexanes to the thf solution and isolated by filtration.

Yield = 1.70 g, 72 %

^{1}H NMR (500 MHz, 329K thf-d_8) δ 7.45-6.92 (m, aryloxide-*H*, 4H), 6.78-6.59 (m, aromatic-*H* and aryloxide-*H*, 8H) 5.80 (s, Ar_3CH, 2H), 2.03 (s, Me*H*, 12H), 1.32(s, ^{t}Bu*H*, 36H).

Mass Spectrometry: (MALDI) m/z 907.601 **[K_4(*m*TP^m)+H]** found. 907.330 calculated for $C_{52}H_{63}K_4O_4$.

Elemental Analysis: C 68.83 %, H 6.89 % calculated. C 66.19 %, H 7.87 % found.

5.3.9 Synthesis of [{U(*m*TP^m)(solv)$_2$}$_2$], 2(*m*TP)

A Schlenk flask was charged with **H_4(*m*TP^m)** (100 mg, 0.132 mmol) and $[K\{N(SiMe_3)_2\}]$ (106 mg, 0.530 mmol) and equipped with a stirrer bar. 1,4-Dioxane (10 cm^3) was added and the resulting yellow solution was stirred for 1 hour at RT. To this solution, a $[UI_4(dioxane)_2]$ (122 mg, 0.132 mmol) solution in 1,4-dioxane was added by cannula transfer from a separate Schlenk flask. The resulting dark green solution was stirred at RT for 24 hours, yielding a green suspension. The pale green precipitate was removed by filtration and the solvent was removed under reduced pressure providing the product as a light dark green solid. Green crystals suitable for single crystal XRD were grown from slow diffusion of hexane vapours into a concentrated solution of **[{U(*m*TP^m)(1,4-dioxane)$_2$}$_2$]** in 1,4-dioxane.

Yield = 252 mg, 41 %.

^{1}H NMR (400 MHz, Benzene-d_6) δ 34.60 (s, aromatic-*H*, 1H), 32.50 (s, aromatic-*H*, 2H), 27.53 (s, aryloxide-*H*, 4H), 18.80 (s, aryloxide-*H*, 4H), 17.41 (s, aromatic-*H*, 1H), 15.76 (s, diox-*H*, 32H), -5.53 (s, ^{t}Bu*H*, 36H), -13.43 (s, Me*H*, 12H), -21.54 (s, Ar$_3$*H*, 2H)
Elemental Analysis: C 61.84 %, H 6.75 % calculated. C 61.65 %, H 6.82 % found.

5.3.10 Reduction of [{U(*m*TP^m)(thf)$_2$}$_2$], 2(*m*TP)(thf), under dinitrogen

[{U(*m*TP^m)(thf)$_2$}$_2$], **2(*m*TP)(thf)**, (315 mg, 0.139 mmol) was dissolved in toluene to provide a dark brown solution. The solution was cooled to −30 °C and added to solid KC_8 (37.6 mg, 0.278 mmol). The reaction mixture was allowed to warm slowly to room temperature and stirred for 16 hours. Analysis by NMR spectroscopy suggested decomposition of 1U-thf to provide several products. These were not isolated cleanly. No evidence of N_2 binding was observed.

5.3.11 Synthesis of [{U(*m*TP^m)}$_2$], 3(*m*TP^m)

An ampoule fitted with a teflon tap was charged with a toluene solution (10 ml) of [U(N")$_2${N(SiMe$_3$)SiMe$_2$CH$_2$}] (2.00 g, 2.785 mmol) and **H$_4$(*m*TP^m)** (2.10 g, 2.784 mmol) and a stirrer bar. The resulting dark brown reaction mixture was heated to 90 °C overnight, during which time the product was formed as a bright green precipitate. After allowing to cool to RT, the green solid **[U(*m*TP^m)]$_2$, 3(*m*TP^m)**, was isolated by filtration, and washed five times with hexane until the washings were colourless.

Yield = 0.426 g, 0.215 mmol, 15 %.

^{1}H NMR (500 MHz, Benzene-d_6) δ 41.16 (s, aromatic-*H*, 1H), 36.46 (s, aryloxide-*H*, 2H), 34.97 (s, aromatic-*H*, 1H), 27.05 (s, ^{t}Bu*H*, 18H), 22.63 (d, *J* = 12.9 Hz, Me*H*, 6H), 21.84 (s, aromatic-*H*, 1H), 19.49 (s, aromatic-*H*, 1H), 18.99 (s, aryloxide-*H*, 2H), 17.91 (s, ^{t}Bu*H*, 18H), 17.24 (s, Me-*H*, 6H), 12.47 (s, aryloxide-*H*, 2H), 6.17 (s, aryloxide-*H*, 2H), 5.20 (s, Me*H*, 6H), 3.59 (s, aromatic-*H*, 1H), 3.57 (s, aryloxide-*H*, 2H), 2.11 (s, aromatic-*H*, 2H), -10.46 (d, *J* = 7.6 Hz, Me*H*, 6H), -10.57 (s, aryloxide-*H*, 2H), -22.89 (s, aryloxide-*H*, 2H), -23.95 (s, Ar$_3$*H*, 2H), -24.31 (s, Ar$_3$*H H*, 2H), -25.47 (s, ^{t}Bu*H*, 18H), -28.71 (s, ^{t}Bu*H*, 18H), -34.40 (s, aromatic-*H*, 2H), -39.15 (s, aromatic-*H*, 2H).
Elemental Analysis: C 63.21 %, H 6.22 % calculated. C 63.12 %, H 6.13 % found.

UV-Vis (toluene) λ_{max}, nm: 284

DOSY NMR Diffusion coefficient (DOSY NMR, d_8-toluene): −9.325 log m^2 s (hydrodynamic radius: 7.638 Å)

Magnetic moment (Evans method) 3.21 μ_B

5.3.12 Synthesis of [{U(*m*TP^t)(thf)$_2$}$_2$], 2(*m*TP^t), *via* solvation of [{U(*m*TP)}$_2$], 3(*m*TP)

[U(N")$_2${N(SiMe$_3$)SiMe$_2$CH$_2$}] (0.780 g, 1.09 mmol) and **H$_4$(*m*TP^t)** (1.00 g, 1.08 mmol) were added to an ampoule with a stirrer bar and dissolved in toluene (10 cm^3). The resulting dark brown reaction mixture was heated to 90 °C for 16 h. After cooling to RT and filtering the light brown solid was extracted into thf. The solvent was removed under reduced pressure and the bright green powder was recrystalised from a concentrated solution of thf at −30 °C to give large single crystals.

Yield was poor and exact amounts were not recorded.

5.3.13 Reaction to target oxidation of 3(*m*TP^m), [U(*m*TP^m)]$_2$, with NCS

3(*m*TP^m) (50 mg, 0.025 mmol) was dissolved in dioxane to provide a bright green solution. A solution of NCS in dioxane (8.3 mg, 0.063 mmol) was slowly added resulting in an immediate colour change to dark brown. Multiple products were observed by ^{1}H NMR spectroscopy. These were not isolated or further characterised.

5.3.14 Reaction to target oxidation of 3(*m*TP^m), [U(*m*TP^m)]$_2$, with TEMPO

3(*m*TP^m) (50 mg, 0.025 mmol) was dissolved in thf to provide a colourless suspension. A bright red solution of TEMPO in thf (9.8 mg, 0.063 mmol) was slowly added to yield a pale pink suspension. The reaction mixture was stirred at room temperature overnight. A pale precipitate was removed by filtration to yield a brown solution. ^{1}H NMR spectroscopy indicated decomposition of **3(*m*TP^m)** but no clean conversion to a new product.

5.3.15 Reaction to target oxidation of 3(*m*TP^m), [U(*m*TP^m)]$_2$, with trimethylamine N-oxide

3(*m*TP^m) (50 mg, 0.025 mmol) was dissolved in dioxane to provide a bright green solution. A solution of trimethylamine N-oxide in dioxane (4.7 mg, 0.063 mmol) was slowly added resulting in an immediate colour change to dark brown. Multiple products were observed by ^{1}H NMR spectroscopy. These were not isolated or further characterised.

5.3.16 Reaction to target oxidation of 3(*m*TP^{m}), [U(*m*TP^{m})]$_2$, with HgI_2

3(*m*TP^{m}) (50 mg, 0.025 mmol) was suspended in thf and cooled to −30 °C. A colourless solution of HgI_2 in thf (11.4 mg, 0.025 mmol) was slowly added. The resulting reaction mixture was allowed to warm slowly to room temperature and stirred overnight. ^{1}H NMR spectroscopy of the resulting dark brown solution indicated that the product was still paramagnetic, indicating unsuccessful oxidation.

5.3.17 Reaction to target oxidation of 3(*m*TP^{m}), [U(*m*TP^{m})]$_2$, with CO

3(*m*TP^{m}) (50 mg, 0.025 mmol) was dissolved in C_6D_6, added to a Young's tap NMR tube and this solution was freeze-pump-thaw degassed. 1 bar of CO was added to the tube and an immediate colour change from bright green to dark brown was observed upon warming to room temperature. ^{1}H NMR spectroscopy indicated decomposition of the starting material into multiple products.

5.3.18 Reduction of 3(*m*TP^{m}), [U(*m*TP^{m})]$_2$, under dinitrogen to afford [K$_4${U(*m'*TP)(NH)}$_2$], 4(*m'*TP^{m})

Under an atmosphere of N_2, at −30 °C, a suspension of KC_8 (55.2 mg, 0.408 mmol) was added dropwise to a toluene solution of **[{U(*m*TP)}$_2$], 3(*m*TP)** (202 mg, 0.102 mmol). The reaction mixture was allowed to warm to RT over 16 h with stirring. The red solution was isolated by filtration from the dark grey solids and volatiles removed under reduced pressure to yield a dark oragne powder. The powder was stirred for an hour in hexane and then isolated by filtration and dried thoroughly under reduced pressure to yield **[K$_4${U(*m'*TP)(NH)}$_2$]** as an orange powder.

Yield = 141 mg, 64 %.

Orange plates suitable for single crystal XRD were formed when the reaction mixture was stored at −30 °C for several weeks.

^{1}H NMR (600 MHz, Benzene-d_6) δ 16.79 (s, aryloxide-*H*, 2H), 15.25 (s, aryloxide-*H,* 1H), 13.60 (s, aryloxide-*H,* 1H), 12.81 (s, ^{t}Bu*H,* 9H), 11.72 (s, ^{t}Bu*H,* 9H), 11.36 (s, aromatic-*H,* 1H,), 11.06 (s, aromatic-*H,* 1H), 8.60 (s, ^{t}Bu*H,* 9H), 8.13 (s, ^{t}Bu*H,* 9H), 7.89 (s, ^{t}Bu*H,* 9H), 7.45 (s, aryloxide-*H,* 1H), 7.29 (s, aryloxide-*H,* 2H,), 6.70 – 6.29 (m, aryloxide-*H,* 2H), 5.41 (s, aryloxide-*H,* 1H), 5.04 (s, Me*H,* 3H), 3.87 (s, aromatic-*H,* 1H,), 3.25 (s, Me*H,* 6H), 2.77 (s, aromatic-*H,* 1H), 0.59

(s, Me*H,* 3H), 0.30 (s, Me*H,* 6H), -0.38 (s, aromatic-*H,* 1H), -0.79 (s, Me*H,* 3H), -1.46 (s, Me*H,* 3H), -1.46 (s, aryloxide-*H,* 2H), -2.96 – -3.32 (m, ^{t}Bu*H*, 9H), -4.36 (s, aryloxide-*H,* 4H), -5.39 (s, ^{t}Bu*H,* 9H), -6.65 (s, ^{t}Bu*H,* 9H), -9.86 (s, aryloxide-*H,* 1H), -14.91 (s, Ar$_3$*H,* 2H), -16.58 (s, aromatic-*H,* 1H), -19.81 (s, aromatic-*H,* 1H).

^{1}H NMR (500 MHz, Toluene-d_8) δ 37.61 (s, arene-*H,* 1H), 27.48 (s, Me*H,* 3H), 26.03 (s, arene-*H,* 1H), 16.74 (s, arene-*H,* 1H), 13.16 (s, ^{t}Bu*H,* 9H), 12.35 (s, arene-*H,* 1H), 11.69 (s, ^{t}Bu*H,* 9H), 11.21 (s, arene-*H,* 1H), 8.69 (s, ^{t}Bu*H,* 9H), 8.21 (s, ^{t}Bu*H,* 9H), 7.63 (s, ^{t}Bu*H,* 9H), 6.49 (s, arene-*H,* 1H), 6.29 (s, arene-*H,* 1H), 4.98 (s, Me*H,* 3H), 3.74 (s, arene-*H,* 1H), 3.56 (s, arene-*H,* 1H), 3.26 (s, ^{t}Bu*H,* 9H), 3.14 (s, arene-*H,* 2H), 3.04 (s, arene-*H,* 1H), 1.47 (s, arene-*H,* 1H), 0.91 (s, arene-*H,* 1H), 0.50 (s, Me*H,* 3H), 0.28 (s, arene-*H,* 1H), -0.47 (s, arene-*H,* 1H), -0.85 (s, Me*H,* 3H), -1.08 (s, Me*H,* 3H), -1.63 (s, arene-*H,* 1H), -2.75 (s, arene-*H,* 1H), -3.11 (s, Me*H,* 3H), -3.16 (s, arene-*H,* 1H), -3.38 (s, Me*H,* 3H), -4.44 (s, Me*H,* 3H), -5.31 (s, ^{t}Bu*H,* 9H), -6.60 (s, ^{t}Bu*H,* 9H), -10.26 (s, arene-*H,* 1H), -15.66 (s, arene-*H,* 1H), -16.60 (s, arene-*H,* 1H), -19.59 (s, arene-*H,* 1H), -30.23 (s, arene-*H,* 1H), -30.44 (s, Ar$_3$*H,* 2H), -34.59 (s, Ar$_3$*H,* 2H).

FTIR (cm^{-1}): 3382 [N-H stretch].

Raman spectroscopy (cm^{-1}): 1138 [N–N stretch]. (powder in glass capillary, wall thickness 120 μm, 785 nm laser, 5 % power, at which no sample decomposition was observed).

Elemental Analysis: C 57.76 %, H 5.78 %, N 1.30 % calculated. C 57.81 %, H 5.86 %, N 1.26 % found.

HRMS-APPI (*m/z*): 2160.89216 calculated for $C_{104}H_{122}K_4N_2O_8U_2$. 2160.86246 found.

5.3.19 Reduction of [{U(*m*TP^{m})}$_2$], 3(*m*TP^{m}), under $^{15}N_2$ to afford [K$_4${U(*m'*TP^{m})(^{15}NH)}$_2$], $^{15}N_2$-4(*m'*TP^{m})

Toluene (10 cm^{-3}) was freeze-pump-thaw degassed and transferred by vacuum transfer onto a powdered mixture of **3(*m*TP^{m})** (300 mg, 0.152 mmol) and KC_8 (82 mg, 0.607 mmol) containing a stirrer bar. The headspace above the frozen mixture was then charged with an atmosphere of $^{15}N_2$ and the mixture allowed to warm to room temperature over 16 h with stirring. Filtration and removal of volatiles from the filtrate under reduced pressure afforded **K$_4$[U$_2$(μ-^{15}N$_2$H$_2$)(*m'*TP^{m})$_2$], ^{15}N-4(*m'*TP^{m})** as an orange powder following washing several times with hexanes.

Yield = 200 mg, 61 %.

Raman spectroscopy (powder in glass capillary, wall thickness 120 μm, 785 nm laser, 5 % power, at which no sample decomposition was observed). 1097 cm^{-1} (N−N stretch); expected value (from reduced mass calculations *cf.* ^{14}NN stretch) = 1092 cm^{-1}.

{^{1}H}^{15}N NMR (51 MHz, Toluene-d_8) δ -4059.58 (s, *N*)

5.3.20 Reduction of [{U(*m*TP^{t})}$_2$], 3(*m*TP^{t}), under dinitrogen to afford [K$_4${U(*m'*TP^{t})(NH)}$_2$], 4(*m'*TP^{t})

Under an atmosphere of N_2, at – 30 °C, a suspension of KC_8 (30 mg, 0.224 mmol) was added dropwise over a few minutes to a brown toluene solution of **[{U(*m*TP^{t})}$_2$]** (130 mg, 0.0560 mmol). The reaction mixture was allowed to warm to RT over 16 h with stirring. The red solution was isolated by filtration from the dark grey solids and volatiles removed under reduced pressure to yield a dark orange powder of **[K$_4${U(*m'*TP^{t})(NH)}$_2$],** which was washed in hexane.

Yield 51 % (71 mg, 0.0280 mmol).

^{1}H NMR (500 MHz, Benzene-d_6) δ 59.03 (s, Ar$_3$*H,* 1H), 52.01 (s, Ar$_3$*H,* 1H), 31.12 (s, arene-*H,* 1H), 25.11 (s, arene-*H,* 1H), 17.95 (s, ^{t}Bu*H,* 9H), 15.73 (s, arene-*H,* 1H), 13.36 (s, arene-*H,* 1H), 10.93 (s, ^{t}Bu*H,* 9H), 10.48 (s, ^{t}Bu*H,* 9H), 9.99 (s, ^{t}Bu*H,* 9H), 7.75 (s, arene-*H,* 1H), 6.68 (s, arene-*H,* 1H), 6.37 (s, ^{t}Bu*H,* 9H), 2.79 (s, arene-*H,* 1H), 2.43 (s, arene-*H,* 1H), 1.63 (s, ^{t}Bu*H,* 9H), 1.52 (s, arene-*H,* 1H), 1.40 (s, arene-*H,* 1H), 1.07 (s, arene-*H,* 1H), 0.93 (s, arene-*H,* 1H), 0.59 (s, ^{t}Bu*H,* 9H), 0.37 (s, ^{t}Bu*H,* 9H), -0.08 (s, ^{t}Bu*H,* 9H), -2.06 (s, ^{t}Bu*H,* 9H), -2.76 (s, ^{t}Bu*H,* 9H), -2.97 (s, arene-*H,* 1H), -3.60 (s, arene-*H,* 1H), -3.95 (s, arene-*H,* 1H), -4.60 (s, arene-*H,* 1H), -5.45 (s, ^{t}Bu*H,* 9H), -6.34 (s, 1H, ArH), -7.05 (s, 1H, ArH), -7.37 (s, ^{t}Bu*H,* 9H), -8.28 (s, ^{t}Bu*H,* 9H), -8.79 (s, arene-*H,* 1H), -10.01 (s, ^{t}Bu*H,* 9H), -13.46 (s, arene-*H,* 1H), -14.26 (s, arene-*H,* 1H), -16.60 (s, arene-*H,* 1H), -18.34 (s, Ar$_3$*H,* 1H), -22.86 (s, Ar$_3$*H,* 1H), -24.56 (s, ^{t}Bu*H,* 9H).

Elemental Analysis: C 61.51 %, H 6.94 %, N 1.12 % calculated. C 61.38 %, H 6.85 %, N 0.95 % found.

HRMS-APPI (*m/z*): [M–2K–Me+3H]$^{+}$ 2408.39006 found; 2408.34317 calculated.

5.3.21 Reaction to target reduction of [{U(*m*TP^{m})}$_2$], 3(*m*TP^{m}) under N_2 in the presence of crown ether 18-crown-6

Under an atmosphere of N_2, at – 30 °C, a brown toluene solution of **3(*m*TP^m)** (76.7 mg, 0.0388 mmol), and 18-crown-6 (41.0 mg, 0.155 mmol) were slowly added to KC_8 (21.0 mg, 0.155 mmol) suspended in toluene. The reaction mixture was allowed to warm to RT over 16 h with stirring. The resulting pale red suspension was filtered to isolate the dark red insoluble product and graphite from the yellow solution. The lack of solubility of the product in aromatic and aliphatic solvents precluded further purification and characterisation, but further reactions with electrophiles did not yield nitrogen-containing products.

5.3.22 Quenching of [K$_4${U(*m*'TP)(NH)}$_2$], 4(*m*'TP^m), with [PyH]Cl to afford NH_4Cl

General procedure from [K$_4${U(*m*'TP)(NH)}$_2$]: A dark red solution of **[K$_4${U(*m*'TP)(NH)}$_2$]** was stirred for 1 hour with excess pyridinium chloride [PyH]Cl (*ca.* 20 equivalents) to afford a colourless suspension. The colourless solid formed was isolated by filtration and washed with thf to remove unreacted [PyH]Cl, dried *in vacuo* and characterised as NH_4Cl.

[K$_4${U(*m*'TP^m)(NH)}$_2$], 4(*m*'TP^m) (87.4 mg, 0.044 mmol). NH_4Cl yield 27% (avg.)

[K$_4${U(*m*'TP^t)(NH)}$_2$], 4(*m*'TP^t) (120 mg, 0.0480 mmol). NH_4Cl yield 52 %.

^{1}H NMR (500 MHz, dmso-d$_6$) δ 7.42 (t, $^1J_{NH}$ = 51 Hz, N*H*, 4H).

NMR spectra of the solutions formed after quenching show no **[{U(*m*TP^m}$_2$]**, **3(*m*TP^m)**, is reformed, and the formation of a diamagnetic set of ligand resonances which are assigned as **H$_4$(*m*TP^m).**

[PyD]Cl yields **D$_4$(*m*^{D}TP^m):** ^{1}H NMR (500 MHz, Toluene-d$_8$) δ 6.96-7.02 (m, aromatic-*H*, 8H), 6.92 (s, aryloxide-*H,* 4H), 5.74 (s, Ar$_3$*H*, 1.5H), 2.07 (s, Me*H*, 12H), 1.45 (s, ^{t}Bu*H*, 36H).

5.3.23 Synthesis of Et_3NDCl

Et_3N (1.50 ml, 10.76 mmol) was added dropwise to a 20 wt % solution of DCl in D_2O at 0 °C (10.76 mmol) and stirred for 5 minutes. The resulting colourless solution of Et_3NDCl was reacted in situ.

^{1}H NMR (400 MHz, Deuterium oxide) δ 3.14 (q, *J* = 7.3 Hz, C*H*$_2$, 6H), 1.24 (t, *J* = 7.4 Hz, C*H*$_3$, 9H).

^{2}H NMR (77 MHz, Water) δ 2.26 (s, 1H, N-^{2}*H*).

5.3.24 Synthesis of Et_3NDBPh_4

$NaBPh_4$ (3.68 g, 10.76 mmol) was dissolved in acetone and added dropwise to the above solution of Et_3NDCl in D_2O at 0 °C. $Et_3N\mathbf{D}BPh_4$ was formed immediately as a colourless precipitate. The solid was isolated by filtration and recrystalised from a mixture of water: acetone (1:1.5) before being dried under reduced pressure.

Yield= 3.60 g, 79 %.

^{1}H NMR (500 MHz, Acetone-d_6) δ 7.40 – 7.24 (m, Ph*H*, 8H), 6.91 (t, *J* = 7.4 Hz, Ph*H*, 8H), 6.86 – 6.59 (m, Ph*H*, 4H), 3.41 (q, *J* = 7.3 Hz, CH_2, 6H), 1.39 (t, *J* = 7.3 Hz, CH_3, 9H).

^{2}H NMR (77 MHz, Acetone) δ 4.52 (s, N-^{2}*H,* 1H).

5.3.25 Quenching of $[K_4\{U(m'TP^m)(NH)\}_2]$, 4(*m'*TP^m), with $[HNEt_3][BPh_4]$ to afford NH_3 and regenerate 3(*m*TP^m), $[U(mTP^m)]_2$

To a stirred dark orange toluene solution of **4(*m'*TP^m)** (168 mg, 0.078 mmol) was added an excess of $[HNEt_3][BPh_4]$ (10 equiv., 0.34 g, 0.78 mmol) at −30 °C . The reaction mixture turned green slowly (30 mins) and was allowed to warm to room temperature with stirring. Filtration to remove excess $[HNEt_3][BPh_4]$ afforded a green solution which was identified by ^{1}H NMR spectroscopy as **3(*m*TP)** in quantitative yield, and dissolved NH_3 in 64 % yield (*vide infra*), based on U. The identity of the removed solid was confirmed as unreacted $[HNEt_3][BPh_4]$ by NMR spectroscopy.

Et_3NDBPh_4: $NH\mathbf{D}_2$ (27 % yield).

To accurately determine NH_3 yield:

To an ampoule containing a dark orange toluene solution of **4(*m'*TP^m)** (232 mg, 0.108 mmol) was added an excess of $[HNEt_3][BPh_4]$ (10 equiv., 0.45 g, 1.08 mmol) at 0 °C. The ampoule was sealed and allowed to warm to room temperature over 1 hr with stirring. Volatiles from the reaction were vacuum transferred onto a degassed solution of 2 M HCl in ethanol in a second ampoule. Removal of all volatiles from this second ampoule under reduced pressure afforded solid NH_4Cl with overall yield 66 % per U. The solid NH_4Cl was then dissolved in dmso and an aliquot was analysed by ^{1}H NMR spectroscopy and calibrated against an internal standard of dimethylsulfone. The yield from this method was calculated as 62 % per U. An average yield of 64 % is thus reported.

To confirm the origin of one NH as from **(*m*TP^{m})** ligand:

The reaction was repeated using [**D**NEt$_3$][BPh$_4$], and ^{2}D NMR spectroscopy confirmed the product is deuterated ammonia NHD$_2$. Accurate yields could not be determined.

5.3.26 Quenching of [K$_4${U(*m*'TP)(NH)}$_2$], 4(*m*'TP^{m}), with DHA to afford NH$_3$

Table 5-3 Amounts and yields for quenching reactions of **4(*m*'TP^{m})**, with DHA

Entry	Compound	Solvent	DHA equivalents	Major products
1	**3(*m*TP^{m})**	benzene	100	NH$_3$, 24%
2	**3(*m*TP^{m})**	toluene	100	NH$_3$, 25%
3	**3(*m*TP^{m})**	benzene	100	NH$_3$, 47%

To a magnetically stirred, dark green, benzene solution of **3(*m*TP^{m})** (−30 °C) was added an excess of reductant, and solid DHA in a teflon-valved ampoule. The mixture was allowed to stir for several hours, then volatiles were collected by vacuum transfer onto a degassed solution of 1.25 M HCl in ethanol. Removal of all volatiles from these under reduced pressure afforded solid NH$_4$Cl.

^{1}H NMR (500 MHz, DMSO-d$_6$) δ 7.42 (t, $^1J_{NH}$ = 51 Hz, N*H*, 4H).

5.3.27 Quenching of [K$_4${U(*m*'TP)(NH)}$_2$], 4(*m*'TP^{m}), with H$_2$ to afford NH$_3$

To a magnetically stirred, dark green benzene solution of **3(*m*TP^{m})** (50 mg, 0.025 mmol) cooled to −30 °C inside a 100 mL ampoule, an excess of K metal was added and the reaction mixture was degassed inside a sealed ampoule. 5 % H$_2$ in N$_2$ was stored in an ampoule over activated molecular sieves for 2 days, before it was used to refill the ampoule containing the frozen reaction mixture (0.21 mmol H$_2$). The mixture was allowed to warm to room temperature with stirring. The volatiles from the reaction were vacuum transferred onto a degassed solution of 1.25 M HCl in ethanol in a second ampoule. Removal of all volatiles from this second ampoule under reduced pressure afforded solid NH$_4$Cl.

Yield = 49 %

^{1}H NMR (500 MHz, dmso-d$_6$) δ 7.42 (t, $^1J_{NH}$ = 51 Hz, N*H*, 4H).

5.3.28 Alkylation of [K_4{U(*m*'TP^m)(NH)}$_2$], 4(*m*'TP^m), to afford [K_2{U(*m*$^{tBu}TP^m$)(NH)}$_2$], 5(*m*TP^m)

To a stirred dark orange toluene solution of **[K_4{U(*m*'TP^m)(NH)}$_2$]** (86.22 mg, 0.040 mmol) was added 2-Iodo-2-methylpropane, ^{t}BuI (6 equiv., 28 µL, 44 mg, 0.24 mmol) at −30 °C. The reaction mixture was allowed to warm to room temperature overnight. The colourless KI by-product was removed by filtration to afford a dark brown solution. Toluene was removed under reduced pressure to afford **5(*m*TP^m)** as a dark orange solid.

Yield = 63 %.

^{1}H NMR (500 MHz, Toluene-d_8) δ 30.23 (s, arene-*H,* 1H), 28.49 (s, arene-*H,* 1H), 21.86 (s, ^{t}Bu*H*, 9H), 21.01 (s, arene-*H,* 1H), 19.39 (s, ^{t}Bu*H*, 9H), 13.79 (s, Me*H*, 3H), 9.73 (s, Me*H*, 3H), 7.33-7.24 (m, arene-*H,* 2H), 5.23 (s, Me*H*, 3H), 5.03 (s, arene-*H,* 1H), 4.85 – 4.79 (m, arene-*H,* 1H), 4.71 (s, ^{t}Bu*H*, 9H), 4.55 (s, arene-*H,* 1H), 4.27 (s, arene-*H,* 1H), 4.04 (s, arene-*H,* 1H), 3.55 (s, arene-*H,* 1H), 3.32 (s, arene-*H,* 1H), 3.24-3.16 (m, arene-*H,* 1H), 2.66 (s, arene-*H,* 1H), 2.47 (s, arene-*H,* 1H), 1.45 (s, Me*H*, 3H), 0.89 (s, Me*H*, 3H), 0.87 (s, ^{t}Bu*H*, 9H), 0.86 (s, ^{t}Bu*H*, 9H), 0.84 (s, ^{t}Bu*H*, 9H), 0.24 (s, Me*H*, 3H), 0.08 (s, ^{t}Bu*H*, 18H), -0.80 (s, Me*H*, 3H), -1.05 (s, arene-*H,* 1H), -1.19 (s, arene-*H,* 1H), -1.42 (s, Me*H*, 3H), -1.65 - -1.75 (m, arene-*H,* 2H), -1.88 (s, arene-*H,* 1H), -2.21 (s, arene-*H,* 1H), -6.20 (s, arene-*H,* 1H), -6.70 (s, arene-*H,* 1H), -11.91 (s, arene-*H,* 1H), -21.99 (s, Ar_3*H*, 1H), -24.33 (s, ^{t}Bu*H*, 9H), -37.97 – -41.01 (m, ^{t}Bu*H*, 9H), -61.11 (s, Ar_3*H*, 1H).

5.3.29 Quenching of [K_2{U(*m*$^{tBu}TP^m$)(NH)}$_2$], 5(*m*TP^m) to afford H_4(*m*$^{tBu}TP^m$)

Excess (0.1 ml) D_2O was added to a solution of **5(*m*TP^m)** (93.5 mg, 0.040 mmol) in toluene and heated to 50 °C for 30 minutes. A colour change from dark brown to colourless was observed. All volatiles were removed under reduced pressure to provide a grey powder. ^{1}H NMR spectroscopy of a benzene-d_6 solution of the product at 298 K indicated alkylation of the ligand to yield, **H_4(*m*$^{tBu}TP^m$)**.

Yields were not recorded.

^{1}H NMR (500 MHz, Benzene-d_6) δ 7.09 (s, aryloxide-*H*, 4H), 7.07 – 6.95 (m, aromatic-*H*, 4H), 6.68 (s, aryloxide-*H*, 4H), 5.49 (s, Ar_3*H*, 1H), 2.05 (s, Me*H*, 12H), 1.43 (s, ^{t}Bu*H*, 45H).

5.3.30 Reaction to target cyanate complex *via* CO addition to 4(*m'*TP^m), [K$_4${U(*m'*TP^m)(NH)}$_2$]

A solution of **[K$_4${U(*m'*TP^m)(NH)}$_2$]** (10.0 mg, 00.0046 mmol) in C_6D_6 was added to a young's tap NMR tube and degassed *via* 3 freeze-pump-thaw cycles. 1 atm of CO was added and the solution was warmed to room temperature. No colour change was observed but clean conversion to a new paramagnetic product was indicated by ^{1}H NMR spectroscopy. This product was not further characterised and accurate yields were not recorded.

^{1}H NMR (500 MHz, Benzene-d_6) δ 58.65 (s, ^{t}Bu*H*, 9H), 52.68 (s, ^{t}Bu*H*, 9H), 47.18 (s, arene-*H,* 1H), 39.73 (s, arene-*H,* 1H), 22.99 (s, arene-*H,* 1H), 19.85 (s, Me*H*, 3H), 16.76 (s, Me*H*, 3H), 13.03 (s, Me*H*, 3H), 11.97 (s, ^{t}Bu*H*, 9H), -2.96 (s, ^{t}Bu*H*, 9H), -4.46 (s, Me*H*, 3H), -5.29 (m, Me*H*, 6H), -7.12 (s, ^{t}Bu*H*, 9H), -8.82 (s, Me*H*, 3H), -12.88 (s, arene-*H,* 1H), -13.95 (s, ^{t}Bu*H*, 9H), -16.30 (s, Me*H*, 3H), -17.31 (s, ^{t}Bu*H*, 9H), -21.24 (s, ^{t}Bu*H*, 9H), -36.23 (s, arene-*H,* 1H).

5.3.31 Stoichiometric silylation of 4(*m'*TP^m), [K$_4${U(*m'*TP^m)(NH)}$_2$]

To a stirred dark orange toluene solution of **4(*m'*TP^m)**, (122 mg, 0.051 mmol) was added $SiMe_3OTf$ (4 equiv., 36.5 µL, 44.9 mg, 0.20 mmol) at −30 °C. The reaction mixture was allowed to warm to room temperature overnight. The volatiles (products, by-products and solvent) were isolated by vacuum transfer. Yields were measured by integration of ^{1}H NMR spectra against an added standard of tri-*tert*-butylbenzene.

^{1}H NMR (500 MHz, Toluene-d_8) δ 0.06 (s, HN(Si*Me$_3$*)$_2$, 18H), 0.1 (s, (Si*Me$_3$*)$_2$O, 18H)

^{29}Si NMR (99 MHz, Toluene-d_8) δ 2.01 (s, HN(*Si*Me$_3$)$_2$), 7.27 (s, (*Si*Me$_3$)$_2$O).

This reaction (or equivalent using **3(*m*TP^m)** and a reductant) was repeated using the conditions shown in Table 5-4.

Table 5-4 Amounts and yields for stoichiometric silylations

Entry	Compound	Reductant (equivs)	Electrophile (equivs)	Major products (yield)
1	**4(*m'*TP^m)**		$SiMe_3I$ (6)	$SiMe_3I$
2	**4(*m'*TP^m)**		$SiMe_3Cl$ (6)	$HN(SiMe_3)_2$

3	**3(*m*TP^m)**	KC_8 (40)	$SiMe_3Cl$ (40)	$(SiMe_3)_2$
4	**3(*m*TP^m)**	K (xs)	$SiMe_3Cl$ (40)	$HN(SiMe_3)_2$ (15 %) $(SiMe_3)_2$
5	**3(*m*TP^m)**	K (xs)	$SiMe_3I$ (40)	$HN(SiMe_3)_2$ (51 %) $(SiMe_3)_2$
6	**4(*m'*TP^m)**		Si Me_3OTf (6)	$HN(SiMe_3)_2$ (33 %) $(SiMe_3)_2O$ (11 %)
Control 1		KC_8 (40)	$SiMe_3I$ (40)	$(SiMe_3)_2$

5.3.32 Reactions to target catalytic silylation of 4(*m'*TP^m), [K_4{U(*m'*TP^m)(NH)}$_2$]

See Table A-3 (Appendix 2) for amounts and yields.

A green solution of **3(*m*TP^m)** was cooled to −30 °C. An excess of reductant was added, and the electrophile was added dropwise. An internal standard of tri-*tert*-butylbenzene was added to allow yields to be determined by ^{1}H NMR spectroscopy after several days (according to Table A-3). The resting state of the catalyst was identified as **3(*m*TP^m)** by ^{1}H NMR spectroscopy.

5.3.33 Synthesis of 6(*m'*TP^m), [K(thf)$_6$][U$_2$(*m'*TP^m)$_2$K(thf)$_2$]

To a stirred, colourless toluene solution of **[{U(*m*TP)}$_2$]**, **3(*m*TP^m)** (50.0 mg, 0.025 mmol, 3 cm^3) was added a red solution of KBn in toluene (8.14 mg, 0.063 mmol, 3 mL) dropwise at −30 °C. The resulting orange suspension was allowed to warm to room temperature over 16 h to afford a red suspension. The product was isolated as a dark red solid insoluble in arene solvents. The solid was dissolved in thf from which dark red crystals of **[K(thf)$_6$][U$_2$(*m*TP^m)$_2$K(thf)$_2$]** could be obtained by slow evaporation.

Yield = 14.6 mg, 0.0055 mmol, 22 %

^{1}H NMR (500 MHz, thf-d_8) δ 66.58 (s, aryloxide-*H,* 2H,), 57.34 (s, aryloxide-*H,* 2H), 47.08 (s, aryloxide-*H,* 2H), 27.47 (s, aryloxide-*H,* 2H), 27.31 (d, *J* = 9.6 Hz, aryloxide-*H,* 2H), 26.97 (s, aryloxide-*H,* 2H), 23.56 (s, aryloxide-*H,* 2H), 21.82 (s, aryloxide-*H,* 2H), 19.37 (t, *J* = 9.6 Hz, aryloxide-*H,* 2H), 15.54 (m, Me*H,* 6H), 15.25 (dd, *J* = 11.3, 2.5 Hz, Me*H,* 6H), 6.87 (s, ^{t}Bu*H,* 18H), 4.01 (s, aryloxide-*H,* 2H), -1.93 (s, ^{t}Bu*H,* 18H), -6.32 (s, Me*H,* 12H), -9.92 (s, aryloxide-*H,*

2H), -11.77 (s, ^{t}Bu*H,* 18H), -14.41 (s, aryloxide-*H,* 2H), -23.67 (s, ^{t}Bu*H,* 18H), -27.69 (s, Ar_3H, 2H).

Elemental Analysis: C 62.18 %, H 6.98 % calculated. C 61.90 %, H 6.98 % found.

5.3.34 Synthesis of 7(*m*TP^{m}), [(U(*m*TP^{m})$_2$(NaOSiMe$_3$)$_3$]

A solution of $NaOSiMe_3$ in benzene (7.01 mg, 0.063 mmol) was added to a frozen solution of **[{U(*m*TP)}$_2$]**, **3(*m*TP^{m})** in benzene (50 mg, 0.025 mmol). The reaction mixture was allowed to warm slowly to room temperature, and stirred over 2 days, giving a yellow solution. The solution was concentrated and then left to stand. A small number of single crystals of **[(U(*m*TP^{m})$_2$(NaOSiMe$_3$)$_3$]** were recovered from the solution after several weeks but accurate yields were not recorded.

^{1}H NMR (500 MHz, Benzene-d_6) δ 46.53 (s, aryloxide-*H,* 8H), 44.17 (s, aryloxide-*H,* 8H), 40.57 (s, arene-*H,* 1H), 40.29 (s, arene-*H,* 1H), 24.11 (s, arene-*H,* 1H), 18.95 (s, arene-*H,* 1H), 17.52 (s, Me*H,* 3H), 16.16 (s, Me*H,* 3H), 13.93 (s, ^{t}Bu*H,* 9H), 12.92 (s, ^{t}Bu*H,* 9H), 10.34 (s, ^{t}Bu*H,* 9H), 5.48 (s, ^{t}Bu*H,* 9H), 2.96 (s, Me*H,* 3H), 2.72 – 2.50 (m, arene-*H*, 4H), 2.12 (s, Me*H,* 3H), 2.00 (s, Me*H,* 3H), 0.91 (s, Me*H,* 3H), 0.47 (s, ^{t}Bu*H,* 9H), 0.29 (s, $Ar_3H,$ 1H), -1.64 (s, ^{t}Bu*H,* 9H), -2.19 (s, Me*H,* 3H), -5.00 (s, Me*H,* 3H), -5.75 (s, $Ar_3H,$ 1H), -6.95 (s, $Ar_3H,$ 1H), -9.83 (s, ^{t}Bu*H,* 9H), -9.93 (s, ^{t}Bu*H,* 9H), -12.97 (s, Ar_3H, 1H), -23.35 (s, $SiMe_3H,$ 9H), -30.05 (s, $SiMe_3H,$ 9H), -38.18 (s, $SiMe_3H,$ 9H).

Me_3Si protons assigned by virtue of lack of coupling to any carbon is HSCQ and HMBC experiments.

^{29}Si NMR (99 MHz, Benzene-d_6) δ 75.26 (s, *Si*Me_3), 45.05 (s, *Si*Me_3).

5.4 Synthetic procedures for Chapter 3

5.4.1 Reaction to target synthesis of [U$_2$I$_2$(*m*TP^{m})(thf)$_4$] from UI$_3$

A Schlenk flask was charged with **H$_4$(*m*TP^{m})** (1.00 g, 1.32 mmol) and KN(SiMe$_3$)$_2$ (1.06 g, 5.30 mmol) and equipped with a stirrer bar. Thf was added and the yellow solution was stirred for 1 hour at RT. To this solution, [UI_3(dioxane)$_{1.5}$] (1.638 g, 2.65 mmol) in thf was added by cannula transfer from a separate Schlenk flask. The resulting dark blue solution was stirred at RT for 24 hours, yielding a pale brown suspension. The colourless precipitate was removed

by filtration providing a brown solution. The thf was removed under reduced pressure to yield a brown solid.

^{1}H NMR and mass spectrometry data were not consistent with the target compound but suggested some formation of **[U_2I_4(*m*TP^m)(thf)$_4$], 8(*m*TP^m)**.

5.4.2 Synthesis of 8(*m*TP^m), [U_2I_4(*m*TP^m)(thf)$_4$]

A Schlenk flask was charged with **H_4(*m*TP^m)** (1.00 g, 1.32 mmol) and [KN($SiMe_3$)$_2$] (1.06 g, 5.30 mmol) and equipped with a stirrer bar. Thf was added and the yellow solution was stirred for 1 hour at RT. To this solution, [UI_4(dioxane)$_2$] (2.44 g, 2.65 mmol) in thf was added by cannula transfer from a separate Schlenk flask. The resulting dark green solution was stirred at RT for 24 hours, yielding a pale green suspension. Colourless precipitated KI was removed by filtration providing a green solution from which the solvent was removed under reduced pressure, yielding **[U_2I_4(*m*TP^m)(thf)$_4$]** as a light green solid.

Yield = 1.87 g, 82 %.

Green crystals suitable for single crystal XRD were grown from slow evaporation of concentrated benzene or thf solutions at room temperature.

^{1}H NMR (500 MHz, THF-d_8) δ13.94 (s, aryloxide-*H*, 4H), 7.53 (s, aryloxide-*H*, 4H), 7.18 (s, ^{t}Bu*H*, 36H), 6.92 (s, aromatic-*H*, 1H), 5.93 (s, Me*H*, 12H), 5.60 (s, aromatic-*H*, 1H), 2.20 (s, aromatic-*H*, 2H), 0.90 (s, Ar_3*H*, 2H).

Elemental Analysis: C 40.37 %, H 4.68 % calculated. C 40.27 %, 4.55 % found.

5.4.3 Synthesis of 8(*m*TP^t), [U_2I_4(*m*TP^t)(thf)$_4$]

A Schlenk flask was charged with **H_4(*m*TP^t)** (1.00 g, 1.08 mmol) and KN($SiMe_3$)$_2$ (0.86 g, 4.33 mmol), a stirrer bar and thf (15 cm^3). The resulting pale-yellow suspension was stirred at RT for 1 hour. A solution of UI_4(dioxane)$_2$ in thf (20 cm^3) was added, yielding a red suspension which was stirred at RT for 16 h. The resulting green suspension was filtered to remove colourless KI, providing a dark green solution. The solvent was removed under reduced pressure to give a bright green solid, which was recrystallised from slow evaporation from concentrated toluene solution.

Yield = 1.92 g, 81%

^{1}H NMR (500 MHz, 330 K, thf-d_8) δ 13.62 (s, aryloxide-*H,* 4H), 10.52 (s, aryloxide-*H,* 4H), 6.93 (s, ^{t}Bu*H,* 36H), 3.82 (s, aromatic-*H,* 1H), 3.51 (s, aromatic-*H,* 2H), 2.66 (s, ^{t}Bu*H,* 36H,), 1.86 (s, Ar_3*H*, 2H), 0.36 (s, aromatic-*H,* 1H,).

Elemental Analysis: C 40.39 %, H 4.56 % calculated. C 40.51 %, H 4.61 % found.

5.4.4 Synthesis of 9(*m*TP^m), [U_2Cl_4(*m*TP^m)(thf)$_4$]

A Schlenk flask was charged with **H_4(*m*TP^m)** (300 mg, 0.397 mmol) and [KN($SiMe_3$)$_2$] (317 mg, 1.589 mmol), a stirrer bar and thf (20 cm^3). The resulting pale yellow solution was stirred at RT for 1 hour. A pale green solution of UCl_4 (378 mg, 0.795 mmol) in thf (20 cm^3) was added, yielding a pale brown solution which was stirred at RT for 16 h. Finely precipitated KCl was removed *via* filtration and the thf was removed under reduced pressure to yield a light brown solid.

Yield = 0.520 mg, 96 %.

^{1}H NMR (500 MHz, thf-d_8) δ13.91 (s, aryloxide-*H*, 4H), 10.78 (s, aryloxide-*H*, 4H), 9.07 (s, aromatic-*H*, 1H), 6.73 (s, ^{t}Bu*H*, 36H), 5.33 (s, Me*H*, 12H), 2.15 (s, aromatic-*H*, 2H), 5.60 (s, aromatic-*H*, 1H), 2.20 (s, aromatic-*H*, 2H), 0.44 (s, aromatic-*H*, 1H), 0.13 (s, Ar_3*H*, 2H).

5.4.5 Synthesis of 9(*m*TP^t), [U_2Cl_4(*m*TP^t)(thf)$_4$]

A Schlenk flask was charged with **H_4(*m*TP^t)** (400 mg, 0.433 mmol) and [KN($SiMe_3$)$_2$] (346 mg, 1.732 mmol), a stirrer bar and thf (20 cm^3). The resulting pale-yellow solution was stirred at RT for 1 hour. A pale green solution of UCl_4 (329 mg, 0.866 mmol) in thf (20 cm^3) was added, yielding a pale brown solution which was stirred at RT for 16 h. KCl was removed as a colourless precipitate *via* filtration and the thf was removed under reduced pressure to yield a light brown solid.

Yield = 0.66 g, 79 %.

^{1}H NMR (500 MHz, thf-d_8) δ 13.33 (s, aryloxide-*H*, 4H), 9.76 (s, aryloxide-*H*, 4H), 5.64 (s, ^{t}Bu*H*, 36H), 3.58 (s, ^{t}Bu*H*, 36H), 2.61 (s, aromatic-*H*, 1H), 2.30 (s, aromatic-*H*, 2H), 1.54 (s, Ar_3*H*, 2H), 0.43 (s, aromatic-*H*, 1H)

5.4.6 Synthesis of 10(*m*TP^m), [(UI{OTtbp})$_2$(*m*TP^m)]

A Schlenk flask was charged with KOTtbp (297 mg, 0.988 mmol) and **[U_2I_4(*m*TP^m)(thf)$_4$]**, **8(*m*TP^m)**, (1.00 g, 0.49 mmol) and equipped with a stirrer bar. Toluene (40 cm^3) was added and the resulting green/brown solution stirred for 16 hours. Light green KI was precipitated as a byproduct, this was removed *via* filtration. The toluene was then removed under reduced pressure to yield the product as a dark green solid.

Yield = 0.78 g, 79 %.

^{1}H NMR (600 MHz, Benzene-d_6) δ13.69 (s, aryloxide-*H*, 4H), 13.27 (s, aromatic-*H*, 1H), 6.98 (s, aromatic-*H*, 1H), 4.79 (s, aromatic-*H*, 2H), 3.81 (s, aromatic-*H*, 2H), 3.45 (s, aryloxide-*H*, 4H), 1.38 (s, ^{t}Bu*H*, 36H), 1.32 (s, ^{t}Bu*H*, 18H), 0.06 (s, ^{t}Bu*H*, 36H), 0.02 (s, Me*H*, 12H), -0.81 (s, Ar_3*H*, 2H).

Elemental analysis: C 52.75 %, H 6.04 % calculated. C 52.83 %, 6.12 % found.

5.4.7 Synthesis of 11, potassium[1,1'-biphenyl]-4,4'-bis(olate)

1'-biphenyl-4,4'-diol (1.00g, 5.37 mmol) and KOH (0.60 g, 10.7 mmol) were added to a round bottomed flask equipped with a stirrer bar. Addition of MeOH (40 cm^3) produced a light green solution that after stirring for 2 hours, turned yellow. The solvent was removed under reduced pressure, providing the product as a colourless solid which was washed in hexane (3 x 30 cm^3).

Yield = 1.08 g, 77 %.

^{1}H NMR (500 MHz, Methanol-d_4) δ 7.12 (d, aromatic-*H,* 4H), 6.58 (d, aromatic-*H,* 4H).

5.4.8 Synthesis of 13(*m*TP^m), [U_2(*m*TP^m)(OTtbp)$_2$]

[(UI{OTtbp})$_2$(*m*TP^m)], **10(*m*TP^m)**, (100 mg, 0.0499 mmol) was dissolved in 1,4-dioxane and slowly added to a vial containing KC_8 (13.0 mg, 0.10 mmol) with stirring. There was a gradual colour change from dark green to brown and the reaction mixture was allowed to stir at RT overnight. The suspension was filtered to remove dark grey graphite. Solvent was removed under reduced pressure to yield **[U_2(*m*TP^m)(OTtbp)$_2$]** as a brown solid.

Yield = 63.56 mg, 62 %

^{1}H NMR (500 MHz, Benzene-d_6) δ 13.15 (s, aryloxide-*H*, 4H), 11.81 (s, aromatic-*H*, 2H), 8.66 (d, $^3J_{HH}$ = 11.2 Hz, aryloxide-*H*, 4H), 5.82 (s, aromatic-*H*, 2H), 5.39 (s, aromatic-*H*, 1H), 4.72 –

4.60 (m, aromatic-*H*, 1H), 3.68 (s, Ar_3H, 2H), 2.11 (s, ^{t}Bu*H*, 36H), 1.23 (s, ^{t}Bu*H*, 18H), 0.10 (s, Me*H*, 12H), -0.01 (s, ^{t}Bu*H*, 36H).

5.4.9 Synthesis of 14(*m*TP^m), [K$_4$][U$_2$I$_2$(*m*TP^m)(N$_2$)(thf)$_4$]

[U$_2$I$_4$(*m*TP^m)(thf)$_4$] (100 mg, 0.0494 mmol) was dissolved in toluene and cooled to −30 °C. The resulting bright green solution was then added dropwise to solid KC_8 (26.7 mg, 0.1977 mmol) and allowed to warm to room temperature overnight with stirring. Colourless KI and dark grey solid C_8 were removed from the resulting suspension by filtration to yield a dark brown solution. Toluene was removed under reduced pressure to yield crude **[K$_4$][U$_2$I$_2$(*m*TP^m)(N$_2$)(thf)$_4$]**. The solid was purified by stirring for 1 hour in hexanes, the dark brown solid was then isolated by filtration and dried under reduced pressure.

Yield = 25.8 mg, 27 %.

^{1}H NMR (500 MHz, Benzene-d_6) δ 42.17 (s, aromatic-*H*, 1H), 28.91 (s, aromatic-*H*, 2H), 28.84 (s, aryloxide-*H*, 4H), 26.80 (s, aromatic-*H*, 1H), 17.11 (s, ^{t}Bu*H*, 16H), 14.98 (s, Me*H*, 6H), -4.17 (s, aryloxide-*H*, 4H), -8.79 (s, Ar_3H, 2H), -9.22 (s, Me*H*, 6H), -13.55 (s, ^{t}Bu*H*, 16H).

Elemental analysis: C 41.80 %, H 4.85 %, N 1.43 % calculated. C 42.1 %, H 4.34 %, N 0.93 % found.

5.4.10 Quenching of 14(*m*TP^m), [K$_4$][U$_2$I$_2$(*m*TP^m)(N$_2$)(thf)$_4$] to yield NH$_4$Cl

[K$_4$][U$_2$I$_2$(*m*TP^m)(N$_2$)(thf)$_4$] (48.29 mg, 0.0247 mmol) was dissolved in benzene and added to a suspension of [PyH]Cl (57.1 mg, 0.49 mmol) in benzene. The suspension was stirred for 30 minutes, and a colour change from dark brown to colourless was observed. The colourless solid was removed by filtration, washed with thf to remove excess [PyH]Cl and the remaining NH_4Cl was dissolved in d_6-dmso. $(CH_3)_2SO$ (4.2 mg, 0.0446 mmol) was added as an internal standard.

Yield of NH_4Cl = 0.0084 mmol, 17 % per U.

^{1}H NMR (500 MHz, dmso-d_6) δ 7.42 (t, $^1J_{NH}$ = 51 Hz, N*H*, 4H).

To confirm that the Hs do not originate from **(*m*TP^m)** ligand:

This reaction was repeated using [PyD]Cl. **[K_4][U_2I_2(*m*TP^m)(N_2)(thf)$_4$]** was prepared in toluene-d_8 and cleanly isolated. **[K_4][U_2I_2(*m*TP^m)(N_2)(thf)$_4$]** (96.6 mg, 0.049 mmol) was dissolved in toluene-d_8 and slowly added to solid [PyH]Cl (115 mg, 0.99 mmol). The suspension was stirred at room temperature for 1 hour to provide a colourless suspension. The reaction mixture was filtered to isolate the colourless solid.

^{1}H NMR (500 MHz, dmso-d_6) no NH_4Cl resonance.

^{2}H NMR (77 MHz, dmso-d_6) δ 7.55 (br, t, N*D*, 4D).

5.4.11 Reaction to target quenching of 14(*m*TP^m), [K_4][U_2I_2(*m*TP^m)(N_2)(thf)$_4$] with $SiMe_3OTf$ to yield $N(SiMe_3)_3$

[K_4][U_2I_2(*m*TP^m)(N_2)(thf)$_4$] (25.8 mg, 0.0132 mmol) was dissolved in toluene to yield a dark brown solution and cooled to −30 °C. Me_3SiOTf (14.3 µL, 0.0792 mmol) was added. Overnight the reaction mixture was allowed to warm to room temperature with stirring. No visible colour change was observed. No paramagnetic resonances remained in ^{1}H spectra of the solution and ^{29}Si INEPT NMR showed no nitrogen containing products.

^{29}Si NMR (99 MHz, Toluene-d_8) δ 42.04 (s, Me_3*Si*OTf), 15.12, (s, IMe_2*Si*-*Si*Me_2I), 7.06 (s, Me_3*Si*-*Si*Me_3).

5.4.12 Synthesis of 14(*m*TP^t), [K_4][U_2I_2(*m*TP^t)(N_2)(thf)$_4$]

[U_2I_4(*m*TP^t)(thf)$_4$] (100 mg, 0.0456 mmol) was dissolved in toluene and cooled to −30 °C. The resulting bright green solution was then added dropwise to solid KC_8 (24.7 mg, 0.183 mmol) and allowed to warm to room temperature overnight with stirring. Colourless KI and dark grey solid C_8 were removed from the resulting suspension by filtration to yield a dark brown solution. Toluene was removed under reduced pressure to yield crude **[K_4][U_2I_2(*m*TP^t)(N_2)(thf)$_4$]**. The solid was purified by stirring for an hour in hexanes, isolated by filtration as a dark brown solid and dried under reduced pressure.

Yield = 31.6 mg, 33 %.

^{1}H NMR contained no sharp paramagnetic peaks. Evidence for the proposed structure is provided *via* quenching reactions detailed below.

5.4.13 Quenching of 14(*m*TP^t), [K$_4$][U$_2$I$_2$(*m*TP^t)(N$_2$)(thf)$_4$] to yield NH$_4$Cl

[K$_4$][U$_2$I$_2$(*m*TP^t)(N$_2$)(thf)$_4$] (24.2 mg, 0.0114 mmol) was dissolved in benzene and added to a suspension of [PyH]Cl (26.4 mg, 0.23 mmol) in benzene. The suspension was stirred for 30 minutes, and a colour change from dark brown to colourless was observed. The colourless solid was removed by filtration, washed with thf to remove excess [PyH]Cl and the remaining NH_4Cl was dissolved in d_6-dmso. $(CH_3)_2SO$ (5.5 mg, 0.0584 mmol) was added as an internal standard.

Yield of NH_4Cl = 0.0055 mmol, 24 % per U.

^{1}H NMR (500 MHz, dmso-d_6) δ 7.42 (t, $^1J_{NH}$ = 51 Hz, N*H*, 4H).

5.4.14 Reaction to target quenching of 14(*m*TP^t), [K$_4$][U$_2$I$_2$(*m*TP^t)(N$_2$)(thf)$_4$] with SiMe$_3$OTf to yield N(SiMe$_3$)$_3$

[K$_4$][U$_2$I$_4$(*m*TP^t)(N$_2$)(thf)$_4$] (20.0 mg, 0.00943 mmol) was dissolved in toluene to yield a dark brown solution and cooled to −30 °C. Me_3SiOTf (10.2 µL, 0.0566 mmol) was added. Overnight the reaction mixture was allowed to warm to room temperature with stirring. No visible colour change was observed. No paramagnetic signals remained in ^{1}H spectra of the solution and ^{29}Si INEPT NMR showed no nitrogen containing products.

^{29}Si NMR (99 MHz, Toluene-d_8) δ 42.04 (s, Me_3*Si*OTf), 15.12, (s, IMe_2*Si*-*Si*Me_2I), 7.06 (s, Me_3*Si*-*Si*Me_3).

5.4.15 Reaction to target synthesis of [U$_2$(*m*TP^m)(N{SiMe$_3$}$_2$)$_2$] from U[N{SiMe$_3$}$_2$]$_3$

U[N{$SiMe_3$}$_2$]$_3$ (100 mg, 0.125 mmol) was dissolved in hexane and cooled to −30 °C. To this purple solution, a solution of **H$_4$(*m*TP^m)** (46.0 mg, 0.0610 mmol) in hexane was slowly added. The reaction mixture was allowed to warm to room temperature and stirred overnight. Crystallisation of the filtered solution yielded only unreacted starting material U[N{$SiMe_3$}$_2$]$_3$.

5.4.16 Synthesis of 15(*m*TP^m), [U$_2$(*m*TP^m)(N{SiMe$_3$}$_2$)$_4$]

A Schlenk flask was charged with **H$_4$(*m*TP^m)** (225 mg, 0.298 mmol) and [U(N'')$_2$(N{$SiMe_3$}$SiMe_2CH_2$)] (450 mg, 0.627 mmol), a stirrer bar and hexanes (20 cm^3). The resulting dark brown suspension was stirred at RT for 16 hours, forming a bright green suspension. The product was isolated by filtration as a yellow precipitate, then recrystallised

by slow evaporation of a concentrated hexane solution to afford yellow plates of **[U_2(*m*TP^m)(N{$SiMe_3$}$_2$)$_4$]**.

Yield = 0.362 g, 65 %.

^{1}H NMR (500 MHz, Benzene-d_6) δ 41.19 (s, aromatic-*H,* 2H), 31.62 (s, aromatic-*H,* 1H), 27.73 (s, aromatic-*H,* 1H), 16.71 (s, aryloxide-*H,* 4H), 3.90 (s, aryloxide-*H,* 4H), 1.50 (s, Me*H,* 12H), -3.03 (s, Ar_3*H*, 2H), -9.76 (s,), -18.51 (s, SiCH_3, 72H).

^{29}Si NMR (C_6D_6, 99 MHz) δ -230.8 (Me_3*Si*).

Elemental Analysis: C 48.85 %, H 7.23 %, N 3.00 % calculated. C 48.66 %, 6.91 %, N 2.78 % found.

5.4.17 Synthesis of 15(*m*TP^t), [U_2(*m*TP^t)(N{$SiMe_3$}$_2$)$_4$]

A Schlenk flask was charged with **H_4(*m*TP^t)** (250 mg, 0.271 mmol) and [U(N")$_2$(N{$SiMe_3$}$SiMe_2CH_2$)] (410 mg, 0.571 mmol), a stirrer bar and hexanes (5 cm^3). The resulting dark brown suspension was stirred at RT for 16 hours, and then cooled to −30 °C for 3 days. The resulting yellow crystalline solid was isolated by filtration and dried under reduced pressure.

Yield = 298 mg, 54 %.

^{1}H NMR (500 MHz, 329.2 K, thf-d_8) δ 7.19-7.05 (m, aromatic-*H,* 4H), 2.29 (s, Ar_3*H*, 2H), 1.29 (s, ^{t}Bu*H,* 36H), 0.89 (s, ^{t}Bu*H,* 36H), 0.88 (s, aryloxide-*H,* 4H), 0.05 (s, aryloxide-*H,* 4H), -2.44 (s, SiMe*H,* 72H).

^{29}Si NMR (thf-d_8, 99 MHz) δ -211.54 (Me_3*Si*).

Elemental Analysis: C 51.89 %, H 7.82 %, N 2.75 % calculated. C 51.72 %, H 7.65 %, N 2.70 % found.

5.4.18 Synthesis of 16(*m*TP^m), [U_2(*m*TP^m)(N{$SiMe_3$}$_2$)$_2$] *via* reduction of 15(*m*TP^m), [U_2(*m*TP^m)(N{$SiMe_3$}$_2$)$_4$]

A Schlenk flask was charged with **[U_2(*m*TP^m)(N{$SiMe_3$}$_2$)$_4$],** (274 mg, 0.223 mmol) and KC_8 (64 mg, 0.447 mmol) and equipped with a stirrer bar. Toluene (10 cm^3) was added and the

resulting dark green solution was stirred for 16 hours at RT, turning dark purple. The toluene was removed under reduced pressure and the product was extracted into heptane. The dark purple product was obtained as a powder following removal of heptane under reduced pressure

Yield = 0.21 g, 74%.

^{1}H NMR (500 MHz, Benzene-d_6) δ 22.22 (s, aromatic-*H,* 2H), 17.50 (s, aromatic-*H,* 1H), 14.62 (s, aromatic-*H,* 1H), 11.85 (s, aromatic-*H,* 4H), 7.50 (s, aromatic-*H,* 4H), 2.11 (s, Me*H,* 12H), 0.89 (s, Ar_3*H,* 2H), -7.94 (s, ^{t}Bu*H,* 36H), -13.33 (s, SiCH_3, 36H).

^{29}Si NMR (C_6D_6, 99 MHz) δ -99.93 (Me_3Si).

Elemental Analysis: C 49.66 %, H 6.38 %, N 1.81 % calculated. C 49.48 %, H 6.49 %, N 1.93 % found.

5.4.19 Reduction of 15(*m*TP^{m}), [U$_2$(*m*TP^{m})(N{SiMe$_3$}$_2$)$_4$] to yield intermediate 17(*m*TP^{m})

[U$_2$(*m*TP^{m})(N{SiMe$_3$}$_2$)$_4$] (50 mg, 0.028 mmol) was dissolved in toluene to provide a bright yellow solution which was cooled to −30 °C. This solution was added dropwise to solid KC_8 (14.5 mg, 0.107 mmol). The mixture was allowed to warm slowly to room temperature and stirred overnight. The resulting dark red solution was filtered to remove dark grey graphite. This solution was used without further purification for the quenching reactions described below.

5.4.20 Reduction of 15(*m*TP^{t}), [U$_2$(*m*TP^{t})(N{SiMe$_3$}$_2$)$_4$] to yield intermediate 17(*m*TP^{t})

[U$_2$(*m*TP^{t})(N{SiMe$_3$}$_2$)$_4$] (30.5 mg, 0.0150 mmol) was dissolved in toluene to provide a bright yellow solution which was cooled to −30 °C. This solution was added dropwise to solid KC_8 (8.10 mg, 0.060 mmol). The mixture was allowed to warm slowly to room temperature and stirred overnight. The resulting dark red solution was filtered to remove dark grey graphite. This solution was used without further purification for the quenching reactions described below.

^{1}H NMR (500 MHz, Toluene-d_8) δ 21.08 (s, arene-*H,* 1H), 13.82 (s, arene-*H,* 1H), 13.30 (s, arene-*H,* 1H), 12.41 (s, arene-*H,* 1H), 10.18 (s, arene-*H,* 1H), 8.17 (s, arene-*H,* 1H), 8.03 (s,

arene-*H,* 1H), 1.72 (s, ^{t}Bu*H,* 9H), 1.35 – 1.16 (m, Ar$_3$*H,* 2H), 0.98-0.79 (m, arene-*H,* 2H), 0.27 (s, arene-*H,* 1H), 0.07 (s, arene-*H,* 1H), -1.17 (s, ^{t}Bu*H,* 9H), -1.52 (s, ^{t}Bu*H,* 9H), -7.32 (s, arene-*H,* 1H) -9.04 (s, ^{t}Bu*H,* 18H), -9.24 (s, ^{t}Bu*H,* 9H), -12.85 (s, ^{t}Bu*H,* 9H), -14.43 (s, ^{t}Bu*H,* 9H).

^{29}Si NMR (99 MHz, Toluene-d$_8$) δ -114.56 (Me$_3$*Si*).

5.4.21 Quenching of Reduced compound 17(*m*TP^{m}) with [PyH]Cl

A solution of **17(*m*TP^{m})** (37.8 mg, 0.027 mmol) was slowly added to solid [PyH]Cl (60 mg, 0.536 mmol). The suspension was stirred at room temperature for 1 hour to provide a colourless suspension. The reaction mixture was filtered to isolate the colourless solid which was washed with thf to removed unreacted [PyH]Cl, dried under reduced pressure and characterised as NH_4Cl, 50 % yield from quantitative NMR with an added standard of dimethylsulfone.

^{1}H NMR (500 MHz, dmso-d$_6$) δ 7.42 (t, $^{1}J_{NH}$ = 51 Hz, N*H*, 4H).

5.4.22 Quenching of Reduced compound 17(*m*TP^{m}) with SiMe$_3$OTf

A toluene-d$_8$ solution of **17(*m*TP^{m})** (0.12 mmol, 20.42 mg) was cooled to −30 °C. SiMe$_3$OTf (8.5 µL, 0.047 mmol) was added. After 30 mins of stirring, the reaction mixture was placed in a −30 °C freezer overnight. 1,3,5-tritertbutyl benzene was added as an internal standard and the reaction mixture was analysed by NMR to confirm production of N(SiMe$_3$)$_3$

Yield = 63 %.

^{1}H NMR (500 MHz, Toluene-d$_8$) δ 0.31 (s, Me*H*, 27H).

^{29}Si NMR (99 MHz, Toluene-d$_8$) δ 2.26 (s, Me$_3$*Si*).

5.4.23 Quenching of Reduced compound 17(*m*TP^{t}) with [PyH]Cl

17(*m*TP^{t}) (11. 85 mg, 7.5 x10^{-3} mmol) was dissolved in toluene to provide a dark green solution. [PyH]Cl (17.3 mg, 0.150 mg) was added and the resulting suspension was stirred at room temperature for 1 hour to provide a colourless suspension. The reaction mixture was filtered to isolate the colourless solid which was washed with thf to removed unreacted [PyH]Cl, dried under reduced pressure and characterised as NH_4Cl.

Yield = 93 % from quantitative NMR with an added standard of dimethylsulfone.

^{1}H NMR (500 MHz, dmso-d_6) δ 7.42 (t, $^1J_{NH}$ = 51 Hz, N*H*, 4H).

5.4.24 Quenching of Reduced compound 17(*m*TP^t) with $SiMe_3OTf$

A toluene-d_8 solution of **17(*m*TP^t)** ($4.42x10^{-3}$ mmol, 6.98 mg) was cooled to −30 °C then added to a young's tap NMR tube. $SiMe_3OTf$ (3.02 µL, 0.016 mmol) was added and the reaction mixture was stored at room temperature overnight. 1,3,5-tritertbutyl benzene was added as an internal standard and the reaction mixture was analysed by NMR. No $N(SiMe_3)_3$ was observed.

5.5 Synthetic procedures for Chapter 4

5.5.1 Synthesis of 18(*m*TP^m), $[K(py)_6][Ce_2(mTP^m)_2K(py)_4]$

H_4(*m*TP^m) (2.00 g, 2.64 mmol) and $[KN(SiMe_3)_2]$ (2.12 g, 10.60 mmol) were dissolved in pyridine to give a bright yellow solution. This solution was added to a solution of $CeCl_3$(thf) (0.842 g, 2.64 mmol) in pyridine, prepared in a rigorously flame dried ampoule. The resulting dark yellow solution was stirred at room temperature overnight before being filtered to remove precipitated KCl. The solvent was removed under reduced pressure to give the product as a bright yellow powder.

Yield = 2.53 g, 73 %.

The powder could be recrystalised from a concentrated solution of pyridine at −30 °C, yielding large yellow block crystals suitable for single crystal XRD.

^{1}H NMR (500 MHz, thf-d_8) δ 10.60 (s, aryloxide-*H*, 4H), 9.99 (s, aryloxide-*H*, 4H), 9.71 (s, aryloxide-*H*, 4H), 9.45 (s, aryloxide-*H*, 4H), 7.59 (s, Ar_3H, 2H), 4.51 (s, Me*H*, 12H), 2.34 (s, ^{t}Bu*H,* 36H), 2.19 (s, Me*H*, 12H), -4.37 (s, ^{t}Bu*H,* 36H)

Elemental Analysis: C 69.76 %, H 6.61 %, N 5.28 %. calculated. C 69.27%, H 6.86 % found.

5.5.2 Synthesis of 18(*m*TP^m)(18c6), [K(18-crown-6)][Ce_2(*m*TP^m)$_2$K(solv)$_4$]

$[K(py)_6][Ce_2(mTP^m)_2K(py)_4]$, **18(*m*TP^m)** (100 mg, 0.0378 mmol) was dissolved in pyridine. This solution was added to one equivalent of 18-crown-6 (10 mg, 0.0378 mmol) dissolved in pyridine. The resulting orange solution was stirred overnight, filtered and then cooled to −30 °C to afford a small number of single crystals of **[K(18-crown-6)][Ce_2(*m*TP^m)$_2$K(solv)$_4$].** Exact yields were not recorded.

5.5.3 Reaction to target oxidation of 18(*m*TP^{m}), [K(solv)$_6$][Ce$_2$(*m*TP^{m})$_2$K(solv)$_4$] with one equivalent of MoO_3

[K(py)$_6$][Ce$_2$(*m*TP^{m})$_2$K(py)$_4$], 18(*m*TP^{m}) (100 mg, 0.0378 mmol) was dissolved in pyridine and cooled to −30 °C. A colourless suspension of MoO_3 in pyridine (5.4 mg, 0.0378 mmol) was added to yield a pale green suspension. The reaction mixture was allowed to warm slowly to room temperature with stirring. Within 4 hours the reaction mixture had turned dark purple. Pyridine was removed under reduced pressure and the dark purple powder was extracted into toluene. From this solution, **[K(py)$_6$][Ce$_2$(*m*TP^{m})$_2$K(py)$_4$]**, **18(*m*TP^{m})** was recovered as a yellow crystalline solid, leaving only diamagnetic products in ^{1}H NMR spectra.

5.5.4 Reaction to target oxidation of 18(*m*TP^{m}), [K(solv)$_6$][Ce$_2$(*m*TP^{m})$_2$K(solv)$_4$] with two equivalents of MoO_3

[K(py)$_6$][Ce$_2$(*m*TP^{m})$_2$K(py)$_4$], 18(*m*TP^{m}) (100 mg, 0.0378 mmol) was suspended in thf and cooled to −30 ° C. A colourless suspension of MoO_3 in thf (10.8 mg, 0.0774 mmol) was added to yield a purple suspension. The reaction mixture was allowed to warm slowly to room temperature with stirring overnight. The suspension was filtered to remove blue $KMoO_3$ and solvent was removed to yield a dark purple solid, which was extracted into pyridine. ^{1}H NMR spectra of the resulting lilac solution indicated that significant amounts of unreacted **[K(py)$_6$][Ce$_2$(*m*TP^{m})$_2$K(py)$_4$]** was still present despite the colour change indicating some oxidation.

5.5.5 Reaction to target oxidation of 18(*m*TP^{m}), [K(solv)$_6$][Ce$_2$(*m*TP^{m})$_2$K(solv)$_4$] with two equivalents of [Cp$_2$Fe]OTf

[K(py)$_6$][Ce$_2$(*m*TP^{m})$_2$K(py)$_4$], **18(*m*TP^{m})** (100 mg, 0.0378 mmol) was suspended in toluene and cooled to −30 °C. A suspension of [Cp$_2$Fe]OTf (14.3 mg, 0.0760 mmol) was added dropwise to this suspension yielding a dark green suspension. The reaction mixture was allowed to warm slowly to room temperature with stirring overnight to yield a dark purple solution. Solvent was removed under reduced pressure to yield a dark purple solid with a broad diamagnetic ^{1}H NMR spectrum.

5.5.6 Reaction to target oxidation of 18(*m*TP^{m}), [K(solv)$_6$][Ce$_2$(*m*TP^{m})$_2$K(solv)$_4$] with one equivalent of [Cp$_2$Fe]OTf

[K(py)$_6$][Ce$_2$(*m*TP^m)$_2$K(py)$_4$], 18(*m*TP^m) (100 mg, 0.0378 mmol) was suspended in toluene and cooled to −30 °C. A suspension of [Cp$_2$Fe]OTf (7.16 mg, 0.0380 mmol) was added dropwise to this suspension yielding a dark green suspension. The reaction mixture was allowed to warm slowly to room temperature with stirring overnight. A blue powder was removed by filtration to yield a dark yellow solution containing **[K(py)$_6$][Ce$_2$(*m*TP^m)$_2$K(solv)$_4$]** and a new diamagnetic product.

5.5.7 Reaction to target oxidation of 18(*m*TP^m), [K(solv)$_6$][Ce$_2$(*m*TP^m)$_2$K(solv)$_4$] with one equivalent of I$_2$

[K(py)$_6$][Ce$_2$(*m*TP^m)$_2$K(py)$_4$], 18(*m*TP^m) (100 mg, 0.0378 mmol) was dissolved in thf and cooled to −30 °C. An orange solution of I_2 in thf (9.70 mg, 0.0380 mmol) was also cooled to −30 °C and added dropwise to this solution. The reaction mixture was allowed to warm slowly to room temperature with stirring overnight to yield a dark blue suspension. The dark blue solid was isolated by filtration but found to be insoluble in organic solvents preventing further characterisation.

5.5.8 Reaction to target oxidation of 18(*m*TP^m), [K(solv)$_6$][Ce$_2$(*m*TP^m)$_2$K(solv)$_4$] with two equivalents of [Cu(OTf)$_2$]

[K(py)$_6$][Ce$_2$(*m*TP^m)$_2$K(py)$_4$], 18(*m*TP^m) (50.0 mg, 0.0193 mmol) was suspended in toluene to and cooled to −30 °C. A colourless solution of [Cu(OTf)$_2$] (14.0 mg, 0.0386 mmol) was added dropwise and an immediate colour change the dark purple was observed. The reaction mixture was allowed to warm slowly to room temperature with stirring overnight. A dark brown precipitate was removed by filtration to yield a lilac solution. Bright blue crystals of unreacted [Cu(OTf)$_2$(py)$_4$] were recovered from the solution after several days. ^{1}H NMR spectra of the lilac solution showed poorly resolved broad, diamagnetic peaks suggesting conversion to a Ce(IV) product.

5.5.9 Reaction to target oxidation of 18(*m*TP^m), [K(solv)$_6$][Ce$_2$(*m*TP^m)$_2$K(solv)$_4$] with one equivalent of [Cu(OTf)$_2$]

[K(py)$_6$][Ce$_2$(*m*TP^m)$_2$K(py)$_4$], 18(*m*TP^m) (50.0 mg, 0.0193 mmol) was suspended in toluene to and cooled to −30 °C. A colourless solution of [Cu(OTf)$_2$] (7.0 mg, 0.0193 mmol) was added dropwise and an immediate colour change the dark purple was observed. The reaction

mixture was allowed to warm slowly to room temperature with stirring overnight. A dark blue precipitate was removed by filtration to yield a lilac solution. Solvent was removed from the solution under reduced pressure to a yield purple solid with a broad diamagnetic ^{1}H NMR spectrum. This product could not be further characterised.

5.6 Crystallographic details

Single crystal X-ray crystallography data on compounds **1(*m*TP^{m})**, **2(*m*TP^{m})**, **2(*m*TP^{t})**, **3(*m*TP^{m})**, **6(*m'*TP^{m})**, **7(*m*TP^{m})**, **8(*m*TP^{m})**, **8(*m*TP^{t})**, **15(*m*TP^{m})**, **15(*m*TP^{t})**, **18(*m*TP^{m})(py)**, **18(*m*TP^{m})(thf)** and **18(*m*TP^{m})(18c6)** were recorded using an Oxford Diffraction Excalibur Eos diffractometer with Mo Kα radiation at 170(2) K. Data on **4(*m'*TP^{m})** was recorded using an Agilent Technologies Supernova dual source Atlas diffractometer using a Cu Kα radiation source at 120(10) K. All structures were solved using SHELXT and least-square refined using SHELXL in Olex2.[8,9] Absorption corrections were applied using *Crysalis PRO* 1.171.38.42b (Rigaku Oxford Diffraction, 2015) or 1.171.37.34 (Agilent Technologies, 2014) software. Analytical numeric absorption corrections used a multifaceted crystal model based on expressions derived by Clark and Reid.[10] Numerical absorption correction was based on a Gaussian integration over a multifaceted crystal model. Empirical absorption correction using spherical harmonics was implemented in SCALE3 ABSPACK scaling algorithm.

No restraints were applied during the refinement of **1(*m*TP^{m})**, **2(*m*TP^{t})**, **4(*m'*TP^{m})**, **6(*m'*TP^{m})**, **15(*m*TP^{t})**, **18(*m*TP^{m})(py)** or **18(*m*TP^{m})(18c6)**.

Three disordered dioxane solvent molecules in the unit cell of **2(*m*TP^{m})** were restrained using RIGU. Two carbon atoms on a disordered molecule of coordinated dioxane were restrained using EADP.

Three disordered benzene solvent molecules in the unit cell of **3(*m*TP^{m})** were restrained using RIGU.

Two disordered benzene solvent molecules in the unit cell of **7(*m*TP^{m})** were restrained using RIGU, an additional disordered benzene solvent molecule in the unit cell was restrained using EADP.

8(*m*TP^{m}) contained three disordered thf solvent molecules in the unit cell, these were restrained using RIGU and EADP. Three of the coordinated thf molecules were also disordered and restrained using RIGU.

Two disordered toluene solvent molecules in the unit cell of **8(*m*TP^{t})** were restrained using RIGU. Two coordinated thf molecules were also disordered and restrained using RIGU. The *tert*-butyl group on aryloxide ring three was rotationally ordered and this was restrained. Aryloxide ring four was also disordered, this was restrained using EADP.

15(*m*TP^{m}) contained a disordered hexane solvent molecule in the unit cell. This was restrained using SADI.

The thf molecules coordinated to the potassium counterion in **18(*m*TP^{m})(thf)** were heavily disordered and restrained using RIGU and EADP.

Table 5.3 Crystallographic data summary for complexes **1(*m*TP^{m}), 2(*m*TP^{m})** and **2(*m*TP^{t}).**

Complex	**1(*m*TP^{m})**	**2(*m*TP^{m})**	**2(*m*TP^{t})**
Chemical formula	$C_{76}H_{109}K_3O_{10}$	$C_{60}H_{78}O_8U{\cdot}4(C_4H_8O_2)$	$C_{144}H_{204}O_{12}U_2{\cdot}2(C_7H_8)$
M_r	1299.93	1517.66	2787.39
Crystal system, space group	Orthorhombic, *Pbca*	Monoclinic, $P2_1/c$	Monoclinic, $P2_1/n$
Temperature (K)	293	170	293
a, *b*, *c* (Å)	25.6438 (4), 18.7211 (3), 31.4669 (5)	16.5248 (2), 14.43675 (19), 29.9231 (3)	18.4887 (4), 23.6606 (5), 23.8438 (5)
α, β, γ (°)	90, 90, 90	90, 90.8081 (10), 90	90, 109.486 (2), 90
V (Å^3)	15106.6 (4)	7137.89 (16)	9833.1 (4)
Z	8	4	2
μ (mm^{-1})	0.23	2.34	1.69
Crystal size (mm)	0.51 × 0.40 × 0.13	0.38 × 0.11 × 0.09	0.49 × 0.18 × 0.07
Absorption correction	Analytical	Analytical	Multi-scan
T_{min}, T_{max}	0.986, 0.996	0.675, 0.888	0.845, 1.000
No. of measured, independent and observed [$I > 2s(I)$] reflections	259142, 12003, 8511	110407, 13051, 10372	234883, 15637, 11362
R_{int}	0.114	0.095	0.171
θ_{max} (°)	24.1	25.4	24.1

$(\sin\theta/\lambda)_{max}$ (Å^{-1})	0.575	0.602	0.575
$R[F^2 > 2s(F^2)]$, $wR(F^2)$, S	0.062, 0.160, 1.03	0.055, 0.127, 1.07	0.083, 0.273, 1.08
No. of reflections	12003	13051	15637
No. of parameters	822	812	800
No. of restraints	0	108	0
H-atom treatment	H atoms treated by a mixture of independent and constrained refinement	H-atom parameters constrained	H-atom parameters constrained
	$w = 1/[s^2(F_o^2) + (0.067P)^2 + 16.324P]$ where $P = (F_o^2 + 2F_c^2)/3$	$w = 1/[s^2(F_o^2) + (0.047P)^2 + 37.596P]$ where $P = (F_o^2 + 2F_c^2)/3$	$w = 1/[s^2(F_o^2) + (0.144P)^2 + 115.666P]$ where $P = (F_o^2 + 2F_c^2)/3$
$(\Delta/\sigma)_{max}$	0.001	0.001	0.602
$\Delta\rangle_{max}$, $\Delta\rangle_{min}$ (e Å^{-3})	0.47, -0.38	1.79, -1.16	2.53, -0.78
CCDC number	-	1829626	1829625

Table 5.4 Crystallographic data summary for complexes **3(*m*TP^m), 4(*m'*TP^m)** and **6(*m'*TP^m).**

	3(*m*TP^m)	**4(*m'*TP^m)**	**6(*m'*TP^m)**
Chemical formula	$C_{60}H_{78}O_8U{\cdot}4(C_4H_8O_2)$	$0.5(C_{118}H_{140}K_4N_2O_8U_2){\cdot}2(C_7H_8)$	$C_{56}H_{69}K_{0.5}O_5U{\cdot}C_{56}H_{66}K_{0.5}O_5U{\cdot}C_{24}H_{48}KO_6{\cdot}2(C_4H_8O)$
M_r	1517.66	1357.65	2772.28
Crystal system, space group	Monoclinic, $P2_1/c$	Triclinic, $P\bar{1}$	Triclinic, $P\bar{1}$
Temperature (K)	170	120	293
a, *b*, *c* (Å)	16.5248 (2), 14.43675 (19), 29.9231 (3)	15.5926 (3), 19.0437 (3), 22.9607 (4)	14.4679 (2), 17.9544 (2), 31.7846 (4)
a, b, g (°)	90, 90.8081 (10), 90	72.471 (1), 78.738 (1), 84.899 (1)	104.563 (1), 93.380 (1), 103.160 (1)
V (Å^3)	7137.89 (16)	6372.9 (2)	7721.94 (17)
Z	4	4	2
Radiation type	Mo *K*a	Cu *K*a	Mo *K*a
μ (mm^{-1})	2.34	8.71	2.20
Crystal size (mm)	0.38 × 0.11 × 0.09	0.35 × 0.09 × 0.03	1.5 × 1.01 × 0.47
Diffractometer	Xcalibur, Eos	SuperNova, Dual, Cu at zero, Atlas	Xcalibur, Eos
Absorption correction	Analytical	Multi-scan *SADABS* 2014/5	Analytical
T_{min}, T_{max}	0.675, 0.888	0.224, 0.923	0.042, 0.408
No. of measured, independent and observed [$I > 2s(I)$] reflections	110407, 13051, 10372	130720, 26434, 22237	136269, 25382, 18477
R_{int}	0.095	0.078	0.084
$(\sin\theta/\lambda)_{max}$ (Å^{-1})	0.602	0.630	0.581

$R[F^2 > 2s(F^2)]$, $wR(F^2)$, S	0.055, 0.127, 1.07	0.044, 0.117, 1.04	0.060, 0.167, 1.03
No. of reflections	13051	26434	25382
No. of parameters	812	1497	1334
No. of restraints	108	26	0
	$w = 1/[s^2(F_o^2) + (0.047P)^2 + 37.596P]$ where $P = (F_o^2 + 2F_c^2)/3$	$w = 1/[s^2(F_o^2) + (0.0763P)^2 + 0.0092P]$ where $P = (F_o^2 + 2F_c^2)/3$	$w = 1/[s^2(F_o^2) + (0.0828P)^2 + 35.4082P]$ where $P = (F_o^2 + 2F_c^2)/3$
$(\Delta/\sigma)_{max}$	0.001	0.001	0.131
$\Delta\rangle_{max}$, $\Delta\rangle_{min}$ (e Å^{-3})	1.79, -1.16	1.74, -3.03	4.24, -2.07
CCDC number	1829624	1829629	1829630

Table 5.5 Crystallographic data summary for complexes **7(*m*TP^{m})**, **8(*m*TP^{m})** and **8(*m*TP^{t})**.

	7(*m*TP^{m})	**8(*m*TP^{m})**	**8(*m*TP^{t})**
Chemical formula	$0.5(C_{125}H_{164}Na_3O_{11}Si_3U_2)\cdot C_6H_6\cdot 0.5(C_{12}H_{11})$	$C_{68}H_{94}I_4O_8U_2\cdot 3(C_4H_8O)$	$2(C_{80}H_{118}I_4O_8U_2)\cdot 3(C_7H_8)$
M_r	1391.64	2239.40	4659.19
Crystal system, space group	Triclinic, $P\bar{1}$	Triclinic, $P\bar{1}$	Orthorhombic, *Pbca*
a, *b*, *c* (Å)	17.9082 (4), 20.6900 (4), 23.3050 (6)	15.8678 (6), 16.2835 (7), 21.4232 (7)	26.7421 (4), 34.4628 (10), 47.5187 (9)
α, β, γ (°)	104.821 (2), 96.165 (2), 105.124 (2)	68.627 (4), 71.761 (3), 62.142 (4)	90, 90, 90
V (Å^3)	7917.0 (3)	4488.4 (3)	43793.7 (17)
Z	4	2	8
μ (mm^{-1})	2.12	5.03	4.13
Crystal size (mm)	0.35 × 0.31 × 0.15	××	0.28 × 0.13 × 0.06
Absorption correction	Multi-scan	Multi-scan	Analytical
T_{min}, T_{max}	0.826, 1.000	0.850, 1.000	0.902, 0.973
No. of measured, independent and observed [$I > 2s(I)$] reflections	134038, 32351, 20372	77490, 14234, 8754	316120, 34673, 17158
R_{int}	0.102	0.135	0.246
θ_{max} (°)	26.4	24.1	24.1
$(\sin\theta/\lambda)_{max}$ (Å^{-1})	0.625	0.575	0.575
$R[F^2 > 2s(F^2)]$, $wR(F^2)$, S	0.077, 0.247, 1.04	0.088, 0.211, 1.03	0.088, 0.244, 1.02
No. of reflections	32351	14234	34673
No. of parameters	1491	824	1831
No. of restraints	72	210	87
H-atom treatment	H atoms treated by a mixture of independent and constrained	H-atom parameters constrained	H-atom parameters constrained

	refinement		
	$w = 1/[s^2(F_o^2) + (0.116P)^2 + 75.463P]$ where $P = (F_o^2 + 2F_c^2)/3$	$w = 1/[s^2(F_o^2) + (0.0796P)^2 + 62.8605P]$ where $P = (F_o^2 + 2F_c^2)/3$	$w = 1/[s^2(F_o^2) + (0.084P)^2 + 891.041P]$ where $P = (F_o^2 + 2F_c^2)/3$
$(\Delta/\sigma)_{max}$	2.537	0.001	0.001
$\Delta\rangle_{max}$, $\Delta\rangle_{min}$ (e Å^{-3})	3.47, -1.24	2.51, -1.31	1.91, -1.11
CCDC number		1478886	

Table 5.6 Crystallographic data summary for complexes **15(*m*TP^{m})**, **15(*m*TP^{t})**, and **18(*m*TP^{m})(py)**.

	15(*m*TP^{m})	**15(*m*TP^{t})**	**18(*m*TP^{m})(py)**
Chemical formula	$C_{76}H_{134}N_4O_4Si_8U_2 \cdot C_3H_7$	$C_{88}H_{158}N_4O_4Si_8U_2$	$C_{124}H_{139}Ce_2KN_4O_8 \cdot C_{30}H_{30}KN_6 \cdot 6(C_5H_5N) \cdot C_5H_2N$
M_r	1911.73	2035.95	3200.12
Temperature (K)	170	293	120
a, *b*, *c* (Å)	12.9013 (3), 18.8759 (4), 21.4638 (4)	13.9480 (2), 22.0637 (6), 22.7281 (8)	19.7601 (5), 21.2195 (5), 22.2052 (6)
α, β, γ (°)	65.3765 (19), 88.1786 (17), 88.3450 (17)	61.433 (3), 82.5811 (19), 83.5341 (17)	79.182 (2), 72.086 (2), 79.394 (2)
V (Å^3)	4748.51 (18)	6081.1 (3)	8622.0 (4)
μ (mm^{-1})	3.55	2.78	0.63
Crystal size (mm)	0.32 × 0.08 × 0.02	0.47 × 0.31 × 0.18	0.30 × 0.27 × 0.15
Absorption correction	Analytical	Analytical	Multi-scan
T_{min}, T_{max}	0.758, 0.971	0.988, 0.994	0.902, 1.000
No. of measured, independent and observed [$I > 2s(I)$] reflections	85138, 16783, 11693	84656, 19285, 14929	197756, 39502, 28962
R_{int}	0.110	0.062	0.088
θ_{max} (°)	25.0	24.1	27.5
$(\sin\theta/\lambda)_{max}$ (Å^{-1})	0.595	0.575	0.649
$R[F^2 > 2s(F^2)]$, $wR(F^2)$, S	0.054, 0.096, 1.02	0.059, 0.152, 1.06	0.067, 0.137, 1.05
No. of reflections	16783	19285	39502
No. of parameters	915	997	1983
No. of restraints	1	0	0
	$w = 1/[s^2(F_o^2) + (0.0184P)^2 + 12.2734P]$ where $P = (F_o^2 + 2F_c^2)/3$	$w = 1/[s^2(F_o^2) + (0.0644P)^2 + 39.4229P]$ where $P = (F_o^2 + 2F_c^2)/3$	$w = 1/[s^2(F_o^2) + (0.0355P)^2 + 21.250P]$ where $P = (F_o^2 + 2F_c^2)/3$
$\Delta\rangle_{max}$, $\Delta\rangle_{min}$ (e Å^{-3})	1.07, -0.64	7.07, -1.07	1.08, -0.96
CCDC number	1478890	-	-

Table 5.7 Crystallographic data summary for complexes **18(*m*TP^{m})(18c6)** and **18(*m*TP^{m})(thf)**.

	18(*m*TP^{m})(18c6)	**18(*m*TP^{m})(thf)**

Chemical formula	$C_{62}H_{72}CeK_{0.5}N_2O_4 \cdot C_6H_{12}K_{0.5}O_3 \cdot 7(C_5H_5N)$	$C_{122}H_{150}Ce_2KN_2O_{10} \cdot C_{50}K_2O_{10} \cdot 6(C_4O) \cdot 2(C_5O) \cdot 2(C_5)$
M_r	1774.28	3228.53
Temperature (K)	120	293
a, *b*, *c* (Å)	14.7870 (3), 19.2736 (5), 20.1571 (6)	15.8958 (3), 18.6385 (3), 19.6721 (3)
α, β, γ (°)	117.438 (3), 91.301 (2), 109.885 (2)	97.210 (1), 113.200 (2), 105.918 (1)
V (Å^3)	4682.4 (2)	4968.52 (16)
Z	2	1
μ (mm^{-1})	0.59	0.57
Crystal size (mm)	0.43 × 0.24 × 0.09	1.87 × 0.84 × 0.67
Diffractometer	SuperNova, Dual, Cu at zero, Atlas	Xcalibur, Eos
Absorption correction	Gaussian	Multi-scan
T_{min}, T_{max}	0.530, 1.000	0.713, 1.000
No. of measured, independent and observed [$I > 2s(I)$] reflections	107276, 17749, 15128	183803, 22757, 17484
R_{int}	0.103	0.070
$(\sin \theta/\lambda)_{max}$ (Å^{-1})	0.610	0.649
$R[F^2 > 2s(F^2)]$, $wR(F^2)$, S	0.054, 0.134, 1.05	0.071, 0.219, 1.52
No. of reflections	17749	22757
No. of parameters	1147	1005
No. of restraints	0	27
$(\Delta/\sigma)_{max}$	0.002	0.781
$\Delta\rangle_{max}$, $\Delta\rangle_{min}$ (e Å^{-3})	1.80, -0.99	2.67, -1.60
CCDC number	-	-

5.7 References for Chapter 5

(1) Ruiz, J.; Astruc, D. *Comptes Rendus l'Académie des Sci. Chem.* **1998**, *1* (1), 21–27.

(2) Mansell, S. M.; Perandones, B. F.; Arnold, P. L. *J. Organomet. Chem.* **2010**, *695* (25–26), 2814–2821.

(3) Monreal, M. J.; Thomson, R. K.; Cantat, T.; Travia, N. E.; Scott, B. L.; Kiplinger, J. L. *Organometallics* **2011**, *30* (7), 2031–2038.

(4) Dormond, A.; El Bouadili, A.; Aaliti, A.; Moise, C. *J. Organomet. Chem.* **1985**, *288* (1), C1–C5.

(5) Westerhausen, M. *Inorg. Chem.* **1991***, 30,* 96-101.

(6) Rosenkoetter, K. E.; Ziller, J. W.; Heyduk, A. F. *Inorg. Chem.* **2016**, *55* (13), 6794–6798.

(7) Kiplinger, J. L.; Morris, D. E.; Scott, B. L.; Burns, C. J. *Organometallics*, **2002**, *21* (26), 5978–5982

(8) Sheldrick, G. M.; IUCr. *Acta Crystallogr. Sect. A Found. Adv.* **2015**, *71* (1), 3–8.

(9) Dolomanov, O. V.; Bourhis, L. J.; Gildea, R. J.; Howard, J. A. K.; Puschmann, H. *J. Appl. Crystallogr.* **2009**, *42* (2), 339–341.

(10) Clark, R. C.; Reid, J. S. *Acta Crystallogr. Sect. A Found. Crystallogr.* **1995**, *51* (6), 887–897.

Appendix 1: Evans method calculation for 3(*m*TP^{m})

U(IV) has the ground state term symbol $^{3}H_{4}$. Unlike in transition metal chemistry, the larger spin-orbit coupling in lanthanide and actinide metals means that the contribution of orbital angular momentum to the magnetic moment cannot be ignored. Spin and orbital contributions combine, according to Russell-Saunders coupling, and the effective magnetic moment is given by Equation A-1, yielding a value of μ_{eff} = 3.58 μ_B.

$$\mu_{eff} = g \times \sqrt{J(J+1)}$$

$$g = \frac{3}{2} + \frac{S(S+1) - L(L+1)}{2J(J+1)}$$

Equation A-1 gives effective magnetic moment, where J is the total angular momentum quantum number (4 for U(IV)), L is the orbital quantum number (5 for U(IV)) and S is the spin quantum number (1 for U(IV)).

To measure the experimental magnetic moment, the Evans Method was employed. 8.60 mg of sample was dissolved in 2.148 g of C_6D_6. A sealed glass capillary containing C_6D_6 was added to the NMR tube with the sample. Using the procedure outlined by Crawford,[1] a shift in frequency of 69.55 Hz of the benzene resonance was measured and calculated to correspond to an experimental magnetic moment of 3.21 μ_B. Details and parameters used in the calculation of paramagnetic susceptibility are given in Tables A-1 and A-2. This experimentally observed value is in good agreement with the calculated value and confirms the +4 oxidation state of the uranium cation.

$$X_M = \frac{3\Delta f}{4\pi F c} - diamagnetic\ correction$$

Equation A-2 Evans method equation, where X_M is paramagnetic susceptibility, Δf is the frequency difference in Hz between the shifted resonance and the pure solvent resonance, F is spectrometer radiofrequency in Hz and c is the concentration of the paramagnetic species in mol mL^{-1}.

	3(*m*TP^{m})
Mass of sample (g)	8.60 x 10^{-3}
Mass of solvent + sample (g)	0.510
Mass of solvent (g)	0.501

Density of solvent (g cm^{-3})	0.950
Volume of solvent (cm^3)	0.528
Shift of peak (ppm)	0.139
Change in frequency (ppm)	1.39×10^{-7}
Change in frequency (Hz)	69.55
Spectrometer frequency (Hz)	5.00×10^{8}
Mass of substance per cm^3 (g cm^{-3})	1.63×10^{-2}
X_g (g^{-1})	2.04×10^{-6}
Solvent Correction (g^{-1})	6.43×10^{-7}
Corrected X_g, (g^{-1})	2.68×10^{-6}
Molecular weight of compound (g mol^{-1})	1976.17
$X_{m'}$ (mol^{-1})	5.30×10^{-3}
Correction for ligand diamagnetism X_m, (mol^{-1})	-1.01×10^{-3}
$X_{m'}$ (cm^3 mol^{-1})	4.28×10^{-3}
μ_{eff} (μ_B)	**3.21**

Table A-1 measurements and parameters used in the calculation of paramagnetic susceptibility

Atoms	Diamagnetic Susceptibility[2] (10^{-6} cm^3 mol^{-1})	Number of Atoms in formula	Total Diamagnetic Susceptibility (10^{-6} cm^3 mol^{-1})
H	-2.9	122	-354
C	-6.0	104	-624
O	-4.6	8	-36.8
			Total -1.01×10^{-3} cm^3 mol^{-1}

Table A-2 Calculation of total diamagnetic susceptibility

References for Appendix 1

(1) Crawford, T. H.; Swanson, J. *J. Chem. Educ.* **1971**, *48* (6), 382.

(2) Kahn, O. *Molecular magnetism*; VCH: New York N.Y., 1993.

Appendix 2: Summary of reactions to target catalytic turnover of $HN(SiMe_3)_2$

As described in Section 2.11.3, the methyl protons in $HN(SiMe_3)_2$ give rise to a ^1H NMR resonance at 0.06 ppm. Integration of this resonance against an internal standard of 2,4,6-tri-*tert*-butylbenzene was used to determine the yield of $HN(SiMe_3)_2$ in simple stochiometric reactions. In reactions with an excess of reductant and Me_3SiOTf, in some cases the yield of $HN(SiMe_3)_2$ determined using this method exceeded the maximum theoretical yield. This result indicates that by-products with coincident resonances are formed during the reaction, adding to the integrated area of the resonance. Whilst ^{29}Si INEPT NMR spectroscopy was used to confirm the presence of $HN(SiMe_3)_2$, integration of Si resonances does not correspond to concentration of material in solution because signal intensity is enhanced by polarisation transfer. Accordingly, exact yields of $HN(SiMe_3)_2$ in the reactions detailed below remain unknown. Despite this, it is possible to infer some information about optimal reaction conditions by comparing the yield of the $(SiMe_3)_2O$ by-product at different reaction conditions. Table A-3 contains the ratio of the integrated areas of the resonance at 0.06 ppm and the resonance at 0.1 ppm, which is assigned as $(SiMe_3)_2O$.

The reactions detailed in Table A-3 show that after approximately 14 days the integrated area of the resonance at 0.06 ppm stops increasing. Addition of further equivalents of Me_3SiOTf after this time leads to a further increase (entry 35). At room temperature and elevated temperatures (80 °C) the kinetically favoured homocoupling reaction is more competitive, yielding $(SiMe_3)_2O$ (entries 3-12) in large quantities. At –30 °C, this side reaction proceeds more slowly. Cs metal can also be used as a reductant, but the reaction is less clean and several diamagnetic products were observed by ^1H NMR spectroscopy (entries 23-24).

The reaction is highly concentration (of $SiMe_3$) dependant. When larger excesses of Me_3SiOTf were added without sufficient dilution (entry 30), formation of $(SiMe_3)_2O$ is once again favoured. It has been noted in similar studies that the heterogeneous nature of the metal reductant (K, Cs) and the active metal complex results in a non-linear relationship between substrate concentration and TON, with catalytic N_2 reduction systems being notoriously sensitive to reaction conditions.[1]

The highest apparent yield of $HN(SiMe_3)_2$, as determined by integration of the resonance at 0.06 ppm, was achieved when 40 equivalents of Me_3SiOTf and excess potassium were stirred with **3(*m*TP^m)** at room temperature in benzene for 11 days, with 100 equivalents of DHA as

the hydrogen source. In this case $(SiMe_3)_2O$ was also produced in high yield (75 % per metal). Similar apparent yields of $HN(SiMe_3)_2$ (entries 1, 2, 35) could be achieved at –30 °C much more cleanly (<7% $(SiMe_3)_2O$).

In addition to $SiMe_3Cl$ and $SiMe_3I$ discussed in Chapter 2, other electrophiles were tested as substrates. The reaction with Me_3SiCH_2Ph (entry 25) did not result in the alkyl group incorporation in the product.

Entry 42 demonstrates that the analogous thorium complex, **3Th(*m*TP^m)**, also provides $HN(SiMe_3)_2$.

(1) Kendall, A. J.; Johnson, S. I.; Bullock, R. M.; Mock, M. T. *J. Am. Chem. Soc.* **2018**, , *140 (7)*, 2528-2563

Table A-3 Reduction and silylation of dinitrogen by **3(*m*TP)**. Comments for each entry explain the effect of different conditions on the reaction. Because the yield of hexamethyldisilazane cannot be accurately quantified by NMR alone, the integral ratio of the resonance at 0.06 ppm to that of the resonance at 0.1 ppm, assigned as the by-product $Me_3SiOSiMe_3$ is provided. Percentage yield of $Me_3SiOSiMe_3$ is given per U atom.

Entry	Compound	Reductant[a]	Solvent	Electrophile	Equivs	Additive	Equivs.	Temp./°C	Time /days	Ratio of 0.06:0.1	by-product[b] $Me_3SiOSiMe_3$	Comments
1	**3(*m*TP^m)**	K	toluene-d_8	Me_3SiOTf	40			-30	6	**289:1**	5%	
2	**3(*m*TP^m)**	K	toluene-d_8	Me_3SiOTf	40			-30	13	**194:1**	7%	
3	**3(*m*TP^m)**	K	toluene-d_8	Me_3SiOTf	40			80	4	**107:1**	7%	
4	**3(*m*TP^m)**	K	toluene-d_8	Me_3SiOTf	40			80	5	**6:1**	135%	
5	**3(*m*TP^m)**	K	toluene-d_8	Me_3SiOTf	40			80	10	**5:1**	173%	
6	**3(*m*TP^m)**	K	toluene-d_8	Me_3SiOTf	40			80	13	**4:1**	170%	
7	**3(*m*TP^m)**	K	toluene-d_8	Me_3SiOTf	200			80	1	**1:182**	5300%	Possibly concentration of $SiMe_3$ radicals is too high to enable productive N-Si bond formation at this concentration.
8	**3(*m*TP^m)**	K	toluene-d_8	Me_3SiOTf	200			80	2	**1:201**	5247%	
9	**3(*m*TP^m)**	K	toluene-d_8	Me_3SiOTf	200			80	6	**1:202**	5248%	
10	**3(*m*TP^m)**	K	toluene-d_8	Me_3SiOTf	40			20	8	**14:1**	51%	
11	**3(*m*TP^m)**	K	toluene-d_8	Me_3SiOTf	40			20	4	**11:1**	123%	
12	**3(*m*TP^m)**	K	toluene-d_8	Me_3SiOTf	40			20	7	**7:1**	141%	
13	**3(*m*TP^m)**	K	toluene-d_8	Me_3SiOTf	40			-30	4	**247:1**	5%	
14	**3(*m*TP^m)**	K	toluene-d_8	Me_3SiOTf	40			-30	7	**247:1**	5%	
15	**3(*m*TP^m)**	K	toluene-d_8	Me_3SiOTf	40			80	4	**8:1**	113%	
16	**3(*m*TP^m)**	K	toluene-d_8	Me_3SiOTf	40			80	7	**7:1**	135%	
17	**3(*m*TP^m)**	K	toluene-d_8	Me_3SiOTf	40	DHA[c]	100	-30	3	**290:1**	3%	
18	**3(*m*TP^m)**	K	toluene-d_8	Me_3SiOTf	40	DHA	100	-30	6	**186:1**	7%	
19	**3(*m*TP^m)**	K	toluene-d_8	Me_3SiOTf	40	DHA	100	-30	10	**163:1**	6%	
20	**3(*m*TP^m)**	K/naph[d]	toluene-d_8	Me_3SiOTf	40			-30	3	**179:1**	6%	
21	**3(*m*TP^m)**	K/naph[d]	toluene-d_8	Me_3SiOTf	40			-30	6	**241:1**	5%	
22	**3(*m*TP^m)**	K/naph[d]	toluene-d_8	Me_3SiOTf	40			-30	10	**151:1**	8%	

23	**3(*m*TP^m)**	Cs	toluene-d_8	Me_3SiOTf	40			-30	2		[e]	Multiple side products.
24	**3(*m*TP^m)**	Cs	toluene-d_8	Me_3SiOTf	40			-30	6		[e]	Multiple side products.
25	**3(*m*TP^m)**	K	toluene-d_8	Me_3SiCH_2Ph	40			-30	2			No alkyl group incorporation.
26	**3(*m*TP^m)**	K	benzene-d_6	Me_3SiOTf	40			20	2	**0**	41%	No $HN(SiMe_3)_2$ formation.
27	**3(*m*TP^m)**	K	benzene-d_6	Me_3SiOTf	40			20	4	**0**	175%	No $HN(SiMe_3)_2$ formation.
28	**3(*m*TP^m)**	K	benzene-d_6	Me_3SiOTf	40			20	7	**0**	170%	No $HN(SiMe_3)_2$ formation.
29	**3(*m*TP^m)**	K	toluene-d_8	Me_3SiOTf	40			-30	2	**80:1**	14%	
30	**3(*m*TP^m)**	K	toluene-d_8	Me_3SiOTf	80			-30	5	**0**	major prod	Possibly concentration of $SiMe_3$ radicals is too high to enable productive N-Si bond formation at this concentration.
31	**3(*m*TP^m)**	K	toluene-d_8	Me_3SiOTf	40			-30	6	**211:1**	6%	Stirred reaction.
32	**3(*m*TP^m)**	K	toluene-d_8	Me_3SiOTf	40			-30	9	**16:1**	78%	Stirred reaction.
33	**3(*m*TP^m)**	K	toluene-d_8	Me_3SiOTf	40			-30	6	**414:1**	2%	Stirred reaction.
34	**3(*m*TP^m)**	K	toluene-d_8	Me_3SiOTf	40			-30	9	**276:1**	3%	Stirred reaction.
35	**3(*m*TP^m)**	K	toluene-d_8	Me_3SiOTf	40+40			-30	14	**552:1**	<3%	40 additional equivs added after 7 days allows reaction to continue.
36	**3(*m*TP^m)**	K	benzene-d_6	Me_3SiOTf	40	DHA	100	20	2	**11:1**		Reaction in benzene achieved by adding an H atom source.
37	**3(*m*TP^m)**	K	benzene-d_6	Me_3SiOTf	40	DHA	100	20	7	**11:1**		
38	**3(*m*TP^m)**	K	benzene-d_6	Me_3SiOTf	40	DHA	100	20	11	**19:1**		
39	**3(*m*TP^m)**	K	benzene-d_6	Me_3SiOTf	40	H_2	1 atm.	20	6	**24:1**	44%	Reaction possible using H_2 as H source.
40	**3(*m*TP^t)**	K	toluene-d_8	Me_3SiOTf	40			20	3	**0**		No $HN(SiMe_3)_2$ formation.
41	**3(*m*TP^t)**	K	toluene-d_8	Me_3SiOTf	40			-30	3	**0**		
42	**3Th(*m*TP^m)**	K	toluene-d_8	Me_3SiOTf	40			20	5	**120:1**	11%	Confirms generality of metal/ligand architecture.
control 1	*none*	KC_8	toluene	TMSI	40							Product is from homocoupling of $SiMe_3$ radicals.
control 2	**4(*m*TP^m)**	none	toluene	TMSI	6							No reaction.

[a] Present in excess, as solid. [b] major by-product is $O(SiMe_3)_2$. Yield per metal atom, measured by quantitative ^1H NMR spectroscopy against an added standard of 2,4,6-tritertbutylbenzene. [c] dihydroanthracene, whose weak C-H bonds are an H atom source. [d] catalytic (1 crystal) naphthalene added to increase solubilisation of K. [e] Several diamagnetic by-products were measured by NMR spectroscopy but not identified.